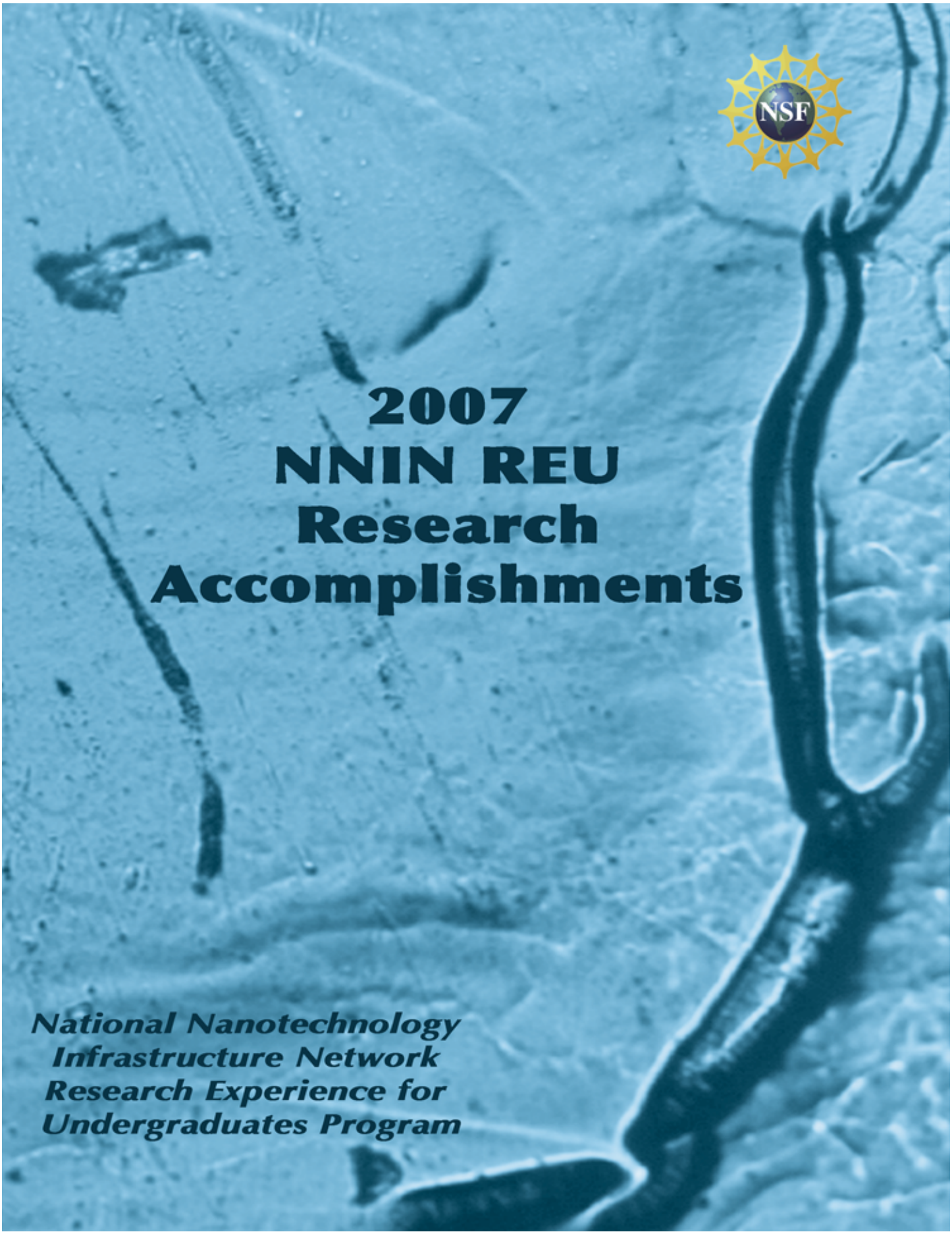

2007 NNIN REU Research Accomplishments

National Nanotechnology Infrastructure Network Research Experience for Undergraduates Program

Table of Contents

Introduction v

NNIN vi

The 2007 NNIN REU Interns, by Site

Cornell University vii
Georgia Institute of Technology vii
Harvard University viii
Howard University..... viii
Penn State University ix
Stanford University..... ix
University of California Santa Barbara x
University of Michigan Ann Arbor.....x
University of Minnesota-Twin Cities xi
University of New Mexico xi
University of Texas at Austin..... xii
University of Washington xii

Blast from the Past.....xiii

The 2007 NNIN REU Research Accomplishments

Biological Applications 2-23

Fluorescence Enhancement of CdSe Quantum Dots with Au Nanocrystals 2
Melissa Aillaud, University of California San Diego

Manipulation of Iron Nanoparticles and Their Effects on Human Colon Carcinoma Cells 4
Ebony Ayres, Hampton University

Fabrication of Multifunctional Atomic Force Microscopy-Scanning Electrochemical Microscopy Probe Arrays 6
Brian Bolz, Manhattan College

Utilization of Surface Acoustic Waves for On-Chip Manipulation of Micro/Nano Particles 8
Ashley Colletti, The Johns Hopkins University

Novel Optical Trapping Particles for Biological Experiments 10
Nathan Friez, Bethel University

Investigating Inter-Domain Regulation of von Willebrand Factor Interactions with Platelets.....12
Ryan M. Harrison, Johns Hopkins University

Watershed Segmentation Algorithm for Medical Confocal Image Analyses Towards *In Vivo* Early Cancer Detection 14
Man Kin Derek Ho, Johns Hopkins University

Study of Silver Nanoparticles Biocidal Impact on *Escherichia coli* Using Optical and AF Microscopy 16
Ruth Enid Kuilan León, UPR, Mayagüez Campus

Protein Functionalization of Nanostructured Polymer Surfaces 18
Ashlee Mangan, Carlow University

Fabrication of a Polymeric Microfluidic Device with Inkjet-Printed Silver Electrodes for Electrokinetic Bioparticle Characterization.....20
Brandon Noia, Duke University

Three-Dimensional Flow-Focusing in Microfluidic Devices 22
Sasha Perkins, University of Florida

Chemistry 24-37

Epitaxial Growth of Germanium and Silicon Nanowires by Chemical Vapor Deposition 24
Christopher J. Hainley, The University of Portland

Parametric Investigation of Picoliter Droplet Interfacial Tension using a Microfluidic Device.....26
Kevin Kelley, Pomona College

Rapid Synthesis of Silver Nanowires 28
Kylee Korte, Bradley University

Directed Self-Assembly for Post-32 nm Lithography 30
Brian Lambson, Columbia University

Factors that Affect the Synthesis of Gold Nanorods.....32
Alice MacQueen, University of Virginia

Cadmium Selenium Quantum Dot Photodiodes.....34
Van Nguyen, University of California, Riverside

Effect of Hydroxide Surface Treatments on Photoluminescence of InP/InGaAs Heterostructures 36
Christina Yeung, Swarthmore College

Electronics.....38-55

Nonvolatile Memory with Multi-Stack Nanocrystals as Floating Gates 38
Kamran Afshari, University of California-Los Angeles

Simulations of Nano-Particle Electro-Luminescence for Novel Near-Field Microscopy.....40
Syed Saad Ahsan, Cornell University

Nanowire-Based Flexible Thin Film Devices.....42
Kevin Baler, Cornell University

ALD on Single/Few Layer Graphene 44
Naresh W. Copeland, Prairie View A&M University

Carbon Nanotube Transistor Fabrication and Reliability Characterization 46
Latisha Crockett, Prairie View A&M University

P-Type Contact Optimization in Nonpolar Gallium Nitride-Based Blue Lasers.....48
Daniel Haeger, Illinois Wesleyan University

Demonstration of a Novel Fabrication Methodology to Produce Complex, Three Dimensional Structures 50
Daniel Linford, University of Rochester

Adhesion and Electromigration Performance of Barrier / Copper Interconnections in CMOS Technologies 52
Nasim Naderseresht, University of California, Berkeley

Post-22 Nanometer Non-Classical CMOS Transistors 54
Austin Nelson, University of St. Thomas

Materials.....56-81

Ohmic n-contacts to Gallium Nitride Light Emitting Diodes.....56
Jonathan Aguilar, Harvard University

Photoelectrochemical Etching of Silicon Carbide.....58
Henry David Babb III, Prairie View A&M University

Self-Assembly and Optical Characterization of Semiconductor and Metallic Nanocrystal Monolayers and Multilayers.....60
Robert Bradley, North Carolina State University

Synthesis, Characterization, and Testing of Polyurethane Nanocomposites 62
Alla Epshteyn, Tufts University

Deterministic Growth of Silicon Nanowires 64
Jonathan Ligda, Shippensburg University

The Role of Surfactants in Aqueous Solution Diffusion in Hydrophobic Nanoporous Thin-Film Glasses 66
Katherine Mackie, Whitworth University

Charge Transport in Gold Nanocrystal Arrays 68
David Marsh, University at Buffalo

Materials Ink Jet Printing of Electronic Structures.....70
Fabiola Nelson, New Jersey Institute of Technology

Fabrication of Low Temperature Solid Oxide Fuel Cells with Ultra-Thin Film Yttria-Stabilized Zircona Electrolytes 72
Amrita Saigal, Massachusetts Institute of Technology

Probing Nanostructures of Biorenewable Polyurethane Collapsed Foams 74
Ryan J. Seelbach, Beloit College

Nanostructured Photovoltaics Using Porous Alumina Templates as Structure-Directing Agents 76
Jessica Sherman, University of Kentucky

Functionalization of Silicon Nanoparticles for Hyperpolarized Magnetic Resonance Imaging 78
Derek Smith, University of Rochester

Spontaneous Alignment in Self-Assembled Block Copolymers for Nanolithography.....80
Mikael Witte, St. Olaf College

Mechanical Devices 82-89

Patterning of Electrical Circuits on Fluidic Assembly Microtiles 82
Andrew Baisch, Carnegie Mellon University

Development of a Three Degrees of Freedom Atomic Force Microscope 84
Courtney Bergstein, Carlow University

Fabrication of Active Probe Structures for Atomic Force Microscopy 86
Mohammad Biswas, Auburn University

Characterization of the DRIE Process for ETWI for Piezoresistive Inertial Sensors.....88
Maria Suggs, Southern Polytechnic State University

Optics.....90-101

Fabrication of Low-Loss GaN/AlN Waveguides for Nonlinear Optics.....90
Aydin Akyurtlu, Virginia Tech

Quantum Dot Light Emitters 92
Rehan Kapadia, University of Texas at Austin

Characterization and Optimization Study of Silicon Evanescent Racetrack Lasers 94
Brian McSkimming, University at Buffalo, State University of New York

Observation of Harmonics in a Uni-Directional Mode-Locked Fiber Laser Incorporating a Carbon Nanotube Saturable Absorber 96
Zachary Nishino, St. John's University

On-Chip Microfluidic Integration of Ultra-High Quality Silicon Optical Microdisk Resonators for Lab-On-Chip Applications 98
William J. Roman, University of Rhode Island

Development of Optical Fiber Packaging for Planar Lightwave Circuits by Microfabrication 100
Kylan Szeto, Rensselaer Polytechnic Institute

Physics 102-115

Modeling the Resolution for Photoacoustic Bio-Microscopy in the Giga-Hertz Frequency Range 102
Chukwunomso Agunwamba, Worcester Polytechnic Institute

Electrical Charge on a Nanofiltration Membrane 104
Kasiem Anderson, Georgia Institute of Technology

Electron Transport in Silver Silicon Composite Film.....106
Ian Broderick, Carleton College

Simulation of Room-Temperature Terahertz Quantum Cascade Lasers with Varying Degrees of Transverse Confinement 108
Nikhil Chandra, Cornell University

Enhanced Laser Cooling Using Ion-Doped Nanopowders: Engineering and Harvesting Atomic Vibrations.....110
Philip Hebda, Purdue University

What Makes Peacock Feathers Colorful? 112
Suntrana Smyth, University of Alaska, Fairbanks

Thermal Transport in Silicon Nanowires 114
Prem Vuppuluri, University of Portland

Process & Characterization.....116-139

Effect of a Magnetic Field on the Synthesis of Single-Walled Carbon Nanotubes.....116
Myriam Alexandre, University of Chicago

Nanowire Sensors.....118
Andrea Boock, Pennsylvania State University at Altoona

Synthesis and Characterization of ZnO and PbI_2 Colloidal Nanoparticles 120
Shin Bowers, Brown University

Maskless Nanolithography Using an Atomic Force Microscope 122
Ian Frank, Pomona College

Photo-CVD Coating of Nanoparticles with Silicon Dioxide 124
Brayden Glad, Duke University

Controlling Fluid Flow to Conducting Polymer Biosensors Using Surface Modification 126
Thomas Gobert, McNeese State University

Synthesis of Palladium Nanoparticles for Methanol Steam Reforming Catalyst.....128
Michael P. Johnson, Dana College

Nanoimprinted Plasmonic Nanoparticles for Biosensor Applications.....130
Emma Kamnang, Corning Community College

Use of Engineered Proteins for Organization of Nanostructures 132
Sarah Lee, Brigham Young University-Idaho

Atomic Force Microscopy Grain Structure Characterization of Perpendicular Magnetic Recording Media.....134
Alexander Luce, University of Arizona

Optical Characterization of Nanostructured Wide Bandgap Semiconductors for Energy Applications.....136
Jessica Smith, Austin College

Investigation of TMAH Release of Stretchable Silicon Networks 138
Allison Solanki, Whitman College

Index 141

Cover Image by Fabiola Nelson .....page 70

Ebony Ayres, Kamran Afshari, Alice MacQueen; photographs of REU interns by various site staff

The National Nanotechnology Infrastructure Network
www.nnin.org
is comprised of the following thirteen sites, and is supported by The National Science Foundation, the NNIN sites, our corporate sponsors and research users.

Cornell NanoScale Science & Technology Facility
Cornell University
250 Duffield Hall • Ithaca, NY 14853
607-255-2329 • http://www.cnf.cornell.edu

Microelectronics Research Center
Georgia Institute of Technology
791 Atlantic Dr NW • Atlanta, GA 30332
404-894-5266 • http://www.mirc.gatech.edu/

Center for Nanoscale Systems
Harvard University
11 Oxford Street LISE 306 • Cambridge, MA 02138
617-384-7411 • http://www.cns.fas.harvard.edu

Howard Nanoscale Science & Engineering Facility
Howard University
2300 6th St NW • Washington, DC 20059
202-806-6618 • http://www.msrce.howard.edu/

Triangle National Lithography Center
North Carolina State University (affiliate)
218A EGRC Box 7911 • Raleigh, NC 27695-7920
919-515-5153 • http://www.tnlc.ncsu.edu/

Center for Nanotechnology Education & Utilization
The Pennsylvania State University
101 Innovation Blvd, Ste 114 • University Park, PA 16802
814-865-5285 • http://www.cneu.psu.edu

Stanford Nanofabrication Facility
Stanford University
420 Via Palou Mall • Stanford, CA 94305-4070
650-735-3664 • http://snf.stanford.edu/

Nanotech: the UCSB Nanofabrication Facility
University of California, Santa Barbara
ECE Engr Science Bldg • Santa Barbara, CA 93106-9560
805-893-7989 • http://www.nanotech.ucsb.edu/

Michigan Nanofabrication Facility
The University of Michigan, Ann Arbor
1301 Beal Ave • Ann Arbor, MI 48109-2122
734-763-6719 • http://www.mnf.umich.edu

Minnesota Nanotechnology Cluster
University of Minnesota-Twin Cities
1-165 ECE Bldg 200 Union St SE
Minneapolis, MN 55455
612-624-8005 • http://www.mintec.umn.edu/

NanoScience @ UNM / CMEM
University of New Mexico
One University of New Mexico MSC 01 1120
Albuquerque, NM 87131
(505) 277-3162 • http://www.chtm.unm.edu/

Microelectronics Research Center
The University of Texas at Austin
J.J. Pickle Research Ctr, 10100 Burnet Rd, Bldg 160
Austin, TX 78758
512-471-6730 • http://www.mrc.utexas.edu/

Center for Nanotechnology
University of Washington
Box 352140 • Seattle, WA 98195-1721
206-616-9760 • http://www.nano.washington.edu/

Corporate Sponsors

• Advanced Micro Devices, Inc. •
• Agilent Technologies •
• Analog Devices, Inc. •
• Applied Materials •
• Canon, Inc. •
• Ebara Corporation •
• Hewlett-Packard Company •
• Hitachi, Ltd. •
• IBM Corporation •
• Infineon Technologies, AG •
• Intel Corporation •
• Intel Foundation •
• LG Electronics, Inc. •
• National Semiconductor Corp. •
• NEC •
• NXP Semiconductors (Philips) •
• Omron Advanced Systems, Inc. •
• Panasonic •
• Qualcomm •
• Renesas Technology Corp. •
• Robert Bosch Corporation •
• Seiko Epson Corporation •
• ST Microelectronics •
• Texas Instruments, Inc. •
• Toshiba Corporation •

Introduction

All photographs in this section were taken by Sascha Anderson

The 2007 NNIN REU Interns at the network-wide convocation, University of California Santa Barbara, August 2007

For an undergraduate student, completing a comprehensive experimental research task in ten weeks can be a very formative and defining experience. Above all, the completion of a challenging task enthuses, but it also tests the many skills of learning and applying the learning, and helps determine the course of life at a very critical stage when one is coming into one's own.

NNIN attempts to provide such an experience by bringing strong collaborations and interesting research problems that undergraduate students can participate in.

The students participating in this effort are on the path of technical education and many are getting their first experience with advanced hands-on research as part of our REU program. The focus on advanced research and knowledge, the strong mentoring and support, the strong exposure to a professional research environment, the strong expectations built into the research and presentations at convocations, the exposure to a wider variety of research conducted by peers and other users in diverse disciplines of science and engineering within the unifying facilities, and the strong scientific and social interactions across the network, have been critical to the compelling experience.

Equally critical is the continuing dedication and effort from our staff, faculty, and graduate students, and the final convocation that happened this year at University of California at Santa Barbara.

This report demonstrates that enthusiastic participating students coupled with the sustained support from staff, faculty, and graduate students leads to major accomplishments and provides the students with confidence in their own abilities and experience to make their own decisions.

I wish the participants the best wishes for future technical careers; NNIN hopes to see them build on this summer's experience, and my thanks to the staff, the graduate student mentors, and the faculty for their participation and involvement. Particular thanks are due to Melanie-Claire Mallison and Lynn Rathbun at Cornell, Angela Berenstein and Mark Rodwell at UC Santa Barbara, and Nancy Healy at Georgia Institute of Technology for their contributions in organizing the logistics of the program and the convocation.

Sandip Tiwari
Director, NNIN

The 2007 NNIN REU Program Staff

Front, from left to right:

Jean Toll, University of Texas at Austin
Melanie-Claire Mallison, Cornell University
Sandrine Martin, University of Michigan
Jennifer Tatham Root, Georgia Tech
Kathryn Hollar, Harvard University
Lynn Rathbun, Cornell University

Back, from left to right:

Michael Deal, Stanford University
Ethan Allen, University of Washington
James Griffin, Howard University
Robert Erhdmann, Penn State University
Angela Berenstein, UC Santa Barbara
Nancy Healy, Georgia Tech

Cornell NanoScale Science & Technology Facility, Cornell University

2007 NNIN REU Interns

First row, from left to right:

Mr. Aydin Akyurtlu ..... page 90
Mr. Thomas Gobert ..... page 126
Ms. Fabiola Nelson ..... page 70
Ms. Sasha Perkins ..... page 22

Second row, from left to right:

Mr. Kamran Afshari ..... page 38
Mr. Suntrana Smyth ..... page 112
Mr. Kylan Szeto ..... page 100
Mr. Nathan Friez ..... page 10

Third row, from left to right:

Mr. Brandon Noia ..... page 20
Mr. Andrew Baisch ..... page 82
Mr. Prem Vuppuluri ..... page 114

Microelectronics Research Center, Georgia Institute of Technology

2007 NNIN REU Interns

First row, from left to right:

Mr. William Roman ..... page 98
Mr. Brian Bolz ..... page 6
Mr. Mohammad Biswas ..... page 86

Second row, from left to right:

Mr. Daniel Linford ..... page 50
Mr. Brian Lambson ..... page 30
Mr. Gerald Lopez ..... *NNIN REU Mentor*

Center for Nanoscale Systems, Harvard University

2007 NNIN REU Interns

First row, from left to right:

Mr. Chukwunomso Agunwamba ..... page 102
Ms. Amrita Saigal ..... page 72

Second row, from left to right:

Mr. Derek Smith ..... page 78
Mr. Ian Frank ..... page 122

Howard Nanoscale Science & Engineering Facility, Howard University

2007 NNIN REU Interns

From left to right:

Mr. Kasiem Anderson ..... page 104
Ms. Ebony Ayres ..... page 4
Mr. Ian Broderick ..... page 106
Ms. Ruth Kuilan León ..... page 16
Mr. Henry Babb III ..... page 58

Penn State Nanofabrication Facility,
The Pennsylvania State University

2007 NNIN REU Interns

From left to right:

Mr. Jonathan Ligda ..... page 64
Ms. Courtney Bergstein ..... page 84
Ms. Ashley Colletti ..... page 8
Ms. Andrea Boock ..... page 118
Ms. Ashlee Mangan ..... page 18

Stanford Nanofabrication Facility,
Stanford University

2007 NNIN REU Interns

Front, left to right:

Ms. Nasim Naderseresht ..... page 52
Ms. Maria Suggs ..... page 88

Back, left to right:

Ms. Latisha Crockett ..... page 46
Mr. Alexander Luce ..... page 134
Mr. Naresh Copeland ..... page 44
Ms. Katherine Mackie ..... page 66
Ms. Allison Solanki ..... page 138

Nanotech @ UCSB,
University of California Santa Barbara

2007 NNIN REU Interns

Front row, from left to right:

Mr. Jonathan Aguilar ..... page 56
Ms. Jessica Sherman ..... page 76
Mr. David Marsh ..... page 68

Back row, from left to right:

Mr. Brian McSkimming ..... page 94
Mr. Daniel Haeger ..... page 48
Mr. Austin Nelson ..... page 54

Michigan Nanofabrication Facility,
University of Michigan Ann Arbor

2007 NNIN REU Interns

Front row, from left to right:

Ms. Emma Kamnang ..... page 130
Ms. Jessica Mae Smith ..... page 136
Ms. Myriam Alexandre ..... page 116

Back row, from left to right:

Mr. Kevin Baler ..... page 42
Ms. Alla Epshteyn ..... page 62
Mr. Philip Hebda ..... page 110

Minnesota Nanotechnology Cluster,
University of Minnesota-Twin Cities

2007 NNIN REU Interns

From left to right:

Mr. Rehan Kapadia ..... page 92
Mr. Brayden Glad ..... page 124
Mr. Mikael Witte ..... page 80
Ms. Christina Yeung ..... page 36
Mr. Ryan Seelbach ..... page 74

Nanoscience @ UNM,
University of New Mexico

2007 NNIN REU Interns

From left to right:

Mr. Shin Bowers ..... page 120
Ms. Melissa Aillaud ..... page 2
Mr. Robert Bradley ..... page 60
Mr. Zachary Nishino ..... page 96
Mr. Michael Johnson ..... page 128

Microelectronics Research Center, University of Texas at Austin

2007 NNIN REU Interns

Front, from left to right:

Mr. Christopher Hainley ..... page 24
Ms. Alice MacQueen ..... page 32
Mr. Man Kin Ho ..... page 14

back, from left to right:

Mr. Nikhil Chandra ..... page 108
Mr. Syed Ahsan ..... page 40

Center for Nanotechnology, University of Washington

2007 NNIN REU Interns

Front, from left to right:

Ms. Sarah Lee ..... page 132
Mr. Van Nguyen ..... page 34
Ms. Kylee Korte ..... page 28

back, from left to right:

Mr. Kevin Kelley ..... page 26
Mr. Ryan Harrison ..... page 12

Blast from the Past

Dear NNIN/NNUN Community:

Believe it or not, this network has been hosting the Research Experience for Undergraduates Program for ten years! For a total of 588 interns! To help mark this momentous anniversary and success, we added this "Blast From The Past" section to the research accomplishments. We contacted all 519 interns from the 1997-2006 programs (most of the email addresses still worked!) and on the following pages are a few words on how they are doing, what they are doing, and how their REU summer with us helped get them there. Enjoy catching up!

Blast From The Past Index, By Year:

YEAR	*INTERN*	*PAGE*
1997	Beyder, Arthur	xiv
1997	Molnar, Paul	xxii
1998	Landwehr McHale, Diana	xxi
1999	Carlson, John	xv
1999	Hvisc, Stacie	xix
1999	Meteer Wiedemer, Jami	xxii
1999	Montanez, Jessica	xxiii
1999	Swint, Ethan	xxvii
1999	Westly, Daron	xxviii
2000	Brown, Austin	xiv
2000	Johnson, Jevon	xx
2000	Slinker, Jason	xxvi
2001	Ercius, Peter	xvii
2002	Graziano, Tom	xviii
2002	Irizarry Rosado, Gizy	xix
2002	Krause, Michael	xx
2002	Pontius, Chris	xxiv
2002	Rey, Diego	xxiv
2002	Vampola, Ken	xxviii
2003	Dejgosha, Siavash	xvi
2003	Farjadpour, Ardavan	xvii
2003	Kone, Ami	xx
2003	Lee, Grace	xxi
2003	Masandi-Shirazi, Ali	xxii
2003	Newton, Andrew	xxiii
2003	Zhao, Yu Jennifer	xxix
2004	Cochran, Peter	xv
2004	Fields Manzini, Diane	xvii
2004	Fraser, Eric	xviii
2004	Olds, Nate	xxiv
2004	Padgaonkar, Vaidehee	xxiv
2004	Shaikh, Shahid	xxvi
2004	Stolyarov, Alexander	xxvii
2004	Vallett, Paul	xxviii
2004	Yang, Allen	xxix
2005	Brettmann, Blair	xiv
2005	Burger, Caitlin	xv
2005	Carson, Ashley	xv
2005	Chestnut, Michael	xv
2005	Doyle, Laura	xvi
2005	Ezeife, Nkemdilim	xvii
2005	Figueroa, Johangel	xviii
2005	Heremans, Joe	xix
2005	Hsu, Derek	xix
2005	Hughey, Jake	xix
2005	James, Miktosha	xx
2005	Johnson, Joy	xx
2005	Kuehl, Ken	xxi
2005	Melton, Andrew	xxii
2005	Montague, Josh	xxiii
2005	Nguyen, Que Anh	xxiii
2005	Noxon, Virginia	xxiv
2005	Scherson, Yaniv	xxv
2005	Shah, Neel	xxv
2005	Soofi, Wafa	xxvi
2005	Symonds, Josh	xxvii
2005	Tippie, Abbie	xxviii
2005	Walker, Brandon	xxviii
2005	Welch, David	xxviii
2006	Adams, Michael	xiv
2006	Ballinger, Andrew	xiv
2006	Bonthera, McIntosh	xiv
2006	Bryan, Sarah	xiv
2006	Coats, David	xv
2006	Cornell, Eva	xvi
2006	Daise III, Henry	xvi
2006	Deng, Luxue	xvi
2006	Harjanto, Dewi	xviii
2006	Henry, Nathan	xviii
2006	Lavenson, David	xxi
2006	Lawrence, Juliet	xxi
2006	Mangan, Niall	xxii
2006	Norvell, Emily	xxiii
2006	Roberson, Leila Joy	xxv
2006	Sanders, Anthony	xxv
2006	Schluneker, David	xxv
2006	Smith, Cary	xxvi
2006	Stoafer, Chris	xxvii
2006	Swaim, Jon	xxvii
2006	Taylor, Dane	xxvii
2006	Velten, Josef	xxviii
2006	Wu, Claude	xxix
2006	Young, Kaylie	xxix

Michael Adams
2006 Harvard University

I graduated from The University of North Carolina at Chapel Hill in May 2007 with a B.S. in Physics, and got a year long internship with IBM. I'm now doing software development work, primarily in Java. After the IBM internship ends, I'm planning to attend a Medical Physics graduate program, for at least a Masters, preferably a PhD.

Thanks, and let me know what the other interns are up to!

Michael

Andrew Ballinger
2006 Georgia Tech

Hey Jennifer,

I'm writing this e-mail for two reasons really, first and foremost I've been meaning to keep you up to date with what I'm doing. My NNIN REU in 2006 has benefited me in enumerable ways. When I got back to the University of North Texas I was asked by the administration at my high school/college to give a series of presentations to students and parents about REU's in general and the NNIN program specifically. The more I was asked to talk about the program, the more I came to realize how much the program has shaped and directed me.

I applied to several schools within the NNIN in order to continue my undergraduate education and decided to go to the University of California - Santa Barbara. We've just started classes here in beautiful Santa Barbara and I'm starting to get to know the research opportunities available here. I heard that the convocation was held here this year, I came up for orientation that same week! I missed you by only a few days and I wish I could have gotten the chance to say hello.

How was the REU program this year? I went online and read a few of the presentations, are there any Final Reports I should watch for? How are you doing? Still busy as ever?

Still missing your pantry, Andrew Ballinger

Arthur Beyder
1997 The Pennsylvania State University

Hi Melanie,

Hope all's well for you and the rest of the bunch at CNF. I am now at Mayo Clinic, being used as an experimental rat, better known as a medical resident. It's actually pretty fun, but a little draining. I've composed a short blurb (below) for you to use as you wish. Ta ta, art

Hard to believe it's been 10 years since that great summer! I have kept up and sharpened my skills over this time and continued working on MEMS. We have recently published several papers and patented a novel Atomic Force Microscope (AFM) cantilever that will surely revolutionize the field (...or, I just hope people notice and use these probes)!

Currently, I am in medicine/research residency at Mayo Clinic, where I will help design and build novel endoscopic tools for futuristic gastroenterology. What if you could perform all of the surgery in a patient's body without ever cutting the skin? Well, this is already happening using a recently developed technique called NOTES (natural orifice transluminal endoscopic surgery).

McIntosh (Mack) Bonthera
2006 Cornell Intel

Hello again Melanie!

Hopefully it's not too late to reply! I am fabulous. This past summer I did an internship with Merck and Co. It is because of my experience with NNIN and funding from Intel that opportunities were open to me and I was selected from many qualified applicants. I am grateful to Intel for this and the whole NNIN family in general. I am hoping to land an internship or co-op with a nanotechnology company for this summer but haven't got one as of yet. Thanks again and I hope to hear from you soon.

Blair Brettmann
2005 Cornell University

I just started grad school at MIT in chemical engineering and am planning on getting my PhD. I'm really thankful that I was able to do the NNIN REU and I hope that the program continues for a long time!

~Blair

Austin Brown
2000 UC Santa Barbara

Hey,

I was an intern in 2000 I think. At UCSB. I'm currently a graduate student at Stanford in the Biophysics program. I'm defending my dissertation later this month, so I should be done soon!

Sarah Bryan
2006 Stanford University

Melanie-Claire -

It was so nice to hear from you! What a big task it must be to try contacting all of your old summer interns!

After spending the summer at the NNIN Stanford site, I decided that I wanted to do research in the nanofabrication field for my graduate work. I am now at Georgia Tech finishing the first semester of my Master's degree in Electrical Engineering. Hopefully I will be continuing on directly to my Ph.D. as of next fall. The NNIN internship was one of the most integral parts of

my decision to enter engineering graduate school and I can't even begin to express all the amazing things I learned! Thank you again!

Sarah Bryan

Caitlin Burger
2005 Cornell University

Hi Melanie-Claire!

I've been doing really well! I'm currently a second year graduate student at Purdue University in West Lafayette, IN. I'm working on my Ph.D. in Materials Engineering, and have been conducting research regarding ultra-thin solid oxide fuel cells. I'm also a Purdue Graduate School senator, and am the acting president of my department's graduate student association. Currently, I teach middle school students about nanotechnology on Saturdays as part of a gifted education program. My summer at Cornell has proved to be an invaluable experience for me!

My time in the NNIN REU helped increase my knowledge base in nanofabrication and gave me my first taste of research. Traveling to the end-of-summer conference at Stanford University is one of my fondest memories from the experience. Giving a presentation helped me realize that I enjoy discussing research with others, and aided in my decision of apply to graduate school. Because of my experience at Cornell, I have discovered the importance of outreach programs in shaping the goals of younger students, and intend to continue participating in educational outreach throughout my professional career.

I hope you and everyone out in Ithaca are doing well!!!!

Caitlin

John Carlson
1999 Cornell University

I am working as a flight controller for the International Space Station program. My primary responsibility is downlinking payload science data and video from the station for the research community.

John Carlson (1999)

Ashley Carson
2005 Georgia Tech

I participated in the 2005 NNIN program at Georgia Tech. I graduated from Clemson University that following spring in 2006. I am now in my second year of graduate school at Georgia Tech in the Biomedical Engineering PhD program. My experience in the NNIN program played a huge role in where I am now. It was my first research experience, and I enjoyed it so much that I decided to pursue my PhD. My main reason for coming to Georgia Tech was because I had such a wonderful experience as an intern. Being here also gave me the opportunity to interact with the 2007 interns here which was very rewarding for me. I hope to be a mentor myself for a future intern!

Ashley Carson

Michael Chestnut
2005 Howard University

Dear Melanie-Claire,

I would first like to thank you, the NNIN program, and the staff at Howard University for the wonderful opportunity that was given to me.

After the program I did research my college campus in the area of nano-electronics. I then took a semester off 'cause I was tired from school, and finished my research by presenting at a summer symposium. In the fall of 2006 I began co-opting at Analog Devices. This was a wonderful experience and I finished my second rotation with them this past summer. I will be getting my Computer Engineering Degree in December, hopefully my Electrical Engineering degree in May, and then pursuing a graduate degree next fall. I hope all is well and I would just like to thank you again for the experience,

Michael D. Chestnut II

David Coats
2006 University of Minnesota

Well Hello Ms. Mallison!

Since I interned at the University of Minnesota in 2006, I have had a whirlwind of a life. Aside from the regular school, I do research in the Optical Coherence Laboratory here at Harvey Mudd College. This latest summer I worked at a functional magnetic resonance imaging laboratory in Singapore. Both experiences have convinced me, however, that my future lies in Finance. I am applying for jobs at a few hedge-funds and hopefully I will be working next year.

- David Coats

Peter Cochran
2004 UC Santa Barbara

Hey,

I was a 2004 intern at UC Santa Barbara researching Atomic Force Microscope anodic-oxidation lithography with Professor Evelyn Hu. Later, I graduated in 2006 with a BSE Mechanical Engineering and Applied Mechanics degree; also was captain of our University of Pennsylvania track team. NNIN REU lead to an industry internship and later several industry career offers a year before graduation! I began at Intel here in New Mexico in our Rotating Engineer Program and am now a career engineer. I have had the opportunity to thank Professor Hu at UCSB many times---she was a great mentor during my NNIN

REU and graciously wrote recommendations for several summer internship applications and two graduate school applications---thank you. I was accepted by the Management Science and Engineering graduate program at Stanford and then chose to attend through Stanford's on line Honors Co-op Program. Nano-science is my academic engineering field along with a decision analysis concentration …Intel pays all costs. No matter how silly it may sound to say my internship at UC Santa Barbara was life-changing, well, it was.

Beyond education and career, I now coach track and field, am an avid soccer player, and volunteer through our Native American education organizations.

Peter A. Cochran

Eva Cornell
2006 University of Minnesota

I'm finishing up my last year of undergraduate work at Gustavus Adolphus College in St. Peter, MN. I'm working on applying to grad schools to study biophysics. My REU definitely helped me clarify my plans and listening to all the talks at the end of the summer helped me realize that biophysics is the field I'm most interested in. I'll know a lot more about my future plans in a few months, but for now I'm looking forward to traveling next summer and then starting work on getting a PhD.

-Eva Cornell

Henry Daise III
2006 Howard University

To Ms. Melanie-Claire Mallison,

Hello to you and how is everything going for you? First, congratulations on the NNIN REU Program and the 10 years of success it has brought to me and the my fellow interns from the program. Lastly, I apologize if this is getting to you late, I have been busy lately and for about the past couple of days, I have been trying to recover, from the week that I had, also below is the update of what, I have done since, the summer of '06.

I am doing fine. Since being an intern in the NNIN program, I have graduated from Morehouse College, in May 2007, with my bachelor's degree in Computer Science. Currently, I am in San Bernardino, California, doing a one year fellowship with the Integrated Technology Transfer Network, at California State University - San Bernardino. Since being in the program, I have gained a stronger appreciation for the science and mathematics. As a result of being in the program, it helped me to get accepted into the current fellowship program and has helped give me a foundation, for studying entrepreneurship and expanded my research interest for graduate school.

Henry Daise III

Siavash Dejgosha
2003 Stanford University

Hi Melanie,

I'm doing great. The internship really stirred an interest in nanotechnology and research. After the internship, I took a research position in a biophysics lab at Cornell which I continued for a year and a half. That work culminated as a co-authorship in a Nature Methods paper published in 2006. I applied for a biophysics PhD program and was about to go to UMich - Ann Arbor, but did not want to spend 5-6 years in the midwest. Following a Masters, also at Cornell, I joined a tech startup in California and am now at Goldman Sachs in New York.

The internship really got me excited about research and technology, and I still follow what I can, but the research path wasn't meant to be. While I do not use the specific knowledge I gained, the introduction to practical research and presentation skills learned have been invaluable studying at school, working at a startup, and now.

Siavash

Luxue (Rose) Deng
2006 University of New Mexico

Melanie,

Hi, I was a NNIN intern in 2006. Currently, I have taken a different road to my career since graduating this past May. I am studying Chinese at Beijing Normal University in Beijing, China, and have been job searching here. I'm not completely sure what job I will end up finding but I know I will be in China for an indefinite amount of time.

The main skills that I acquired during my time with NNIN were research skills and presentation. It was the first time I presented in from of 60 plus people. I think it was a great experience and allowed me to get an idea of what academic research is like. Although I right now I am not completely sure if I want to become a full time researcher, it did help me see my options. I know now that if I did want to attend graduate school in the sciences it is not a far off option.

I hope you get quite a few updates. It'll be interesting to see where everyone is at right now.

-Rose

Laura Doyle
2005 Georgia Tech

Hi Melanie-Claire,

The NNIN program actually wasn't too far from my mind recently because I ran into one of my fellow REUs when I was doing grad school visits. It was great to see her and check up on how she's doing, so I think that getting updates on as many

REUs as possible is absolutely fantastic! My "Blast From the Past" follows:

My research career sure has blossomed since doing an NNIN REU in the summer of 2005. I used the conference presentation skills I learned there when I gave a podium presentation at the Biomedical Engineering Society conference that following October. Since then, I've kept up with my research. The skills I learned as an REU and the contacts I made at the Georgia Tech site helped me get into all the graduate schools I applied to. Right now I'm enjoying my first year in a BME PhD program at Johns Hopkins. Doing the NNIN internship was a fantastic experience for me and I firmly believe that it helped get me where I am today.

Thanks a lot for putting in the effort to organize this. I hope you'll e-mail us all a link to the finished copy when the time comes.

Take care, Laura

Peter Ercius
2001 UC Santa Barbara

Hi Melanie,

It is hard to believe that the program has been going for 10 years now. It was a great experience for me, and I actually think about it often. The program encouraged me to do research on nanotechnology, in fact. I graduated from Cornell University in 2003 with a B.S. in applied and engineering physics, and decided to continue on in the same program for a PhD. The lure of the newly built nanotechnology building was too much for me to resist. I started working for Professor David Muller who does materials and microelectronics research with transmission electron microscopes. I collaborate with IBM researchers on a 200keV scanning/transmission electron microscope with support from the Semiconductor Research Corporation (SRC). I image copper wires and interconnects from computer chips in three dimensions using a technique called electron tomography to help characterize and predict their performance. I hope to finish my doctoral studies soon and plan to find a job working with a high tech company such as IBM. All of the people involved in the NNUN program were great and spending the summer at UCSB was a valuable experience.

That is what I have been up to. I'm looking forward to hearing about other interns from my program. I'll try to stop by some time to say hello since I'm still here at Cornell.

Peter

Nkemdilim (Kemdi) Ezeife
2005 Cornell Intel

Melanie-Claire,

I have been doing well since my participation in the NNIN program 2 summers ago. I graduated from Temple University in January 2007 with a B.S. in chemistry (Magna cum laude) and I am now a first year student at Temple University School of Medicine. My experience in the NNIN REU program helped me to get into medical school and has provided me with a good perspective into how academic research is done which may prove useful to me in the future. I wish the best of luck to you and the program's continued success.

-Nkemdilim (Kemdi) Ezeife

TUSM Class of 2011

P.S. I give my thanks for the Intel sponsorship as well.

Ardavan Farjadpour
2003 Cornell University

Hi Melanie-Claire,

It is a real treat to hear from you. My summer at the CNF in 2003 was really the start of my academic research career. My work on electronic devices and the experience gained working in a top-notch clean room environment definitely helped in making my decision to go to graduate school. I discovered my main research interests in computational nanophotonics the summer following the (formerly) NNUN REU program—at the IBM Almaden Research Center in California—and am now in my 4th year at MIT working on a masters in Computation for Design & Optimization and a doctorate in Materials Science & Engineering. I made a lifelong friend at the CNF in Mike Campolongo who I keep in regular contact with and have visited many times in the years since. That summer in '03 was a formative one and I have very happy memories of my time in Ithaca; it was a special summer for me.

I hope all is well with you and your son. I will definitely stop by and say hello the next time I am in Ithaca visiting my old friend Mike C.

All the best, Ardavan

Diane Fields Manzini
2004 Cornell University

Melanie!!

I know everyone from my year still talks about how we miss our wonderful summer of 2004! Such a great time, valuable experience and wonderful people!

I graduated in 2006 from Virginia Tech with my B.S. in materials science. Then I started working at Cree Inc. in Raleigh, NC as a process engineer on in their LED fab. I was in the clean room decked out in a bunny suit everyday just like my summer at Cornell.

But I actually got married October 6th and I moved with my husband up to Groton, CT. We're only here till December and then the Navy is sending us off to Hawaii for a few years! I'm really excited! I'm hoping to get a job with the Navy or with a

contractor on base once we get there. (Of course I'm also hoping to spend a lot of time on the beach!)

Aloha! Diane Manzini (Fields)

Johangel (Joe) Figueroa
2005 University of Minnesota

Hi Melanie:

I was part of the 2005 REU team in the University of Minnesota. Since my internship I graduated from my Bioengineering/ Biotechnology degree and worked in the start-up process of one of the biggest mammalian cell culture plants of the world (Amgen, P.R.). I'm currently working in another Biotech plant start-up, this time in Indiana and pursuing my Masters degree in Biotech/Bioinformatics from John Hopkins University.

I hope everyone from the 05' is doing great....

Later; Joe

Eric Fraser
2004 UC Santa Barbara

Hi Melanie-Claire, great to hear from you.

I can't wait to see the research accomplishments of this year's class and read updates on my classmates! Here is mine.

After my NNIN REU, I graduated with a degree in Physics from Pomona College. My REU research in Shuji Nakamura's lab at UCSB formed the basis of my experimental thesis about deep-UV light emitting diodes. After studying physics, I started studying law and business at the University of Chicago and will graduate with joint JD/MBA degrees in 2009. Of course, my REU gave me substantive science and engineering knowledge and research skills. More importantly, however, it refined my analytical thinking and helped me to discover and explore the delicate balance between science, law, and business. Now I can talk with friends and family about not only the benefits of LEDs, but also how the patent system fuels scientific research and how research, in turn, drives business.

Eric M. Fraser

Tom Graziano
2002 UC Santa Barbara

Good hearing from you:

Currently I am working on nuclear reactor core control equipment at Knolls Atomic Power Laboratory in Schenectady, NY (i.e. not nanofab). I loved my internship though at UC Santa Barbara—it was an experience I will never forget. I would love to hear from my friends to see how they are doing.

-Tom

Dewi Harjanto
2006 University of Minnesota

I'm finishing my final year of undergraduate work at Olin. I am currently in the process of applying for graduate school—specifically, I'm looking for Ph.D. programs in bioengineering. The REU summer program really solidified my interest in pursuing research in academia.

Dewi

Nathan Henry
2006 Cornell University

Hi Melanie-Claire,

How are you doing? I know it has been a long while since we have seen each other or talked. So, I am in Italy right now. These keyboards are so hard to type on cause everything is in weird places. Italy is grand. Lovely city with many old artworks and buildings. I am staying in Turino, learning Italian and culture. This place is so different from America, much slower pace. I like it a lot. I don't want to come back to the US, but will have to sometime to finish my degree.

Below is my statement:

Partaking in the REU has offered me many treats. First, the REU offered me a rare glimpse into nanotechnology and fabrication. Being an EE, a greater appreciation is understood on chip design and fabrication along with present and future electrical technology. I met an amazing mentor, Ali Gokirmak, who dedicated much of his time and friendship into me and the project. And if life wasn't grand already, I spent a blissful summer in Ithaca's natural beauty. The summer spent working on nanowires, eating with Ali, and jumping into gorges is one that still reigns supreme in my mind.

I am soon to graduate with my degrees in EE and BME this coming December. I have had an offer from my mentor, Ali, to do a PhD at the University of Connecticut on continuing the research into Crystallization of A-Si Nanowires for TFTs. I have also been researching jobs in the medical field with a passion to work on medical implants of the cochlear and retinal. It's another fork in life's roadway, and to tell you honestly, I have no idea where I will venture, and I love it!!!"

I hope my statement makes it into the books. If not, it is ok. At least you will know my opinion on the REU and my outlook for the future. I have included a couple of pictures of me taken in China. I am not if I told you or not, but Jon Swaim and I hungout in Beijing. Great times and lots of adventures. But I have to run to class. Interested in how you have been and how last years REU went. Bye M-C!

Nathan

Joe Heremans
2005 Cornell University

Hello,

Sorry for the near deadline submission. T'wasn't my intention to cut it this close but this fell right in my midterms and some rather interesting data collection. I attached the blurb in word form if you prefer, otherwise the body is just as follows:

A year after my internship at Cornell University in 2005, I graduated from the University of Michigan and moved onto my PhD studies in electrical engineering at University of California, Santa Barbara. My time working as an REU solidified my wish to pursue graduate school and continue my path in academia. The skills and techniques I learned in the clean-room stick with me here at UCSB. I am currently a second year graduate student working for Prof. David Awschalom, researching the spin manipulations of Nitrogen-Vacancy centers in diamond for possible use in quantum computing. The past few months I have been using every fabrication trick I learned both from the staff at the Cornell NanoFab and the staff and fellow graduate students here at the UCSB NanoFab to process on my tiny 1mm by 1mm diamond sample.

Hope all is well in Ithaca, Joe

Derek Hsu
2005 Stanford University

Hi Ms. Mallison,

After my NNIN REU at Stanford, I spent the next two years finishing up my B.S. degree at Northwestern. Due to my increased interest in research as a result of my experience from NNIN, I worked as a research assistant at my school last summer, using Local Electrode Atom Probe tomography to conduct microanalysis and modeling of TiNi-based shape memory alloys for cardiovascular stents applications. Eventually, I continued this research into my senior capstone project, and received from my department the Hilliard Award for Undergraduate Research and Design for my project. Also, I collaborated with a team of five undergraduates, combining my experimental results with their computational modeling. Later, our team received the First Prize Award for the ASM Undergraduate Design Competition.

I have benefited greatly from the NNIN REU because the experience gave me confidence in my abilities as a student, and paved the road for my interest and dedication to research in the past two years and beyond. Currently, I am working at the NET Lab in Oregon, using thermodynamic simulations to develop models for alloy oxidation behavior in ultra-supercritical steam turbines. I plan on enrolling in an MSE Ph.D. program next fall.

Once again, thank you for the chance of experiencing the NNIN REU program. I will definitely encourage other undergraduates to apply for the internship in the future. Thank you.

Sincerely, Derek Hsu

Jake Hughey
2005 Georgia Tech

Melanie-Claire,

I'm doing well. In May I graduated from Vanderbilt in biomedical engineering and math. Most of the summer I just relaxed. I am beginning my first year in the PhD program in bioengineering at Stanford, with a Bio-X Bioengineering Fellowship. With my research, I hope to combine microfluidics and systems biology in order to gain a quantitative understanding of cell behavior. Since my research project for my NNIN REU at Georgia Tech was about synthesis of metal nanoparticles, the overlap in technical details is rather small. Nonetheless, my NNIN REU experience taught me the universal lesson that science is hard, so success requires perseverance and ingenuity. Plus, that summer at Georgia Tech was awesome.

Jake Hughey

Stacie Hvisc
1999 Stanford University

Hi Melanie,

Here's an update for me:

After my REU, I graduated from Cornell with my B.S. and M.Eng. in engineering physics and started working on some very large things. My first job was working on the National Ignition Facility (NIF) at Lawrence Livermore National Laboratory (LLNL). This is a laser that takes up an entire building and quite opposite from the VCSEL's (vertical cavity surface emitting lasers) that I researched in my REU. I worked on a few other projects at LLNL before taking a leave of absence to return back to school.

Currently, I am working on my PhD at the University of Arizona, College of Optical Science. My research group is involved in designing and fabricating large optics, especially large telescopes. My research is on field-dependent aberrations in misaligned optical systems. While I may not be working in nanofabrication anymore, I am grateful for the introduction to research my REU provided and for the opportunity to say that I have worked on all sorts of projects, from the very small to the very large.

Stacie Hvisc

Gizy Irizarry Rosado
2002 Cornell University

Hello Melanie!

It is nice to hear from you. Here is my "Blast from the Past" story:

My name is Gizaida Irizarry Rosado from Puerto Rico and I participated in the 2002 REU Summer Internship program. It was a very rewarding experience and it was a first step in my

career path. After REU, I participated in other undergraduate Internship programs until I graduated from the Mechanical Engineering Department of the University of Puerto Rico Mayaguez Campus. In 2003, I worked in Merck Sharp and Dohme of Barceloneta, Puerto Rico as an engineering student in the Engineering Department. In 2004, I worked in the Research and Development Center of Guidant at Minnesota. In 2005, I started working in the San Juan Office of The Trane Company as a Mechanical Engineer for the Applied Sales Department and have being working there since. To be part of Trane, I had to successfully complete an intensive six-months training in La Crosse, Wisconsin in the field of HVAC: Products, Designs, Analysis and Components. These past years in Trane have being very challenging and of great professional growth for me.

This year, I also enrolled in the University of Puerto Rico Rio Piedras Campus to pursue a Master's Degree in Business Administration. Hopefully, I will complete this MBA in 2010.

I encourage any student that wants to be successful to participate in summer Internship programs. These programs provide you with good learning and great experience. Thanks! Gizy

Miktosha James
2005 University of Texas at Austin

Since the internship I have had some amazing opportunities. I just finished working for NASA this summer. Graduation is approaching this December. The experience of the REU opened my eyes to explore or areas of engineering. From then on things have gotten better by the years. I was with child when I did the REU and after the internship I knew that I could accomplish anything. I am right now working on a project that is leaning toward a patent.

Thank you for giving me a chance to prove myself. My son is about to be two and I am a success all because someone looked past my personal life and gave me a chance to create a successful path. THANK YOU for the bottom of my heart.

Miktosha James

Jevon Johnson
2000 The Pennsylvania State University

Hi Melanie,

Good to here from you, I definitely look back on those months at Penn State with fond memories. Since completing the experience in 2000, I went on to finish my last two years of college at Xavier University of Louisiana with a B.S. in Biology. I started med-school in the fall of 2002 at the University of Southern California Keck School of Medicine and got my M.D. in 2006. Soon after this I started my residency in psychiatry at UC Davis Med Center. I am currently in my second year of the four year program. During this time period I got married and my wife and I are expecting our first child in February.

Although hands-on research has not played a major role in my career up until this point, my experience with the REU program definitely taught me the importance of bench work research in respect to future developments in applicable science.

I hope everything is going well with you too and it was good hearing from you.

Jevon J. Johnson

Joy Johnson
2005 Cornell Intel

Presently, I am a MS/PhD student at MIT in Electrical Engineering on both an MIT Presidential Fellowship and the Intel GEM PhD Fellowship. I interned at Intel for two summers in the Flash Memory Group, including speaking on behalf of Intel at the 2007 NNIN REU Convocation at UC Santa Barbara and attending the GEM National Conference 2007 in Las Vegas. I volunteer with MIT's SEED Academy working with underrepresented minorities in engineering on Saturdays. I am just doing SEED and grad school right now. I graduated from NCSU, Magna Cum Laude with degrees in Electrical and Computer Engineering in May of 2007.

That's pretty much it, Joy

Ami Kone
2003 Howard University

Hello Melanie,

This is Mimi. It is a pleasure to hear from you. I am now the process engineer in concrete manufacturing company, CEMEX. I am currently living in Ontario, CA, only 3 hours from Santa Barbara, where we had our end of internship presentation.

I hope that everything is going well with you all. I would like to thank you all, especially the Howard University group, for contributing to my professional development.

Best Regards, Mimi

Michael Krause
2002 Cornell University

Hello Melanie-Claire,

I am doing well, graduating ~4.5 years ago with my BSEE degree. I am working at a major global automotive supplier as a senior engineer in the Chicago area. I married my wife, Melissa, in early 2006 and we are expecting our first child (a girl) at the end of 2007 to the beginning of 2008. The NNUN internship was extremely helpful in preparing me for the fast pace, creative design environment I work in today.

Thank you for the learning opportunity that helped open doors. Sincerely, Michael Krause

Ken Kuehl
2005 University of Minnesota

Hello Melanie-Claire!

I hope things are going well and I hope the program is healthy and running well. It was a really good experience for me and I hope others are getting that as well!

Since I completed my internship (Summer of 2005) I have graduated, started grad school and begun a full-time job. I was between my junior and senior years and I graduated that next spring, May 06. I started a full-time job at Raytheon Co. in Tucson in August after working with a professor from the Materials Science department at the University of Arizona over the summer. I am working with a group that works with design engineers to infuse some manufacturing know-how into the development. I started my MS degree in Materials Science Engineering in the Spring '07 semester and am progressing slowly and steadily at this point. Things are going well and I am still talking with a couple of people that I met a couple of summers ago once a month or so.

Hope that's what you are looking for and I hope things are going well! Ken Kuehl

Diana Landwehr McHale
1998 Cornell University

Hi Melanie-Claire,

10 years-wow! I was an REU student in the summer of 1998, at Cornell. I worked for Prof. Craighead trying to pattern biological materials to aid in the growth of nerve cells. I continued the research during my senior year at Cornell. After graduation, I moved to Boston and coached Novice Women's Rowing at Boston College for 3 years. Then I moved to Denver, and I got my masters in Transportation Engineering from the University of Colorado. I am currently married, working as a Traffic Engineer in Denver, and we are anxiously awaiting the birth of our first child (actually my due date is today!!).

Good luck, I hope you hear from lots of us!! I was just cleaning out a filing cabinet and found all my REU stuff (which I saved of course!) and it seems soooo long ago! Denver is great, but around this time of year I am always missing Ithaca a little more!

Hope this finds you well, Diana (Landwehr) McHale

David Lavenson
2006 University of New Mexico

Life since my NNIN REU has been full of great opportunities. After completing the research program and the convocation, I headed back to Lehigh University as President of my fraternity, the Kappa Alpha Society. I attended the AIChE national student convention in November of 2006 and presented my work in the student poster contest. I secured an internship the summer after my junior year (summer of 2007) with Air Products and Chemicals, Inc. in St. Louis, Missouri. I worked in process control and quality assurance fields at the manufacturing site.

I'm now currently the Vice President of our student chapter of AIChE and Vice President of the Interfraternity Council during my senior year. I'm interviewing with companies like Merck, Exxon Mobil, and Arkema, while also considering graduate school at UCSB, U of Washington, UCLA and UCSD. I'm also doing research with my department on the Weissenberg phenomena in the blending of oil additives for automobile engines.

Since my summer in UNM, I've been able to do so much more in my life related and unrelated to my career. The experiences, friends and connections I made from the program are ones I will never forget and would like to extend many thanks to everyone in the program for their hard work.

Have a good one! DML

Juliet Lawrence
2006 Howard University

Hello there,

After the summer program, with the help of Melanie-Claire and my mentors from Howard Nanoscale Facility, my summer paper was published in the undergraduate Journal of Young Investigators (JYI). I've also been able to get a full time job within a month of my graduation from USC as a Safety Engineer Associate for the city of Los Angeles with a salary that's to die for. During my time here I've learned that there is a real need for safety regulations in the field of nanotechnology, so now I'm trying to find out what I need to do in order to get involved in the world of nano-science to protect both the pioneers that are leading this scientific research and the consumers that will eventually be benefiting from it.

Thank you NNIN REU for a wonderful summer experience and the foundation I'll use to jumpstart a career with endless possibilities.

Juliet Lawrence

Grace Lee
2003 Stanford University

Hi Melanie,

Great to hear from you! Fantastic that the program has grown tremendously. I've gain so much insight from the program and are still in touch with some of my peers from the program.

Here's a quick update on what I've been up to since the program. I got my Masters in Economics and is now working for Accenture doing management consulting work for financial institutions, as well as doing strategic analysis on sustainable practices. Although the day to day isn't pertaining to the research I did in undergrad, many of the skills I've gained are still applied on a daily basis.

Again, great to hear from you. Please give me updated on the progress. Best in your endeavors!

Smiles, Grace H. Lee

Niall Mangan
2006 University of Michigan

We are pleased to inform you that your article, "Influence of N on the electronic properties of GaAsN alloy films and heterostructures," M. Reason, Y. Jin, H.A. McKay, N. Mangan, D. Mao, R.S. Goldman, X. Bai, and C. Kurdak, has been published online today, 20 November 2007, in Journal of Applied Physics (Vol.102, Issue 10): URL: http://link.aip.org/link/?JAP/102/103710. DOI: 10.1063/1.2798629

Your article may be accessed via the issue's table of contents at this link: http://link.aip.org/link/?JAP/102/10/htmltoc

Ali Masandi-Shirazi
2003 Cornell University

Hello Melanie-Claire,

Hope all is well with you and the rest of the CNF staff. The memory of those good old days of summer 2003 is one of the most vivid in my brain. I kind of diverged from the field of nanofabrication and entered a field with more math :D.

I am a 3rd year PhD student now at ECE Dept. UC-San Diego in the field of signal processing and machine learning. The CNF REU experience helped me a lot in getting to a good graduate school and I want to thank you all.

Please convey my regards to the other CNF staff especially Rob Illic and Mike Skvarla.

Sincerely, Ali Masnadi-Shirazi

Andrew Melton
2005 Stanford University

Melanie-Claire,

Josh Symonds just forwarded me your message requesting updated information on what we've been up to since completing the NNIN REU program. Hoping that it is still not too late, here is what I've been up to:

After completing the NNIN REU program at Stanford, I was absolutely sure that I wanted to go to graduate school and pursue a career in research, so during my final undergraduate year at the University of Portland, I applied to electrical engineering Ph.D. programs at several graduate schools around the country. I am quite sure that my experience with the NNIN REU program was helpful in getting me admitted to most the schools to which I applied. I chose Georgia Tech from and started as a Ph.D. student in August 2006. I was a graduate teaching assistant for my first two semesters and am currently a graduate research assistant with a group that is focused on optoelectronic and ferromagnetic materials growth.

I found out the summer before moving to Atlanta that Josh Symonds (one of my fellow NNIN REUers at Stanford) was going to be starting graduate school at Georgia Tech at the same time as me. We've been roommates since moving here, which has worked out very well. We often reminisce about the fun we had during our REU summer, as it was a very positive experience for both of us.

~Andrew Melton

Jami Meteer Wiedemer
1999 The Pennsylvania State University

After my NNUN REU internship at Penn State in 1999, I finished my BS EE at Notre Dame. In 2000, I started an MS/PhD program in EE at Cornell, during which I worked in CNF (both old and new facilities). While at Cornell, my adviser hosted an REU intern each of two summers, and I had a chance to work with both of them. After completing my PhD in January 2005, I started working as a device engineer at Intel in Hillsboro, OR, as part of the team developing Intel's high-κ metal-gate 45 nm technology. On a personal note, my husband Matt and I were married in October 2005.

During my participation in the NNIN/NNUN REU program, I gained valuable exposure to a micro/nano-fabrication facility and a multi-disciplinary research environment. Although I had some similar experience through my undergraduate program, the REU program was good preparation for graduate school, as it provided a more realistic taste of the persistence and discipline required to survive in research.

Paul Molnar
1997 UC Santa Barbara

Melanie-Claire, I'm glad to hear the REU is still going strong! Here is my recent bio:

After graduating from Cornell with an MEng degree in '99, I have been working for Nortel as a software engineer. I have recently completed a Certificate in Software Engineering Management from the University of Texas at Austin. I have worked on various projects at Nortel including: a graphical voice prompt editor, a graphical programming environment for an Interactive Voice Response system, a streaming video server, a speaker verification system, and a Unified Messaging system. I am currently living in Holbrook, New York.

I look forward to the final product! Cheers, Paul Molnar

Josh Montague
2005 Cornell Intel

Hi Melanie,

Good to hear from the CNF again. A brief summary of what I've been up to:

I participated in the NNIN REU program the summer before my senior year at Colby, so I went back and finished my undergrad program with a degree in physics and mathematical science. I was accepted to, and deferred a year from, the graduate physics department at the University of Colorado at Boulder (where I am, now). During the year after undergrad, I taught physics at a private high school in Massachusetts (Phillips Academy - Andover). That was a great experience for me, and I can definitely see myself getting back into teaching at some point.

Now I'm a first year grad student at CU, and just trying to keep my head above water! Classes are intense, and I'm TA-ing a first year physics lab, as well. I'm still trying to find a lab group to get involved with for research in the future... it's a work in progress.

My summer at CNF definitely helped me realize how much I enjoy scientific research. I had an amazing experience working under Mike Guillorn, and I'm thinking I may get into some research here that is similar to what I did over there that summer.

That's about all from this end. Good luck with the compilation and I look forward to hearing about everyone else!

-Josh Montague

Jessica Montanez
1999 The Pennsylvania State University

Hey Melanie,

It is great to hear from you. I look at the NNUN REU internship as one of my best internships because it was the first work experience I ever had and it opened the doors for me to other exciting and rewarding internship and work opportunities as well. At NNUN REU I learned what working in a professional environment is, what research is about, how to do presentations, and many other things. I was also impressed and honored of being able to work in such a high-tech environment and with the leaders in the field of nanotechnology. In addition, this internship was a very high paying one and very well organized too. Having the opportunity to travel to Stanford University to present the results of my research was a really nice added bonus. Thanks for a great experience!

This internship allowed me to find other work opportunities at the Department of Energy Lawrence Berkeley National Lab in California, Eastman Chemical Company in Tennessee and Kraft Foods in Illinois. Having all these opportunities allowed me to discover that I wanted to work in environmental issues and thus, I currently work for the U.S. Environmental Protection Agency.

Jessica

Andrew Newton
2003 Cornell University

Hi Melanie!

I hope you are doing well. Here is my story:

After the completion of the NNUN REU program at Cornell University, I returned to Kansas State University and graduated in 2004 with a B.S. in Electrical Engineering and an emphasis in Bioengineering. I started law school in the fall of 2004 at The University of Kansas School of Law and I graduated in May 2007 with my Juris Doctor degree. Upon law school graduation I moved to San Diego, California and have recently begun my career as an Intellectual Property (IP) attorney with the law firm of Fish & Richardson P.C. My practice specialties include Patent Prosecution and IP litigation. My education and REU experience provided me with an amazing and unique background which helped me obtain a job at the largest IP law firm in the world.

Thank you for your time and I hope you have a great day!

Andrew Newton

Que Anh Nguyen
2005 Stanford University

Ms Mallison -

I attended NNIN in the summer of 2005 at Stanford University. There I worked with Professor Bruce Clemens in the Materials Science and Engineering Department.

Now I am just across the bay at UC Berkeley, where I am a Chancellor's Fellows and NSF Graduate Research Fellows. I am about halfway through the 2nd year of my PhD program. My research in the MSE department involves metal-oxide nanostructures for applications in electrochemical devices, like dye sensitized solar cells and Li-ion batteries.

NNIN was a great learning opportunity for me. I really enjoyed the research I did at Stanford and became sure that I wanted to attend graduate school after finishing my BS. And so far, graduate school has been great. There are definitely ups and downs, but overall I am very happy with what I am doing.

I hope that all is well for you and a happy 10th to NNIN !

Emily Norvell
2006 UC Santa Barbara

Since my internship at UCSB during the summer of 2006, I am still in school working towards my undergraduate degree in Materials Engineering with a minor in Environmental Studies at Cal Poly, San Luis Obispo. This past summer I worked as an intern at Lockheed Martin in order to contrast working at a company with doing research at a university. I also attended a leadership program on sustainability in Slovakia for 18 days. I'm still not entirely sure if I want to go to grad school but I'm definitely interested and I was really inspired by the research I

did at UCSB regarding new solar cell technology. The experience gave me a base on the topic of solar cells with which I've become very interested in and have been looking into for career/research opportunities. I also appreciated the exposure to the grad student lifestyle of having direct control of what you're working on and think it is a life that I could live.

Emily Norvell

Virginia Noxon
2005 Howard University

Hey Melanie!

I have done a lot since my first REU with NNIN in 2005. I am now a senior at Emory and Henry and my past two summers, 2006, 2007, have been full of fun and adventure. I did another REU at the University of South Alabama on proteins in breast cancer for the 2006 summer. This past summer I went abroad to Ireland and Italy for 6 weeks. Major fun over there, which included seeing The Who in Cork. Other than those summers, I have been working at my classes and I am now getting ready to apply to graduate school to get a PhD in a field of biology. I hope this helps.

Take care, Virginia Noxon

Nate Olds
2004 Georgia Tech

Hi Ms. Mallison,

Since graduation a year ago I've been able to get two job offers, and am currently working on my 3rd. I'll never forget one interview where I was asked to prepare a presentation. I immediately thought it strange, but remembered my experience as a NNIN REU. I found my research presentation from that summer, dusted it off, and used it for the interview. It came in rather handy even for an interview!

Regards, Nate

Vaidehee Padgaonkar
2004 Cornell University

Hi Melanie,

How are you doing? Here is my update for the book:

Since my summer as an NNIN REU (summer 2004), I graduated from University of Michigan, Ann Arbor, with a Bachelors in Electrical Engineering. Shortly after graduation, I moved to Oregon to work for Intel Corp. as a Product Development Engineer. My team provides hardware and software support for speedpath debug.

Although I didn't pursue research, NNIN did give me exposure to a state-of-the-art clean room and a great fabrication experience! I learned a lot and I feel the exposure to fabrication is something every Electrical Engineer should have. At Intel, there are many stages a processor goes through before it gets sold to the customers (i.e. Dell, Apple, etc.). Although I don't work in the clean room at Intel, the NNIN experience gives me insight to that portion of the product life cycle just before it comes to our debug lab.

On a separate note -- the research project I was working on while at Cornell was in Professor Michael Lipson's group under the guidance of a post-doc Sameer Pradhan. He and his wife also works for Intel in Oregon now, and I meet up with them from time to time. Small world, huh?! When I first moved to Oregon from Michigan, they were the only people I knew! So NNIN and my particular project also helped me in this way when I started my job at Intel. =)

I am doing great out here. Oregon is a very outdoorsy place - I have had a chance to enjoy white water rafting, snowboarding, and the many hiking trails they have around here.

Hope everything is well with you!

Take care, Vaidehee

Chris Pontius
2002 The Pennsylvania State University

Thanks for the inquest! Nothing special but here you go:

I participated in the NNUN REU program the summer of 2002 under Dr. Pantano at Penn State. I completed my bachelor's degree in biotechnology at the Rochester Institute of Technology, Rochester NY, in 2005. After graduation I took a worked for Wyeth Pharmaceuticals, Rouses Point NY, for 2 years as an LC Chemist.

With the announcement that the facility would be closing Dec 2009, I found new employment with a contract pharmaceutical manufacturer in Norwich, NY. I perform quality assurance testing on a variety of finished drugs and active components. I also help write and validate the methods used to test these products. My experience at Penn State opened my eyes to the instrumentation side of science. I had intended to go to graduate school for molecular microbiology but I've now discovered the lucrative business of analytical separations. Thanks REU!!!

Sincerely, Christopher Pontius

Diego Rey
2002 Cornell University

Since my REU experience at Cornell I've made the long journey ... back to Cornell ... and I'm still here! After getting my BS in Electrical Engineering from the University of California at Santa Barbara I embarked on a quest for a PhD in Biomedical Engineering. Cornell officially started its BME department the same year that I graduated from UCSB and with the great

reputation for interdisciplinary work that I had experienced as an REU I decided to come back.

I joined Professor Carl Batt's laboratory where I develop and use nanoparticles for cancer imaging and therapies. In addition, through taking advantage of the entrepreneurial resources at the Cornell Johnson School of Management, I'm in the process of starting diagnostics company, Bold Diagnostics. The plan is to continue with the company full time after Cornell.

How did the REU experience get me here? Through working with graduate students I got a glimpse into the social and professional life in grad school. Experiencing the research environment at Cornell was the deciding factor in my decision to join. I also met Carl Batt through my REU experience. All in all, I really wouldn't be here if it weren't for the REU program.

Can't wait to see the BFTP! Diego

Leila Joy Roberson
2006 Cornell University

Hello Lynn,

Sorry for the late response. Hope things are going well for you and the rest of the CNF staff members.

This summer I am working in a lab at Texas A&M University in the Department of Biochemistry and Biophysics. I will be graduating in December of this year, and I will be looking for a job. If you hear of anything (e.g., through Intel), or if you guys are hiring at Cornell (?), please let me know! Please tell Melanie-Claire I said hello.

Regards, Leila Joy Roberson

Anthony Sanders
2006 Stanford University

Hey!

Forgive me if this isn't the most formal email that I've ever written, but I just graduated and I'm pretty excited! How's everything going? I debated on whether I would go to grad school immediately, or work first and then go. I applied to seven different companys and three different Graduate schools. I've been blessed to land a job in New Mexico with Sandia National Labs. I've been hired into their OYOC program. For a two year commitment, they will pay for my Master's Degree, and they will also pay me to go to graduate school. I'll be attending Texas A&M University in the fall in the Solid State and Nano-Engineering Department.

I just wanted to thank you guys for everything! Every job that I interviewed with took a look at my resume, saw Stanford, and I could tell they pretty much made up their mind to hire me right then. I received offers from every company that I applied to, so again, I just wanted to say thank you!

On another note, I hear that two of my friends were accepted into the 2007 program. I think that's great, and they are excellent students! I know that they are excited because they asked me at least 10 questions a day! Of course I told them exactly what they needed to succeed....Cheesecake Factory on Thursdays! Thanks again, and take good care of my fellow panthers for me.

Sincerely, Anthony Sanders

Yaniv Scherson
2005 UC Santa Barbara

Hi!

I'm a first year graduate student in Mechanical Engineering at Stanford University. REU helped me gain research skills, experience, and a great recommendation while also solidifying my choice to go to graduate school for a PhD. I am doing great and loving graduate school!

David Schluneker
2006 Georgia Tech

Ms. Mallison,

Here's my update. Hope you're getting a bunch!

The biggest effect my NNIN summer had was to make me want to do more research. It really shifted my focus from industry internships and job hunting to trying to find more research opportunities and graduate school.

Currently, I am in my senior year of college. When I came in as a college freshman I had no thought of going to graduate school. However, my experience in the NNIN REU program really opened my eyes. It helped me learn a great deal more about graduate school. Based on the new information, I began to realize that graduate school appeared to be the more fitting path for my interests. Right now I'm working on graduate school admissions papers trying to find the right school instead of going through the job search.

Overall, the NNIN program helped me in a number of ways. The experience was priceless. I can't count the times interviewers and hiring managers have asked me to elaborate on this experience. In fact, I will be re-presenting the material worked with at an on-site interview in the next week.

Dave Schluneker

Neel Shah
2005 Stanford University

Hello Melanie,

Below is a short paragraph of my recent mischief. Enjoy!

I have graduated from Harvey Mudd College with a B.S. in Engineering. I received Departmental Honors and High

Distinction awards during graduation. Currently I am working at Medtronic Diabetes in Northridge, CA. I design electronic wireless systems for insulin pumps. In a couple of years I plan to obtain a Masters either in Medical Devices or Electronics Communication. The REU at Stanford University University was the doorway to my shift from an aerospace engineering career to a medical engineering career. Working with Dr. Griffin was my first taste of engineering with biological systems. It was also my first hands-on experience with the emerging field of nanotechnology and sparked an interest in the field that remains very much alive to this day.

Shahid Shaikh
2004 Harvard University

I just graduated from UCSB this past June. I did apply to graduate schools and got into one (WPI) for my PhD in Chemical Engineering. However, they didn't offer me any money, so I deferred the decision for a year, and will apply for some type of assistanceship or researchship for Fall 07. I'm also going to apply to more schools for Fall 07 in Environmental engineering in California and try to specialize in water.

Why Environmental engineering? Well, now I'm working with the Alameda County Water District as a Water Quality/ Operations Intern for up to a year, and they said that if I attend Cal or Stanford, they'll pay for me. So, I'm going to give that a shot and apply to those schools, as well as some others. Anyways, that's about it for me over here. Hope to hear from you soon.

Regards, Shahid

Jason Slinker
2000 Cornell University

Hi Melanie,

Actually, my REU experience at Cornell has had a tremendous influence on my subsequent graduate and postdoctoral research experiences. First of all, I had such a good time working for my REU PI, Professor George Malliaras, that I ultimately came to work for him as a graduate student at Cornell. It helped, of course, that the CNF staff helped me complete a successful project so that George would want me back. The REU program put me a step ahead--it looks great on the resume, the research connection directly paid off, and the skills carried over to my graduate research. We were able to complete about 4 or 5 projects involving significant nanofabrication over the course of my Ph.D on organic light-emitting devices.

Now I am working as a postdoctoral scholar with Professor Jackie Barton at Caltech. My project leans even more heavily on nanofabrication as I am making miniaturized devices for multiplexed protein analysis. My previous nanofabrication experience has enabled me to make a fast transition to a completely new area of research and make devices with a high degree of independence. OK, that's it for me.

It ends up that Keith (MCM notes: Keith Slinker, 1998 CNF REU, and Jason's brother) is now working at Lockheed Martin in Dallas, TX, largely due to his knowledge and expertise with electron beam lithography. Think the Cornell REU had anything to do with that? I'll try to bug him for you. My pleasure to help. Thanks Melanie.

Enjoy, Jason

Cary Smith
2006 Cornell Intel

You know I always come to see you when I visit. I'm sure you'll be around next time….

This summer I am an REU at Carnegie Mellon. I see Erica every now and then when I'm here. Mack is not that far away from me either—he's in Philadelphia on an internship as well. I was in Taiwan for the month of May learning Chinese. Jon and Nate are in China for the remainder of the summer doing the same. Everyone else, I have no idea where or what they are doing. ;-) We'll tell all of your students that the CNF's 29th year was better. lol

I have been filling out graduate school applications over the past few months. A little about what I am doing in my career. I am doing research with my department working with nano-materials here at Jackson State University. I am applying to graduate school and will be pursuing a Masters in Industrial Engineering and a MBA. I am strongly awaiting graduation in May 2008 where I will receive a BA in Physics with a minor in Management. I hope everything is well, and hope to see you soon.

Your favorite REU student, Cary Smith

Wafa Soofi
2005 Georgia Tech

Hi Jennifer!!

Thank you so very very much for taking care of recommendation letters for me! Now that all of my decisions finally came in, I need to tell you all about my plans! I've decided to accept an internship in the Summer Undergraduate Clinical Research Program at the UT Health Science Center and M.D. Anderson Cancer Center. Both are located in the Texas Medical Center, right across the street from Rice University. It's actually a joint program with Rice, so I'll be getting course credit for my work this summer. It's a very multifaceted program - there's an anatomy class we take, plus a lab where it looks like we'll actually be dissecting real human cadavers, which should be very interesting. Then there are the clinical rotations - I'll be shadowing doctors in pediatrics, OR, ER, OB/GYN, internal medicine, and a few other fields.

Finally (what I'm most excited about), there's the clinical research. I've been assigned to work in the department of radiation physics. I don't know much about my project yet, but I do know it involves improving tumor-targeting techniques in cancer radiation treatment by relying on implanted landmarks,

rather than external ones. Anyway, it sounds really exciting, and I can't wait to get started. And it'll be in Houston, and I'll have a car, so I'll have the freedom to pop home whenever I want, as well as do all sorts of fun Houston-y things while I'm here. So: Thank you thank you thank you for the letters! I couldn't have done it without you ;)

So, after some very careful thought, I've decided I want to go into medicine after graduating from Rice.

Thanks very much, and have a wonderful day!!!

Wafa

P.S. How is the MiRC gang doing? Hope it's not too hot yet!

Chris Stoafer
2006 UC Santa Barbara

Hi Melanie-Claire,

Here is my current life description: After experiencing the internship with NNIN in the summer of 2006, I returned to school at, Cal Poly, San Luis Obispo, and participated in an internship with Lawrence Livermore National Laboratories. In this internship I conducted research in plasma and beam physics. I am now finishing up my undergraduate career and applying to graduate school. I plan to attend graduate school in either plasma, nuclear, or particle physics. I am also looking into studying and research the physics of quantum computing at graduate school. My experience with the NNIN internship seem to be crucial in my applications for graduate school. These graduate school plans are to commence in the Fall of 2008. I eventually plan to use my experience in a research and development career in industry or with a national lab.

Hope everything is going well and hope you correct me for any grammar or other mistakes in my paragraph. Thanks again.

-Chris Stoafer

Alexander Stolyarov
2004 Harvard University

Alexander (Sasha) Stolyarov (REU04) is at Harvard University Engineering and Applied Sciences in the 2nd year of a PhD program in applied physics.

Jon Swaim
2006 Cornell University

Hey Mel,

I'm great! I graduate in one month and then I'm off to China for 3 months to teach English. It doesn't look like I'll be coming to Cornell next year for grad school, but I was accepted into Imperial College London, so that's cool. Jon

Ethan Swint
1999 Cornell University

It's good to hear from you! Say hello to Garry Bordonaro and Mike Skvarla for me. I'm now working on an ECE PhD at Virginia Tech in Switched Reluctance Machines, which I should finish up. I earned an BSME from the University of Texas at Austin in robotics before that, and I married the girl I met in '99 during my REU there. Going into the program I was quite interested in MEMS, but even though I enjoyed my work there, the summer helped me realize that I prefer to spend a bit more time in the daylight and not in the clean room. The short courses we attended there, e.g. Rathbun's vacuum technology course, have also come in handy during my academic and professional endeavors.

Thanks for the memories!

-Ethan

Josh Symonds
2005 Stanford University

I was hesitant to reply to your email when I got it, since I had yet to take a qualifying exam and I felt my future was too uncertain to commit to a book, lest I jinx it! But I finally have notification that I've passed them all, so I can finally divulge my status.

Anyway! I'm doing a Ph.D. program in physics at Georgia Tech, working with a group in the chemistry department. The NNIN REU played a big part in helping me determine what I liked about academia and how I wanted to continue my work in graduate school. Of course, I'm sure it made the admissions process easier, and I'm quite glad it went smoothly!

Incidentally, one of my roommates since coming to Tech in August '06 has been a fellow NNIN REU student that I lived with in Stanford. He happened to enroll in a different Ph.D. program here, and was the only person I knew in Atlanta! It has worked out wonderfully, life is good.

Thanks! Josh Symonds

Dane Taylor
2006 University of Washington

Dear Melanie-Claire Mallison,

I am Ashutosh Shastry, the Research Associate with Karl Bohringer at University of Washington, Seattle who had mentored Dane Taylor for the NNIN Summer REU program of 2006. You'd be pleased to know that our work has been accepted at Transducers 2007 and we are also writing a journal paper.

Thank you very much for sparing the time and thought.

Sincerely, Ashutosh Shastry, Ph.D.

Abbie Tippie
2005 Harvard University

Abbie Tippie (REU05) is in a Phd Program in Optics at the University of Rochester.

Paul Vallett
2004 University of New Mexico

Hello! Wow, that certainly was a long time ago...

Since the summer of 2004 at UNM, I finished my chemistry degree at the University of Vermont. I completed research with Professor Dan Savin over the next two years on synthesizing and characterizing block copolymers for use in biological systems. I also spent the summer of 2006 and 2007 working at the National Renewable Energy Laboratory in Golden Colorado with John Turner, working on systems to use solar energy to split water and make hydrogen. Those research projects have been extremely interesting and hopefully should be published soon.

I applied to graduate schools in the fall of 2006 and was accepted to Berkeley, Stanford, and UC Boulder's Physical Chemistry departments. I decided to pursue my doctorate degree at UC Boulder, primarily so I could continue research at the Renewable Energy lab.

In the spring of 2007 I decided to defer attending graduate school for a year to do something different and spent some more time in Vermont. I ended up being a chemistry teacher at a private high school called the Vermont Commons School. I'm enjoying teaching and will continue to teach in various forms until the springtime when I will move back out to Colorado. I am looking forward to getting back to doing research at school, however, and I am glad for the opportunity that the NNIN REU gave me to jump start my career doing research!

Hope all is well! - PV

Ken Vampola
2002 Cornell University

It was nice to see you at the convocation. It was an interesting experience to see the whole REU from the other side as a mentor. (This summer, I mentored Jonathan Aguilar.)

I am in the Ph.D. program at UC Santa Barbara. I am working to make ultraviolet LEDs brighter and more efficient. I do a considerable amount of process design and development. These are skills that I learned and developed during my summer at Cornell. Outside of school, I am involved in a number of extracurriculars, including the UCSB triathlon team.

-Ken

Josef Velten
2006 University of New Mexico

Hello,

I'm now doing graduate work at UT Dallas's Alan MacDermit Nanotechnology Institute, studying dye sensitized solar cells, working on my way to a PhD. I could reasonably say that the internship that I took through NNIN made me seriously look at a career in nanotechnology research, considering it is what I am doing now. Not sure what else to add here. The internship was probably the most enjoyable summer I had during my time as an undergrad.

Brandon Walker
2005 Cornell Intel

Hello MCM,

How are you doing? I am doing great. I am in my second your of graduate school at the University of Iowa, Department of Chemistry (Ph.D program). I am a GAANN fellow. I work for Dr. Amanda Haes and my research focus entails the use of nanoparticle technology in combination with molecular beacon systems for improved pathogen detection. There is a lot more to say about it but I am very short for time. I have just completed my departmental seminar and I am eager to start the comps. procedure in the spring.

Regards, Brandon M. Walker

David Welch
2005 The Pennsylvania State University

I'm doing as well as any graduate student can. I am in the first year of a PhD program in Bioengineering at Arizona State U. I successfully completed my undergraduate degree at Tulane University even though Katrina did her best to prevent it.

The NNIN program was the start to my research career and likely helped me land an REU the following summer at the University of Minnesota. Thanks for the experience.

-David Welch

Daron Westly
1999 Cornell University

Daron graduated from the University of South Florida and then joined the staff of the Cornell NanoScale Facility in 2001. He is now one of the CNF's Electron Beam Lithography Engineers.

Claude Wu
2006 Georgia Tech

Dear Jennifer,

How are you? How was the NNIN REU internship this year?

I have graduated from UCLA recently with a bachelor degree in electrical engineering. A picture from my commencement is attached. As of now, I am in a training program for Bible truth and church services. It is a full-time program with strict regulation and schedule. Still, I plan to continue to study at a grad school after the training.

I sure miss you and the other interns and the time we spent together at Georgia Tech. I am sure you also had a good time with the REU interns this year. Hope that in the future we will have chance to have a reunion.

Keep in touch, Claude Wu

Allen Yang
2004 Cornell University

Melanie,

I did my REU program at Cornell University in the summer after my junior year of undergrad. I made a lot of friends that summer along with doing interesting research.

I am now currently a third-year chemical engineering graduate student at Cornell working in the lab of David Erickson. My research interests lie in the development and study of optofluidic transport, which is a chip-based system for moving small objects using guided optical energy. I still do my fabrication work in the CNF, which is continually changing and improving itself.

The REU was instrumental in my post-undergrad career decisions. The research experience in developing nanotechnology opened me to a world of cutting edge research I had not known about previously. I still talk to my program PI and we converse about many things, including his lab's ongoing research. When the first opportunity arose, I became a mentor for the same REU program in which I participated, and that was a very rewarding experience. The REU program was great for me, and thanks to Melanie for allowing me to help contribute to it and make it better.

Kaylie Young
2006 University of Washington

Ms. Mallison,

After participating in the NNIN program at the University of Washington during the summer of 2006, I have continued to conduct research in the field of nanotechnology. Currently I am a senior at Brown University working on my thesis project which involves functionalizing magnetic magnetite (Fe_3O_4) nanoparticles with functional molecules such as chemotherapy drugs. I am working on developing a new, inexpensive linker chemistry that (i) allows monodisperse Fe_3O_4 nanoparticles, originally synthesized in organic solvent, to be water soluble and (ii) allows for the attachment of functional molecules to these particles for drug delivery, bio-imaging, bio-separation, enhanced MRI contrast, etc.

My experience with the NNIN program was one of the best academic experiences I have had in college. I was able to network with professors who are very well known in the nano field, which is extremely helpful when it comes to applying for graduate programs, and meet some of my future colleagues. Additionally, my work from the summer of 2006 was published in the online undergraduate journal JYI (Journal of Young Investigators). I am currently applying to graduate programs in chemistry.

Thank you for doing this Ms. Mallison! It will be very interesting to see what everyone is up to. I am applying to work with my NNIN advisor (Younan Xia who is now at Washington University in St. Louis) for grad school and am also considering Cornell's program.

Thanks! Kaylie Young :)

PS: I wanted to share with you a recent achievement of mine which has led to an article on the Brown homepage. http://www.chem.brown.edu/undergraduate/kyoung.html

Yu Jennifer Zhao
2003 Stanford University

Hi Melanie,

I participated in the NNUN REU back in 2003 at Stanford, and I graduated from Cornell's Material Science Engineering in 2005. I've been working at GE's Global Research Center in the Edison Engineering Development program for the past 2.5 years. I've worked on exciting technologies such as MEMS, photovoltaics, and fiber optic sensors. The REU program was definite an eye opener for me. I got to experience laboratory research first hand and worked with world class scientists, plus it was so much fun! Thank you for the great opportunity. I recommend the program for all undergrads interested in research!

Jennifer Zhao

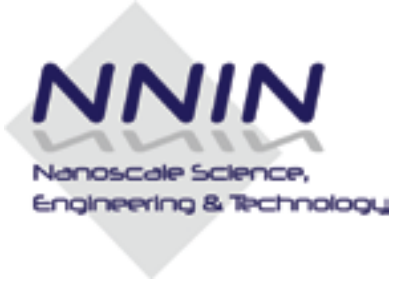

2007 NNIN REU Research Accomplishments

Fluorescence Enhancement of CdSe Quantum Dots with Au Nanocrystals

Melissa Aillaud

Bioengineering, University of California San Diego

NNIN REU Site: Nanoscience at the University of New Mexico
NNIN REU Principal Investigator: Ravi Jain, Electrical and Computer Engineering, Center for High Technology Materials, University of New Mexico
NNIN REU Mentor: Li Wang, Electrical Engineering, Center for High Technology Materials, University of New Mexico
Contact: maillaud@ucsd.edu, jain@unm.edu, liwang@unm.edu

Abstract

Linear and nonlinear fluorescence were studied in cadmium selenium quantum dots (CdSe QDs) with gold nanocrystals (Au NCs). Linear photoluminescence measurements in CdSe QDs and Au NCs mixed solutions (1:1 and 5:1 mixing ratio by weight) showed significant fluorescence-intensity quenching effect, compared to a QDs-only sample. Another set of thin film samples gave over 3 times of enhancement in the nonlinear florescence measurement.

Introduction

Semiconductor QDs are nanoparticles with unique optical properties. Those properties, like large two-photon absorption coefficient, narrow emission and broad absorption spectra, and size-tunable fluorescence, have made them good substitutes for dyes that are typically used as fluorescent tags in biological applications. To understand and improve the QDs' efficiency in such applications, surface plasmon enhanced fluorescence was studied. The optical properties of small metal particles have been an attractive field of study for years, since they interact with incident light strongly and change the optical properties significantly. Such extraordinary properties can be explained by the excitation of coherent free electron oscillations, or surface plasmon polaritons. As a result of the high polarizability induced by such modes, a strong electrical field develops about the nanocrystals surface. This locally-enhanced electromagnetic field can be helpful to achieve enhanced fluorescence.

Materials and Experimental Design

We investigated the changes in fluorescence intensity for two sets of thin film samples. The first set is composed of a monolayer of 5-nm-diameter CdSe QDs, a monolayer of 4.5 nm Au NCs and a separating section consisting of 4, 5, 14, 16 and 18 layers of polymethyl methacrylate (PMMA) to control the distance between the monolayers of QDs and NCs. The second set consists of a monolayer of 4.3 nm in diameter CdSe quantum rods (QRs) and the same monolayer of Au NCs. This set was assembled in a similar way as the first set, but using varying layers of amorphous silicon dioxide (SiO_2) to separate the QRs and gold monolayers. The setup of the linear fluorescence measurement is shown schematically in Figure 1. An argon laser was used to excite the sample, and the fluorescence was collected by two lenses and sent to a monochromator.

A photon-multiplier tube (PMT) and a lock-in amplifier were used to increase the sensitivity and signal-to-noise ratio of the setup. The nonlinear fluorescence measurement was done in a similar way except that: a mode-locked Ti-sapphire laser (wavelength ~ 800 nm, pulse width ~ 200 fs, repetition rate ~ 76 MHz and peak power > 10 kW) was used instead of the argon laser. Also to eliminate the loss introduced by the monochromator, we collected the fluorescence directly with a PMT.

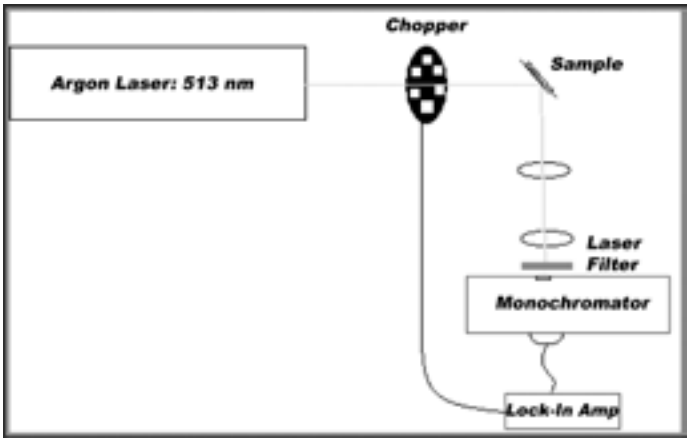

Figure 1: Schematic of linear experimental setup.

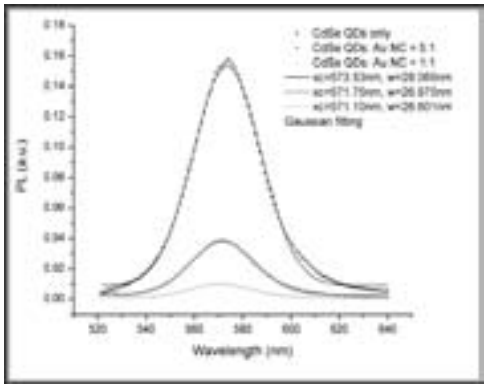

Figure 2: Photoluminescence intensities for samples in solution: Linear Experiment.

Results and Discussion

In the beginning, linear fluorescence measurements were done with QD/Au solutions mixed at different ratios: samples with QDs only, and QD/Au mixed at 1:1 and 5:1 ratios were compared. The results are shown in Figure 2. The QDs-only sample showed the strongest fluorescence, and the more Au NCs in the other two samples, the less fluorescence they gave. From the curve-fitting, we were not able to distinguish any significant center wave-length or full-width-at-half-maximum changes for all three samples tested. Although it seems to be quenching with more gold in the solution, the results are inconclusive since there are too many uncertainties, like re-absorption of fluorescence by Au NCs and uncontrollable spacing between QDs and NCs.

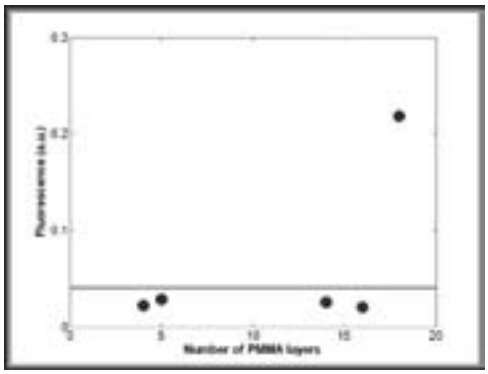

Figure 3: Average photoluminescence intensities for thin-film samples with PMMA: Linear Experiment.

Having this in mind, we obtained the QD/Au thin film samples which had the nanoparticles separated at "specific" distances using PMMA layering in between them. This batch of samples consisted of thin films with QDs only, and QDs and gold NCs separated with 4, 5, 14, 16 and 18 PMMA layers. We noted, though, that the samples had visible surface unevenness, which is why, during the linear and nonlinear experiments, we decided to scan through the sample with the laser and obtain an average of the intensities. For the QD/Au thin film samples with PMMA layering, Figure 3 shows the average of the fluorescence intensities for varying PMMA layers in the linear experiment. The red line represents the average intensity for the QDs-only sample. From the intensity plots generated with the fluorescence data obtained, there is no significant fluorescence quenching or enhancement in these samples.

The 18-layer PMMA sample seems to be totally different from others, and we believe that there might have been some mistakes during fabrication (possibly the PMMA layers folding upon themselves). Figure 4 shows the data obtained for the nonlinear fluorescence experiments on the same samples with PMMA layering. Without considering the 18-layered sample, over 3-fold of fluorescence enhancement has been observed in the 4-layered sample compared with the CdSe QDs only sample (red line). Furthermore, the optimum spacing seems to be smaller than 4-layered thickness. To further investigate the optimum spacing between the CdSe QDs and Au NCs, thinner and more precisely controlled layers are needed.

The final set of samples consisted of QR/Au thin films fabricated more precisely with SiO_2 layering to separate the nanoparticles from each other. The surface of the samples was much more even than the previous set of samples; unfortunately, we could not perform the planned experiments because of laser malfunction.

Conclusions and Future Work

We have shown that over 3-fold of nonlinear fluorescence enhancement in CdSe QDs monolayer with Au NCs can be obtained. Future work will be done with the last set of samples when the laser is available, but similar results are expected for the nonlinear experiments. Once this is done, we will be able to calculate the optimal distance between the nanoparticles and fabricate the QD/NC particles so that they can be used in biological applications.

Acknowledgements

I would like to acknowledge and give special thanks to Prof. Ravi Jain and Li Wang. Also, thanks to our collaborators in Prof. Brinker's lab; Robert Bradley and Shisheng Xiong. Special thanks to the National Nanotechnology Infrastructure Network Research Experience for Undergraduates Program and National Science Foundation for funding my participation in this project. Muchas gracias a mi familia.

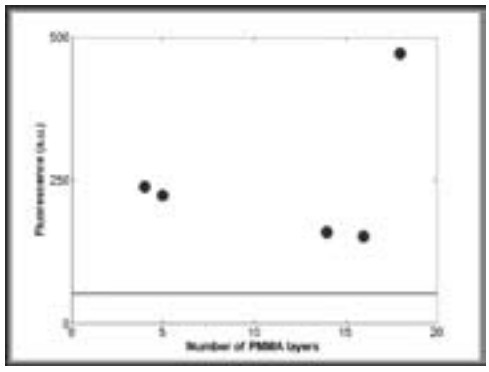

Figure 4: Average photoluminescence intensities for thin-film samples with PMMA: Non-linear Experiment.

Manipulation of Iron Nanoparticles and Their Effects on Human Colon Carcinoma Cells

Ebony Ayres

Pharmacy Practice/Pharmaceutical Sciences, Hampton University

NNIN REU Site: Howard Nanoscale Science and Engineering Facility (HNF), Howard University
NNIN REU Principal Investigators: Dr. Gary L. Harris and Dr. Winston Anderson, HNF, Howard University
NNIN REU Mentor: Nefertiti Patrick-Boardley, Applied Physics, University of Michigan
Contact: ebony.ayres@pipeline.hamptonu.edu, gharris@msrce.howard.edu

Abstract

Magnetic nanoparticles (MNPs) were synthesized to evaluate the influence of various polymer coatings on particle size, zeta potential, and cellular uptake. Stock solutions of gum arabic (GA), chitosan, and polyethylenimine (PEI) at 2% by weight were added to the MNP solutions. The particle size was obtained with the vibrating sample magnetometer and Malvern Zetasizer. The coated particles were on average approximately 100 nm. The zeta potential of the particles was acquired with the Malvern Zetasizer. Results revealed a negative surface charge for each of the coatings at low concentrations. Increased amounts of PEI demonstrated the ability to alter the surface charge from negative to positive. The live/dead (LD) assay showed that PEI coated particles demonstrated toxic effects with a LD 50 ≈ 100 μg iron/millions cells. In contrast, GA and chitosan-coated MNPs were the least toxic to the human colon carcinoma cells (HCT-166) with a LD 50 > 1000 μg iron/millions cells. Being non-toxic is important because it relates the biocompatibility of the nanoparticles with the body system.

Introduction

Colon cancer is one of the most prevalent and fatal types of carcinoma disease [1]. There are several studies dedicated to optimizing cancer therapy through the use of nanotechnology applications [2]. Magnetic field hyperthermia (MFH) makes use of MNPs, such as magnetite. When coated in glycomolecules, like GA and chitosan, a crab shell derivative, it is thought that MNPs are more likely to be taken up by cancer cells than by healthy cells because cancer cells require more energy to proliferate. Also, because cancer cells are negatively charged, it's interesting to note whether surface charge affects particle uptake across the cell membrane's phospholipid bilayer. With an accumulation of MNPs in or around cancerous cells, an alternating magnetic field (AMF) causes hysteresis heating. Hysteresis heating around 42º-45ºC leads to the apoptosis of cancerous cells while leaving healthy cells unharmed [3].

However, MFH is most effective if the MNPs are at an optimal size, concentration, adhesiveness, and strength. The goals of this experiment were to manipulate the physical and chemical surface properties of magnetic nanoparticles (MNPs) by coating them with polymer and to evaluate how these polymers influence surface charge. Additionally, we sought to determine the cell viability when exposed to polymer-coated MNPs.

Methods/Materials

The MNPs were synthesized via wet chemistry techniques. A 2:1 molar solution of iron (III) chloride and ferrous chloride was added to 20 mL of deionized water. An alkaline solution was prepared by adding 15 mL of reagent NH_4OH to 65 mL of deionized water. The latter solution was stirred for approximately 5 minutes on a magnetic stir plate. The Fe^{2+}, Fe^{3+} solution was added drop-wise to the alkaline solution. It is believed that pouring the iron solution into the alkaline solution would result in smaller particles; however a slower reaction rate correlates with more uniform particles. The MNP solution was stirred for 1 hour and washed via centrifugation. The MNPs were redispersed with deionized water via ultrasonication. This process was repeated about six times or until the pH of the suspension was comparable to that of the deionized water. The polymer-coated MNPs were synthesized via the same method with the addition of 2% polymer solution after ultrasonication.

Overall, four types of MNPs were used: naked, chitosan-coated, GA-coated, and PEI-coated. The Malvern Zetasizer was used to measure size and zeta potential. Size measurements were verified via magnetic susceptibility analysis. A live/dead cell assay was performed with each particle type at concentrations from 31-8000 μg iron/million cells.

Results and Discussion

Size analysis via vibrating sample magnetometer and dynamic light scattering (Malvern Zetasizer) showed that the naked particles were 3.84-60.4 nm. The smaller sizes represent primary particles, and the larger sizes represent agglomerates. The coated particles were about 100 nm. Zeta potential results, which correlate with electrophoretic mobility, showed that the nutrient medium for cells (DMEM) in which the particles were suspended for testing rendered all the particles negatively charged. PEI had

the strongest negative charge at -6.9 mV. It was interesting to note that PEI and chitosan-coated MNP's exhibited a negative charge in DMEM even though PEI and chitosan are cationic polymers. The live/dead cell assay showed that the LD 50 results for GA, chitosan, and PEI were 6700, 1450, and 106 μg iron/ millions cells, respectively (see Figure 1).

The particle size retrieved via the two size analysis techniques gave size measurements which were consistent with predicted and literature results. The MNPs were tested in DMEM solution to more accurately simulate the body system. In this solution, all the coatings, even those which are typically positively charged, rendered a negative surface charge. The PEI coated MNPs were very toxic to the cells at higher concentrations, which could cause rejection if used in the human body. Although chitosan particles were promising in relation to their biocompatibility, GA best reflected the live/dead cell assay results of particles with no coatings.

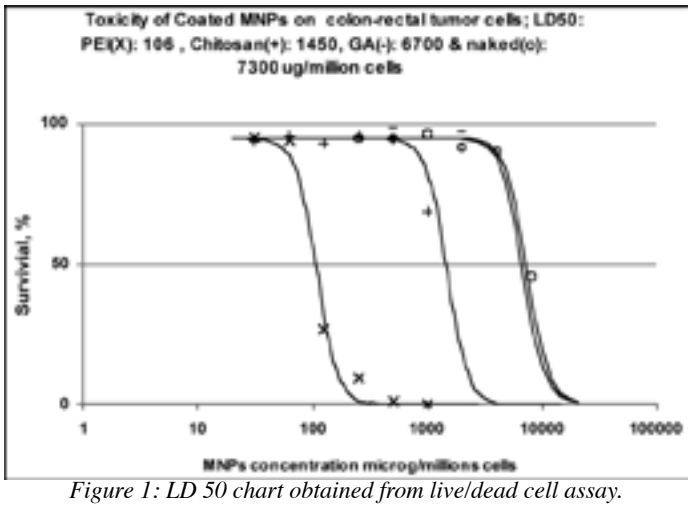

Figure 1: LD 50 chart obtained from live/dead cell assay.

Summary

Polymer-coated MNPs imparted an overall negative charge. The live/dead cell assay showed that overall GA was the least toxic to the colon carcinoma cells meaning that it would be the most biocompatible. Further studies need to be done to identify and optimize surface coatings that could render a positive surface charge. Additionally, particle uptake of the coated MNPs needs to be observed via TEM imaging.

Acknowledgments

I would like to thank my PIs, Dr. Gary L. Harris and Dr. Winston Anderson, my mentor, Nefertiti Patrick-Boardley, Dr. Otto C. Wilson, Dr. Patrick Mehl, HNF staff, National Nanotechnology Infrastructure Network REU Program, and the National Science Foundation for their efforts and support.

References

[1] National Cancer Institute. Colon and Rectal Cancer Homepage. <www.cancer.gov/cancertopics/types/colon-and-rectal>.

[2] Cuenca A., Jiang H., et al. Emerging Implications of Nanotechnology on Cancer Diagnostics and Therapeutics. Wiley Interscience 2006: 459.

[3] Ivkov R., DeNardo S., et al. Application of High Amplitude Alternating Magnetic Fields for Heat Induction of Nanoparticles Localized in Cancer. Clin Cancer Res 2005; 11 (19 Supply): 7093s.

Fabrication of Multifunctional Atomic Force Microscopy-Scanning Electrochemical Microscopy Probe Arrays

Brian Bolz

Electrical Engineering, Manhattan College

NNIN REU Site: Microelectronics Research Laboratory, Georgia Institute of Technology
NNIN REU Principal Investigators: Dr. Christine Kranz and Dr. Boris Mizaikoff, Chemistry and Biochemistry, Georgia Institute of Technology
NNIN REU Mentor: Dr. Heungjoo Shin, Chemistry and Biochemistry, Georgia Institute of Technology
Contact: bbolz.student@manhattan.edu, christine.kranz@chemistry.gatech.edu, gt7018b@mail.gatech.edu

Abstract/Introduction

Combined atomic force scanning electrochemical microscopy (AFM-SECM) probes integrated with micro/nano-electrodes enable simultaneous collection of electrochemical information along with high resolution topological imaging [1-3]. Thereby, an innovative technique for correlating surface chemical activity and topography during a single sample surface scan is provided. In the present research, a batch fabrication process at the wafer level was developed for incorporating an array of four AFM-SECM cantilevers with recessed electrodes. The electrode was located at a defined distance from the tip apex enabling separation of correlated topographical and electrochemical information. The bifunctionality of the individual probes is demonstrated by AFM imaging and electrochemical characterization of the integrated electrodes.

The presented development was at the forefront of combined scanning probe technology providing sub-microelectrode integrated AFM probe arrays for the first time.

Fabrication

Multifunctional cantilever arrays were fabricated from a 4″ silicon-on-insulator (SOI) wafer consisting of a device layer of 10 μm silicon (Si), a stop etch layer of 1 μm silicon dioxide (SiO_2) and a handle layer of 500 μm Si. This procedure is conducted using a batch process involving the development of over three hundred microchips on a single wafer. Each microchip contains four gold (Au) pad openings and four cantilevers of various heights and widths.

First, the device silicon layer AFM tips were fabricated using an isotropic reactive ion etching (RIE) process. The AFM tip surface was insulated by a 500 nm plasma enhanced chemical vapor deposition (PECVD) silicon nitride (SiN) layer. An etch mask for backside Si etch was patterned by successive 6 μm PECVD SiO_2 layer deposition and wet etching. The electrode layer is then patterned using lift-off process of 100Å titanium and 2000Å gold deposited using an e-beam evaporator. Another 500 nm PECVD SiN layer insulated the metal layer. Four gold pads were exposed by an RIE process for electrical connection to individual electrodes for electrochemical measurements. Each cantilever profile was defined by etching the SiN and the silicon device layers with RIE and inductively coupled plasma (ICP) etching processes respectively. The backside of the microchip was then etched through ICP. Each cantilever chip was then removed from the host wafer and focused ion beam (FIB) technology was used to open each tip electrode and shape the AFM tip [1].

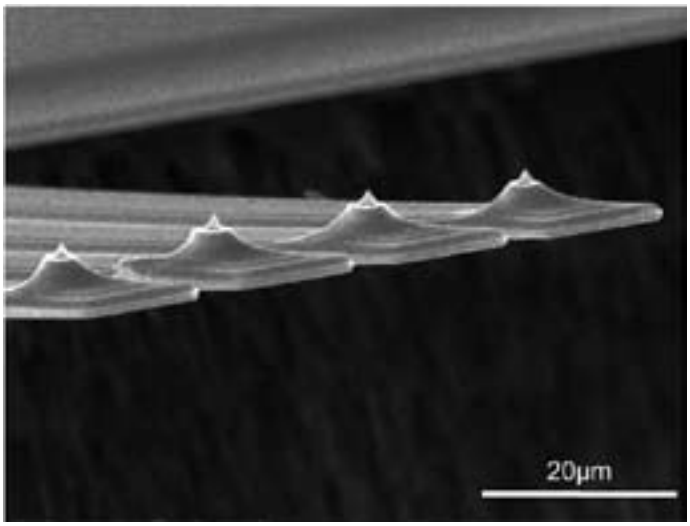

Figure 1: SEM image of a fabricated AFM-SECM probe array.

Results and Conclusions

An AFM-SECM probe array is shown in Figure 1. Each cantilever chip contains four separate cantilevers with 20 μm or 16 μm spacing between each tip apex. The imaging quality of the cantilever was tested.

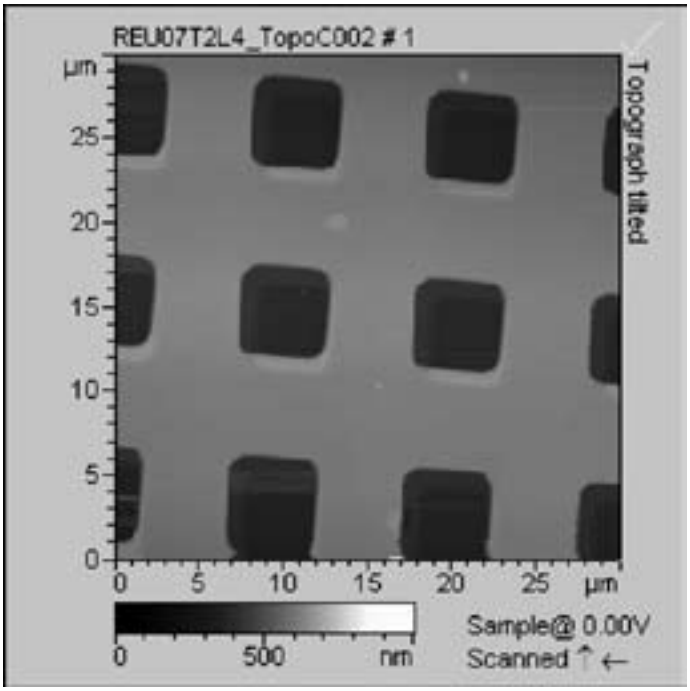

Figure 2: AFM of a test grid recorded with a single cantilever from the array.

The AFM laser was focused on one of the cantilevers and scanned across a model sample; the AFM image is shown in Figure 2. The change in color along the lower edge of each etched region is related to the spot size of the used laser, which results in an overlapping readout of two neighboring cantilevers.

The electrochemical functionality of the cantilever array was then tested by cyclic voltammetry (CV) in 0.1 mol/L $K_4Fe(CN)_6$ in 0.5 mol/L KCL in a potential range from 0V-0.6V. CVs were recorded before and after focused ion beam (FIB) milling (Figure 3). As shown in the voltammograms, the current level before tip milling is in the low pA range, which indicates good insulation. The same test was then conducted after tip milling. The measured steady state current of 1.68 nA is in good agreement with the expected theoretical value for the given electrode size.

Finally the free vibration of the cantilever in air was recorded and the spring constant of the cantilevers was calculated to be 0.95-1.2 N/m which is comparable to that of commercial cantilevers. The frequency response of the cantilevers in air was also conducted using a mean-square displacement which verified that the AFM-SECM cantilevers have a resonant frequency of 69.1 kHz, also comparable to commercial cantilevers [1].

In conclusion, the first known AFM-SECM integrated probe array was successfully fabricated using microfabrication techniques suitable for production on a wafer level. The gold microelectrodes were integrated recessed from the tip apex allowing simultaneous topographical and electrochemical imaging. The AFM-SECM cantilever performance as AFM cantilevers was verified and is comparable to that of commercial cantilevers and electrochemical functionality was demonstrated by cyclic voltammetry.

Future Work

Simultaneous topographical and electrochemical imaging will be demonstrated with one of the four cantilevers of the array. Parallel readouts from each cantilever are anticipated in the future with a modified AFM set-up. Reducing the size of the integrated microelectrode will result in improved resolution for electrochemical imaging. Ultimately, individual modifications of each electrode of the cantilever array with biosensing layers or pH sensing layer will allow multiple parameter readouts during AFM imaging.

Acknowledgements

I would like to thank Dr. James Meindl, Jennifer Root, and the staff at MiRC for providing a pleasant work environment. Also thanks to my mentor Dr. Heungjoo Shin for his close work, and Christine Kranz and Boris Mizaikoff for providing the topic for the research project. Finally, I would like to recognize the National Nanotechnology Infrastructure Network REU Program and the National Science Foundation for their funding and support during this project.

References

[1] C. Kranz, G. Friedbacher, B. Mizaikoff, A. Lugstein, J. Smoliner, E. Bertagnolli, "Integrating an Ultramicroelectrode in an AFM Cantilever: Combined Technology for Enhanced Information"; Anal. Chem., 73, 2491, (2001).

[2] A. Lugstein, E. Bertagnolli, C. Kranz, A. Kueng, B. Mizaikoff, "Integrating micro- and nanoelectrodes into AFM cantilevers using FIB techniques"; Appl. Phys. Lett., 81, 349 (2002).

[3] H. Shin, P. Hesketh, B. Mizaikoff, C. Kranz, "Batch Fabrication of AFM Probes with Recessed Integrated Ring Microelectrodes at a Wafer Level"; Anal. Chem, 79, 4769-4777, 2007.

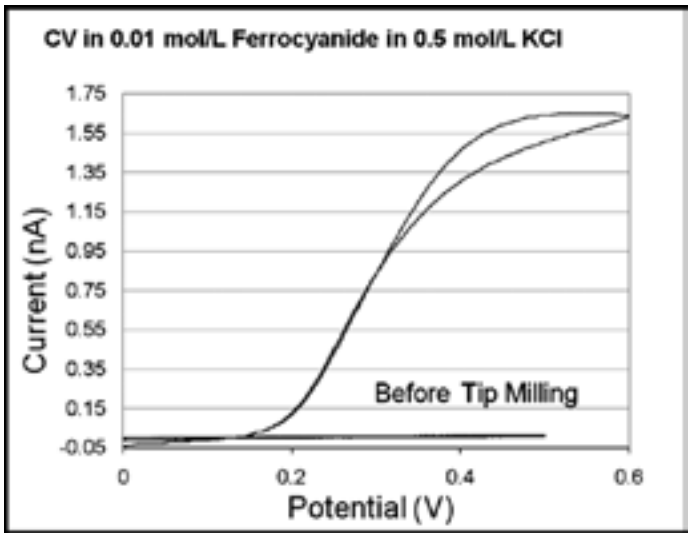

Figure 3: CV recorded at the integrated electrode of the cantilever.

Utilization of Surface Acoustic Waves for On-Chip Manipulation of Micro/Nano Particles

Ashley Colletti

Biomedical Engineering, The Johns Hopkins University

NNIN REU Site: Penn State Center for Nanotechnology Education and Utilization, The Pennsylvania State University
NNIN REU Principal Investigator: Dr. Tony Jun Huang, Engineering Science and Mechanics, The Pennsylvania State University
NNIN REU Mentors: Jinjie Shi and Xiaole Mao, Engineering Science and Mechanics, The Pennsylvania State University
Contact: ashleycolletti@jhu.edu, junhuang@psu.edu, jus239@psu.edu, xum101@psu.edu

Abstract

The on-chip integration of microfluidic and surface acoustic wave (SAW) systems provides a promising platform for potential applications such as cell patterning, cell sorting and separation, high throughput screening in drug development and testing, and ultrafast mixing. In this study, we integrated polydimethylsiloxane (PDMS) microchannels with inter-digitated transducers (IDTs) on a piezoelectric substrate to enable the on-chip manipulation of micro/nano particles. Photolithography techniques were utilized to define the micropattern for both the microchannels and IDTs. The mold for the PDMS microchannels was fabricated via deep reactive ion etching (DRIE) on a photoresist-patterned silicon (Si) wafer. Precision control of polystyrene (PS) micro/nano particles is achieved by generating standing SAW within the microchannel using IDTs. Through careful arrangement of microchannels and IDTs, one-dimensional and two-dimensional patterning of micro/nano particles in the microchannel can be achieved.

Introduction

In recent years, much interest has been expressed in the development of robust, integrated lab-on-a-chip systems which serve a multitude of purposes in engineering, medicine, and biochemistry. In this study, our goal was to design, fabricate, and test an on-chip integrated microelectromechanical systems (MEMS) device that would enable aggregation of micro/nano particles within a microchannel at the pressure anti-pressure nodes of standing SAW.

Microfluidic channels provide a controlled region for study, taking advantage of laminar flow, low Reynolds numbers, and high surface area to volume ratios [1]. The underlying mechanism for particle patterning stems from wave theory, where two approaching waves converge and undergo positive interference to form standing waves. In this project, a piezoelectric substrate was used due to the fact that it functions as an energy interface, converting between electrical and mechanical forms of energy. Thus, when a form of electrical energy, voltage, is applied across an electrode on a piezoelectric substrate, mechanical vibrations of the substrate result, and SAW propagate across the medium, perpendicular to the IDT. Arranging two IDTs in either parallel or angled patterns enables precise 1D or 2D patterning, respectively, at the pressure nodes of the standing SAW.

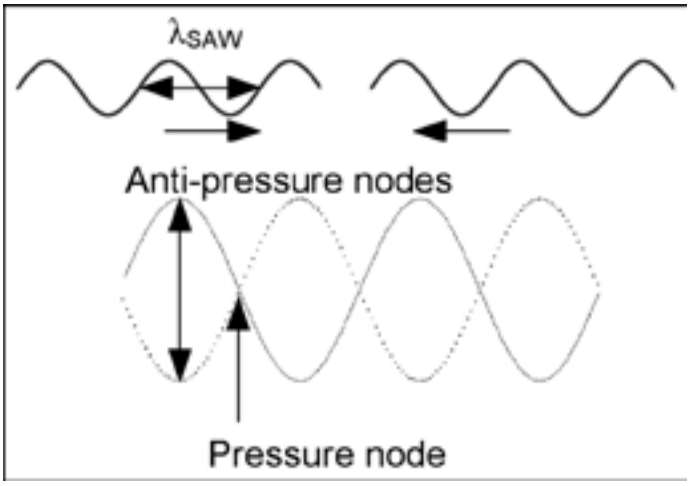

Figure 1: The underlying mechanism for particle manipulation: the combination of two converging SAWs into one standing SAW.

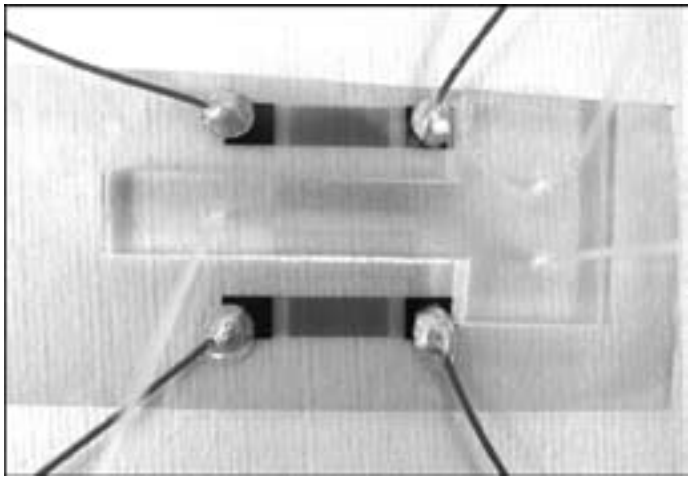

Figure 2: On-chip combined acoustic and microfluidic systems: titanium/gold IDTs with wires bonded and PDMS microchannel with polyethylene tubing, ready for testing.

Experimental Procedure

Photolithography techniques were implemented in both the fabrication of the IDTs and microchannels. First, IDT and microchannel masks considering a variety of parameters were designed on AutoCAD. Based on the orientation of the IDTs and microchannels, both 1D and 2D patterning systems were designed.

Both masks were written on a laser writer, and contact lithography was used for the patterning of the Si wafer for the microchannel mold and the piezoelectric IDT substrate. Following, the photoresist-patterned Si wafer underwent DRIE, which etched into the exposed areas of the wafer, creating a Si mold for microchannels. PDMS was mixed and poured over the mold and cured, and the microchannels were released. To complete the IDT fabrication, an adhesive layer of titanium (Ti) was deposited, followed by a layer of gold (Au), by metal evaporation onto the photoresist patterned piezoelectric substrate. Finally, the Ti/Au electrodes were revealed by a chemical liftoff process, removing any remaining photoresist/Ti/Au.

Device integration challenges were overcome by relying on reactive ion etching (RIE) to pre-treat bonding surfaces of both the PDMS microchannel and piezoelectric substrate. Immediately following low-power oxygen RIE, microchannels were aligned with the IDTs under a microscope. Wires were bonded to the IDT electrodes, and polyethylene tubing was inserted into the microchannel inlets and outlets.

The device testing experimental setup consisted of an radio frequency (RF) signal generator first connected to a power amplifier, which was then connected to both IDTs. An oscilloscope recorded the signal voltage and frequency. The integrated MEMS device was placed on the stage of an inverted optical microscope for testing. Specified flow rates of micro/nano particle containing fluid were delivered to the polyethylene tubing by a syringe pump.

Results and Conclusions

In conclusion, we have developed an effective method for the on-chip manipulation of micro/nano particles. When an alternating current (AC) signal was applied across the surface of both IDTs, aggregation of micro/nano particles within the microchannels did occur successfully at the pressure nodes of the standing SAW. Both 1D and 2D patterning of micro/nano particles was achieved, resulting in an aggregated line or grid of dots, respectively. Patterned particles ranged in size from 460 nm to 10 μm in diameter.

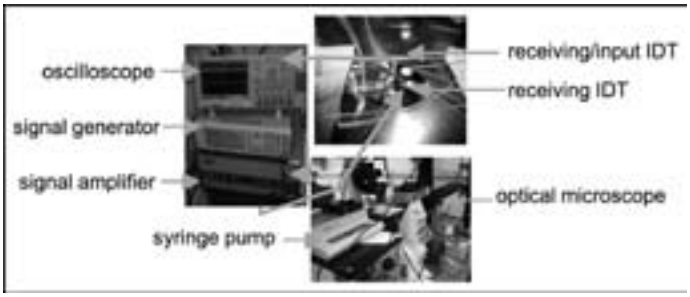

Figure 3: Experimental setup consisting of signal generator, power amplifier, MEMS device, syringe pump, inverted optical microscope, and oscilloscope.

Future Work

This work boasts a multitude of applications, particularly in pharmaceuticals, biology, and biochemistry. Future work involving the patterning of cells would be applicable to drug discovery, development, and testing. This technique could potentially be used to affix the positions of cells and provide a uniform environment for monitorable testing during high throughput screening. Cell responses to variations in dosage amount, frequency, and other factors could be observed. Secondly, functionalizing molecules with polystyrene micro or nano particles could lead to improvements in molecular sorting and deoxyribonucleic acid (DNA) analysis techniques. Finally, microfluidic in-channel mixing, which is often difficult to attain in laminar microfluidic systems, could be achieved efficiently by selective functionalization and patterning of molecules.

Acknowledgements

The author wishes to thank Dr. Tony Jun Huang, Jinjie Shi, and Xiaole Mao of the Penn State Bio-NEMS Group for their support and motivation throughout the project, the Penn State Nanofabrication Facility and staff for assistance and patience with fabrication, and the Penn State Center for Nanotechnology Education and Utilization and the National Nanotechnology Infrastructure Network Research Experience for Undergraduates Program for this incredible opportunity. She would also like to thank the NNIN and NSF for funding.

References

[1] Squires, T. M., Quake, S.R.; "Microfluidics: Fluid physics at the nanoliter scale; Revs of Modern Physics, 77, 977-1026 (2005).

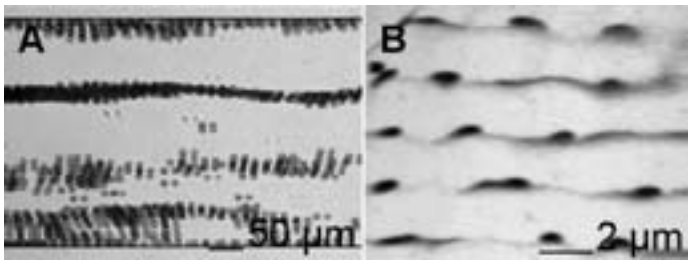

Figure 4: 1D patterning of 10 µm (A) and 2D patterning of 1 µm (B) polystyrene microparticles at pressure nodes of standing SAW.

(Note new publication; "Focusing Microparticles in a Microfluidic Channel with Standing Surface Acoustic Waves"; J. Shi, X. Mao, D. Ahmed, A. Colletti, and T.J. Huang. Received 1st January 2007, Accepted 1st January 2007, First published on the web, 1st January 2007, www.rsc.org/loc | Lab on a Chip.

Novel Optical Trapping Particles for Biological Experiments

Nathan Friez

Applied Physics, Bethel University

NNIN REU Site: Cornell NanoScale Science & Technology Facility, Cornell University
NNIN REU Principal Investigator: Dr. Michelle Wang, Physics, Cornell University
NNIN REU Mentors: Dr. Chris Deufel and Scott Forth, Physics, Cornell University
Contact: frinatm@bethel.edu, mdw17@cornell.edu, cd77@cornell.edu, sf73@cornell.edu

Abstract

Optical trapping is a powerful technique used to investigate the mechanical properties of the molecular motors that govern cellular processes. In order to examine such mechanisms, trappable "handles" must be developed that can be used for attachment to biological samples. This project involves the design and fabrication of cylindrical trapping particles to be used in measuring forces and torques exerted on deoxyribonucleic acid (DNA), in addition to optimizing existing fabrication protocols. In previous work, the entire top surface of a cylinder was chemically functionalized for binding to DNA. During the first stage of this project, this protocol was repeated with slight modifications in order to generate cylinders which dramatically reduced the unwanted precessing of particles in an optical trap, thereby minimizing measurement noise. The second stage principally dealt with fabricating smaller cylinders (600 nm height, 300 nm diameter) to allow for more accurate and precise measurements. Progress in this area has proved challenging, likely due to having approached the optical limits of the nanofabrication tools being used. It may ultimately prove more beneficial to design and fabricate a new type of trapping particle.

Introduction

There have been a myriad of uses for optical traps in the field of single molecule biophysics, with special emphasis on systems involving DNA. Briefly, an optical trap can be described as an instrument that uses collimated light, normally provided by a single mode laser, which is brought into a tight focus by high numerical aperture (NA) objective lenses to trap dielectric particles. The principal forces involved in an optical trap are the scattering force (a result of the momentum of photons) and the gradient force, which is the force that actually does the trapping. The scattering force "is proportional to the light intensity and acts in the direction of the propagation of light" while the gradient force is "proportional to the spatial gradient in light intensity and acts in the direction of that gradient" [1]. The diameter of the particles is on the order of the wavelength light that is being used.

In this project we used crystalline quartz, which is birefringent, as our substrate for fabricating cylindrical trapping particles in order to make measurements of torque and force on DNA in an angular optical trap. In addition to being a well understood fabrication material, quartz was used since "angular trapping occurs in particles made from materials such as quartz, in which the extraordinary axis of the crystal is more easily polarized [due to the birefringent nature of quartz] than the ordinary axes" [2]. When such a particle is positioned in an electric field, a polarization is induced on the particle. Any misalignment between the electric field and the polarization of the particle results in a torque [3]. By monitoring the ellipticity introduced in the trapping beam by this particle, the torque can be determined with great accuracy (typically ~ a few kT).

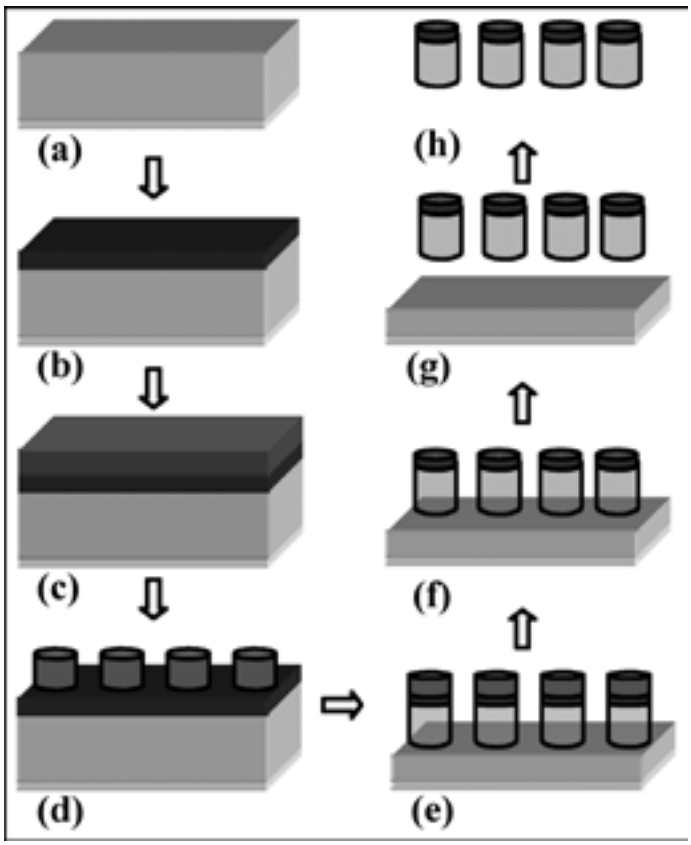

Figure 1: Optimized protocol.

Fabrication

The primary purpose of this project was to master and improve the existing cylindrical nanoparticle fabrication protocols [4]. Figure 1 outlines the optimized fabrication protocol. Part (a) depicts the initial step in our protocol; here a thin anti-reflective coating (ARC) has been applied (this coating was used to prevent unwanted ring like structures from appearing on the wafer from the reflective chucks used in the exposure process). In (b) the top surface has reacted with 3-aminopropyltriethoxysilane (APTES); this is the functionalized area to which we want to attach a biological molecule. Approximately 660 nm of OIR 620-7i has been spun onto the wafer in part (c).

A 10x stepper is used to expose the pattern in (d). Section (e) depicts the first anisotropic dry etch (CHF_3/O_2 used as etching gas). Etching times were selected such that particles of height ~ 1 micron were generated.

In the next step, part (f), the resist is removed by sonicating the cylinders/wafer in an acetone solution. The resist was successfully separated from the cylinder, leaving behind the APTES layer for attachment to streptavidin protein. The cylinders, in section (g), have been cleaved using a microtome blade. Finally, part (h) depicts the end product; from here a sample chamber will be prepared and the localized APTES on the top of the cylinders has to be reacted with streptavidin in order for use in an optical trap.

Summary

A protocol for the production of anisotropic quartz cylinders for use in novel optical trapping experiments was successfully performed with improvements made over the published protocol. Further optimization of the fabrication protocol would involve reducing the overall size of the cylinder. Initial attempts proved challenging due to the optical limits of the nanofabrication tools being reached.

In addition, it may be possible to further refine and improve the trapping handles by employing new particle geometries or perhaps considering alternate fabrication substrates.

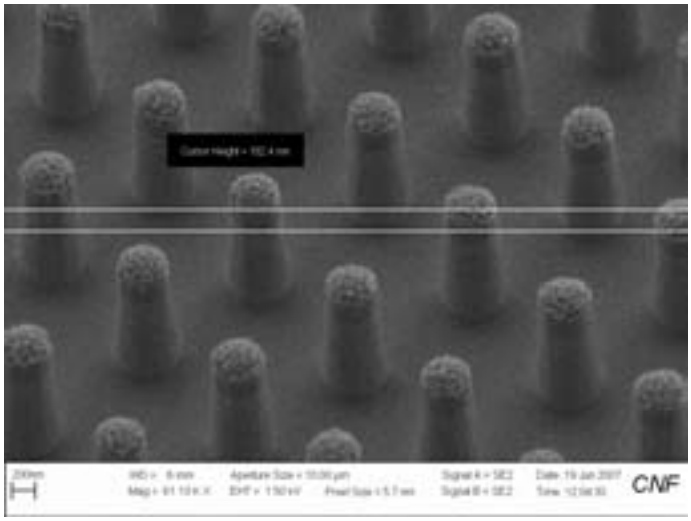

Figure 2, top: Quartz cylinders with resist on top after anisotropic dry etch is performed.

Acknowledgements

I would like to thank my principal investigator, Dr. Michelle Wang, my mentors, Dr. Chris Deufel and Scott Forth, the National Nanotechnology Infrastructure Network Research Experience for Undergraduates Program, the National Science Foundation, and the Cornell NanoScale Facility and staff without which this research would not have been possible.

References

[1] Svoboda, K., "Biological Applications of Optical Forces," Annual Reviews, <www.annualreviews.org>, 249 (1994).

[2] La Porta, A. and M.D. Wang, "Optical Torque Wrench: Angular Trapping Rotation and Torque Detection of Quartz Microparticles," Physical Review Letters Volume 92, Number 19 (2003).

[3] Ibid.

[4] Deufel, C. et al, "Nanofabricated quartz cylinders for angular optical trapping: torque detection during DNA supercoiling," Nature Methods Vol. 4, 223 (2007).

Investigating Inter-Domain Regulation of von Willebrand Factor Interactions with Platelets

Ryan M. Harrison

Biomedical Engineering & Economics, Johns Hopkins University

NNIN REU Site: Center for Nanotechnology, University of Washington
NNIN REU Principal Investigator: Wendy Thomas, Bioengineering, University of Washington
NNIN REU Mentors: Dr. Shivani Sharma, Dr. AnYue Tu, and Dr. Olga Yakovenko, Bioengineering, University of Washington
Contact: rharrison@jhu.edu, wendyt@u.washington.edu, aytu@u.washington.edu

Abstract/Introduction

Von Willebrand factor (vWF), a large multimeric blood plasma protein, is integral to *in vivo* platelet aggregation and clot formation (Figure1) [1]. Of particular interest are the shear dependent interactions between the A_1-domain of vWF and platelet glycoprotein (GP) Ib_α [2]. Weak, transient bonding between these two partners anchors platelets and vWF long enough for other glycoprotein and integrin mediated bonds to form [3]. Disruption of these transient bonds, such as mutations that abolish the shear dependence of the interaction, lead directly to clinical illnesses such as von Willebrand disease, the most common hereditary blood clotting disorder [1]. To detect the presence of inter-domain regulation within vWF, we investigated the interaction of platelets with the isolated A_1, $A_1A_2A_3$, $D'D_3A_1A_2A_3$ and $\Delta D'D_3$ ($A_1A_2A_3D_4B_1B_2B_3C_1C_2C_k$) domains of vWF under flow conditions. In addition, we conducted ristocetin induced platelet aggregation (RIPA) assays to verify construct functionality, and enzyme linked immunosorbent assays (ELISA) to quantitate construct surface absorption.

Results

ELISA, which were visualized at A_{650} with a horseradish peroxidase (HRP)/HRP antibody system developed by Invitrogen, revealed nonlinear concentration dependence as well as variable coat concentration for the different constructs tested — multimeric vWF, A_1, $A_1A_2A_3$, $D'D_3A_1A_2A_3$. Construct size dependent adsorption was observed as expected — A_1 coated at ~24%, $A_1A_2A_3$ at ~58% and $D'D_3A_1A_2A_3$ at ~67% of multimeric vWF coating (data not shown).

RIPA assays verified the functionality of the dimeric ($D'D_3A_1A_2A_3$ and $\Delta D'D_3$), but not monomeric (A_1 and $A_1A_2A_3$) constructs. RIPA assays rely on the fact that platelets, in combination with ristocetin (antagonist) and a cross linker should aggregate in solution. In Figure 2, our negative control (platelets + vWF) shows no aggregation, while our positive control (platelets + vWF + ristocetin) and dimeric constructs (platelets + construct + ristocetin) aggregate in solution. This reveals that both vWF and dimeric constructs are functionally active in solution; that is, they bind platelets with high affinity in the presence of a ristocetin antagonist. For monomeric, the paradigm is the opposite— platelets + vWF + ristocetin + monomer should actually inhibit platelet aggregation versus platelets + vWF + ristocetin. No platelet aggregation inhibition was consistently observed, suggesting that our A_1 and $A_1A_2A_3$ were functionally inactive. This is curious, considering that A_1 is widely known to inhibit platelet aggregation in the presence of ristocetin (or botrocetin, a close analog) [2,4].

Flow chamber experiments were conducted for plates coated with multimeric vWF, A_1, $A_1A_2A_3$, $D'D_3A_1A_2A_3$ and $\Delta D'D_3$ in the range of 0.0025 Pa to 16 Pa wall shear stress. Platelet interactions occurred for all constructs other than A_1 and $A_1A_2A_3$, where the interaction is quantified as the number of platelets bound to the surface in two minutes under flow conditions. Bovine serum albumin (BSA)-coated plates were used as a negative control and a baseline threshold for platelet interactions; that is, constructs

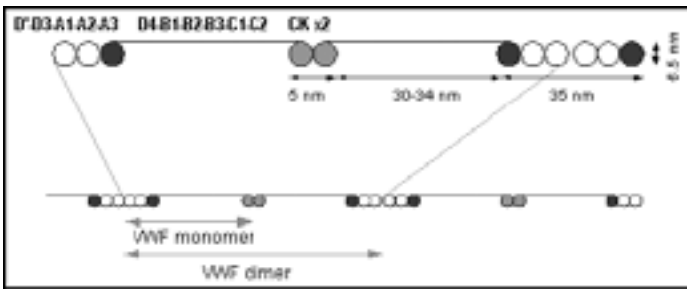

Figure 1: Domain-level structure of von Willebrand factor.

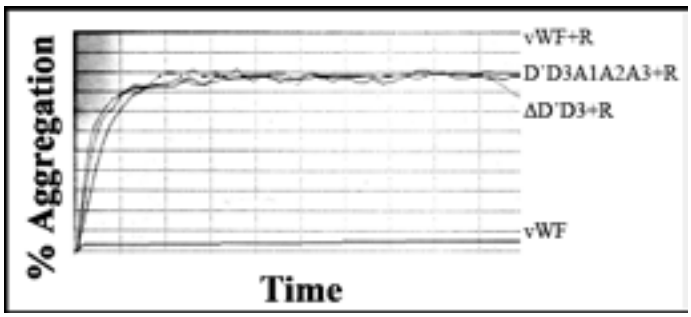

Figure 2: RIPA assay for dimeric vWF constructs.

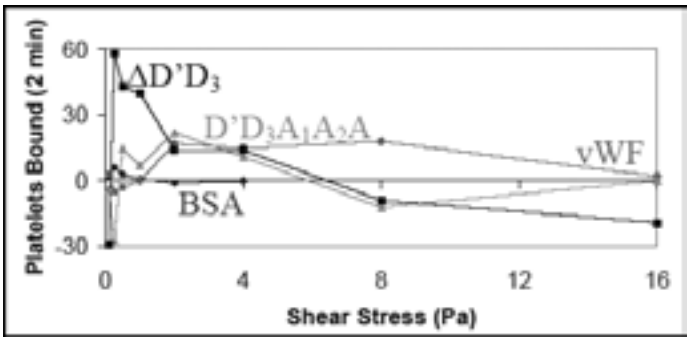

Figure 3: Flow chamber experiment comparing the shear-dependent platelet binding of vWF constructs.

that bound less platelets than BSA, such as A_1 and $A_1A_2A_3$, were considered nonspecific and discounted.

Four experiments were performed in the same conditions on separate days and Figure 3 shows the results from one representative/typical experiment. Note that the $\Delta D'D_3$ construct experiences peak platelet binding at a much lower shear than both multimeric vWF and $D'D_3A_1A_2A_3$. This demonstrates that the $\Delta D'D_3$ domain has a role in regulating the shear dependence of vWF platelet interactions.

Furthermore, at high shear (> 2 Pa), platelets tend to detach from the dimeric constructs while platelet binding occurs throughout the entire high shear range for multimeric vWF.

Methods

Flow chamber experiments were conducted with circular parallel plate flow chambers (Glycotech) following the protocol of Dogget, et. al. 2003 [5]. Variable concentrations of multimeric vWF (Haematologic Technologies Human von Willebrand factor VIII Free, Cat#: HCVWF0191, Stock 210 μg/mL), A_1, $A_1A_2A_3$, $D'D_3A_1A_2A_3$ and/or $\Delta D'D_3$ were coated onto 35 mm round polystyrene petri dishes (Corning) via a 90 minute incubation at 37°C. Recombinant vWF-A_1 [6] and $A_1A_2A_3$, $D'D_3A_1A_2A_3$ and $\Delta D'D_3$ were prepared and isolated as previously described [7]. vWF construct coated dishes were mounted to the flow chamber, suffused with a platelet rich suspension isolated from healthy donor whole blood and visualized under a 10X light microscope (Nikon) [5]. RIPA assays were conducted following the protocol of Cruz, et. al. 2000 [2].

Conclusion

This study reveals that inter-domain regulation does indeed occur in vWF platelet interactions. Flow chamber experiments demonstrate that the D'D3 domain regulates shear dependent platelet binding by inhibiting low shear vWF platelet interactions by an, as of yet, undetermined mechanism. One possible mechanism is that the $D'D_3$ domain inhibits the A_1 domain at low shear, preventing GP Ib_α binding. However, at high shear, vWF and $D'D_3$ are elongated by shear forces, exposing the A_1 domain.

While in general agreement with our findings, the elongation theory does not explain the discrepancy between the dimeric constructs and vWF platelet binding at high shear. Repeating flow chamber experiments with GP Ib_α coated polystyrene beads instead of intact platelets and characterization under an atomic force microscope are needed to cement our findings as well as to test mechanistic hypothesizes.

Acknowledgements

I would like to thank the Lenting Laboratory (University Medical Center Utrecht, Utrecht, the Netherlands) for their generous donation of vWF constructs, Greg Mize (University of Washington, Biochemistry) for aggrometer usage and the Thomas Laboratory for hosting me. Research funded by the National Nanotechnology Infrastructure Network Research Experience for Undergraduates Program and National Science Foundation.

References

[1] Wagner DD. (1990) An. Rev. Cell. Bio. 6:217242.
[2] Cruz MA, et. al. (2000) J. Bio. Chem. 275.25:1909819105.
[3] Doggett TA et. al. (2002) Biophys. J. 83:194–205.
[4] Fukuda K et. al. (2005) Nature Struct. Mol. Bio. 12:2:152159.
[5] Doggett TA et. al. (2003) Blood 102:1:152160.
[6] Cruz MA et. al. (1993)) J. Bio. Chem. 268.28:2123821245.
[7] Ulrichts H et. al. (2006). J. Biol. Chem., 281.8:46994707.

Watershed Segmentation Algorithm for Medical Confocal Image Analyses Towards In Vivo Early Cancer Detection

Man Kin Derek Ho

Department of Biology, Johns Hopkins University

NNIN REU Site: Microelectronics Research Center, The University of Texas at Austin
NNIN REU Principal Investigator: Dr. John X. J. Zhang, Biomedical Engineering, The University of Texas at Austin
NNIN REU Mentor: Karthik Kumar, Electrical Engineering, The University of Texas at Austin
Contact: derekho@jhu.edu, john.zhang@engr.utexas.edu, kkumar@mail.utexas.edu

Abstract

This REU project successfully demonstrated an automated image segmentation technique to overcome artifacts from *in vivo* images and provide real time, accurate analysis of nuclear size, density, and nuclear-cytoplasmic ratio, critical visual markers of epithelial precancers. The algorithm was first calibrated using optical images of microfluidic droplets, and then applied on confocal images of oral cavity tissues. All images were segmented successfully to provide accurate count (95% with 6.2% standard deviation) of cells or droplets.

Introduction

Cancer is a serious global healthcare problem, accounting for over 6.5 million deaths annually. Although widely considered a disease of the developed world, 60% of cancers occur in developing countries, where low per-capita healthcare expenditure, unreliable infrastructure and facilities render advanced cancer screening technologies inaccessible. In lieu of these factors, we have developed a low-cost, handheld, microelectromechanical systems (MEMS)-based *in vivo* confocal microscope for sub-cellular-resolution imaging of tissue towards early detection of epithelial precancers from which 85% of cancers originate. Currently, endoscopic procedures are performed for biopsy samples and images are manually segmented for initial testing of pre-cancer. However, this results in long turnaround time, high costs, discrepancies among different segmentation methods, and inconvenience for patients. An advanced algorithm is therefore needed to provide fast, low-cost, standardized results which are essential for *in vivo* pre-cancer detection.

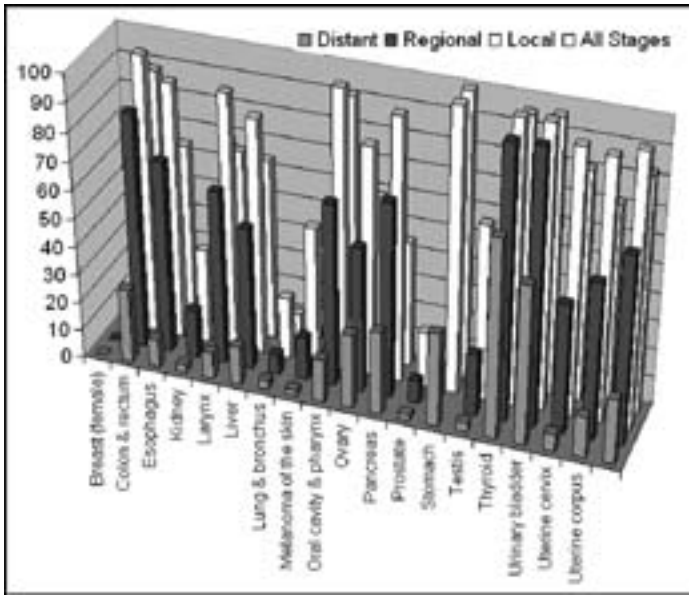

Figure 1: Statistics showing survival rates vs. cancer diagnosed at different stages.

Algorithm Outline

The image was imported into MATLAB® and converted to grayscale for faster processing using inbuilt functions. **Imclearborder** was used to eliminate incomplete nuclei and only account for complete and visible ones. The gradient magnitudes were calculated and the threshold was increased to outline cell membranes.

The normal watershed transform usually over-segments so we used the more advanced marker-controlled watershed transform. Foreground objects were marked with local maxima to ensure only wanted objects were accounted for. **Strel** and **graythresh** were used to mark the background in black against the resized white foreground markers. In order to only count minima at

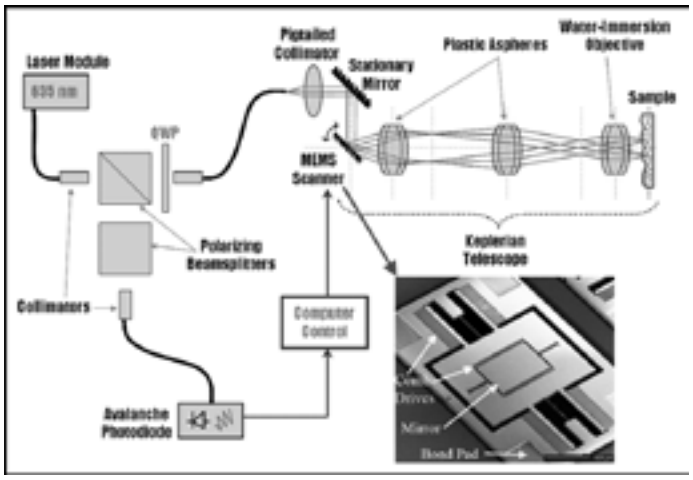

Figure 2: Illustration of our imaging setup with top view of microscanner shown (Inset).

markers and not the entire image, **imimposemin** was used and the transformation was initialized at this point.

To visualize how the watershed function worked, the image was viewed as a topographical surface. The algorithm started at a minima of each marked object and expanded uni-directionally until it reached an edge of another region. The watershed transform was an accurate way to count and segment marked regions. **Bwlabel** labels connected components of the image, which allowed **numObjects** and **Regionprops** to give numerical statistics about the segmented image. Based on results from previous trials, parameters were set up to remove false counts. All nuclei sizes were put into an array and a mean nuclei size was calculated, together with a histogram displaying the occurrences vs. size.

Algorithm Calibration

The algorithm was first calibrated using optical images of droplets in microfluidic channels. Microfluidic channels were fabricated using polydimethylsiloxane (PDMS) with rapid prototyping. A clean silicon wafer was coated with hexamethyldisilazane (HMDS) to ensure good adhesion between silicon and photoresist. Photoresist SU-8 2250 was applied to produce a master of appropriate thickness and the wafer was spun at 1860 rpm for 30 seconds. Under soft lithography, the wafer was exposed to UV light for 50 seconds and developed for 3 minutes. On developing, features of microfluidic channels are transferred to the resist, and the master fabrication is complete. PDMS was poured onto the wafer after applying Sigma-Cote to reduce adhesion between the PDMS and wafer, cured for 45 minutes at 70°C, and peeled to form channels. The master can be used in this manner to reliably reproduce thousands of channels based on a design.

Water droplets dyed with various colors were injected at different arms of the microfluidic channel. The fusion efficiency was observed when different flow rates were applied and the algorithm was capable to segment and count droplets with 93% accuracy and 8.7% standard deviation. Over-segmentation occurred when many droplets did not fuse together. Based on that, an additional criterion was implemented to minimize inaccurately segmented droplets.

Results and Conclusion

Medical confocal images were used for a more rigorous and robust testing of the algorithm. Images were taken from porcine oral cavities with our confocal microscope. The algorithm provided 95% accuracy and 6.2% standard deviation to hand-segmentation. Although over-segmentation did occur, the mistaken segmented regions were obvious in that they were not nuclei based on size and could therefore be discarded.

The results show that our image segmentation algorithm can analyze images taken in vivo and detect nuclei to a good extent. Our algorithm, together with our hand-held *in vivo* microscope, can provide real-time, biopsy-free results.

Future Work

Bayesian Classifiers can be implemented to detect specific object shape and size, which allows an observation of different cancer stages and an idea of what types of treatments are needed. A GUI can be written for easier usage and other research groups can benefit from automated image segmentation versus manual counting. Also with each image there are different objects and signals in them, thus performing a Fourier Transform can be useful in image analysis.

Acknowledgements

I would like to thank the NSF, NNIN Research Experience for Undergraduates Program, Dr. Sanjay Banerjee, NNIN Facility, and Zhang Research Lab at UT Austin.

References

[1] K. Kumar, K. Hoshino, H.J. Shin, R. Richards-Kortum and X.J. Zhang, "High-reflectivity Two-Axis Vertical Combdrive Microscanners for Sub-cellular Scale Confocal Imaging Applications", Proceedings of International Conference on Optical MEMS and their Applications (Optical MEMS '06), August 21-24, Montana, USA, 2006.

[2] Brette L. Luck, Kristen D. Carlson, Alan Conrad Bovik, Rebecca R. Richards-Kortum, "An Image Model and Segmentation Algorithm for Reflectance Confocal Images of *In Vivo* Cervical Tissue," IEEE Image Proc., V14, #9, pp. 1265-1276, Sep. 2005.

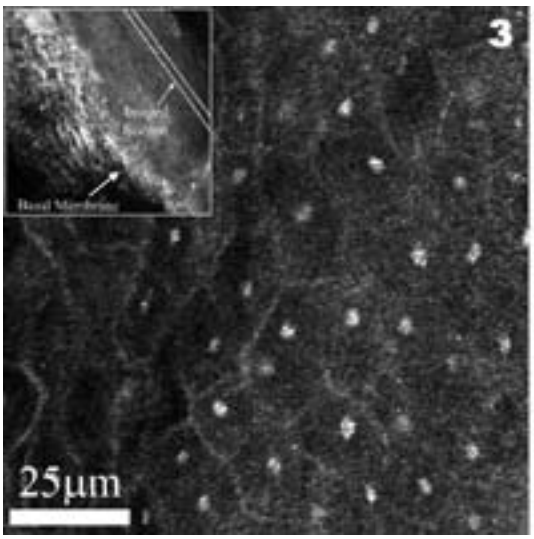

Figure 3: Porcine oral tissue. Inset: Epithelium and basal layer.

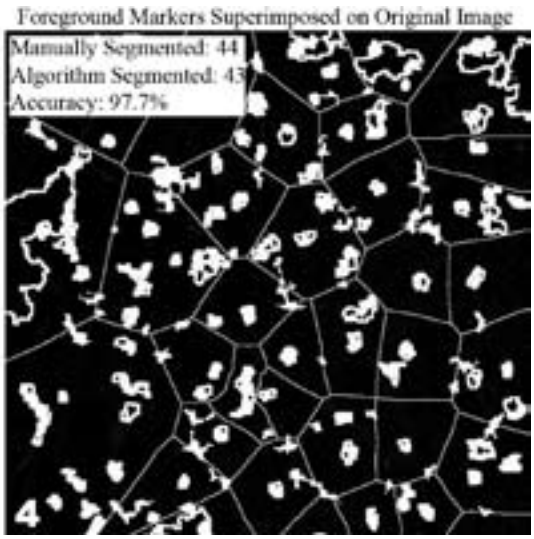

Figure 4: Segmented image with markers shown using our algorithm.

Study of Silver Nanoparticles Biocidal Impact on Escherichia coli Using Optical and Atomic Force Microscopy

Ruth Enid Kuilan León

Chemical Engineering, University of Puerto Rico, Mayagüez Campus

NNIN REU Site: Howard University Nanoscale Science and Engineering Facility, Howard University
NNIN REU Principal Investigator: Dr. James W. Mitchell, Chemical Engineering, Howard University
NNIN REU Mentor: Dr. Tina Brower-Thomas, Chemical Engineering, Howard University
Contact: rkl21656@uprm.edu, jwm@msrce.howard.edu, tbthomas@msrce.howard.edu

Abstract

Silver's biocidal properties have been known to affect cellular metabolism and inhibit cell growth; therefore it is expected that it will affect *Escherichia coli*, a bacteria known as one of the many species of bacteria living in the lower intestines of mammals. One of the primary adverse effects of the bacteria is the ability to cause food-borne illness. Atomic force microscopy (AFM) is a high-resolution imaging technique that can resolve features as small as an atomic lattice in real space. One of its many advantages is that it allows molecular scale resolution in liquid or without vacuum; therefore it has been immediately extended to biological systems. The focus of the present study was to investigate the structural and surface alterations induced in *E. coli* by the exposure of silver nanoparticles and image these changes using AFM. It is expected we will obtain easily achievable images by AFM with different orientations in space and accurate measurements of the morphology of normal versus affected *E. coli*. Optical microscopy was used for preliminary experiments to confirm that silver nanoparticles can affect the *E. coli* [1-3].

Objective

Investigate the effects induced on *Escherichia coli* when exposed to a biocidal compound such as silver nanoparticles and image them using optical and atomic force microscopy.

Materials and Methods

Surface Characterizations. Silver/silicon (AgSi) and Si wafer samples were studied using AFM. AgSi samples were prepared by DC magnetron sputtering of Ag and Si targets to deposit films onto a Si wafer. The Ag content for the samples was expected to be from 18-20%. Characterization was done by observing patterns on the surface topography and by studying data provided by the AFM, such as the average roughness of each sample. Contact and tapping mode was used, the latter being the ideal method because of its use in biological applications.

Preparation of Bacteria Samples. *E. coli* was grown in two different mediums: brain heart infusion (BHI) broth and nutrient agar. Flame inoculation was used to probe the *E. coli* into glass slants containing each medium. *E. coli* slants were left in an incubator at 37°C overnight to observe bacterial growth. After bacterial growth was evident, slants were labeled as stock solutions.

Serial Dilutions. Phosphate buffer was used to prepare solutions of decreasing bacterial concentration (10^{-1} to 10^{-6}) from *E. coli* BHI stock solution. These were labeled according to their bacterial concentration. The most diluted solutions (10^{-4} to 10^{-6}) were plated in a BHI agar and left to incubate at 37°C overnight to observe and quantify colonies.

Optical Microscopy. *E. coli* BHI stock solution and diluted solutions were observed on depression slides by optical microscopy using a (40x) objective. 500 μL of each *E. coli* solution were added to the slides with a sterile pipette. *E. coli* behavior was observed and recorded for 5 minutes prior to exposure to silver nanoparticles.

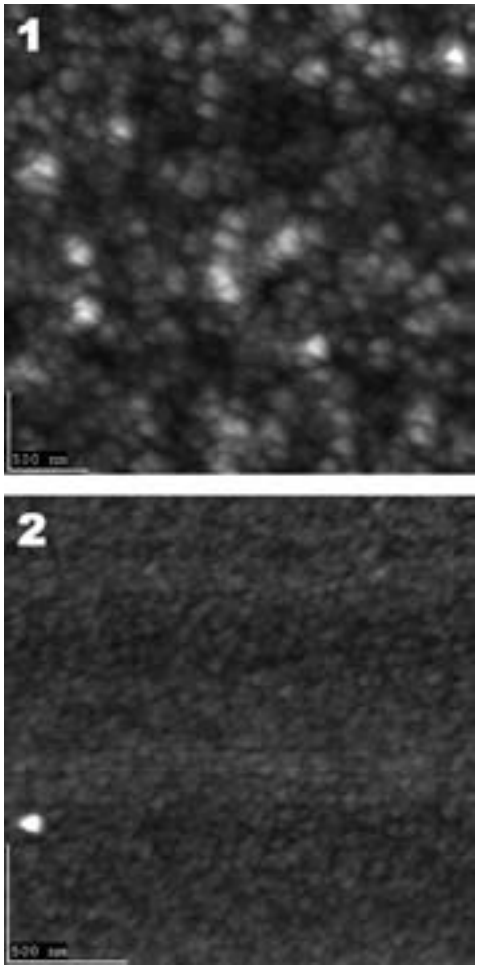

Figure 1, top: AgSi (3 µm scan) (Ra: 8.27 nm).

Figure 2, bottom: Si (3 µm scan) (Ra: 0.829 nm).

Silver Nanoparticles. Ag nanoparticle solution was prepared in a RPMI 1640 medium. This solution contained 10^{14} Ag nanoparticles per milliliter. Slides containing *E. coli* were exposed to 200 μL of Ag nanoparticles solution after 5 minutes of observation. *E. coli* behavior after exposure to Ag nanoparticles was observed for 35 minutes.

Results and Conclusions

Surface Characterization. Different patterns were observed when imaging surfaces by non-contact mode on the AFM. When the Si wafer samples were studied, surface topography images seemed smooth and very uniform contrary to AgSi samples that showed a rougher and more complex surface topography. AgSi samples appeared to have small scattered clusters along the surface. When average roughness (Ra) data was obtained, it showed that Si wafer surfaces had a (Ra = 0.829 nm) and that AgSi samples had a (Ra = 8.27 nm), confirming what was previously observed on surface topography images. Additionally, when the (Ra) for the AgSi sample and Si wafer sample were subtracted, a value of approximately 7 nm was obtained. This value confirmed that silver nanoparticles were embedded in the surface since it was the expected value for the size of the silver nanoparticles when prepared by DC magnetron sputtering. (See Figures 1 and 2.)

***E. coli* and Silver Nanoparticles.** Before silver nanoparticles exposure, *E. coli* seemed healthy and moving freely in solution. *E. coli* was observed for a period of 35 minutes after exposure to silver nanoparticles solutions. During the 35 minute period, the *E. coli* movement began to decrease and *E. coli* began to collide with each other forming clusters. After the 35 minute period, the *E. coli* movement stopped completely and a large number of clusters were observed. (See Figures 3 and 4.)

Future Work

Future work is expected to include: further study of surface characterization of AgSi and Si wafer surfaces by AFM, and *E. coli* growth on mica surfaces. In both studies, *E. coli* will be exposed to silver nanoparticles and the *E. coli* behavior will be observed *ex-situ* and *in-situ,* anticipating that it will die. Additionally it is expected that quantifying the *E. coli* in each sample will enable calculation of the rate at which the *E. coli* dies.

Acknowledgements

I thank the National Nanotechnology Infrastructure Network Research Experience for Undergraduates, the National Science Foundation, the CREST Nanomaterials Center, and the Howard Nanoscale and Engineering Facility for the opportunity. Also a special thanks to: Dr. James W. Mitchell, Dr. Tina Brower-Thomas, Mr. James Griffin, Dr. Gary Harris, Dr. Chichang Zhang, Mr. Andy Yuen Hai Ting, Mr. William Rose, and all my new friends at Howard University.

References

[1] Braga, P.C.; Ricci, D. Antimicrob. Agents Chemother. 1998, 42(1), 18-22.

[2] Doktycz, M.J.; Sullivan, C.J; Hoyt, P.R; Pelletier, D.A.; Wu, S.; Allison, D.P. Ultramicroscopy. 2003, 97, 209-206.

[3] Binnig, G.; Quate, C.F. Phys. Rev. Lett. 1985, 56(9), 930-933.

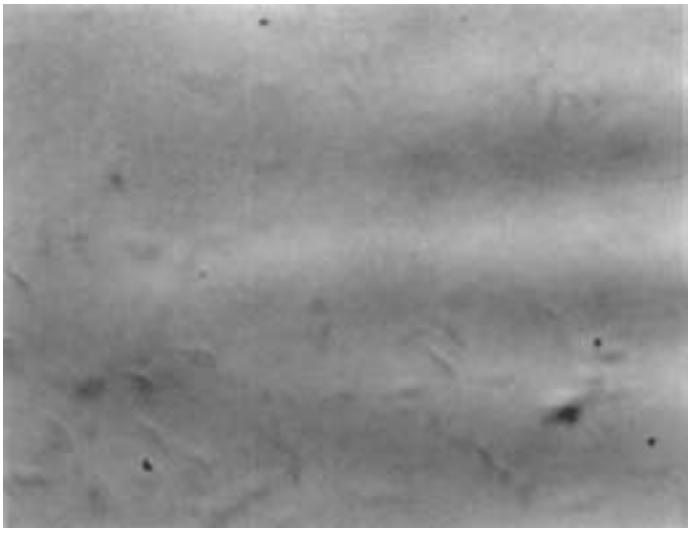

Figure 3: Before exposure to silver nanoparticles.

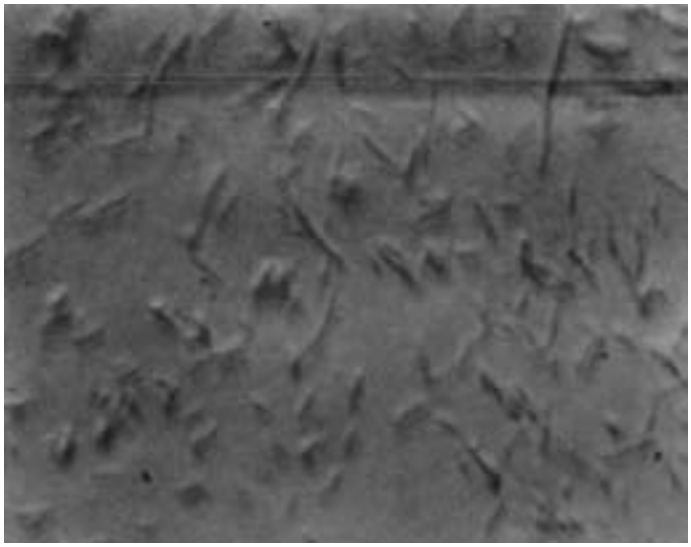

Figure 4: 40 minutes after exposure.

Protein Functionalization of Nanostructured Polymer Surfaces

Ashlee Mangan

Chemistry, Carlow University

NNIN REU Site: Penn State Center for Nanotechnology Education and Utilization, The Pennsylvania State University
NNIN REU Principal Investigator: Dr. Melik C. Demirel, BioNanoMaterials Lab, The Pennsylvania State University
NNIN REU Mentor: Dr. Serhan Boduroglu, BioNanoMaterials Lab, The Pennsylvania State University
Contact: ashlee73184@yahoo.com, mdemirel@engr.psu.edu

Abstract

Immobilization of proteins on polymer surfaces is of great interest for applications in biosensing, cell and tissue culturing, and medical device coating. This research studied the functionalization of a fluorescent protein on a structured polymer surface. Copolymerization of 4-trifluoroacetyl-[2.2]paracyclophane and 4-amino-[2.2]paracyclophane by a vapor deposition technique result in the formation of slanted, columnar, porous structures of the copolymer poly(*o*-trifluoroacetyl-*p*-xylylene-*co*-o-amino-*p*-xylylene-*co*-*p*-xylylene), (PPX-$COCF_3$-NH_2). The coupling of green fluorescent protein (GFP) to the structured and planar (control) polymer surfaces was studied by chemisorption (i.e. using a linking reagent, hexamethylene diisocyanate (HMDI)) and physisorption (i.e. without any linker). The fluorescence intensity of GFP on the surfaces was measured by an optical microscope and the data was analyzed using imaging software. The fluorescence intensity on the structured surfaces was higher than planar surfaces. This method will open a new wealth of applications to functionalize proteins that have desired functional groups for biomedical applications.

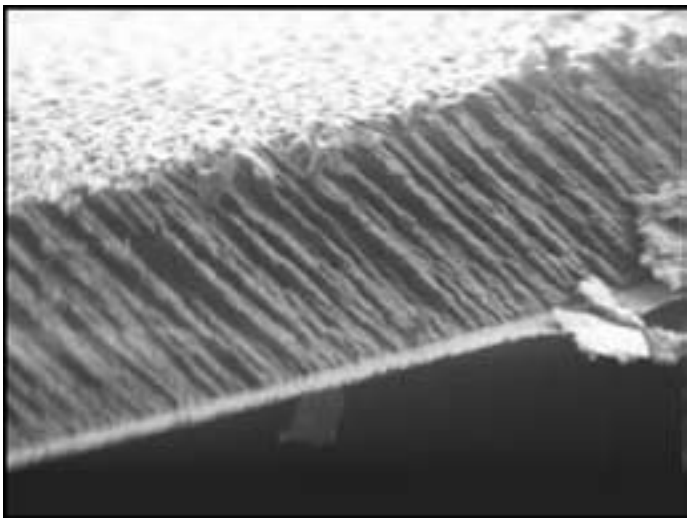

Figure 1: Cross sectional SEM image of a structured PPX film [2].

Introduction

Nanostructured poly(p-xylylene) (PPX) films are of great interest because of their unusual physical and chemical properties such as surface chemistry, morphology, and topology [1]. Nanostructured PPX films have increased surface area which enhances the efficiency of functionalization, and this is the significant difference between a planar and structured surface (Figure 1) [2]. Planar surfaces have functional groups only on the top surface whereas structured surfaces have spaces between the columns of porous polymer strands, which provide more functional groups available for attachment to proteins.

Experimental Procedure

Surface functionalization was achieved by placing the films into a flame dried 50 mL round-bottom flask. First 5 mL of anhydrous toluene, 30 μL of HMDI, and a small amount of catalyst (di-n-butyl tin dilaurate) were added to the flask and the top was capped. The reaction was let go for 4 hours. The film was removed from the flask, washed subsequently with toluene and placed in the desiccator to dry for 20 minutes.

GFP coupling to the surfaces was achieved by measuring 5 mL of GFP solution into a 50 mL round-bottom flask. The film in the desiccator was removed, placed into the flask, submerged, and the flask was capped. The reaction was let go overnight. The film was removed from the flask and placed in the desiccator to dry for 20 minutes. The film was removed from the desiccator, washed subsequently with deionized water and placed in the desiccator to dry. The schematic of protein coupling onto a functionalized structured PPX surface is shown in Figure 2.

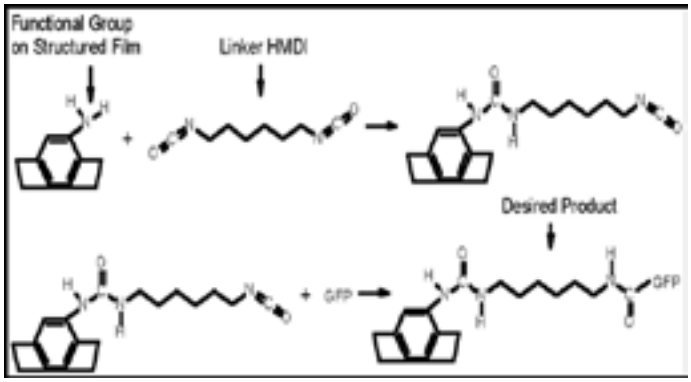

Figure 2: Schematic of protein coupling to PPX surfaces.

GFP imaging was performed using the Olympus Fluoview 300 confocal laser scanning microscope with a single-line 488 nm blue laser using the 40X oil objective. The intensity per field analysis was performed using ImagePro Plus 5.0 [3].

Results and Conclusions

Using the crosslinking agent (HMDI) surface coupling between the reagent and the amino groups on the film was achieved. To characterize the surface of the film, it was run on the FT-IR spectrometer and the resulting spectrum showed 2 peaks that were indicative that the surface coupling reaction linked the amino surface to the coupling reagent (HMDI). The spectra of the unreacted film and HDMI coupled film is shown in Figure 3. The IR spectrum shows an amide bond peak (between 1630-1695 cm^{-1} for the C = O stretching and between 3300-3500 cm^{-1} for a secondary amine). An isocyanate peak at 2200 cm^{-1} is also observed.

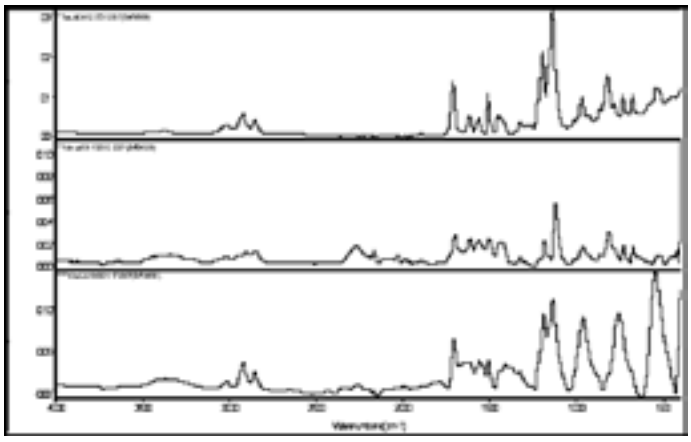

Figure 3: IR spectra: amino film (bottom line), amino film with HMDI (middle line), amino film with GFP (top line) [3].

Next, GFP was attached to the free isocyanate group on the surface. In addition to the fluorescence imaging of PPX surfaces, an IR spectrum confirmed the coupling of GFP to the surface (Figure 3). The spectrum shows that the free isocyanate group has reacted with the GFP.

The GFP intensity was measured in four different conditions using the confocal microscope: (i) a planar PPX-$COCF_3$-NH_2 surface where the GFP is linked with HMDI (planar-chemisorption); (ii) a structured PPX-$COCF_3$-NH_2 surface where the GFP is linked with HMDI (structured-chemisorption); (iii) a planar PPX-$COCF_3$-NH_2 surface where the GFP is adsorbed to the surface without a linker (planar-physisorption); and (iv) a structured PPX-$COCF_3$-NH_2 surface where the GFP is adsorbed to the surface without a linker (structured-physisorption). The fluorescence intensity results are shown in Figure 4 [3].

Figure 4 shows that nanostructured PPX films have higher intensities compared to planar PPX films. It was also observed

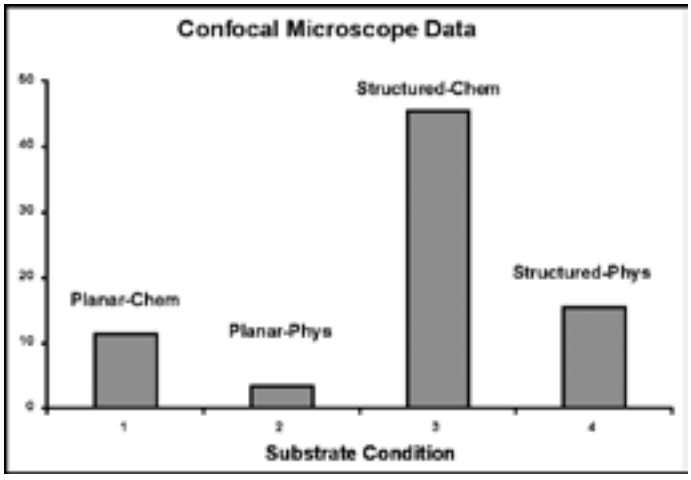

Figure 4: Fluorescence intensity results.

that GFP physisorption on nanostructured PPX films is higher than planar PPX films. This is due to the increased surface area and the porosity of nanostructured PPX films. However, the overall GFP attachment is highest when the GFP is chemisorbed to the nanostructured PPX surface. Novel surface properties can be obtained by coupling reagents attached to the structured PPX film. Therefore, the surface may be incorporated into medical devices or other engineering device applications [3].

Future Work

Another proposal would be to functionalize nanostructured PPX surfaces with RGD peptides, seed cells onto the film and monitor the cell growth. The amino acid sequence of RGD interacts with integrin receptor sites and is found in the extracellular matrix; therefore, it is suggested that cells would be highly attracted to the RGD peptides on the surface and increase cell growth.

Acknowledgments

I would like to thank Dr. Melik C. Demirel, Dr. Serhan Boduroglu, the National Nanotechnology Infrastructure Network REU Program, the NSF, and the Penn State Nanofabrication Facility staff and coordinators.

References

[1] Cetinkaya, M., Boduroglu, S., Demirel, M.C. "Growth of Nanostructured Thin Films of Poly(p-xylylene) Derivatives by Vapor Deposition", Polymer, Vol.48, pg. 4130-4134, (2007).

[2] Demirel, M.C., Boduroglu S., Cetinkaya, M., Lakhtakia, A. "Spatially Organized Free-Standing Poly(P-xylylene) Nanowires Fabricated by Vapor Deposition", Langmuir, Vol. 23, pg. 5861-5863, (2007).

[3] Mangan, A., Boduroglu, S., Demirel, M.C. "Protein Functionalization of Structured Poly(p-xylylene) Films", Materials Science and Engineering:C, submitted, (2007).

Fabrication of a Polymeric Microfluidic Device with Inkjet-Printed Silver Electrodes for Electrokinetic Bioparticle Characterization

Brandon Noia

Biomedical and Electrical and Computer Engineering, Duke University

NNIN REU Site: Cornell NanoScale Science & Technology Facility, Cornell University
NNIN REU Principal Investigator: Prof. Brian Kirby, Mechanical and Aerospace Engineering, Cornell University
NNIN REU Mentor: Benjamin Hawkins, Biomedical Engineering, Cornell University
Contact: brn2@duke.edu, bk88@cornell.edu

Abstract

We are developing an inkjet printing technique for patterning electrodes on polymeric substrates to create microfluidic devices for bioparticle applications. Electrode deposition is important for actuating electrokinetic phenomena in microfluidic devices, and polymeric substrates are becoming increasingly common. Dielectrophoretic (DEP) forces are induced via application of a spatially non-uniform electric field and are directly dependent on the sign and magnitude of the Clausius-Mossotti factor. Accurate characterization of particle response when subject to spatially varying electric fields is essential for successful implementation of DEP-based particle sorting and manipulation techniques. We propose a microfluidic device that will (a) characterize Clausius-Mossotti factors for biologically relevant particles and media, and (b) allow for easy and inexpensive fabrication outside of a clean room environment. Particle characterization is conducted using an interdigitated electrode design in a polymeric microchannel. A Dimatix inkjet printer is used to deposit micro-scale electrodes onto Zeonor 1020R using a silver nano-ink (PChem Assoc.). Electrode resolutions of approximately 70 μm have been accomplished using these techniques, which are compatible with applications on a biological scale. The inkjetting protocols developed allow for fast, inexpensive fabrication of our device and rapid prototyping for future research.

Summary

We are developing inkjet printing techniques for the rapid prototyping and manufacture of polymeric microfluidic devices that require on-device electrodes. Microfluidic devices have been produced utilizing DEP forces for particle sorting [1]. Proper functioning of these devices requires accurate characterization of DEP mobility. We desire a DEP characterization device that is cheap and easy to manufacture outside of a clean room environment. Cyclo-olefin copolymer substrates, such as Zeonor, are ideal for this application since they are inexpensive and mechanically resilient. The deposition of highly conductive electrodes on these substrates is necessary to generate locally non-uniform electric fields.

Dielectrophoretic forces are felt by mobile, polarizable particles subject to spatially-varying electric fields. Analytical modeling of these forces is possible when idealized particles are considered. However, accurate modeling becomes difficult when dealing with biological particles such as cells, which are of non-uniform shape and composition, and are subject to multiple double-layer effects. The magnitude and sign of the DEP force is dependent on the Clausius-Mossotti factor (f_{cm}) (Figure 1). This factor measures the difference in complex permittivity ($\tilde{\varepsilon}$) between a particle and a medium in which it is suspended. The complex permittivity is a relation of the permittivity (ε) and frequency-dependent conductivity (σ) of a given material. Under a negative DEP force, a particle will be repelled from regions with a high electric field, whereas positive DEP corresponds with movement toward higher electric fields.

$$\left\langle \vec{F}_{DEP} \right\rangle = \pi \varepsilon_m a^3 \,\mathrm{Re}\left[f_{CM}\right] \nabla \left| \vec{E} \right|^2$$

$$f_{CM} = \frac{\tilde{\varepsilon}_p - \tilde{\varepsilon}_m}{\tilde{\varepsilon}_p + 2\tilde{\varepsilon}_m}$$

$$\tilde{\varepsilon} = \varepsilon + \frac{\sigma}{j\omega}$$

Figure 1: Equations for dielectrophoresis and the Clausius-Mossotti factor.

Our proposed device for characterizing DEP mobility relies on interdigitated electrodes crossing a microfluidic channel (Figure 2). The electrodes alternate positive and negative to create a non-uniform electric field. By varying voltage amplitude at a given frequency and known flow rate, a graph of the trapping voltages against drag and sign of the DEP force can be obtained.

Electrode deposition was achieved on Zeonor 1020R using a Dimatix Materials Printer (DMP-2800), a tabletop inkjet printer. To be jettable, an ink must not have large agglomerates of particles or settle quickly, and should have low viscosity and surface tension. Modifications were made to the PFI-300 (PChem Assoc.) silver ink to produce a jetting, conducting ink. The pH of the ink was raised to 5.4 using a solution of 5:1 deionized (DI)

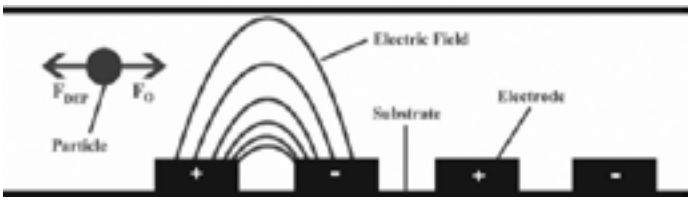

Figure 2: Side view of the proposed dielectrophoretic mobility characterization device, where F_0 denotes Stokes' drag force.

water to ammonium hydroxide, altering interparticle potentials and resulting in smaller aggregations. The ink was then filtered through a 0.8 μm filter to remove any remaining large particles. DI water could then be added to increase fluid volume and decrease concentration. Solutions of up to 5:1 DI water to ink were tested, with 1:2 yielding the best results with regards to jettability (Figure 3). The surfactant Triton X-100 was added in small amounts to later inks prior to filtering, which resulted in better electrode conductivity. A ratio of 40:1 Triton X-100 to ink resulted in the most effective jetting while maintaining conductivity.

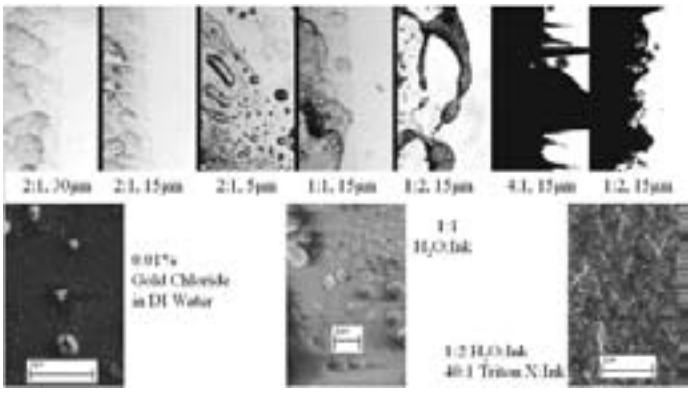

Figure 3: Various inks printed on a Zeonor 1020R substrate given in ratio of DI water to ink.

The Dimatix inkjet printer had to be tuned for functional ink jetting. Even after filtering, particle settling and ink evaporation resulted in clogging at the nozzle head. A 0.1 second purge cycle, during which a pressure increase forcefully pushed ink through the nozzles, was run every 300 seconds to remove clogs and keep the ink fresh. No heat was applied to the nozzle or to the Zeonor substrate, and voltage amplitudes were adjusted specifically for each nozzle.

Using these techniques and materials, we were able to produce promising results. Conductive silver electrodes were successfully printed onto a Zeonor substrate. We were only able to resolve the printed silver features down to about 1 mm. This was due in part to some variability in the angle at which the silver droplets would leave the print head. We hope to be able to produce smaller resolutions in the future. The device has been printed on paper using a model ink with 90 μm resolution (Figure 4), which is sufficient to actuate DEP forces in biological

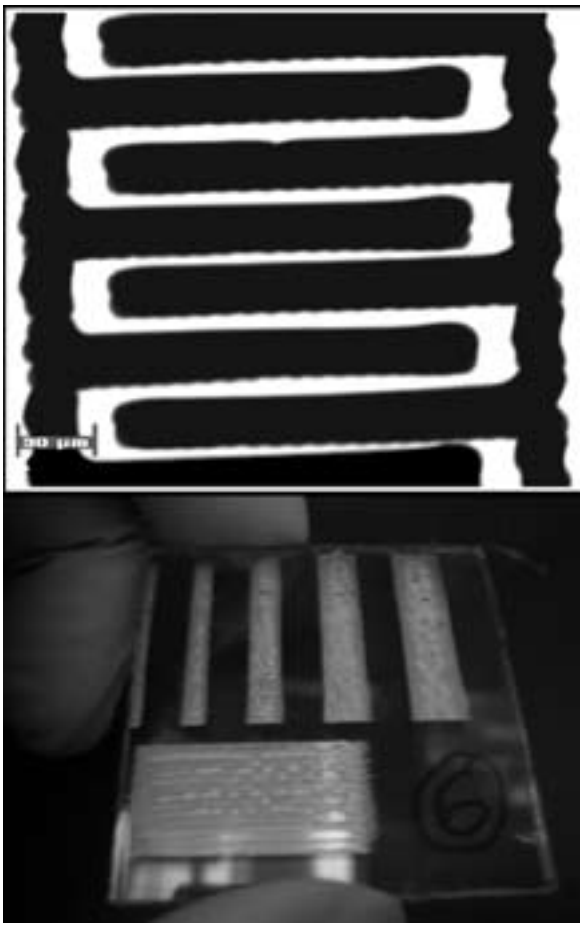

Figure 4: Top; High resolution printing of DEP characterization device with model ink on paper. Bottom; Ihe electrodes printed on Zeonor, with researcher's hand for scale. Ihe electrodes all conduct along their entire length and are of different widths. The far left is 1mm wide.

particles. Electrode adherence to the Zeonor substrate has been tested with several solvents, including ethanol, isoporopynol, and acetone. Adherence can be improved by depositing a 3-Mercaptopropyltrimethoxysilane monolayer onto the Zeonor substrate prior to electrode printing, though this is necessary only if the electrodes are subject to relatively large mechanical stresses. We believe that our inkjet manufacturing techniques will allow electrode-based microfluidic devices to be easily produced, paving the way for future rapid prototyping applications.

Acknowledgements

Benjamin Hawkins and Brian Kirby for their guidance and support. The National Nanotechnology Infrastructure Network Research Experience for Undergraduates Program, National Science Foundation, and the Intel Foundation for funding. All the staff and faculty at the Cornell NanoScale Facility.

References

[1] Hawkins, B.G., Smith, A.E., Syed, Y.A., and Kirby, B.J., Anal. Chem., 2007.

Three-Dimensional Flow-Focusing in Microfluidic Devices

Sasha Perkins

Materials Science and Engineering, University of Florida

NNIN REU Site: Cornell NanoScale Science & Technology Facility, Cornell University
NNIN REU Principal Investigator: Dr. Carl Batt, Department of Food Science, Cornell University
NNIN REU Mentors: Matthew Kennedy, Electrical Engineering, Cornell University;
Clarissa Lui, Biomedical Engineering, Cornell University
Contact: slperks@ufl.edu, cab10@cornell.edu, mjk67@cornell.edu, csl42@cornell.edu

Introduction

Over the recent years, an interest in hand-held devices applicable in forensics and biological applications which need fast and efficient data analysis has increased through the research of lab-on-a-chip systems and bead-based detection technology [1]. In this research, three-dimensional hydrodynamic flow-focusing has been obtained in a two layer polydimethylsiloxane (PDMS) microfluidic device. Using sheath flow, this device employs a microfluidic manifold to focus fluorescent particles in three dimensions ensuring that the particles will be confined to the focal volume of the optical fibers embedded into the deoxyribonucleic acid (DNA) analysis microchip. The flow-focusing performance of this device has been characterized as a prelude to its integration into a hand-held particle-counter microchip. The geometry of the inputs and liquids of different viscosities were tested in order to achieve the most effectively focused stream. Through laser scanning confocal microscopy, the focused stream, using polyvinyl alcohol as a sheath fluid, was found to have a width of about 15 μm and a height of about 25 μm. In addition, successful calcium cross linking of sodium alginate microfibers was seen in this device with confocal microscopy through the diffusion of sheath fluid into the focused stream, within a channel of 100 μm by 100 μm cross section.

Experimental Procedure

The microfluidic device was constructed through two layer soft lithography [2]. Channels of 100 μm depth and 100 μm width were fabricated by spinning SU-8 100 photoresist onto blank silicon wafers at 2900 rpms for 35s. The distance between the inlets in the patterns did not affect the focused stream as much as the dimensions of the actual channels. After spinning the resist on the silicon wafers, the wafers were pre-baked for 10 min at 65°C and then soft-baked for 30 min at 95°C. The wafers were exposed to ultraviolet light through a patterned chrome mask at 600 mJ/cm^2 for 8s, three times. The exposed wafers were then baked for 10 min at 95°C [3]. After developing the wafer, polydimethylsiloxane (PDMS) was poured on the patterned silicon wafers and cured in an oven for 2 hr at 60°C. After curing the PDMS, the two layers of PDMS were placed into an oxygen plasma asher and then aligned under a contact aligner. Polyethylene tubing was attached to the inlets and outlets of the flow cell with epoxy. A final product of a flow cell, seen in Figure 1, shows the flow cell before being characterized.

Different geometries and different solutions of various viscosities, such as ethylene glycol, glycerol, Tris-HCL with EDTA (TE buffer), and polyvinyl alcohol were tested as sheath fluid and sample flow solutions to see the size and location of the focused stream with the fluorescent beads. The rate of the syringe pump was also considered. The velocity of the beads on the focused stream was also calculated to see how fast the beads could be detected. The focused stream was characterized under a Leica confocal microscope.

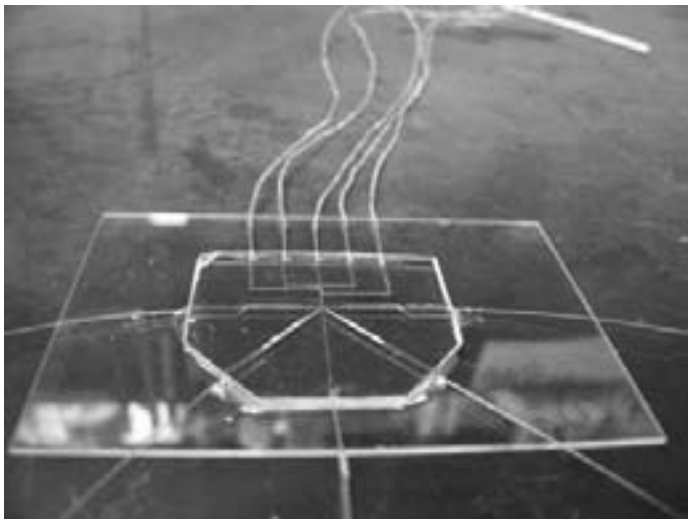

Figure 1: Assembled flow cell with channels that have a cross section of 100 µm by 100 µm.

Results and Conclusions

The most effective pattern was designed with a symmetrical setting with the sheath fluid channels joining the central channel from both sides and from the top and shortly after, sheath fluid would connect from both sides and the bottom as shown in Figure 2. The dimensions of the side sheath fluid channels were 50 μm wide, while the central channel was 100 μm wide. TE buffer

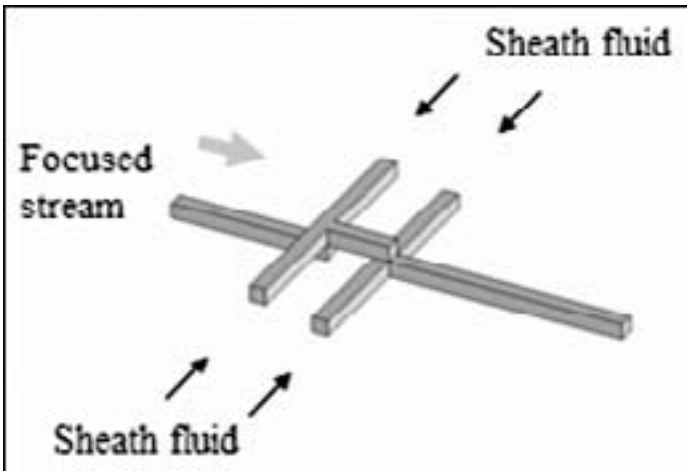

Figure 2: Schematic drawing of flow cell with 50 μm wide central channel and 100 μm wide sheath fluid channels.

(with 80% glycerol to increase its viscosity) was used to carry the sample and flowed at 3 μl/min. (TE buffer is commonly used as a buffer for DNA.) Polyvinyl alcohol was pumped as sheath fluid at 13 μl/min. This version provided a focused stream with a width of about 15 μm and a height of about 25 μm in the center of the central channel as shown in Figure 3. A more circular focused stream was characterized because the side channels did not provide high pressure in the central channel which would cause the focused stream to be more oblong.

The velocity of 5 μm-in-diameter fluorescent beads was about 10 cm/s ± 2 cm/s in the focused stream. The velocity of the beads was calculated based on 20 streak-length measurements using pixel size and the rate at which the images were scanned. Also, due to the diffusion caused in the central channel in the flow cells designed, alginate microfibers were fabricated using sodium alginate in the sample flow and calcium chloride as sheath fluid. The sample flow was pumped at 1 μl/min and the sheath fluid was pumped at 333 μl/min [4].

Future Work

Particles need to be analyzed to test the usability of the microfluidic device, by attaching the optical fibers in the microchip. Some work was done during this research to create bioluminescent microfibers using Renilla Luciferase in the sample flow and adding coelenterazine substrate to the microfibers after making them in the flow cell. However, the glow was not able to be seen.

Acknowledgements

Intel Foundation, National Nanotechnology Infrastructure Network, Cornell NanoScale Science and Technology Facility, National Science Foundation, Dr. Carl Batt, Matthew Kennedy, and Clarissa Lui.

References

[1] Gardeniers, J. G. E, et al. "Lab-on-a-chip systems for biomedical and environmental monitoring", Analytical and Bioanalytical Chemistry, Vol.378, Number 7, Pages 1700-1703 (April 2004).

[2] Sundararajan, N. et al. "Three-Dimensional Hydrodynamic Focusing in Polydimethylsiloxane (PDMS) Microchannels", Journal of Microelectromechanical Systems, Volume 3, No. 4, Pages 559-568 (August 2004).

[3] "NanoTM SU-8." MicroChem. Rev 2/02. http://microchem.com/products/pdf/SU8_50-100.pdf

[4] Shin, S et al. "On the Fly Continuous Generation of Alginate Fibers Using a Microfluidic Device", June 6, 2007. Langmuir 2007, 23, 9104-9108, ACS Publications. Retrieved from http://pubs.acs.org/cgi-bin/article.cgi/langd5/2007/23/i17/pdf/la700818q.pdf.

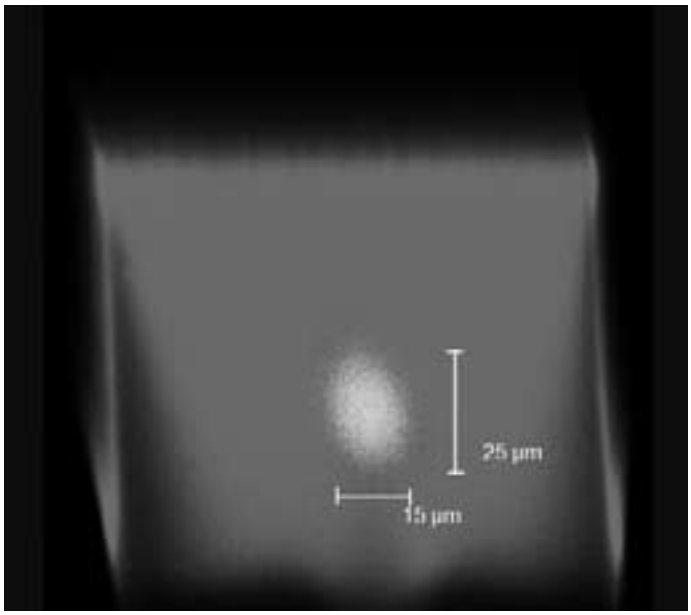

Figure 3: Cross-section view of focused stream under confocal microscope. The focused stream had a 25 μm height and a 15 μm width.

Epitaxial Growth of Germanium and Silicon Nanowires by Chemical Vapor Deposition

Christopher J. Hainley

Mechanical Engineering, The University of Portland

NNIN REU Site: Microelectronics Research Center, The University of Texas at Austin
NNIN REU Principal Investigator: Prof. Emanuel Tutuc, Electrical Engineering, The University of Texas at Austin
NNIN REU Mentor: Kamran Varahramyan, Electrical Engineering, The University of Texas at Austin
Contact: chainley@up.edu, etutuc@mer.utexas.edu

Abstract

Germanium (Ge) and silicon (Si) nanowires promise to become useful in the further miniaturization of integrated circuits because they allow for precise structuring at scales of 20-50 nm [1]. In order to accurately characterize the electrical properties of nanowires, a necessary ingredient to any semiconductor device integration route, a reproducible process to fabricate them must be established. Chemical vapor deposition (CVD) presents itself as a useful technique in the fabrication of nanowires by utilizing the vapor-liquid-solid (VLS) mechanism, which also allows for the heterogeneous integration of semiconductor nanowires.

Using 2% diluted SiH_4 and GeH_4 in He as precursor gases in controlled pressure and temperature conditions, and with gold (Au) nanoparticles as catalysts for VLS wire growth, epitaxial growth of Ge and Si nanowires on silicon <111> wafers is demonstrated.

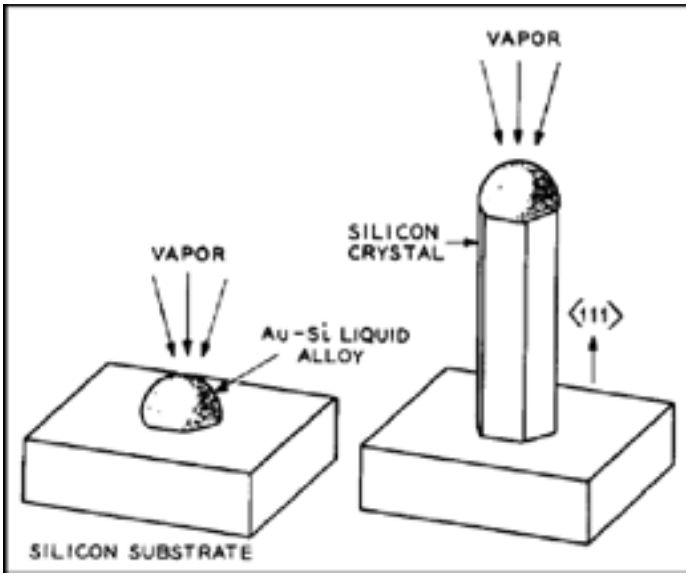

Figure 1: VLS whisker growth [1]. (a) Initial Au droplet absorbs precursor vapor and becomes supersaturated Si-Au alloy. (b) Si from the supersaturated droplet migrates to the crystal lattice of the substrate and forms a silicon whisker in the <111> direction.

Introduction

The VLS growth mechanism of highly anisotropic silicon crystals, or "whiskers," was introduced by Wagner, et al. (Figure 1) [2]. Their study concluded that whisker growth required an impurity and that supersaturated liquid alloy droplets existed on the whisker tips. Subsequent studies have demonstrated reduced whisker sizes down to the nanoscale in silicon [3,4], germanium [5], and III-V compounds [6].

CVD of silicon and germanium nanowires utilizes VLS transport, in which a gold catalyst provides lower dissociation energy (rather than the bare substrate) for the decomposition of the carrier gas, H2, from the precursor, Si or Ge, in the following reactions at the vapor-liquid interface:

$$SiH_4(g) \rightarrow Si + 2H_2(g)$$
$$GeH_4(g) \rightarrow Ge + 2H_2(g)$$

The semiconductor material then diffuses through the droplet, which is liquid at growth temperatures as it forms an eutectic alloy with the Au. Once supersaturated, the semiconductor atoms are incorporated into the crystal lattice at the liquid-solid interface, with epitaxial growth in the <111> direction.

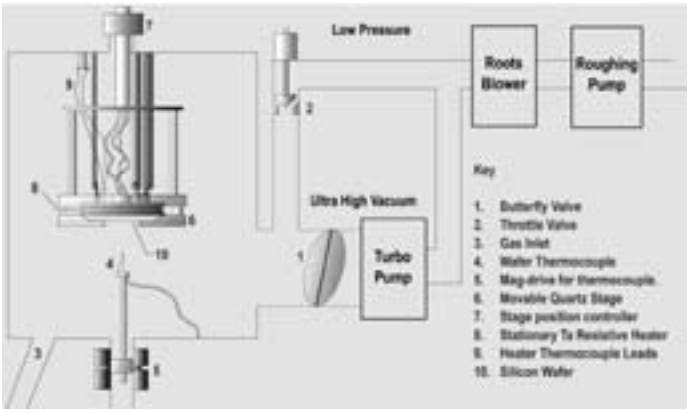

Figure 2: Schematic representation of the CVD apparatus used in the study.

Process

The growth apparatus (Figure 2) used here was a cold wall CVD reactor containing a tantalum (Ta) resistive heater encased in quartz, with operating pressure range of 10^{-8} Torr to 20 Torr. A 1/4 inch gap existed between the wafer and the heater, causing a difference in heat transfer when a precursor gas was or was not present. Thermocouples directly contacting the filaments monitored heater temperatures. Heater voltages and current were also monitored. An unfixed thermocouple measured the wafer temperature.

Silicon <111> wafers were prepared by a 45 second hydrofluoric acid (HF) dip, rinsed, and transferred within 10 minutes to a high vacuum ($\sim 5.0 \times 10^{-6}$ Torr) metal deposition chamber. After depositing a 10Å gold (Au) film, the wafer was transferred into the CVD chamber (approximately 1 hr after HF dip).

Germanium nanowires were produced in a two step process. First, the wafer temperature was raised to 400°-450°C for 5-10 minutes in order for the Au film to coalesce into droplets. The wafer temperature was then lowered within 30 min to a specified temperature, ranging from 230° to 280°C, and GeH_4 was introduced. The reactor pressure was maintained at 10 Torr.

Similarly, silicon nanowires were produced by raising the wafer temperature to 530°-580°C in 60-90 min and introducing SiH_4 into the chamber, maintaining reactor pressure at 10 Torr.

Results

In order to establish Ge wire growth, a series of growths at substrate temperatures of 300°C, 275°C, and 240°C were performed. High temperatures produced tapered wires, a result of the combination of axial and conformal growth. Figure 3 shows the scanning electron microscopy (SEM) data of Ge wire growth carried out at a pressure of 10 Torr and a substrate temperature of ~ 240°C. The measured nanowire growth rate was ~ 1.5 μm/hr, with a nanowire aspect ratio of 33:2.

Si wires were produced at a growth pressure of 10 Torr, with wafer temperatures of 580°C, 550°C, and 530°C. Epitaxial growth was less pronounced than in the Ge growths. Figure 4 shows, at 2 hours, a silicon wire growth maintained at a pressure of 10 Torr and wafer temperature of ~ 580°C. The axial nanowire growth rate was ~ 5 μm/hr, with a nanowire aspect ratio of 40:1. The wires grown at a higher temperature showed a significant surface roughness.

Future Work

The current apparatus separates the heater from the wafer, which results in a wafer temperature dependence on the precursor pressure as well as a large temperature gradient between the heater and wafer. To mitigate these issues, a replacement boron nitride heater will be installed directly contacting the wafer, also allowing for higher wafer temperatures during growth.

Once grown, the nanowires will be deposited onto dielectric wafers, and we will fabricate three terminal, back-gate devices with metal contacts, allowing electronic properties to be characterized.

Acknowledgments

I would like to thank Prof. Tutuc, Kamran Varahramyan, Junghyo Nah, En-shao Liu, and James Ferrara for their help in familiarizing me with the project, Ms. Melanie-Claire Mallison and Ms. Jean Toll for their work in helping me to participate in this program, and National Science Foundation, the National Nanotechnology Infrastructure Network REU Program, and Dr. Banerjee for assisting in funding this research.

References

[1] H.J Fan, P. Werner, M. Zacharias, Small 2006, 701.
[2] R. S. Wagner, W. C. Ellis, Appl.Phys.Lett. 1964, 4, 89.
[3] Y. Wu, R. Fan, P. Yang, Nano Letters 2002, 2, No. 2, 83.
[4] Y. Wu, P. Yang, J.Am. Chem. Soc. 2001, 123, 3165.
[5] H. Dai, D. Wang, Angew. Chem.Int.Ed. 2002, 41, No. 24, 4783.
[6] X. Duan, C.M. Lieber, Adv.Materials, 2000, 12, No. 4, 298.

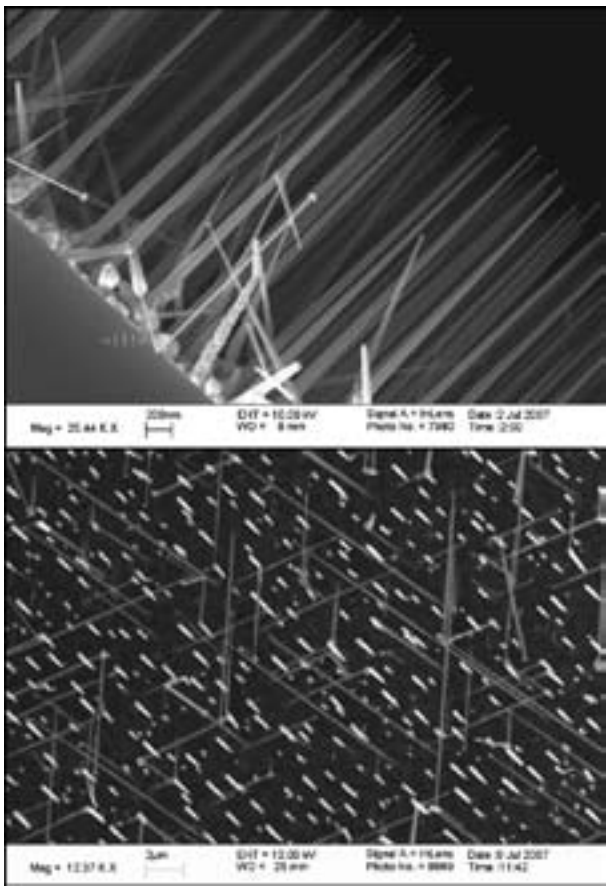

Figure 3, top: Cross-sectional SEM image of showing growth along the three <111> directions, predominately vertical, demonstrating epitaxial Ge nanowire growth on a Si substrate.

Figure 4, bottom: Top down SEM image of silicon nanowires. The three <111> growth directions, aside from the normal to the substrate, can be clearly seen.

Parametric Investigation of Picoliter Droplet Interfacial Tension using a Microfluidic Device

Kevin Kelley

Chemistry and Physics, Pomona College

NNIN REU Site: Center for Nanotechnology, University of Washington
NNIN REU Principal Investigator: Dr. Daniel Chiu, Chemistry, University of Washington
NNIN REU Mentor: Gavin Jeffries, Chemistry, University of Washington
Contact: kevin.kelley@pomona.edu, chiu@chem.washington.edu

Abstract

The transport and detection of nanoscale objects has become an essential part of sub-cellular biochemical research and with it the use of droplets as controllable confined volumes. To fully understand and utilize the chemical environment of droplet systems, it is necessary to elucidate the physical properties of the droplet interface, namely through studying system parameters such as the interfacial tension. The interfacial tension (IFT) is an important physical factor for designing and calculating fluidic dynamics in microfluidic droplet systems. In fluid dynamics, the capillary number (Ca) represents the relative effect of viscous forces versus surface tension acting across an interface between two immiscible liquids. Using Ca, it is possible to simulate fluidic channels and better aid in design, and explain phenomenon.

Introduction

This project seeks to investigate changes in the interfacial tension as a function of the following factors: ion concentration, surfactant type, surfactant concentration, and oil type. The interfacial tension of numerous individual droplets was measured by examining the deformation and restoration dynamics of the drops through a microfluidic channel constriction. Droplet generation parameters were independently varied and results were captured using fast imaging techniques. This video data was analyzed using a mathematical model of droplet dynamics, coded with the program Labview, which calculated the interfacial tensions.

These results will attempt to further clarify the quantitative relationship among the key factors, and should provide general trends for the interfacial tension as system variances are made, allowing future research the ability to predict the effect on droplet formation when used in microfluidic devices for bio-analytical applications.

Design and Fabrication

This microfluidic approach to measure IFT observes the response of individual droplets in a carrier fluid to deformation. A microfluidic tensiometer device should; (a) produce controllably sized droplets, (b) accelerate the droplets, and (c) induce drop deformation and restoration. We designed a system to generate aqueous plugs using a T-junction with an aqueous inlet and an oil inlet. To achieve independent control of the inter droplet distance as well as the droplet velocity, they are accelerated via flow focused oil lines coming from a single inlet.

Droplet deformation occurs in a flow field generated by a microchannel constriction. We experimentally determined that a constriction width of 200 μm induces modest deformations, to which the Taylor theory applies. A thickness of about 200 μm throughout was determined to be optimal.

Silicon masters patterned with SU-8 photoresist were fabricated using photolithography as described in detail elsewhere. Briefly, in order to create channels of 200 μm thickness, it was necessary to successively spin two 100 μm layers of SU-8. These were exposed to UV through a patterned mask, and then developed using propyl glycol methyl ether acetate (PGMEA).

To form the microchannels, the pattern on the master was replicated in poly(dimethylsiloxane) (PDMS) and then sealed with oxygen plasma to a coverslip with a thin layer of spin-coated PDMS. It was necessary to coat the coverslip with PDMS because the generation of aqueous droplets required channels with four hydrophobic walls to prevent wetting by the aqueous phase of the walls of the channel.

To address the microchannels, access holes to the channels were punched with a 16-gauge needle. Polyethylene tubing (PE 100) was inserted into the access holes and then attached to a microinjector, with the aqueous and two oil inlets having their own respective injector.

Parameters Tested

The continuous phase type and its viscosity have significance on the experiment. High viscous oils generally make very stable small droplets easier than low viscosity oils. The compatibility of the oil with the sample is also important since biological samples require low mass transfer between the oil and water and vice versa to maintain droplet constant concentrations.

Surfactants are known to reduce the interfacial tension at the oil-water interface and are necessary to create stable droplets in most systems. Similarly, different types of surfactants have varying compatibilities with both the continuous and dispersed phases.

When using biological samples, the pH of the system becomes important. The ion concentration is dependent on the pH. An investigation of the affects of ion concentration on the affects of interfacial tension is thus important.

Results and Conclusions

Interfacial tension was calculated by using a custom built Labview program that would track the vertical deformation of the droplets as a function of position. By measuring the time for drop shape relaxation, the interfacial tension could be calculated.

The results demonstrate that interfacial tension correlates positively with oil viscosity, negatively with surfactant concentration, and negatively with ion concentration (Figures 1-3). The three surfactant types tested (Gran Surf 77, Tween 20, and Span 85) were found to have no correlation with the interfacial tension (not shown). It is well known that surfactant concentration correlates negatively with interfacial tension. The fact that ion concentration correlates negatively with interfacial tension was a surprising result. Intuitively, we would expect that an increase in ions would cause the water phase to be more dissimilar to the oil phase, which would cause an increase in interfacial tension.

In conclusion, we successfully developed a microfluidic device that rapidly measured interfacial tension of picoliter droplets, and have shown that surface active components indeed affect the interfacial tension. These results can be used to extrapolate interfacial tension values so as to extrapolate the optimal microfluidic chip design

Acknowledgements

I would like to thank NSF and the National Nanotechnology Infrastructure Network REU Program for making this all possible. Special thanks to my PI, Dr. Daniel Chiu, and especially my mentor, Gavin Jeffries, for all his time and help.

References

[1] Cabral, J.T., and Hudson, S.D.; "Microfluidic approach for rapid multicomponent interfacial tensiometry"; Lab on a Chip, 6, 427-436 (2006).

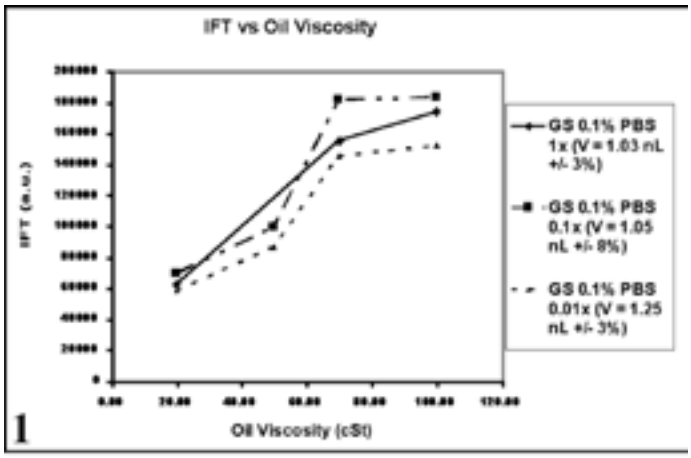

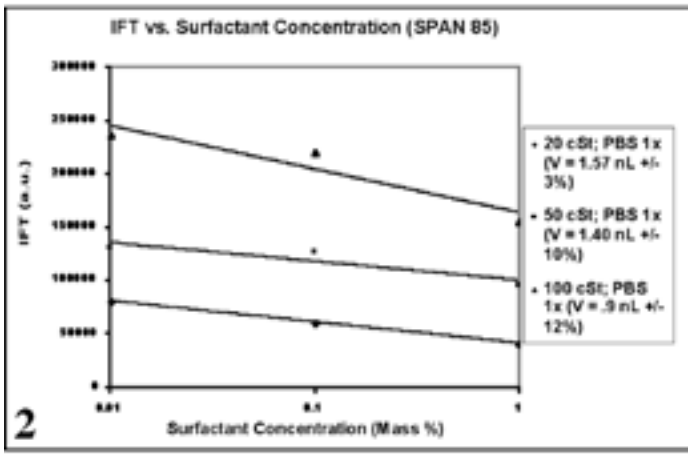

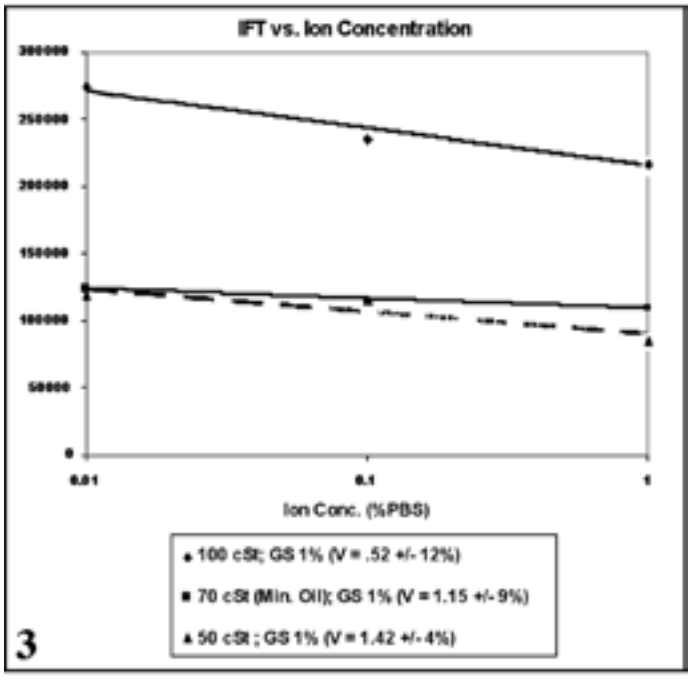

Figure 1: IFT as a function of oil viscosity at three different ion concentrations.

Figure 2: IFT as a function of surfactant concentration for three different oils.

Figure 3: IFT as a function of ion concentration for three different oils.

Rapid Synthesis of Silver Nanowires

Kylee Korte

Chemistry, Bradley University

NNIN REU Site: Center for Nanotechnology, University of Washington
NNIN REU Principal Investigator:Professor Younan Xia, Chemistry, University of Washington
NNIN REU Mentor: Dr. Sara Skrabalak, Chemistry, University of Washington
Contact: kkorte@mail.bradley.edu, xia@biomed.wustl.edu, skrabs@u.washington.edu

Abstract

The presence of either copper(I) or copper(II) chloride in the polyol reduction of silver nitrate facilitates the production of silver nanowires. Silver nanowires have applications in many areas, including electronics and catalysis. These wires are produced quickly (in approximately one hour), with the synthesis being easily performed in disposable glass vials, using only pipettes to deliver reagents. Specifically, silver nitrate is reduced by ethylene glycol in the presence of poly(vinylpyrrolidone) (PVP) and copper(II) chloride. PVP acts as a stabilizing agent, while the copper chloride likely controls the rate of silver(I) reduction and initial seed formation. Our results indicate that both the copper and chloride ions are necessary to synthesize the wires; otherwise, ill-defined silver particles are formed. Scanning electron microscopy (SEM) has been used to characterize the wires.

Introduction

Metallic nanostructures have a wide range of properties and applications. These properties and applications are determined by the shape, size, structure, and composition of the nanostructures. The presence of various ions has been shown to influence the shape and size of metallic nanostructures produced via the polyol method. For example, previous research done by the Xia group has shown that the presence of iron(II) or iron(III) ions in the polyol synthesis facilitates the growth of silver nanowires or cubes, depending on the concentration of the iron ions [1]. A study of copper salts has shown that the presence of copper(I) or copper(II) chloride in the polyol reduction of silver nitrate allows for the production of silver nanowires, which can be used in many areas, including electronics and catalysis [2].

Experimental Procedure

The polyol method involves the reduction of a metal salt precursor by a polyol, a compound containing multiple hydroxyl groups. The polyol used in this synthesis, ethylene glycol, served as both the reducing agent and solvent. 5 mL of ethylene glycol was heated at 150°C for one hour with stirring (260 rpm). This pre-heating was done in disposable glass vials placed in an oil bath. 40 μL of a 4 mM $CuCl_2 \cdot 2H_2O$/ethylene glycol solution was added, and the solution was allowed to heat for 15 minutes. 1.5 mL 114 mM PVP/ethylene glycol was then added to each vial, followed by 1.5 mL 94 mM $AgNO_3$/ethylene glycol. All reagents were delivered by pipette. The reaction was stopped when the solution became gray and wispy, after approximately one hour. The reaction was stopped by submerging the vials in cold water. The product was washed once with acetone and three times with deionized water.

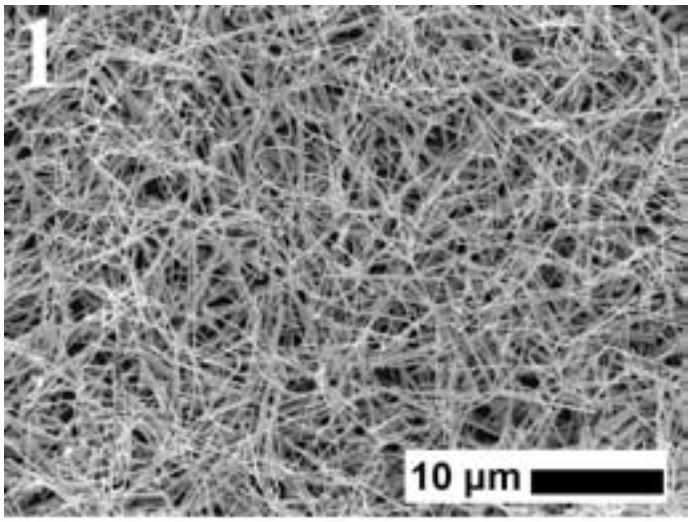

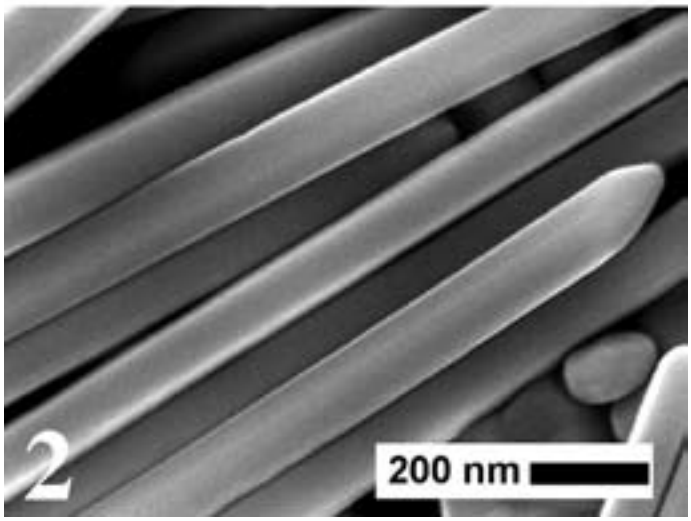

Figure 1: SEM of silver nanowire.

Figure 2: Higher magnification SEM of silver nanowires.

Results and Conclusions:

The produced wires were relatively uniform in shape and size. They had a pentagonal cross-section, as determined by scanning electron microscope (SEM), and were, on average, approximately 10-50 μm in length.

These wires were also present in high yield (approximately 90% relative to other structures) and were produced in approximately one hour after the addition of all reagents. Figures 1 and 2 show SEM images of the wires produced.

One of the advantages of this particular synthesis is its simplicity. To avoid supersaturation of the reaction media and thus particle formation, typically a syringe pump is required to controllably add reagents. Here, we are able to prepare silver wires in high yield without a syringe pump, which may not be available in all laboratories due to costs. The vial setup allows the reaction to be scaled up by simply running the reaction in additional vials. This setup of vials also allows a range of variables, such as concentration or temperature, to be tested at once.

To elucidate the role of copper(II) chloride, several controls were run. Sodium chloride and copper(II) nitrate were used to test the effect of each ion on this synthesis (sodium and nitrate ions are spectators and should have no effect on this synthesis). As shown in Figure 3, when only copper(II) nitrate is present, only particles are produced. Similarly, as shown in Figure 4, when only sodium chloride is present, only particles are produced. However, when both copper(II) nitrate and sodium chloride were added, wires were produced, indicating that both ions are necessary for wire growth.

Previous reports indicate that chloride ions can help stabilize initial silver seeds, preventing agglomeration, while Cl^-/O_2 has been shown to etch seeds [3]. To further investigate the function of copper(II) in this synthesis, further experiments were performed using copper(I) chloride. As with copper(II) chloride, copper(I) chloride facilitates silver wire formation. This result suggests that the redox behavior of the copper additives helps to control the reduction of silver nitrate and avoid initial supersaturation.

Future Work

To better understand this proposed mechanism, trials run in an inert atmosphere are now underway to determine the role of oxygen in this synthesis.

Acknowledgments

Special thanks to my mentor, Sara Skrabalak, for her guidance and support. I would also like to thank Professor Younan Xia, the other members of the Xia group, and Dr. Ethan Allen. This research was supported by the 2007 National Nanotechnology Infrastructure Network Research Experience for Undergraduates and the National Science Foundation. Thank you to all for a memorable summer!

References

[1] Wiley, B., et al; "Polyol Synthesis of Silver Nanostructures: Control of Product Morphology with Fe(II) or Fe(III) Species"; Langmuir, 21, 8077-8080 (2005).

[2] Xia, Y., et al; "One-Dimensional Nanostructures: Synthesis, Characterization, and Applications"; Advanced Materials, 15, 353-389 (2003).

[3] Wiley, B., et al; "Polyol Synthesis of Silver Nanoparticles: Use of Chloride and Oxygen to Promote the Formation of Single-crystal, Truncated Cubes and Tetrahedrons"; Nano Letters, 4, 1733-1739 (2004).

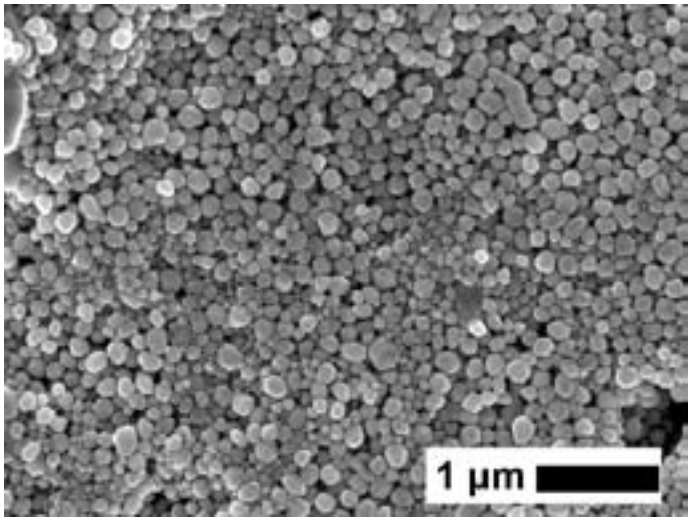

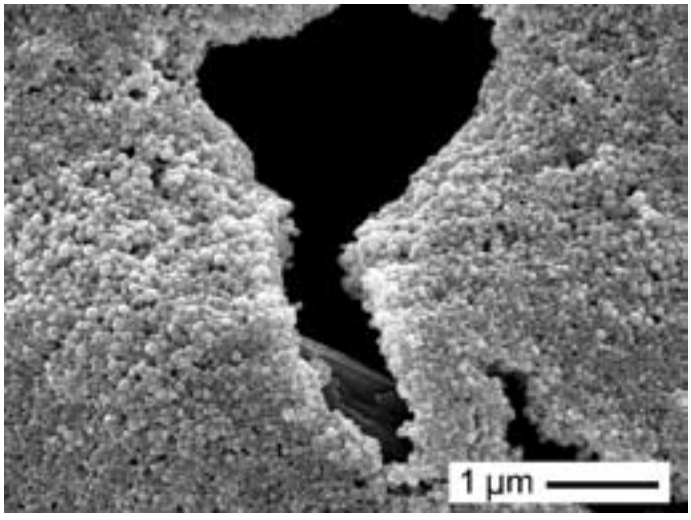

Figure 3, top right: SEM of sample produced in the presence of copper(II) nitrate (no Cl present).

Figure 4, bottom right: SEM of sample produced in the presence of sodium chloride (no Cu present).

Directed Self-Assembly for Post-32 nm Lithography

Brian Lambson

Electrical Engineering, Columbia University

NNIN REU Site: Microelectronics Research Center, Georgia Institute of Technology
NNIN REU Principal Investigator: Raghunath Murali, Microelectronics Research Center, Georgia Institute of Technology
NNIN REU Mentor: Gerald Lopez, Electrical Engineering, Georgia Institute of Technology
Contact: bjl2109@columbia.edu, rm206@mail.gatech.edu

Abstract

Like many large polyaromatic hydrocarbons (PAHs), C96 self-assembles into well-ordered supramolecular structures due to π-π interactions between adjacent molecules. Because densely packed monolayers of C96 fibers are easily obtained on silicon or silicon oxide (SiO_2) via standard deposition techniques such as spin-coating or drop-coating, C96 is an attractive candidate for microelectronics applications. This project explores the possibility of using directed self-assembly to attain long-range ordering of C96 fibers for use in post-32 nm lithography. In this method, top-down lithography defines the pattern placement, and C96 self-assembly defines the pattern line-width. Experimental results demonstrate consistently strong C96 fiber alignment with 250 nm and 125 nm chromium (Cr) trenches, suggesting that with further process optimization, directed C96 self-assembly may be a viable extension of traditional lithography techniques.

Introduction

In lithography, the term "critical dimension" refers to the smallest feature size that can be accurately reproduced using a given technology. If current rates of progress in electronic device scaling are maintained, sub-16 nm dimensions will be reached within the next decade [1]. Optical lithography, currently the standard lithography technique for large-scale semiconductor fabrication, has achieved critical dimensions at the 32 nm node, but rising costs and fundamental limits may restrict its use at future nodes.

We seek to extend traditional lithography for post-32 nm critical dimensions using a technique called directed C96 self-assembly. C96 is a large polyaromatic hydrocarbon (PAH) that self-assembles on silicon or SiO_2 into long fibers 2-3 nm in diameter, as shown in Figure 1. Looking down over the substrate, C96 self-assembly results in a dense two-dimensional fiber network that can serve as an etch mask to transfer the pattern onto the substrate [2]. In this case, the critical dimension of C96 self-assembly is the fiber width. The primary drawback of existing C96 self-assembly methods is that C96 fibers tend to orient randomly, rendering the resulting patterns unusable for many practical applications.

Our objective is to develop a method to control the orientation of C96 fibers. One candidate is directed self-assembly, in which patterned features created by traditional lithography techniques direct the self-assembly of C96 fibers. Top-down lithography defines the pattern placement, and C96 self-assembly defines the pattern line-width. In our experiment, we qualitatively examine the interaction of C96 fibers with patterned metal trenches and determine the degree to which C96 fiber orientation is correlated to trench direction.

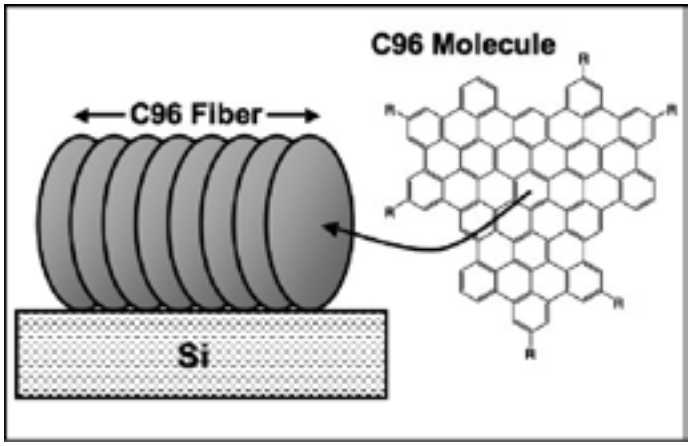

Figure 1: C96 self-assembly mechanism.

Experimental Procedure

A silicon wafer was first patterned via electron-beam lithography (EBL), followed by a metal liftoff. Line/space patterns—parallel lines of fixed width—were patterned onto ZEP 520A resist using a JEOL JBX-9300FS EBL system, with line-widths ranging from 125 nm to 1 μm. After developing the resist, we evaporated 8 nm Cr on the sample and performed a liftoff process using n-methyl-pyrrolidone. The end result was a pattern of parallel Cr trenches, 8 nm deep and 125 nm to 1 μm wide.

C96 deposition was accomplished using one of two methods, dropcast or spincast. In both methods, we first dissolved crystalline C96 in chloroform ($CHCl_3$) at a concentration of 10^{-5} M. Dropcasting involves applying several drops of the C96 solution directly onto a patterned sample and allowing the solvent to evaporate overnight. Spincasting differs from dropcasting in that we spun the sample at 1000 rpm for 60 seconds immediately after depositing the C96 solution, eliminating the need for overnight evaporation.

Before imaging the sample, all C96 molecules that had not bonded covalently to the silicon substrate were removed with chloroform via Soxhlet extraction. Once clean, the sample was imaged using an atomic force microscope (AFM), which allowed us to determine the location and orientation of the C96 fibers. Though the AFM has excellent vertical resolution, lateral resolution is dependent on the width of the probe tip, approximately 25 nm. Therefore, imaged fibers appeared about ten times their actual width of 2-3 nm, limiting our ability to quantitatively analyze the surface patterns.

Results

Samples were prepared using the experimental procedure for Cr line-widths of 1 μm, 250 nm, and 125 nm. Our conclusions are based on qualitative observations regarding the correlation between the C96 fiber orientation and the trench walls, as seen in AFM images.

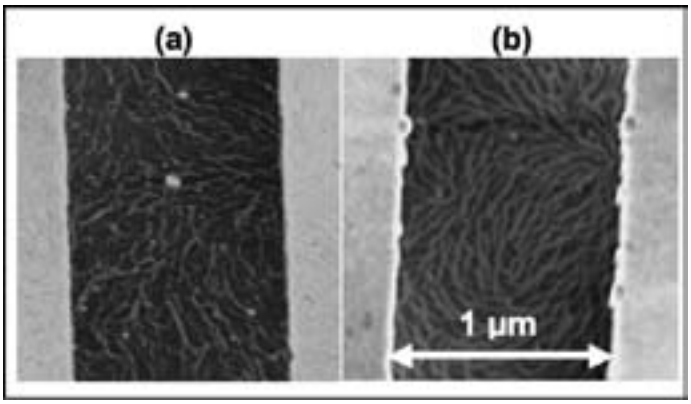

Figure 2: 1 µm trenches, (a) spincoated and (b) dropcoated.

We first noted that dropcast deposition is preferable to spincast deposition. The spincast samples, such as the sample shown in Figure 2a, demonstrated incomplete C96 fiber formation and limited correlation with the trench direction. In Figure 2b, a dropcast sample with the same 1 μm Cr line-width yielded much more robust fiber formation, but equally lacked correlation with the trench direction.

For 250 nm and 125 nm Cr line-widths, however, dropcast samples demonstrated excellent C96 fiber alignment, as shown in Figures 3 and 4. Additionally, on the 125 nm samples, we observed consistency perpendicular to the trench direction—there were approximately two C96 fibers in parallel in each trench. These results confirm the ability to influence C96 fiber alignment using a directed self-assembly method.

Conclusions

We developed and tested a procedure that allows for long-range control of C96 fiber alignment using a directed self-assembly method. First, we showed that C96 fibers tend to self-align with 250 nm-wide patterned Cr trenches. Later, in 125 nm trenches, we observed a significant degree of control over the number of fibers that align in parallel in each trench.

We conclude that, with optimization, directed C96 self-assembly has the potential to be used in large-scale semiconductor fabrication as a practical lithography technique offering sub-32 nm critical dimensions.

Acknowledgements

I would like to thank Gerald Lopez, Dr. Raghunath Murali, Dr. James Meindl, Dr. Jonas Jarvholm, Jennifer Root, and the Tolbert Group for their assistance. This project was funded by Georgia Tech, the National Nanotechnology Infrastructure Network Research Experience for Undergraduates Program, and the National Science Foundation.

References

[1] "Lithography," in International Technology Roadmap for Semiconductors, 2005.

[2] J. Jarvholm, "Etch resistance for highly aromatic monomolecular etch masks," Atlanta: Georgia Tech, 2007.

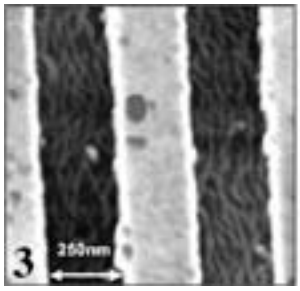

Figure 3, left: 250 nm trenches, dropcoated.

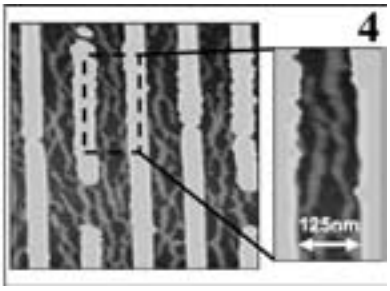

Figure 4, right: 125 nm trenches, dropcoated.

Factors that Affect the Synthesis of Gold Nanorods

Alice MacQueen

Biology and Biochemistry, University of Virginia

NNIN REU Site: Microelectronics Research Center, The University of Texas at Austin
NNIN REU Principal Investigator: Brian A. Korgel, Chemical Engineering, The University of Texas at Austin
NNIN REU Mentor: Danielle K. Smith, Chemical Engineering, The University of Texas at Austin
Contact: alicem@virginia.edu, korgel@che.utexas.edu, dsmith@che.utexas.edu

Introduction

Gold nanorods have two plasmon resonance peaks in their absorbance spectra: a higher-energy peak related to their diameter and a lower-energy peak associated with their length. Typically, the low energy peak occurs at ~ 750 nm. Nanorods with an optical signal within the 700-1000 nm range are interesting for medical imaging of tissue at cellular resolutions. This range corresponds to an "optical window" where light absorption is minimal, thus allowing deeper tissue penetration. For example, we have previously explored the use of near-infrared two-photon luminescence (TPL) for epithelial pre-cancer cell detection [1]. Lengthening the nanorods shifts the lower-energy plasmon to longer wavelengths, improving the optical penetration depth.

In this project, we focused on synthesizing gold (Au) nanorods with longitudinal plasmon peaks around 900 nm. We prepared colloidal Au nanorods using a seed-mediated approach and studied the effect of the additives hydrochloric acid (HCl) and sodium sulfide (Na_2S) [2]. Then, we measured absorbance spectra of the Au nanorods, and quantified the nanorod aspect ratios using transmission electron microscopy. Longitudinal plasmon resonances were red-shifted to wavelengths as long as 994 nm by adding both Na_2S and HCl.

Experimental Procedure

Gold nanorods were synthesized in aqueous solutions using a seed-mediated approach. Au seeds were first prepared by adding sodium borohydride (0.01 M, 600 μL) to a preparation of cetyltrimethylammonium bromide (CTAB, 0.1 M, 9.75 mL) and hydrogen tetrachloroaurate (0.01 M, 250 μL), and stirring for two minutes. Next, 12 μL of this gold seed solution was injected into a growth solution containing CTAB (0.1 M, 9.5 mL), silver nitrate (0.01 M, 75 μL), Au tetrachloroaurate (0.01 M, 500 μL), and ascorbic acid (0.1 M, 55 μL). Additional compounds were combined with this "typical" growth solution to adjust the wavelength of the longitudinal plasmon peak.

In the first experiment, hydrochloric acid (0.1 M, varying amounts between 50 and 2000 μL) was added just before injecting the seed solution. The second experiment involved adding sodium sulfide (Na_2S, 0.1 M), which quenches the growth solution [2]. Na_2S was added in two molar ratios of sulfur (S) to metal (M, both Au and Ag) at different times following seed injection (both 15 and 30 minutes afterwards, in a 2:1 and 4:1 S:M ratio). In the third experiment, both hydrochloric acid (0.1 M, amounts between 50 and 1000 μL) and Na_2S (0.1 M, 4:1 S:M ratio at 30 minutes) were added to the growth solution.

The Au nanorods were purified by two cycles of centrifugation at 8500 rpm for 10 minutes, followed by suspension in deionized water. Nanorods were characterized using UV-Vis spectroscopy and transmission electron microscopy.

Results

Experiment 1. Adding up to 500 μL of HCl shifted the lower-energy plasmon resonance peak out to a maximum of ~ 800 nm.

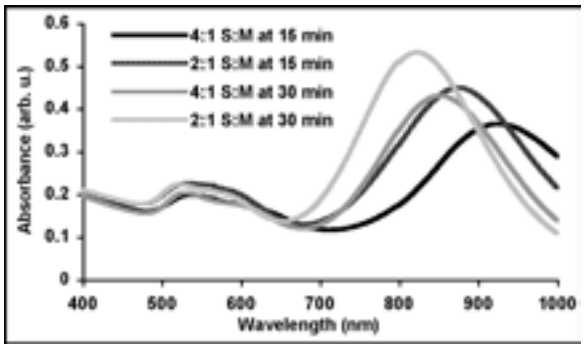

Figure 1: Addition of sodium sulfide to the growth solution.

Larger HCl additions seemed to poison the growth solution, blue-shifting the low-energy peak back toward the wavelength of the control (Figures 1 and 4B). Adding more HCl also lowered the yield of rods, as evidenced by the decreased absorbance ratio between the low- and high-energy peaks. A higher transverse peak, relative to the longitudinal plasmon peak, precluded formation of a higher population of spheres (gold particles without a longitudinal dimension).

Experiment 2. Injecting Na_2S at a larger S:M ratio and shorter time into growth shifted the longitudinal plasmon farther to the red (Figure 2). Changing the time of addition had a greater effect on nanorod length than varying S:M. Also, nanorod yield decreased while red-shifting the longitudinal plasmon.

Experiment 3. Adding Na_2S and up to 100 μL of HCl red-shifted the maximum wavelength of the second plasmon peak to 994 nm. Additional HCl lowered the rod yield and blue-shifted the longitudinal peak away from the 994 nm maximum. As shown in

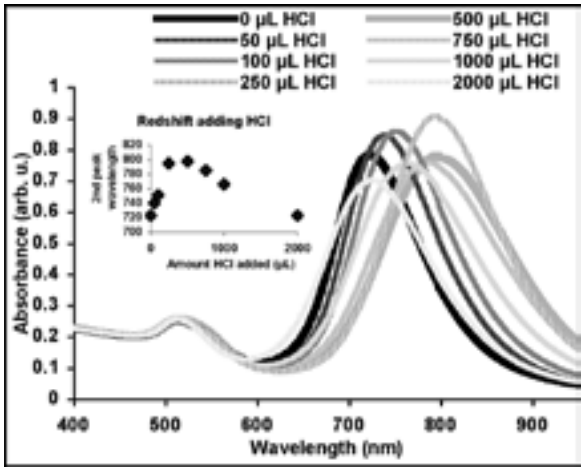

Figure 2: Addition of hydrochloric acid to the growth solution.

Figure 3, adding both Na_2S and HCl during rod growth lowered the longitudinal peak height; thus, rod yield was compromised by including these additives. However, Figure 4C exhibits nanorod samples with an absorbance peak positioned near the lower energy boundary of the "optical window" for cellular imaging, making them interesting agents for TPL imaging.

Conclusions

Longitudinal plasmon resonances were red-shifted as far as 994 nm with the addition of 100 μL 0.1M HCl followed by Na_2S in a 4:1 S:M ratio 30 minutes after the growth reaction was seeded. Adding Na_2S alone could not mimic this result; rods obtained with only Na_2S had a longitudinal peak red-shifted to 925 nm, and were obtained in much poorer yield. Adding HCl alone resulted in nanorods with a longitudinal peak having a maximum red-shift of 800 nm. Larger HCl additions blue-shifted this peak wavelength away from this maximum. Rods with the most potential for TPL imaging were obtained by adding 50 μL 0.1M HCl and. Na_2S at a 4:1 S:M ratio at 30 min, and had a longitudinal peak at 915 nm.

Future Work

Future work could involve increasing the monodispersity of the gold nanorod lengths in these altered procedures, as indicated by the breadth of the longitudinal plasmon peak. The yield of rods could also be increased by more delicately tuning the ratio of sodium sulfide or the time at which it is added.

Acknowledgements

Many thanks to Danielle Smith, Michael Rasch, and Dr. Brian Korgel for their guidance, Jean Toll for her help and organization, and to the National Nanotechnology Infrastructure Network Research Experience for Undergraduates Program, National Science Foundation, and Dr. Sanjay Banerjee for funding this work.

References

[1] Durr, N; Larson, T; Smith, D; Korgel, B; Sokolov, K; Ben-Yakar, A; "2-Photon Luminescence Imaging of Cancer Cells Using Molecularly Targeted Gold Nanorods"; Nanolets. V0 A-E (2007).

[2] Zweifel, D.; Wei, A.; "Sulfide-Arrested Growth of Gold Nanorods"; Chem. Mater., 4256-4261 (2005).

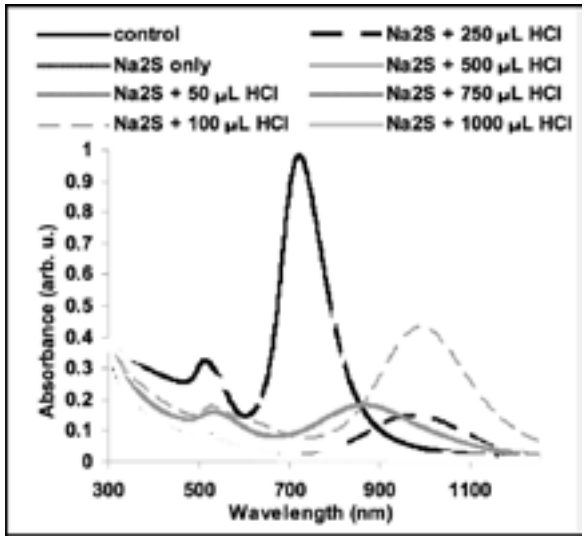

Figure 3: Addition of both HCl and Na_2S to the growth solution.

Figure 4, right: TEMs of gold nanorods synthesized in the presence of various additives with the most red-shifted second plasmon peak.

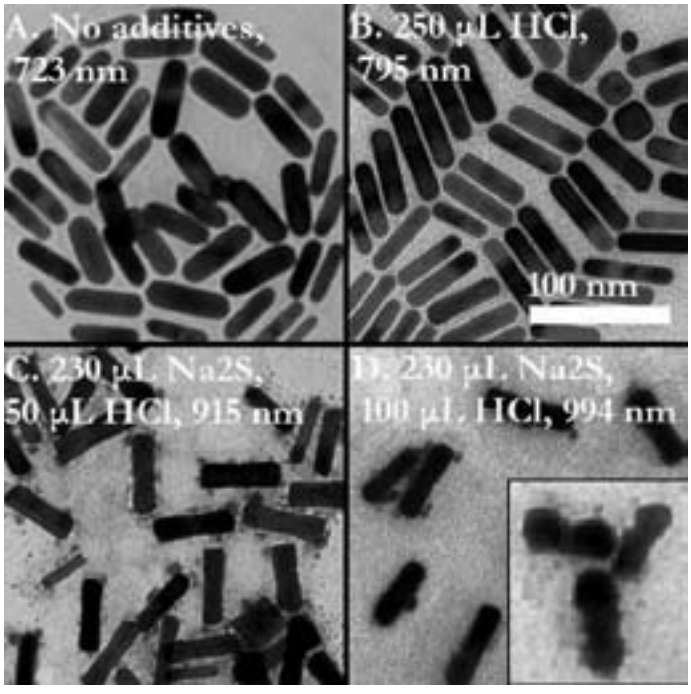

Cadmium Selenium Quantum Dot Photodiodes

Van Nguyen

Chemical Engineering, University of California, Riverside

NNIN REU Site: Center for Nanotechnology, University of Washington
NNIN REU Principal Investigator: Dr. Daniel Gamelin, Chemistry Department, University of Washington, Seattle
NNIN REU Mentor: Paul Archer, Chemistry Department, University of Washington, Seattle
Contact: van.nguyen002@email.ucr.edu, gamelin@chem.washington.edu, archerp@u.washington.edu

Abstract

A simple cadmium selenium (CdSe) quantum dot photodiode was assembled. The device is composed of two electrodes, indium tin oxide (ITO) and ITO/titanium dioxide (TiO_2) plates, two layers of 3-mercaptopropionic acid, and a thin layer of CdSe quantum dots. With this simple configuration, photocurrents up to 0.5 μA were detected under room light excitation. In addition, the diode photocurrent action spectra closely resembled the absorption spectrum of the parent colloidal CdSe quantum dots, indicating CdSe-TiO_2 coupling. Most interestingly, cyclic voltammetry scans revealed the photodiode properties of the device.

Introduction

The emission and absorption spectra of CdSe quantum dots are highly tunable making this one of the most studied nanocrystalline semiconductors. TiO_2 is widely used as an anode material in photovoltaic cells due to its superb performance as a charge carrier. Therefore, a CdSe/TiO_2 coupled system is expected to be an efficient and tunable photoanode.

In the past, CdSe and CdSe/TiO_2 systems have been grown from their precursors on a substrate [1,2]. Such methods yield a densely packed, well-connected nanocrystalline structure, in which the CdSe absorbs visible photons, while the TiO_2 network acts as a charge transfer system. In previous reports, however, the size and shape of the CdSe quantum dots could not be precisely controlled. In contrast, direct deposition of as-prepared quantum dots on TiO_2 coated substrates fails due to poor CdSe-TiO_2 coupling.

Here, we demonstrate an alternative method to assembling an effective photoanode using colloidal CdSe quantum dots and an intermolecular linker, 3-mercaptopropionic acid. The acid linker is a bifunctional molecule in which the thiol group on the linker binds to the CdSe quantum dots, while the carboxylic acid group attaches to the TiO_2 network.

Experimental Procedure

Chemical Preparation. Colloidal CdSe quantum dots were synthesized using the hot injection method as described in Qu, et al., 2001 [3]. By washing extensively with butanol and toluene, excess ligand in solution and on the surface of the CdSe quantum dots were removed. The bare nanocrystals were then suspended in tetrahydrofuran (THF) (Solution 1). In addition, 3-mercaptopropionic acid was diluted in ethanol (Solution 2). Lastly, 0.66 mmol of TiO_2 nanoparticles and 5 drops of polystyrene spheres were suspended in 10 ml of ethanol (Solution 3).

Electrode Preparation. Indium tin oxide (ITO) was chosen due to its transparency and low cost. ITO plates were cut into rectangular pieces, approximately 0.5 × 1.0 in. in dimension. After cleaning with ethanol and toluene, half of the cut ITO plates were spin-coated with Solution 3. These plates were then annealed at 450°C for 30 minutes. Before being stored under dry condition, the plates were rinsed thoroughly with ethanol.

Device Assembly. Solution 2 was drop-coated onto the TiO_2 coated ITO plate. When most of the ethanol had evaporated, Solution 1 was deposited. It took a few hours for the THF to evaporate. After that, an uncoated ITO plate was offset on top, and the whole device was secured using binder clips. Finally, copper tapes were pasted on the edges of the electrodes to enhance electrical connections. The cross sectional view of the device is shown in Figure 1.

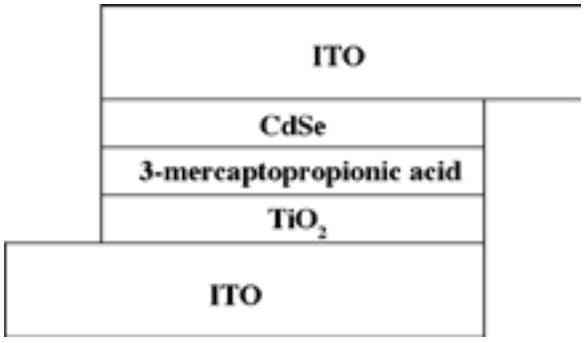

Figure 1: Device configuration (drawing not to scale).

Characterization. All measurements were done using MicroAutoLab-TypeII apparatus.

Result and Conclusions

In Figure 2, the incident photo-to-current conversion efficiency, IPCE4, spectra resembled the absorption spectrum of CdSe colloidal quantum dots at wavelengths longer than 520 nm. In

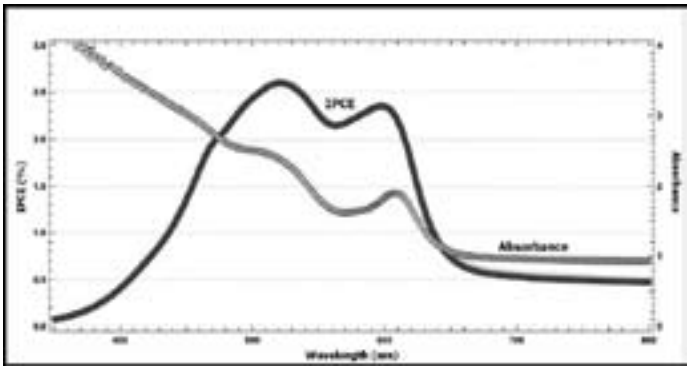

Figure 2: Photocurrent action and absorbance spectra (monochromator rate at 1.44 nm/s; applied potential at1.0 V).

other words, CdSe quantum dots were producing current under photo-excitation.

The most cyclic voltammetry characteristics of the device are presented in Figure 3. The observed current at 1.0 V is 13 times greater than that at -1.0 V. In addition, the cell shows ohmic behavior from 0.0 V-1.0 V. This cyclic voltammetry scan provides strong evidence that the cell possesses photodiode characteristics.

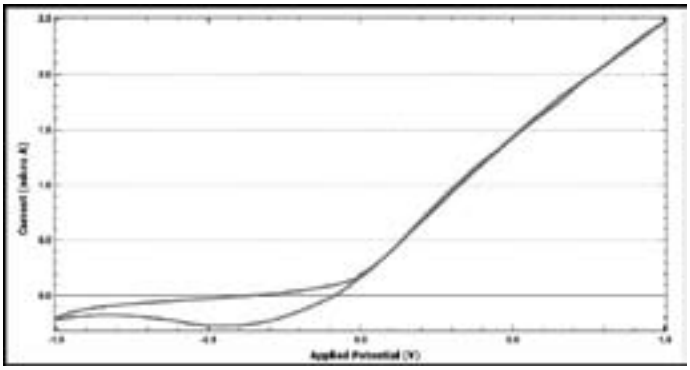

Figure 3: Cyclic voltammetry scans (scan rate at 0.001 V/s; 25 cm below a 20 halogen lamp).

The proposed photoelectrical mechanism of the CdSe-TiO_2 coupled system involves electron tunneling. Upon irradiation, CdSe quantum dots absorb energy and promote electrons from the valence band to the conduction band (exciton generation). The applied voltage then helps inject the excited electrons into the TiO_2 network, and subsequently into the ITO and the closed circuit. Since the valence band offsets between CdSe and either TiO_2 or ITO are large, the holes are confined to the CdSe. In contrast, the conduction band offsets between CdSe and TiO_2 and ITO are relatively small. With sufficient applied potential, electrons could "hop" from the plain ITO plate to re-fill electron deficiencies (see Figure 4).

The probability of successful electron tunneling decreases exponentially with distance. Thus, the ideal position of the holes is in the middle of the film. If the film were too thick, electron tunneling would be greatly inhibited. If the film were too thin, there would not be enough CdSe quantum dots to absorb the photons.

The film used in this project was fairly thick (~ 50 μm). Since the absorption spectrum of the CdSe-TiO_2 system increased dramatically at shorter wavelength (< 500 nm), most photons were absorbed well before they reached the middle region. As a result, charge separation was less efficient and less photocurrent was detected. The decrease in IPCE at wavelengths shorter than 520 nm in Figure 2 is therefore due to the large film thickness.

In conclusion, CdSe-TiO_2 coupled photoelectrodes were successfully prepared using 3-mercaptopropionic acid as a linker. A simple device assembled from these photoelectrodes showed high sensitivity to various wavelengths and possessed photodiode properties.

Acknowledgements

We thank Ethan Allen for laboratory coordination and all members in the Gamelin group at UW for friendly and professional collaboration. Funding for this project was provided by the National Nanotechnology Infrastructure Network Research Experience for Undergraduates Program and National Science Foundation.

References

[1] Diguna, L. J.; Shen, Q.; Kobayashi, J.; Toyoda, T. Applied Physics Letters, 2007, Vol. 91.

[2] Robel, I.; Kuno, M.; Kamat, P. V. J. Am. Chem. Soc. 2007, 129, 4136-4137.

[3] Qu, L.; Peng, A. Z.; Peng, X. Nano Letters, 2001, Vol.1, No. 6, 333-337.

[4] Liu, W; Salley, G.; Gamelin, D. J. Phys. Chem. B 2005, 109.

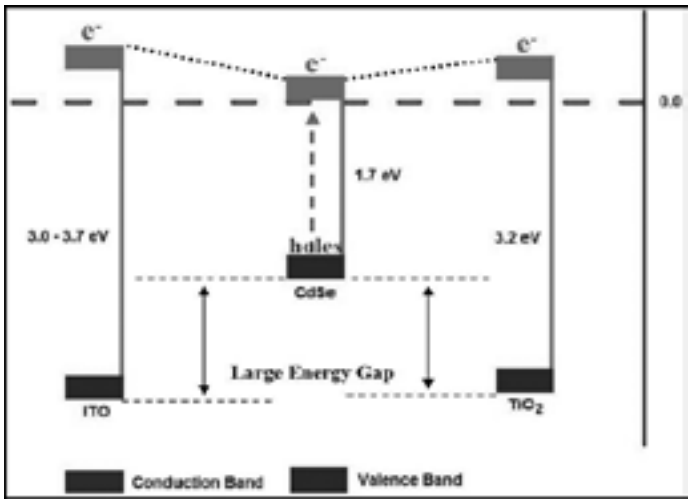

Figure 4: Electron tunneling.

Effect of Hydroxide Surface Treatments on Photoluminescence of InP/InGaAs Heterostructures

Christina Yeung

Engineering, Swarthmore College

NNIN REU Site: Minnesota Nanotechnology Cluster, University of Minnesota-Twin Cities
NNIN REU Principal Investigator: Joey Talghader, Electrical and Computer Engineering, University of Minnesota-Twin Cities
NNIN REU Mentor: Jan Makowski, Electrical and Computer Engineering, University of Minnesota-Twin Cities
Contact: cyeung1@swarthmore.edu, joey@ece.umn.edu, makowski@umn.edu

Abstract/Introduction

It has been previously shown that the surface recombination velocity of exposed indium gallium arsenide (InGaAs) quantum wells can be significantly reduced by permanently placing the heterostructure in a hydroxide solution or by forming a hydroxide crystalline layer [1]. The focus of this experiment is to use temporary hydroxide treatments, which do not form a crystal layer, to improve surface quality. A step was etched into an indium phosphorus (InP)/InGaAs heterostructure to expose a quantum well. Next, half of the sample (perpendicular to the step) was covered with photoresist and the whole sample was treated with buffered oxide etch and various concentrations of sodium hydroxide (NaOH) solution. After stripping the resist, the covered side was compared to the treated side to measure the difference in photoluminescence. The measurements show that the surface treatments did not reliably improve surface quality. Specifically, with a 90% confidence level, it was determined that a 1 mM NaOH, 30 minute treatment had no effect.

The ultimate goal of this research was to improve a device being developed for nanomechanical tuning of electron states.

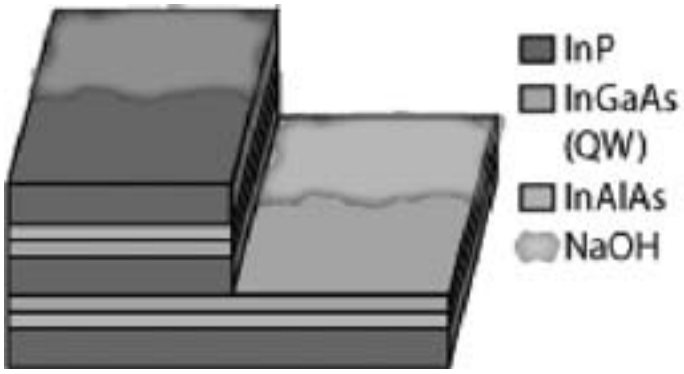

Figure 1: Four regions of the sample used in the experiment (With InP Cap/Exposed InGaAs Well, Treated or Not Treated).

Theory

InP/InGaAs Heterostructures. A quantum well is formed in a semiconductor when a thin semiconductor with a lower band gap (ex: InGaAs) is sandwiched between two thicker layers of a different semiconductor (ex: InP) with a higher band gap. Electrons within the middle layer are confined to the 2-dimensional plane of the well.

Surface Recombination. When the layer above the quantum well is etched away, the well is "exposed." The incomplete bonds at the surface create trap states. Trap states are energy levels between the conduction band and the valence band at which electron-hole pairs recombine non-radiatively. Chemical bond passivation is used to slow trapping and recombination.

Photoluminescence (PL). When photons are absorbed by a semi-conductor, electrons within the compound are excited to higher energy states. When these electrons recombine to their original state through radiative recombination, photons are emitted. The amplitude and wavelength of the emitted light can be measured to further characterize the semi-conductor which produced the PL. Because PL intensity decreases when many electron-hole pairs recombine non-radiatively at the surface, a low PL indicates a large amount of surface recombination.

Experimental Procedure

To measure the effect of the hydroxide treatment on exposed quantum wells, steps were etched into the InP/InGaAs heterostructures, exposing the quantum wells. A standard photolithography process using 1818 photoresist was used to cover half the sample with photoresist. Next, the sample was etched in a solution of HCl: H_3PO_4:CH_3COOH (1:1:2) for 120 seconds, a solution of H_2SO_4:H_2O_2:H_2O (1:8:500) for 120 seconds, and, again, a solution of HCl:H_3PO_4:CH_3COOH (1:1:2) for 90 seconds.

Because it was expected that the surface treatment only affected the exposed quantum well, the treated and untreated regions of the capped quantum well were used to check the experimental procedure. A great difference in PL of the capped regions would indicate a systemic error in the experiment.

After etching, photoresist was painted onto half of the sample (perpendicular to the step). (A standard photolithography process was not used because the developer may chemically passivate the exposed quantum well bonds.) Then, an eye-dropper was used to form a bubble of NaOH solution on the sample. After various times of treatment, the sample was rinsed with deionized (DI) water and a solvent rinse.

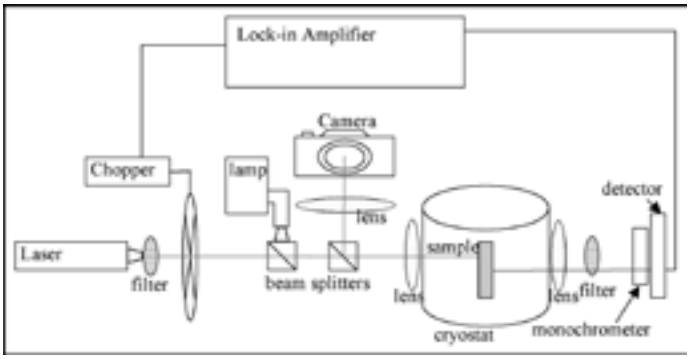

Figure 2: Apparatus for measuring photoluminescence.

The PL of four points on each of the four resulting regions was measured using the apparatus shown in Figure 2 from a frequency of 800 nm to 1750 nm, at room temperature.

Results and Conclusions

The average maximum PL of the untreated side is 1.56 pA (standard deviation = 1.26) while the average maximum PL of the treated side is 1.43 pA (standard deviation = 1.43). The means are statistically similar, with a confidence level of 90%. Treatments from 1 mM to 10 M and treatment times from 1-30 minutes were tested. A student t-test was used to analyze the data because previous experiments showed that the variation across the sample after etching, but before surface treatment, was about 100%. Therefore, only an improvement of above 100% could be attributed to the surface treatment, and not sample variation. Other experimental data indicates that the photoresist itself did not effect the PL of the samples.

Future Work

While it can be concluded that a 1 mM NaOH solution treatment for 30 minutes did not significantly improve the PL of the heterostructure, other concentrations and treatment times may have an effect. However, when the concentration was increased to 1M, the photoresist was etched away on the sample and so the control side was not preserved. A different photoresist may prevent this phenomenon.

It was also observed that longer or stronger treatments triggered a chemical reaction that resulted in a dark-colored film on the surface of the heterostructures. It would be worthwhile to experiment with other hydroxide solutions, such as potassium hydroxide (KOH), to determine if the formation of the film could be prevented. It would also be interesting to repeat this experiment, but allow a crystal layer to form, just to see if the previous results of Yablonovitch could be duplicated with this experimental apparatus.

Acknowledgments

I would like to thank Dr. Joey Talghader and Jan Makowski for their guidance. I would also like to thank Dr. Doug Ernie, the University of Minnesota ECE REU program coordinator, and the NFC staff for their efforts.

This study was funded by the National Science Foundation through the National Nanotechnology Infrastructure Network Research Experience for Undergraduates Program at the University of Minnesota, Twin Cities.

References

[1] E. Yablonovitch, H.M. Cox, T.J. Gmitter. "Nearly ideal electronic surfaces on naked InGaAs quantum wells", Appl. Phys. Lett., March 21, 1988, Volume 52, Issue 12, pp. 1002-1004.

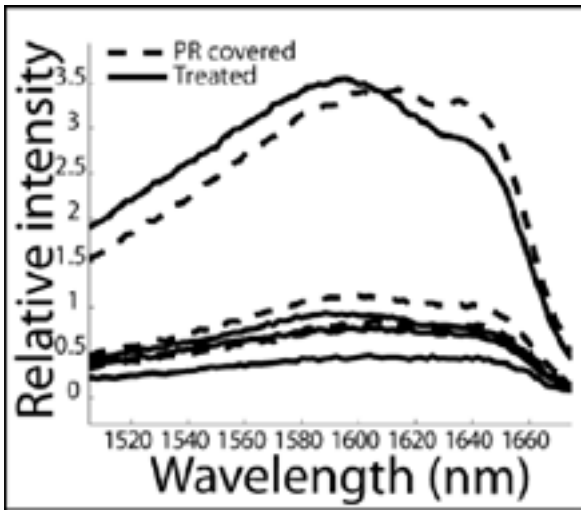

Figure 3: PL of exposed quantum well treated in 1 mM NaOH solution for 30 minutes.

Nonvolatile Memory with Multi-Stack Nanocrystals as Floating Gates

Kamran Afshari

Electrical Engineering, University of California-Los Angeles

NNIN REU Site: Cornell NanoScale Science & Technology Facility, Cornell University
NNIN REU Principal Investigator: Prof. Edwin Kan, Electrical & Computer Engineering, Cornell University
NNIN REU Mentor: Tuo-Hung Hou, Electrical & Computer Engineering, Cornell University
Contact: kafshari@ieee.org, kan@ece.cornell.edu

Abstract

Nonvolatile memory technologies are focusing on devices with longer retention, faster read and write, higher bit density, improved endurance, and low-voltage program/erase characteristics. Nanocrystal (NC) memories are promising for realizing high-density nonvolatile storage with the inherent advantage of low-voltage operation [1]. Recently carbon molecules in the form of fullerenes (C_{60}), known as "bucky balls," also have been incorporated in non-volatile memory devices [2] with its advantages of mono-disperse nature and molecular size. In this project, various memory structures with self-assembled multi-stacked gold, platinum, and C_{60} nanocrystals as floating gates have been fabricated and characterized. In two-layer nanocrystal structures, the C_{60} bottom layer acts as an additional barrier to prevent charge back-tunneling from the upper layer, improving retention time without a commensurate penalty in program time. The upper nanocrystal layer functions as additional charge storage to provide sufficient memory window.

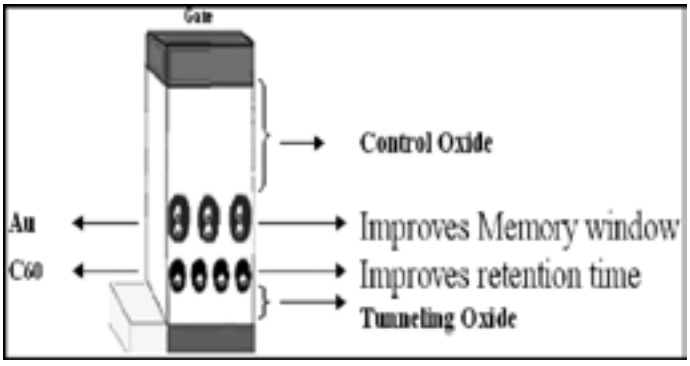

Figure 1: Schematic of the double-layer nanocrystal memory.

Introduction

Figure 1 shows the cross section of a double-layer nanocrystal memory device. By applying enough positive bias across the gate, electrons will quantum-mechanically tunnel through the thin tunneling oxide. If the lower-layer nanocrystal is designed so that it is energetically unfavorable for charge storage due to its small size, electrons will step through the lower nanocrystal layer, and get stored in the second layer nanocrystal. After taking away the applied potential, the energy penalty for electrons in the second layer to tunnel back into the first layer is larger enough, again due to the large charging energy associated with the small size. The first-layer nanocrystal acts as a part of tunneling barrier to provide prolonged retention time. The same concept applies to the hole storage when negative bias is applied. Charging nanocrystals with electrons and holes can require different gate biasing due to different properties of nanocrystals, which also contribute to different retention time characteristics.

The goal was to engineer the best structure such that one can obtain a memory device with an optimal memory window and retention time. This required the optimization of the tunneling oxide thickness, nanocrystal diameter and the choice of a nanocrystal material.

Experimental Procedure

P-type wafers with a doping level of 10^{15} cm^{-3} were used in this study. The device isolation was achieved by the local oxidation isolation (LOCOS). 2-3 nanometers of tunneling oxide was grown on the active region in a diluted oxygen ambience using an atmospheric-pressure furnace. Each wafer was named separately.

Sample 1 (S_1) was the control device without any floating gate, sample 2 (S_2) had a single-layer gold (Au) nanocrystal as a floating gate, S_3 had a double-layer Au nanocrystal floating gate, S_4 had a single-layer C_{60} nanocrystal floating gate, S_5 had a double-layer C_{60} and Au nanocrystal floating gate, and S_6 had the same structure as S_5 but with a thinner thickness of tunneling oxide.

The Au nanocrystals were deposited through e-gun evaporation while the C_{60} nanocrystals through the thermal evaporation. For those samples with double-layer nanocrystals, 2-3 nm of evaporated silicon dioxide (SiO_2) was inserted between two layers. After the floating-gate formation, 20-30 nm of control oxide was deposited through a plasma-enhanced chemical vapor deposition (PECVD), followed by chromium and aluminum evaporation as the control gate. Finally the control gate was patterned to finish the device fabrication. The device was now measured, and memory window and retention time for different configurations were compared.

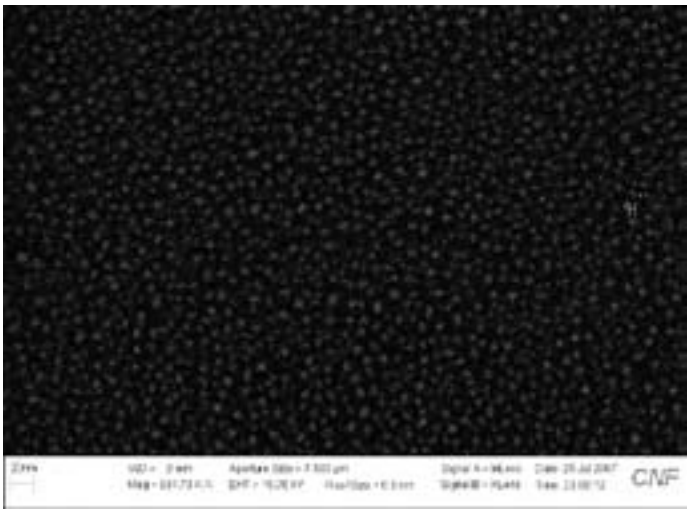

Figure 2: SEM image of Au nanocrystals on SiO_2 surface.

Results and Conclusions

After 1.2 nm Au deposition on the tunneling oxide, the minimization of local energy at the Au/SiO_2 interface reshaped the thin film into discontinuous and spherical Au nanocrystals, as shown in the scanning electron microscopy (SEM) image (Figure 2). The diameter of each nanocrystal was about 5 nm.

To measure the memory window, we performed multiple capacitance-voltage (CV) sweeps from inversion to accumulation and back again. The observed hysteresis of the CV curves indicated memory effect through charge storage. Figure 3 represents the memory window obtained from a double-layer C_{60} and Au floating gate.

We then measured the retention time for each configuration, and as demonstrated in Table I, we compared the values to obtain the optimal configuration for a memory device. Based on the results we concluded that double-layer nanocrystal floating gates with C_{60} as the bottom layer and Au as the upper layer would give the best memory device in terms of memory window and retention time. Since mono-dispersed C_{60} has a diameter of about 1 nm, it performed best in blocking back-tunneling of electrons and holes from the upper layer to the channel in this project.

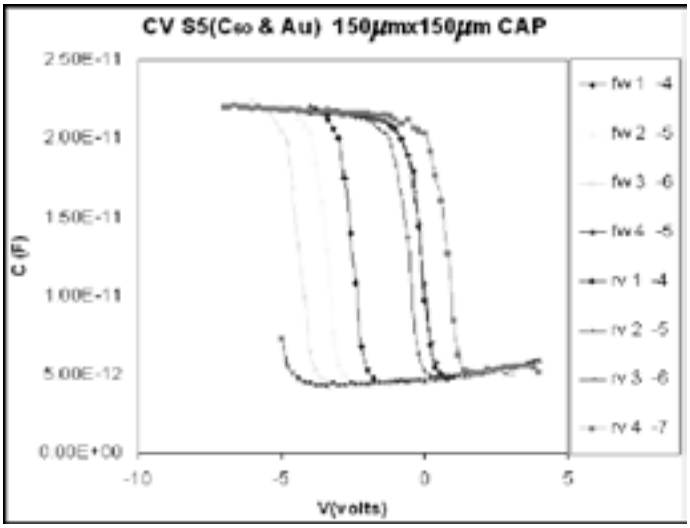

Figure 3: Memory window for a double-layer C_{60}/Au NC memory.

Future Work

More tests will be performed to study the behavior of these memory devices under short-pulse program/erase operations. The retention time will be further improved by incorporating high-κ material as the tunneling dielectric. Finally, the control oxide thickness can be scaled to eliminate short channel effects in the sub-micron gate-length devices.

Acknowledgements

This work has been supported by Cornell NanoScale Science & Technology Facility, National Nanotechnology Infrastructure Network Research Experience for Undergraduates Program, and the National Science Foundation. I would like to thank Edwin Kan, Tuo-Hung Hou, Daniel Ruebusch, CNF staff, and the rest of the Kan group for their guidance and support.

References

[1] Hanafi, H.I.; Tiwari, S.; Khan, I. , "Fast and long retention-time nano-crystal memory," Electron Devices, IEEE Transactions on Volume 43, Issue 9, Sept. 1996 Page(s):1553-1558.

[2] Hou, Tuo-Hung; Ganguly, Udayan; Kan, Edwin C, "Programable molecular orbital states of C60 from integrated circuits," Appl. Phys. Lett., vol. 89, 253113 (2006).

Run#1 Tunneling oxide = 2.41nm
Run#2 Tunneling oxide = 2.72nm
Voltage sweep (-2 to 5 V)

Sample #	Nanocrystal Layer/s	Run#1		Run#2	
		Mem-win(V)	Reten_t (S)	Mem-win	Reten_t
S1	Control	0	0	0	0
S2	Au	5.8	400	5.4	NA
S3	Au & Au	NA	NA	NA	NA
S4	C60	2.4	240	2.8	250
S5	C60 & Au	3	1100	4.1	5100
S6	C60 & Au	4.7	500	4.4	5000

Table 1: Summary of memory window and retention time.

Simulations of Nano-Particle Electro-Luminescence for Novel Near-Field Microscopy

Syed Saad Ahsan

Applied and Engineering Physics, Cornell University

NNIN REU Site: Microelectronics Research Center, The University of Texas at Austin
NNIN REU Principal Investigator: Dr. John X.J. Zhang, Biomedical Engineering, The University of Texas at Austin
NNIN REU Mentors: Ashwini Gopal and Kazunori Hoshino, Biomedical Engineering, The University of Texas at Austin
Contact: ssa27@cornell.edu, John.Zhang@engr.utexas.edu

Abstract

We simulated two-dimensional electro-luminescence (EL) performances of organic multi-layered quantum dot light emitting diodes (QD-LEDs), through iterative time-step calculations. Simulations were run for LED anode-cathode pairs of various overlapping length. Our simulation results showed that: (1) nearly all recombination happened on the QD mono-layer; (2) when the spatial overlap was zero, the area of emission could be further decreased to 50 nm under driving current densities at the mA/cm^2 level; and (3) with increasing driving current, the decay time of the excitons significantly slow down leading to the saturation of neighboring QDs, and therefore loss in resolution.

Introduction

The resolution of near-field optical signals, captured at a distance shorter than the wavelength of the emitted light, is determined by area of light emission rather than Rayleigh diffraction. Near-field scanning optical microscopes (NSOMs) use this phenomenon on scanning probe microscopes (SPM). Light emitting diodes (LEDs) can be incorporated on the probe tip leading to aperture free NSOMs [1]. We have fabricated a silicon microprobe integrated with a nanometer-sized LED, consisting of organic quantum dots (QD) on the tip, for NSOM. The physical properties of the QD-LED directly define the spectral range and imaging resolution due to the quantum confinement effects.

Methodology

We applied the Poisson equation using the charge distribution to solve the potential which was consequently used to determine charge transport. We then ran a time-step process until steady-state solution was achieved. Quantum tunneling is assumed over nanocrystal energy barriers.

Device Schematic (refer to Figure 1)

The LED was designed to have ohmic electrode contacts, organic transport layers and a monolayer of capped nano-particles. Our two-dimensional simulations varied the lengths of the spatial overlap between the two electrodes. All simulations were done in MATLAB®.

Algorithm Outline

The algorithm basically divided our LED device into many subdivisions. Each subdivision being 10 nm wide and 2 nm tall, which was consequently the resolution of our two-dimensional solution. To decrease run time, we found the smallest device width after which the position-dependent variable distributions did not change significantly. For no spatial overlap, our device was 500 nm.

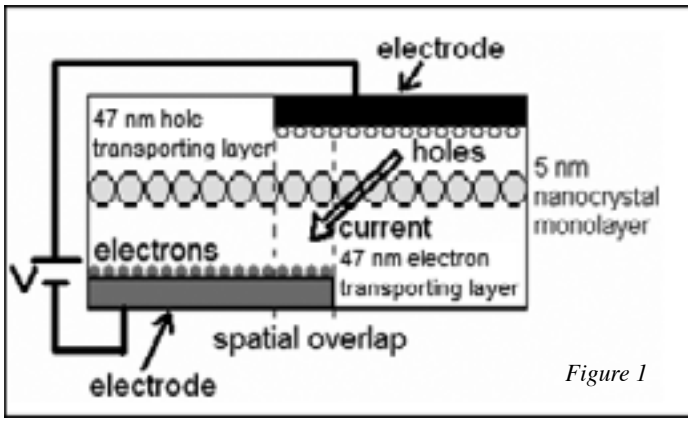

Figure 1

We assumed several variables that were functions of position such as potential, electric field, and carrier transport. Each iteration solved the potential using the charge distribution, and found the new charge distribution from finding charge transport determined from potential. We ran these iterations until the steady state condition [3] was reached:

$$\nabla J_n/q = -\nabla J_p/q = Bnp \qquad (Recombination)\ (1)$$

where the divergence of the current densities over the charge of the carriers, q, was equal to the recombination that occurred at each division. The Langevin recombination constant B was equal to 10^{-18}m^3/sec.

Potential

The potential was determined using the charge distribution by solving the Poisson equation [2]:

$$\nabla^2\Phi = q\,(p-n)/\varepsilon \quad (2)$$

where ε represents the permittivity of free space, p and n represent the hole and electron carrier concentrations and Φ represents the potential. After defining relevant boundary conditions, we numerically solved the potential employing matrices.

Charge Transport

Assuming that carrier injection was due to thermionic emission at the ohmic electrodes, the carrier density at the electrodes was approximated [3] as $10^{24}/m^3$ for holes at the cathode and the electrons at the anode.

We assumed that the charge transport [2] was composed of drift and diffusion:

$$J_p = q(\mu_p pE + D_p \nabla p) \qquad (3)$$

$$J_n = q(\mu_n nE + D_n \nabla n) \qquad (4)$$

where μ represents the mobility variable, D represents the diffusion variable and E represents the electric field. Mobility and diffusion were also functions of position being dependent on electric field [2] as in an electron-hopping like model:

$$\mu_{n/p} = \mu_{0\,n/p} \sqrt{(E/E_{pf})} \qquad (5)$$

$$D = \mu KT/q \qquad (6)$$

where $\mu_{0\,n/p}$ is the mobility constant, and E_{pf} is the activation field related to disorder equal to 10^7 V/m. The mobility constant for each carrier at its respective transport layer was 10^{-10} m^2/Vs and in the other layer as 10^{-12} m^2/Vs [3]. Treating our equations like vectors, we calculated each dimensional component.

Across the nanocrystal monolayer, we found charge flow by taking quantum transmission rates over square wells or barriers using one-dimensional Boltzmann-Maxwellian velocity distributions. The energy diagram was found in previous literature [4] assuming that the transporting layers were PBD, TPD, and the nanocrystals were CdSe.

Exciton Kinetics

We assumed that light originated from Forster energy transfers into the nanocrystal monolayer with a slow diffusion limit [5]. We only considered the excitons formed in the nanocrystal monolayer presuming that most of the excitons would form in the monolayer. Because the diffusion coefficient is inversely related to the decay rate squared, $\tau_{exc}^{\ 2}$, we assumed a modestly long τ_{exc} of 100 ns which would correspond to relatively slow exciton diffusion for CdSe nanocrystals.

Results And Discussion

The recombination profile (see Figure 2) shows that exciton formation occurs only on the nanocrystal monolayer. We expect that since the monolayer is also the most radiative part of the device, the light emission should be easily confined to these nanocrystals. This also verifies our initial assumptions that only the excitons formed on the monolayer are important in computing Forester energy transfers.

Figure 2

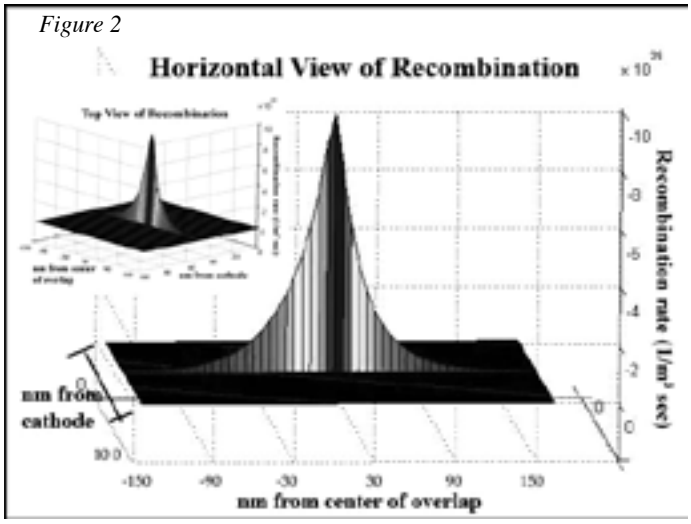

Additionally when spatial overlap is zero (see Figure 3), the area of light emission is further confined to 50 nm inside the monolayer at low voltages.

At higher driving currents, the low exciton limit [5], where the exciton injection rate < τ_{exc}^{-1}, is not fulfilled anymore as nanocrystals get more than one exciton (see Figure 4), produced biexcitons and led to slower decay rates. When this happened, there was a loss of resolution implying that the tradeoff for low exciton diffusion was lower light intensities.

Acknowledgements

I would like to acknowledge the National Science Foundation, the National Nanotechnology Infrastructure Network Research Experience for Undergraduates Program, and Dr. Sanjay Banerjee for the support. I would also like to thank the Zhang research lab and especially God.

References

[1] K. Hoshino et al., MEMS, p.743 (2007).
[2] S. Chang et al., Proc. SPIE, p. 26-1 (2006).
[3] B. Crone et al., J. Appl. Phys., p.833 (1998).
[4] Zhao et. al., J. Appl. Phys., p.3207 (2004).
[5] K. Kohary et. Al., J. Appl. Phys., 114315 (2006).

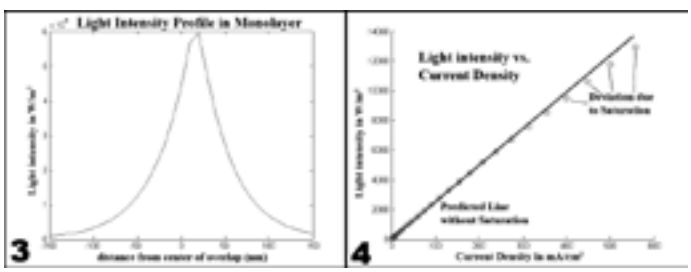

Nanowire-Based Flexible Thin Film Devices

Kevin Baler

Materials Science and Engineering, Cornell University

NNIN REU Site: Michigan Nanofabrication Facility, The University of Michigan Ann Arbor
NNIN REU Principal Investigator: Prof. Wei Lu, Electrical Engr. and Computer Science, University of Michigan Ann Arbor
NNIN REU Mentor: Eric Dattoli, Electrical Engineering and Computer Science, University of Michigan Ann Arbor
Contact: kb263@cornell.edu, wluee@umich.edu, dattoli@umich.edu

Abstract

High-performance flexible thin film transistors (TFTs) were fabricated on plastic substrates using lightly tantalum (Ta)-doped tin dioxide (SnO_2) nanowires as the channel material. High densities of crystalline SnO_2 nanowires were dry-transferred directly onto plastic substrates, followed by lithographic patterning of resist, sputtering of chromium/gold (Cr/Au) contacts and a silicon dioxide (SiO_2) insulator layer, and a second lithography process to define a top Cr/Au gate. The top-gated TFT structures exhibit both mechanical flexibility and excellent electrical properties under cyclic tension experiments. Charge carrier mobility was estimated to be as high as 160 $cm^2/(V•s)$—two orders of magnitude higher than that of conventional amorphous-silicon or organic TFTs. The low-cost nanowire growth and dry-transfer processes make this approach a cost-effective means to fabricate flexible TFT's. SnO_2 nanowire-based transparent TFT (TTFT) devices were also fabricated on glass substrates optimized for transparency using sputtered Sn doped indium tin oxide (ITO) electrodes (annealed at 200°C) and a photocured hard-baked epoxy as a gate dielectric (SU8-25 20%, MIBK; Microchem Corp.). Although highly transparent, higher contact resistance was observed for TTFT devices using ITO contacts, additional improvements to these devices need to be further explored.

Introduction

Metal oxide nanowires have attractive electrical and optical properties (i.e. high electron mobility and optical transparency) that make them ideally suited for use in high performance TFTs on low-temperature substrates. In this work, we report on the performance of lightly Ta-doped SnO_2 nanowires incorporated into flexible polyethylene terepthalate (PET) based top-gated TFTs. High density dry transfer of previously synthesized single-crystalline nanowires enables subsequent low-temperature device fabrication without sacrificing device performance [1,2]. The performance of these devices show field effect mobilities in excess of 100 $cm^2/(V•s)$ and on/off ratios > 10^5 which are a marked improvement over existing conventional amorphous-silicon and organic semiconductors [3-5]. Additionally, high optical transmittance of SnO_2 nanowires suggests that TFT devices could be designed for high transparency as well as flexibility [1].

Device Fabrication

Ta-doped SnO_2 nanowires were synthesized with the method described by Dattoli et. al. [1]. After growth, nanowires were dry transferred onto the PET substrate (100 μm thick) in one direction to maximize the number of parallel nanowires (Figure 1, bottom inset). A photolithography process was used to define the Cr/Au source and drain contacts, followed by 360 nm sputter deposition of the SiO_2 gate insulator and definition of the Cr/Au gate contact. All electrical measurements were carried out in air at room temperature.

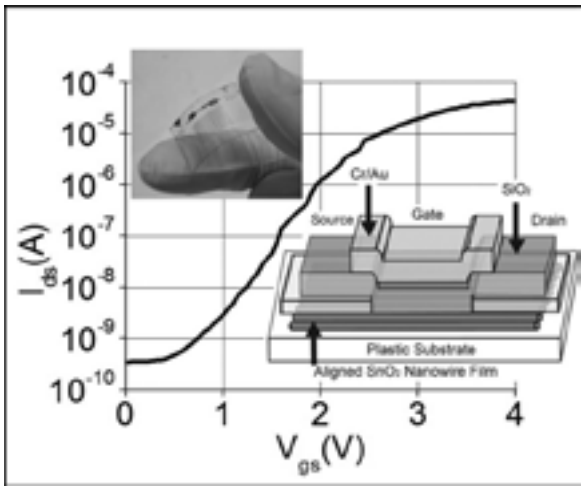

Figure 1: Logarithmic scale gate sweep characteristics of an unbent plastic TFT device shown in the upper inset. Bottom inset depicts the device architecture.

Results and Conclusions

As a result of Ta doping, the TFTs behaved like n-type enhancement-mode transistors [1]. Doping of the SnO_2 nanowires reduced the contact resistance in the TFT devices, evidenced by the ohmic behavior in the linear regime current-voltage (I_{ds}-V_{ds}) characteristics (Figure 2). Devices showed negligible gate leakage at both source and drain. The field-effect mobility, μ_{fe} ranged from 55 $cm^2/(V•s)$ to 160 $cm^2/(V•s)$ and coincided with mobilities measured on similar SnO_2 nanowire-based TTFTs [1]. The mobility was estimated from low-bias (1V) transconductance

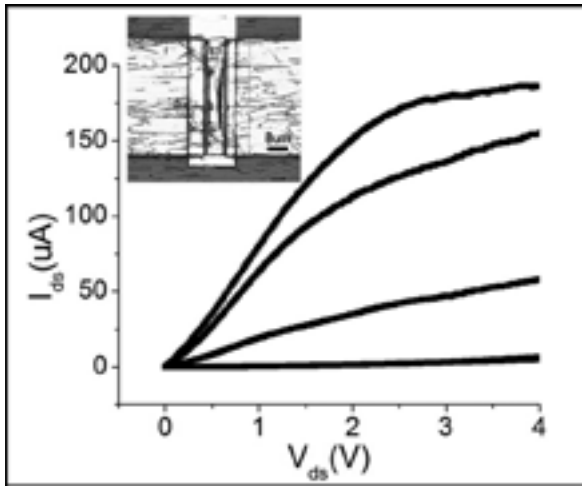

Figure 2: Voltage sweep characteristics of an unbent plastic TFT device shown in the inset.

measurements, and the capacitance of the nanowire "film" was approximated using the formula for an infinite plane ($\varepsilon_0 \bullet 3.9/t_{ox}$) [1]. An on/off ratio of > 10^5 was achieved within a 5V gate bias range with a 1V bias at the source (Figure 1). The channel length and width of this device is 8 μm and 47 μm respectively (Figure 2, inset).

The TFT radius of curvature was used to quantify the degree of compression during bending measurements. The radius of curvature was measured with ImageJ by analyzing photographs of the TFTs during compression (Figure 3). TFTs were tested before and during compression at 8 mm. The gate sweeps in Figure 3 are at a 1V source bias and show high gate mobilities above 100 $cm^2/(V\bullet s)$ for both bent and unbent conditions. This device (Figure 3, lower inset) has a channel length of 3.3 μm and width of 66 μm. At the 8 mm radius of curvature, there is a decrease in the maximum current and ~ 66% reduction in field effect mobility, μ_{fe}.

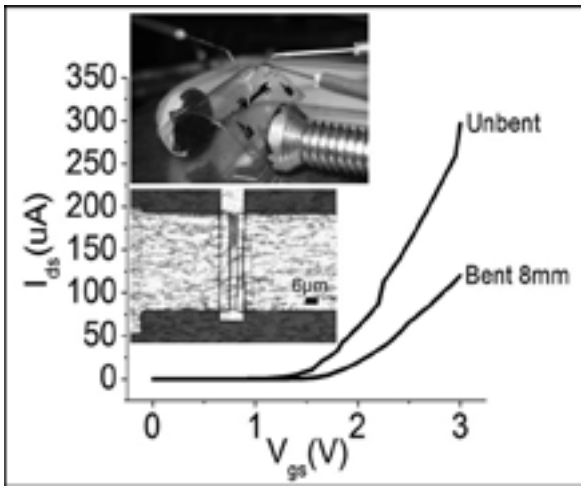

Figure 3: Gate sweep characteristics of an unbent and bent plastic TFT device (insets) taken during compression.

TFT devices were also tested after ten repeated compressions at curvatures from 20 mm to 4 mm. Gate sweeps at decreasing radii of curvature (Figure 4) show μ_{fe} above 100 $cm^2/(V\bullet s)$ and on/off ratios > 10^4. Like devices tested during compression, lower radii of curvatures show an 80% reduction in field effect mobility, and an order of magnitude reduction of the on/off ratio. Even after these reductions, the TFT performance characteristics in compression are still above comparable devices [3-5].

Future Work

The highest fabrication temperature was 150°C which shrank the PET substrate on the order of microns. This shrinkage encumbered alignment of subsequent mask layers. Future processing should maintain temperatures lower than 90°C to minimize plastic substrate shrinkage. Finally, highly transparent TTFT devices using ITO contacts were obtained but showed high contact resistances. Future TTFTs could have thinner SU-8 insulating layers or separate annealing of ITO to minimize sheet resistance prior to spin coating SU-8.

Acknowledgements

This work was funded by the Intel Foundation, the National Nanotechnology Infrastructure Network Research Experience for Undergraduates Program (NNIN REU), the National Science Foundation (NSF) and used the Michigan Nanofabrication Facility (MNF). I acknowledge everyone at UM, my friends and family.

References

[1] Dattoli et. Al; Nano Lett., 2007, 7, (8), pp 2463-2469 In press.
[2] McAlpine et. Al; Proceedings of IEEE, 93, 7, 1357-63 (2005).
[3] Ohta et. Al; Appl. Phys. Lett. 88, 103506 (2006).
[4] Cao et. Al; Adv. Func. Mater. 16, 2355-2362 (2006).
[5] Yoon et. Al; PNAS, 102, 13, 4679 (2005).

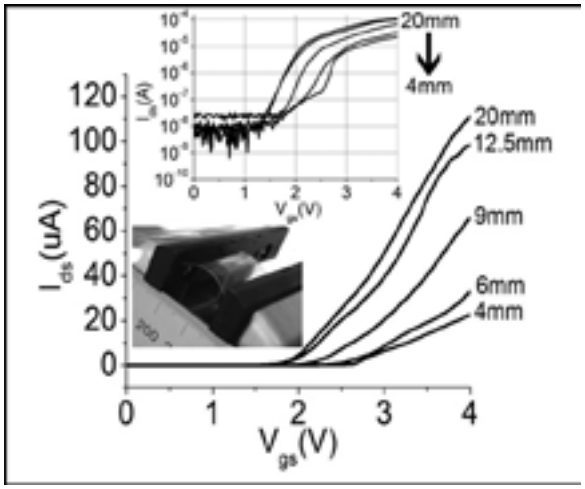

Figure 4: Gate sweep characteristics of the same plastic TFT device tested after 10 compressions of decreasing radius (20-4 mm) shown in the bottom inset. Upper inset shows log scale representation of the same data.

Atomic Layer Deposition on Single/Few Layer Graphene

Naresh W. Copeland

Electrical Engineering, Prairie View Agricultural & Mechanical University

NNIN REU Site: Stanford Nanofabrication Facility, Stanford University
NNIN REU Principal Investigator: Professor Hongjie Dai, Chemistry Department, Stanford University
NNIN REU Mentor: Xinran Wang, Physics Department, Stanford University
Contact: ncopeland@pvamu.edu, hdai1@stanford.edu, xinranw@gmail.com

Introduction

Due to the limitations of silicon based transistors, as the dimensions are continuously scaled down, there exists the need to find materials that produce more promising electrical properties such as high mobility, nearly ballistic channel and ohmic contact. Carbon based materials, especially single-walled carbon nanotubes (SWNTs), are among the most promising materials thus far. Yet due to the uncontrollability of chirality and position of SWNTs, the large scale integration is still unachievable. Recently, single layer graphene, which is a one atom thick layer of carbon, was discovered to be stable. Due to the structure of graphene, electrons can travel through the material at the same speed, acting as if they have no mass. Graphite, from which graphene is derived, can be grown in a controlled manner leading to the possibility of large-scale integration particularly in the development of field effect transistors. Another unique advantage of graphene materials is their band gap is inversely proportional to the width of the material, as you will see in Figure 1 [1], which indicates that the smaller it is the more potential energy it has, which is a very attractive semiconducting quality. The development and fabrication of such a device however, is nontrivial. Due to graphene being hydrophobic, we must coat the surface of the graphene with a material which will allow for the bonding of the high dielectric material, aluminum oxide (Al_2O_3), serving as the top gate. We used atomic layer deposition (ALD) to deposit the Al_2O_3, and after we coated the graphene, we checked our results using atomic force microscopy (AFM).

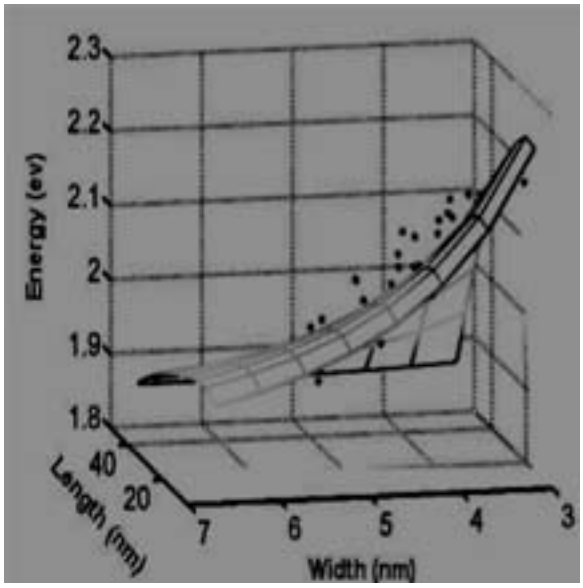

Figure 1: Energy band inversely proportional to the width of the graphene ribbon.

Experimental Procedure

The first stage of our experiment was the development of single layer graphene (SLG). This involved a process named micromechanical cleavage. In this process we cleaved off layers from a $10 \times 10 \times 2$ mm block of highly oriented pyrolytic graphite using scotch tape. Once we achieved relatively thin sheets of graphite on our tape, we contacted the tape against the substrate at varying angles. Next, we investigated our substrate under the 5x/20x optical microscope for signs of graphene which reflects a pale pinkish/purplish color when viewed under the microscope. We proceeded, from this point, by calcining our chip at 470°C for 20 minutes which burned away tape residue and any impurities on the surface. We confirmed our findings using the atomic force microscopy (AFM) system.

Our next step was to deposit the high dielectric oxide layer on the surface. However, since graphene is hydrophobic, we needed to test a control sample, with graphene only, along with a sample soaked for an hour in fluorescein (FITC) and a sample soaked for an hour in deoxyribonucleic acid (DNA), both of which are hydrophilic chemicals. By doing this, we expected the graphene to bond with the high dielectric oxide and uniformly layer over the samples. We proceeded to the atomic layer deposition system, which uses two precursor gases H_2O and tri-methyl aluminum (TMAl). The two gases pulsed respectively and reacted with the surface of the substrate to form the high dielectric, Al_2O_3 (oxide), on the surface. Each cycle put a 0.1 nm layer of Al_2O_3 on the surface and we performed 80 cycles resulting in 8 nm of Al_2O_3. After the ALD was completed, we took more AFM images of our samples to observe and conclude our results.

Results and Conclusions

We were able to conclude from our AFM images that the control sample did have some oxide on the surface however, we were uncertain as to why this would happen because we did not think that any Al_2O_3 would exist on the surface at all. We believe that

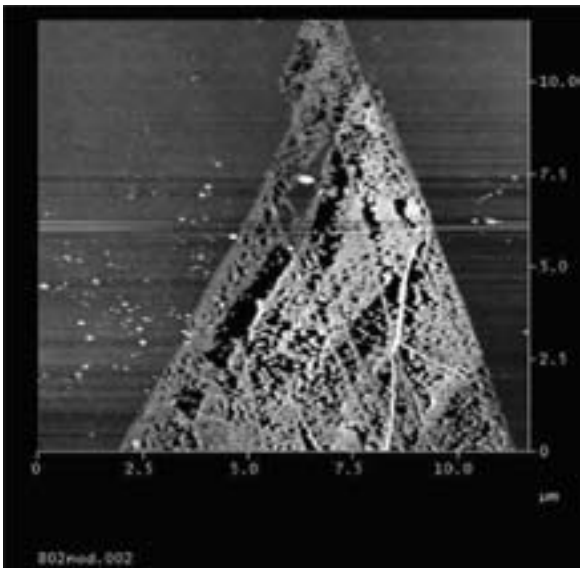

Figure 2: Control sample after ALD.

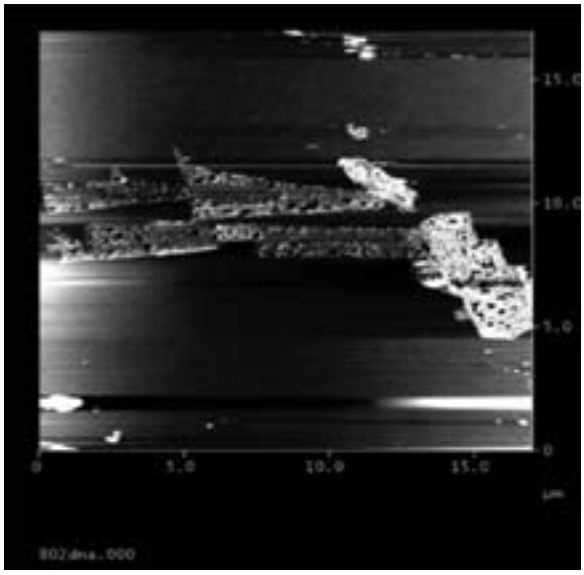

Figure 4: Graphene sample soaked in DNA for one hour after ALD.

this was a result of defects in the graphene. Perhaps the dangling bonds reacted with the Al_2O_3 and caused the dielectric to form. There existed a minimal amount of oxide on the surface, as shown in Figure 2.

We then investigated the sample with the FITC coating and we noticed more Al_2O_3 build up on the surface of the graphene, however it was still not uniformly distributed on the surface as you can see in Figure 3. We also noticed that the Al_2O_3 layer was patterned in blotches which indicated to us that the FITC may have reacted with the graphene forming undesirable bonds.

Lastly, we observed the sample coated with DNA, which had produced the best results thus far. There was considerably more oxide on the surface than both of the previous experiments. The Al_2O_3 was still not uniform over the surface, however, as you can see in Figure 4. We were slightly disappointed by this outcome because our lab had successfully coated carbon nanotubes with DNA in a prior research experiment, so we believed that this would work.

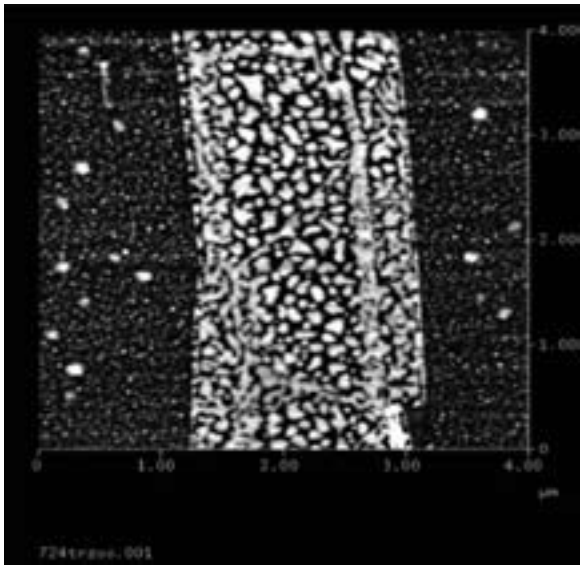

Figure 3: Graphene sample soaked in FITC for one hour after ALD.

Future Work

We will attempt to try more hydrophilic chemicals to achieve a uniform distribution of the Al_2O_3 (oxide) layer. Once achieved, we will etch the graphene down to a narrow ribbon and use the e-beam to pattern contacts on the graphene sample. Once the pattern is made, we will use metal sputtering to deposit the metal contacts on the graphene sample. We will then test the electrical properties of the device and compare with a chemistry method being tested in the lab.

Acknowledgements

I would like to thank my PI, Professor Hongjie Dai, for allowing me the opportunity to work in his lab this summer. I want to acknowledge my mentor Xinran Wang and the Dai Lab for all of their help and effort to help me this summer. I also want to thank Mike Deal and Maureen Baran and the whole Stanford Nanofabrication Facility staff. Last, but certainly not least, I want to thank the Intel Foundation for their financial support, and National Nanotechnology Infrastructure Network Research Experience for Undergraduates Program and Melanie-Claire Mallison for providing this opportunity.

References

[1] Yang, Li. " Quasiparticle Energies and Band Gaps of Graphene Nanoribbons" Jun. 2007: arXiv:0706.1589v1. 11 Jun. 2007 <http:// cond-mat.mes-hall>.

Carbon Nanotube Transistor Fabrication and Reliability Characterization

Latisha Crockett

Electrical Engineering, Prairie View Agricultural & Mechanical University

NNIN REU Site: Stanford Nanofabrication Facility, Stanford University
NNIN REU Principal Investigator: Dr. Philip Wong, Electrical Engineering, Stanford University
NNIN REU Mentor: Deji Akinwade, Electrical Engineering, Stanford University
Contact: lcrockett1@pvamu.edu, hspwong@stanford.edu, dejia@stanford.edu

Abstract

Carbon nanotubes (CNT's) are molecular-scale tubes of graphitic carbon with outstanding properties. CNT's are stronger than steel, harder than diamonds, and also posses unique electrical characteristics such as the following: high electrical conductivity, very high tensile strength, highly flexible, high thermal conductivity, and good field emission of electrons. They have the ability to increase the tensile strength and halt crack propagation in concrete, provide stronger yet lighter sports equipment, produce artificial muscles, stronger bridges, are instrumental in production of a space elevator, and act as transistors/diodes/resistors in computer circuits. However, commercial applications have been gradual due to high production costs and issues concerning reliability. When exposed to oxygen or a natural atmosphere, the nanotubes degrade within a few days. Therefore, we suspended CNT's in various polymers which provided a medium that should protect the carbon nanotubes from the atmosphere.

By placing the suspended CNT's on devices that were built on silicon wafers, we were capable of measuring the CNT electrical characteristics. Therefore, we were able to observe how the CNT's degrade with time while being suspended in various polymers. The goal was to discover a polymer that increased the amount of time that CNT's remain effective, and hence greatly enhanced their stability and utilization.

Introduction

The proposed problem is that carbon nanotubes are degrading too quickly in ambient air. Therefore, the point of the study is to experiment with different polymers to passivate the nanotubes and increase their working lifetime. It was hypothesized that carbon nanotubes coated with a polymer will not degrade as quickly as those not coated with polymers. The theoretical implication of the study included the fact that the exact causes of CNT degradation are not known, and the results should determine how the atmosphere changes the quality of the CNT.

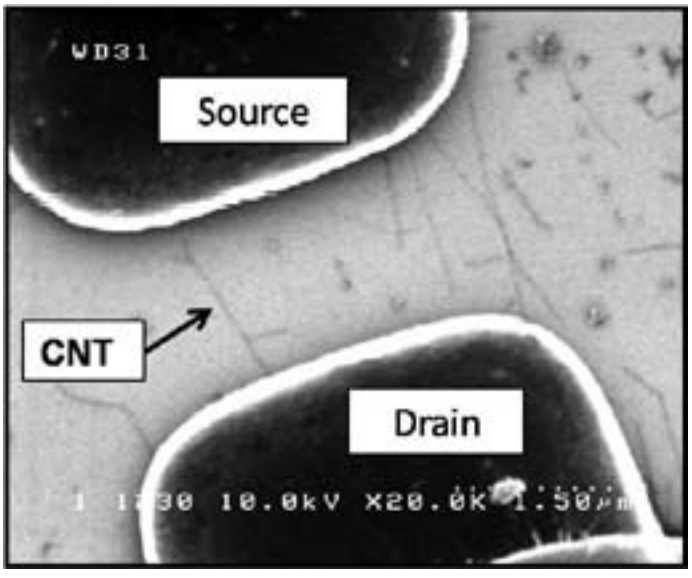

Figure 1: SEM image of CNT connected via the source and drain electrodes on the device.

Experimental Procedures

The experimental design revolved around a plan to build devices, on silicon wafers, which were capable of testing the electrical characteristics of CNT's, and then placing the CNT's on the devices. The CNT's were in the form of a liquid solution which contained completely dispersed CNT's as shown in Figure 1. In order to build the devices and coat them with the polymer, four photolithography steps utilizing different masks were required. Mask one: gold/chrome deposit and liftoff. Mask two: source drain electrodes for CNT. Mask three: isolation to separate devices via gold/chrome etching. Mask four: polymer deposit and polymer etch from bond pad. (Note: The CNT's were deposited using the dielectrophoresis (DEP) method. Experiments were completed to find the etch rate for each polymer, which was removed using the dry etching process.) Figure 2 displays a cross-section of the method for building the device, and the deposition of the CNT's and polymer.

Results

The first run results were flawed due to an issue concerning oxide breakdown, which occurred with those wafers that originally consisted of a 10 nm oxide layer. The calculated

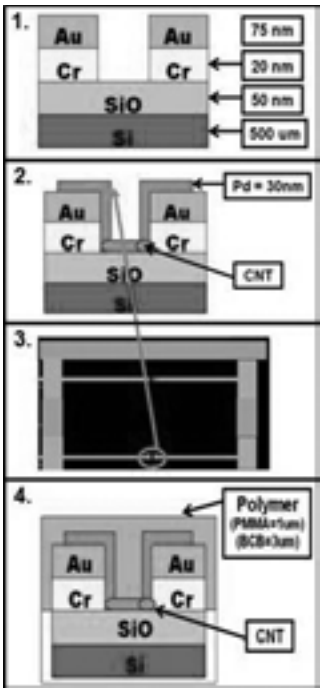

Figure 2: Cross section of four mask method.

voltage breakdown (VB) equaled 100 V. However, the measured VB was 10 V. The remaining runs utilized wafers which consisted of a 50 nm oxide layer which prevented further occurrences of oxide breakdown.

Repeatability test were completed to understand how the probing process may affect the results. One repeatability test showed that when the devices are probed once and a voltage sweep is applied continuously over a set period of time, the results are repeatable. However, the results are not repeatable when the devices are probed multiple times and a voltage sweep is applied each time the device is re-probed. During the first run of the multi-probed repeatability test, the gate and drain current dropped significantly after the eighth device probing was complete.

After the four mask method was complete, the wafer with no polymer had a 69% yield of good devices (see Figure 3), while the wafer covered with polymethyl methacrylate (PMMA) had a 33% yield, and the wafer covered with benzocyclobutene (BCB) had a 7% yield.

A high drain current is desired, because drain current behaves as a conductor. Gate current behaves as an insulator; therefore it needs to be relatively small. The electrical characteristics of the same devices were measured and compared each day to observe the amount of time that elapsed before CNT degradation was noticed (see Figure 4). The CNT's on the wafer without the polymer and the wafer coated with PMMA degraded at

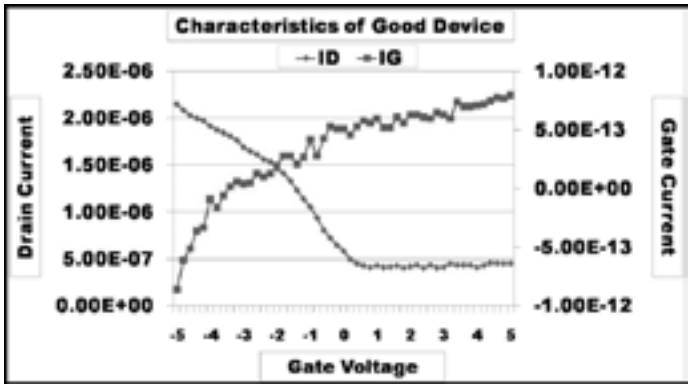

Figure 3: Example of a good semiconductor device.

approximately the same rate. However, on day eight of the experiment, 8% of the devices on the wafer without the polymer remained functional, while 31% of those on the wafer covered with PMMA remained functional. After three days, 0% of the devices on the wafer covered with BCB remained functional.

Conclusion and Future Work

The results led us to conclude that passivation does not appear to improve CNT lifetime, multiple probing appears to degrade the results, and BCB processing degrades CNT yield. The future work involves repeating the experiments with other polymers to observe how the polymers alter the CNT lifetime.

Acknowledgements

The author wishes to thank the National Nanotechnology Infrastructure Network Research Experience for Undergraduates Program, National Science Foundation, Intel Foundation, Deji Akinwade, Dr. Philip Wong, Dr. Noe Lozano, Maria Suggs, Mike Deal, and Maureen Baran.

References

[1] Sedra, Adel S., and Kenneth C. Smith. Microelectronic Circuits. New York: Oxford University Press, 2003.

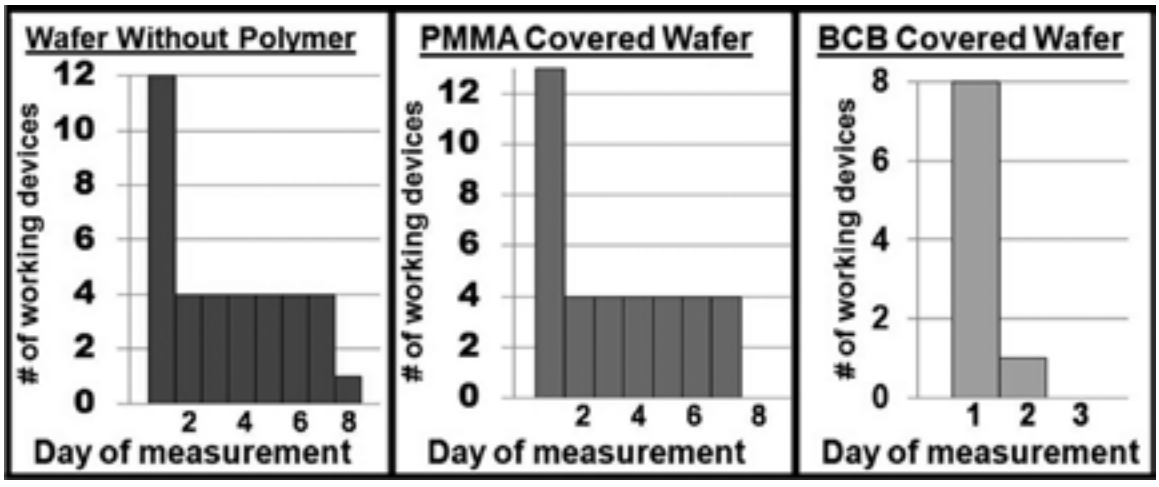

Figure 4: Results of degradation rates for each wafer.

P-Type Contact Optimization in Nonpolar Gallium Nitride-Based Blue Lasers

Daniel Haeger

Economics, Illinois Wesleyan University

NNIN REU Site: Nanotech—The UCSB Nanofabrication Facility, University of California, Santa Barbara
NNIN REU Principal Investigator: Shuji Nakamura, Materials Department, University of California, Santa Barbara
NNIN REU Mentor: Robert M. Farrell, Electrical and Computer Engineering, University of California, Santa Barbara
Contact: dhaeger@iwu.edu, shuji@engineering.ucsb.edu, rmf@ece.ucsb.edu

Abstract

Polar gallium nitride (GaN)-based blue lasers have been hindered by poor yields in their fabrication. Nonpolar GaN-based blue lasers, which are grown along a different crystal plane than polar GaN-based blue lasers, show great promise for increasing laser yields and lifetimes. They lack the polarized electric field inherent in c-plane GaN substrates. Continuous-wave (CW) operation of nonpolar lasers has been recently achieved, yet they are hindered by their low lifetimes relative to polar blue lasers. Initial measurements suggest that a large increase in lifetime can be realized by reducing the resistance across the p-type metal contacts of the laser. Contacts schemes were tested using a circular transfer length method (CTLM) structures. Significant improvements in the p-type contact resistance have been realized by optimizing metallization schemes, thermal annealing conditions, and doping levels.

Introduction

GaN and related materials have been around for over a decade and are extremely useful blue and near-UV light emitting diodes and lasers. Their uses include ultra high density optical storage, lighting sources, high resolution printing and advanced medical imaging applications [1].

Non-polar GaN substrates are inherently difficult to grow and appropriate metal contacts with work functions higher than p-GaN are difficult to find [2]. The metals are typically more difficult to deposit due to higher evaporation temperatures and consequently are less reliable. Experiments have shown that the majority of the resistance is across the p-type contact resistance, so they are the best candidate for optimization at this point. Typically contacts for polar p-GaN use some combination of platinum (Pt), palladium (Pd), and gold (Au) contacts. Research has also shown that the resistance can be significantly reduced by growing a highly doped, p^{++}, layer on top of the p-GaN just beneath the contacts [2].

Experiment

The p-GaN M-plane substrates were grown by Mitsubishi Chemical. The top 20 nm p^{++} layer was grown by metal-organic chemical vapor deposition techniques. The sample was then rapid thermally annealed at 750°C in nitric oxide (N_2O_2) for 15 minutes. Then 100 nm of silicon oxide (SiO_2) was deposited on top of the p-GaN as a protective layer during processing. The CTLM contacts were fabricated with standard photolithography techniques. The spacing varied between 5 μm to 100 μm. Then we used a 20 minute UV ozone de-scum followed by a 1 minute buffered hydroflouric acid (HF) wet etch and a 30 second hydrochloric acid (HCl) dip. The metal contacts were then put down with standard electron beam deposition techniques. The liftoff was preceded by a 30 second sonication in 70°C deionized water. Depending on what contacts we were making, we would repeat the process to make a set of 100-250 nm gold pads on top of the contacts to protect them during testing. Then I-V curves were obtained for three sets of CTLM's on each sample using a standard 2-probe arrangement. The data was aggregated and the contact resistances were determined at the 250 μA current level.

Results and Discussion

Figure 1 shows the specific contact resistivity as a function of the bis-cyclopentadienylmagnesium (CP_2Mg) flow rate (in standard cubic centimeters). The flow rate of the dopant gas during the metal-organic chemical vapor deposition (MOVCD) process

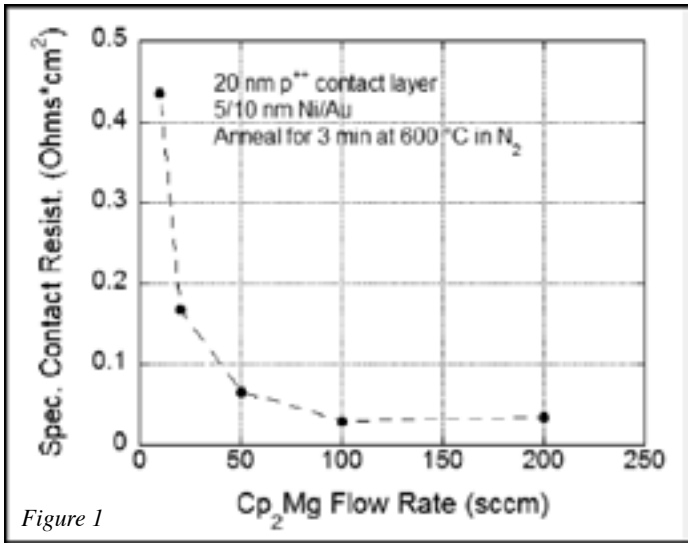

Figure 1

was varied for different samples. 100 sccm was found to be the ideal flow rate. More research is needed to optimize the specific contact resistivity between the 100 and 200 sccm flow rates. With the Ni/Au contacts in the first sample run the I-V curves were found to be considerably non-ohmic, and the resistances and several orders of magnitude higher than the literature on C-plane contacts suggested they should be.

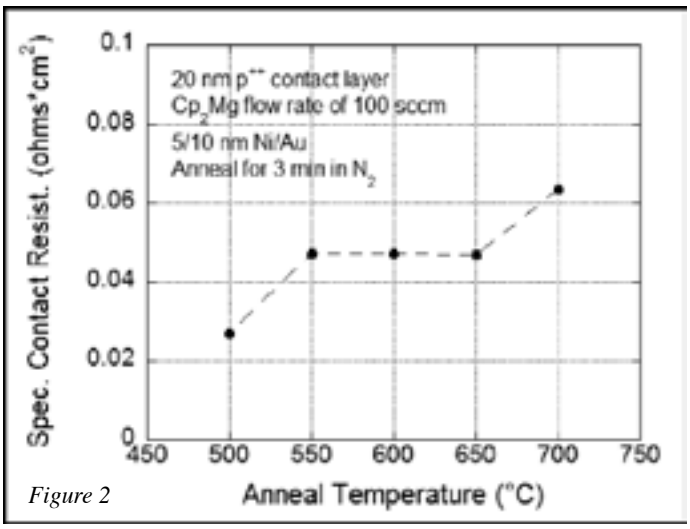

Figure 2

Then the anneal temperature of the Ni/Au contacts themselves was varied (Figure 2). We found considerable difference across the anneal temperatures. We still kept the original anneal temperature for the p-GaN the same for each sample. The overall numbers were around the same order of magnitude as the previous flow series. The I-V curves were slightly more linear, but still far from ohmic. However we determined that the nickel was perhaps not the best metal for the contacts and then varied the metallization scheme for the contacts.

The metallization scheme proved to be our most significant. We found that different metals provided an order of magnitude decrease in contact resistivity. We tried using metals with higher work functions since those seem to have lower contact resistance. The Pt/Pd/Au (7/7/100nm) proved to be the best scheme (Figure 3). Not only was the resistance lower, but most of the I-V curves were nearly perfectly ohmic. At higher spacing the curves were more linear, but at the lower spacing (5 to 10 μm) the curves looked slightly like a p-n junction I-V curve. We later tried several variations of the Pt/Pd/Au scheme and were able to optimize the thickness as well.

Contact Metals	Specific Contact Resistivity (Ω*cm^2)
Pt/Pd/Au	***0.0051***
Ni/Au Annealed in N_2 O_2	0.0106
Ni/Au Annealed in N_2	0.0115
Pd/Au	0.0497
Ti/Au	0.1306

Figure 3

Summary

We found an optimum metal scheme and thickness for the contacts. We also optimized the surface treatments and wet etching processes. Our best contacts were nearly ohmic and the calculated specific contact resistivities were on the order we hoped for. We still have some work to be done with optimizing the flow rate and doping levels of the top p^{++} layer of the p-GaN, but the improvements made so far should give an order of magnitude increase in the laser lifetime and efficiency of the next batch of fabricated lasers.

Acknowledgements

I would like to thank the National Nanotechnology Infrastructure Network Research Experience for Undergraduates Program for their funding and support, as well as everyone in the Nakamura research group at UCSB, especially Robert Farrell.

References

[1] Farrell, B., Haeger, D., et al. "Continuous-Wave Operation of AlGaN-Cladding-Free Nonpolar m-plane InGaN/GaN Laser Diodes"; Japanese Journal of Applied Physics, Vol. 46, (2007).

[2] Kim, H., et al. "Interfacial reaction effect on the ohmic properties of a Pt/Pd/Au contact on p-type GaN"; Journal of Vacuum Science and Technology, Vol. 22, (2004).

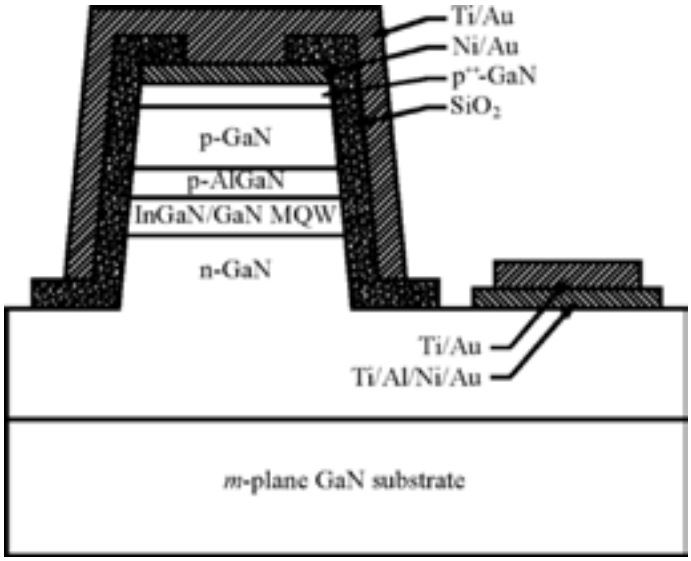

Figure 4: A cross sectional view of the laser [1].

Demonstration of a Novel Fabrication Methodology to Produce Complex, Three Dimensional Structures

Daniel Linford

Physics, University of Rochester

NNIN REU Site: Microelectronics Research Laboratory, Georgia Institute of Technology
NNIN REU Principal Investigator: Muhannad Bakir, Electrical Engineering, Georgia Institute of Technology
NNIN REU Mentor: Hang Chen, Chemistry and Electrical Engineering, Georgia Institute of Technology
Contact: dlinford@mail.rochester.edu, muhannad.bakir@mirc.gatech.edu

Abstract

Fabrication of high aspect-ratio three-dimensional (3D) microstructures has many important applications in modern microchip technology. A micro-electro-mechanical system (MEMS) fabrication procedure is presented that can produce high aspect-ratio 3D metal structures, which may be used for (but is in no way limited to) electronic, optical, chemical, and/or fluidic interconnection. This represents the interdisciplinary marriage of a number of highly disparate device technologies. The aforementioned MEMS structures were produced through micro-fabrication procedures, including spinning photoresist, post and pre-baking, developing, curing, electroplating, polymer decomposition, and seed layer etching. Some of the applications of the structures which were fabricated using this method include coplanar waveguides, inductors, and microfluidic filters. The primary focus of this research was to develop an enabling process technology to meet the fabrication and integration needs of generic 3D complex device structures.

Introduction

This study was performed in an attempt to demonstrate a novel fabrication methodology for producing complex three-dimensional microstructures. Although this method extends far beyond the creation of high aspect ratio copper pillars, the most comparable previous fabrication methodology was for that purpose.

In the past, there have been many different proposed fabrication methodologies for creating high aspect ratio copper pillars. These included the copper pillar bump process [5,6] and a method involving through silicon vias [2,3,4,6] wherein the silicon is etched following copper filling of the holes (known as "vias").

The pillar bump process involved patterning a layer of photoresist and then electroplating into the resist openings [5,6]. This method was severely limited in several ways, including the fact that it was extremely difficult to electroplate copper into high aspect ratio resist openings and it was very difficult to fabricate high aspect ratio vias in resist [6]. This process, therefore, was typically only able to achieve comparably low aspect ratios (usually, < 5.)

The other process essentially involved creating vias in a silicon wafer and then electroplating into the resultant vias [2,3,4,6]. Via creation was usually done either by etching or laser-ablation [6]. Next, an oxide layer would be deposited onto the wafer, followed by the deposition of a seed layer. The via would be filled with copper through an electroplating process. Finally, the silicon wafer would be etched away (using potassium hydroxide (KOH)) to leave behind the high aspect ratio copper pillars. There were also several problems with this process, to which several solutions were proposed. One such problem was the creation of voids during electro-deposition inside the vias due to the non-uniform current densities resulting from the local geometry of the sample. One proposed solution to this problem was the use of an aspect ratio dependent electro-deposition process, whereby the current density was continuously varied as a function of time [3]. Moreover, it is difficult to bond the resulting pillars to the wafer containing the circuitry.

It has been well established that it is possible to create high aspect ratio polymer pillars [1,7]. These have been mainly been used in attempts to create electrical-optical I/O devices (such as micro-electro-optical-mechanical systems or MEOMS) [1,7].

During a previous REU project, sidewall metallization of polymer pillars for use as chip I/Os was investigated [7], and it was shown to be possible to create copper pillars with aspect ratios exceeding 20:1. Under that method, polymer pillars were created, and then a seed layer was deposited onto them. Once the seed layer had been created, copper was electroplated onto the side wall of the pillar. Finally, the polymer was removed through thermal decomposition. What remained was a high aspect ratio structure [7].

The method proposed here extends that previous work and uses a similar process to create structures with a more complex geometry. Some of the structures created were square spiral inductors, coplanar waveguides, an electromechanical chuck, and a microfluidic filter.

Experimental Procedure

Two different fabrication methodologies were created, capable of creating ~ 50 μm and ~ 140 μm tall polymer pillars respectively (which would directly affect the height of the resulting structures). They differed in that the taller pillars were created by spinning two layers of polymer (Avatrel®) on the substrate surface. Herein, the sample with two layers of Avatrel shall be denoted as being produce through the "2-spin process."

A single layer of Avatrel 2090P polymer photoresist was spun on a silicon dioxide coated silicon wafer at 600 RPM for 40 seconds (twice for the 2-spin process.) The wafer was then pre-baked for 45 minutes on a hot plate at 108°C. Then the wafer was exposed for 25 seconds in an EVG620 mask aligner (50 seconds for the 2-spin). Following the exposure, the wafer was post baked for 20 minutes at 108°C in an oven. The wafer was then developed using an Avatrel development solution. Following this development, the wafer was inserted into a PlasmaTherm reactive ion etcher (RIE) for a minimum of 3 minutes for descumming. After the descum, the wafer was cured in the Lindberg furnace at a temperature of 160°C for 2 hours. After having been cured, the wafer was metallized using the Unifilm sputterer (with 300Å of titanium, 3000Å of copper, and 300Å of titanium). This thin layer of metal acted as a seed layer for the copper electroplating which would occur later in the procedure.

A second layer of Avatrel was then spun on top of the wafer, again at 600 RPM for 40 seconds (this is done twice for the 2-spin process.) The wafer was then pre-baked once more, and then exposed using the mask aligner (for 30 seconds for the single spin process and 37 seconds for the 2-spin process). Once again, the wafer was post baked at 108°C for 20 minutes, following which the wafer was again developed. The wafer was placed into the RIE for a minimum of an additional 3 minutes. The wafer was then placed into a buffered oxide etchant (BOE) to remove the 300Å layer of titanium on its surface. The top surface of the wafer was then electroplated using a copper sulfate solution, a copper anode and the wafer as the cathode. The wafer was then thermally decomposed in the Lindberg Furnace for 2 hours at 450°C to remove the Avatrel. To remove the remaining seed layer, the wafer was placed into a copper etching solution produced from a 1:1 ratio of hydrogen peroxide and ammonium peroxide.

Results and Conclusions

A novel fabrication methodology for producing complex, 3D structures was demonstrated to be feasible. Several different structures with various different interdisciplinary applications were constructed. In addition, process optimization has been performed. An aspect ratio of ~ 17.1:1 was achieved, as measured via images from the Hitachi scanning electron microscopy (SEM).

Future Work

In the future, additional work can be done on building taller structures, or structures with more complex geometries. Work can also be done on providing a computational model of the various stresses, strains, and forces induced on the structures to determine the origins (and theoretical magnitudes) of the several different kinds of deformations that were observed to occur on the structures during the fabrication process.

Acknowledgments

The author would like to thank the National Science Foundation and, in particular, the National Nanotechnology Infrastructure Network, for allowing me to be involved in this REU program. Gratitude should also be extended to the Georgia Institute of Technology, the Microelectronics Research Center (MiRC) and its staff, and, in addition to the author's mentor, Hang Chen, and principal investigator, Muhannad Bakir. Likewise appreciation should be extended to Mrs. Jennifer Tatham Root and her assistants. Finally, acknowledgment needs to be given to Dr. James Meindl.

References

[1] Bakir, M, Gaylord, T, Martin, K, & Meindl, J (2003). Sea of Polymer Pillars: Compliant Wafer-Level Electrical-Optical Chip I/O Interconnections. IEEE Photonics Technology Letters, 15.

[2] Dixit, P, Miao, J, & Preisser, R (2006). Fabrication of High Aspect Ratio 35 micrometer Pitch Through-Wafer Copper Interconnects by Electroplating for 3-D Wafer Stacking. Electrochemical and Solid-State Letters. 9.

[3] Dixit, P, & Jianmin, M (2006). Aspect-Ratio-Dependent Copper Electroplating Technique for Very High Aspect-Ratio Through-Hole Plating. Journal of the Electrochemical Society. 153.

[4] Dixit, P, Xu, L, Miao, J, Pang, J, & Preisser, R (2007). Mechanical and Microstructural Characterization of High Aspect Ratio Through-Wafer Electroplated Copper Interconnects. Journal of Micromechanics and Microengineering. 17.

[5] He, A, Osborn, T, Allen, S, & Kohl, P (2006). Low-Temperature Bonding of Copper Pillars for All-Copper Chip-to-Substrate Interconnections. Electrochemical and Solid-State Letters, 9.

[6] Keigler, Arthur, & Wu, Bill, & Liu, Zhen (2006, August). Copper Deposition for Pillars and Vias. Semicon. Manufacturing, 7(8).

[7] Shodeinde, Tajudeen (2006). Sidewall Metallization of High Aspect Ratio Perpendicular Polymer Structures for Chip I/O Interconnections. NNIN REU 2006 Research Accomplishments.

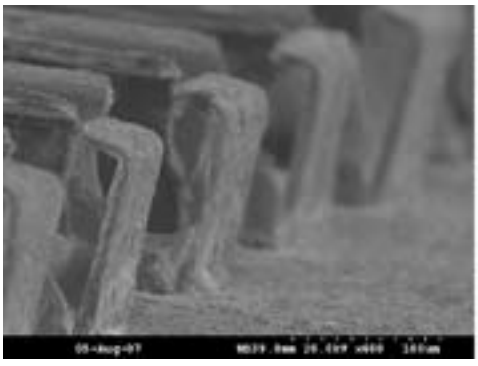

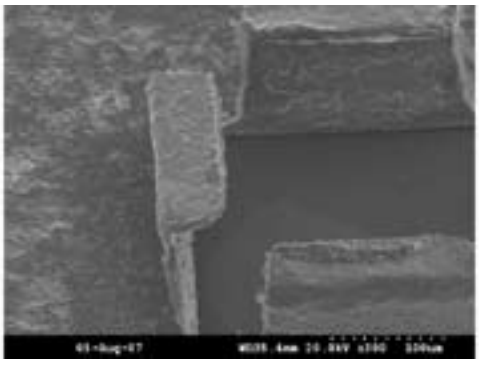

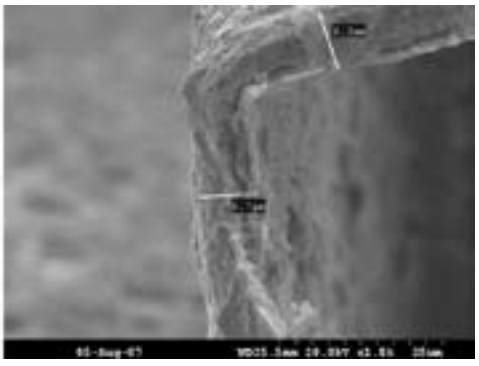

Adhesion and Electromigration Performance of Barrier / Copper Interconnections in CMOS Technologies

Nasim Naderseresht

Electrical Engineering and Computer Science, University of California, Berkeley

NNIN REU Site: Stanford Nanofabrication Facility, Stanford University
NNIN REU Principal Investigator: Prof. Reinhold Dauskardt, Dept. of Materials Science and Engineering, Stanford University
NNIN REU Mentor: Ryan Birringer, Dept. of Materials Science and Engineering, Stanford University
Contact: nasimnader@snf.stanford.edu, dauskardt@stanford.edu, ryan34@stanford.edu

Introduction and Motivation

Electromigration (EM), the movement of metal atoms due to the flow of current, can cause failure in interconnects in complementary metal oxide semiconductor (CMOS) circuits. EM performance in copper (Cu) interconnect structures is largely related to the diffusion of copper atoms along the barrier layer interfaces. It has been shown that the mobility of copper atoms is closely related to the adhesive strength of this copper / barrier layer interface [1]. In the past these properties have usually been assessed separately.

Previously, Zhou et al. [2] reported that there was an increase in electromigration mean-time-to-failure as the interlayer adhesion increased. Lane et al. [1] showed that when the interface debonding energy of a copper / barrier layer is small, the void growth rate during EM is higher. This is presumably due to more mobile copper atoms. This again shows a connection between EM and adhesion.

In our work, we are developing a novel technique for characterizing EM performance and adhesion of a copper/barrier layer simultaneously. Once this technique is developed, it will provide a unique tool in optimizing EM performance in the next generation of integrated circuits and nanoelectronics. Using thin film fracture mechanics techniques, adhesion in copper / barrier film stacks was analyzed in the presence of electromigraton. The crack propagation rate or velocity, v, was measured versus applied strain release rate, G (which is a measure of adhesion). This was measured while different current densities were applied. X-ray photoelectron spectroscopy (XPS) was performed on the fracture surfaces to see if the failure does indeed occur at the Cu/barrier interface.

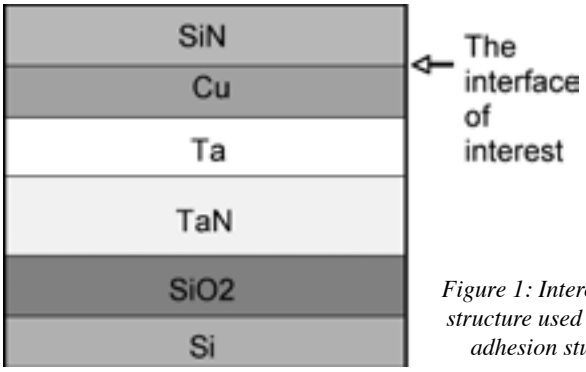

Figure 1: Interconnect structure used in EM/ adhesion studies

Experimental Method

Samples were obtained of typical multilayer interconnect structures, as shown in Figure 1. Copper was the main conducting layer and silicon nitride (SiN) was the barrier layer on top. The SiN layer was etched off at the ends in order to make contact areas. 85% aqueous phosphoric acid at room temperature was used. The resistance was measured every 5 minutes until the SiN was removed.

As shown in the schematic diagram in Figure 2, the crack propagation rate or velocity, v, was measured versus applied strain release rate, G (which is a measure of adhesion) by using standard subcritical double-cantilever beam fracture mechanics method. This was measured while different current densities were applied.

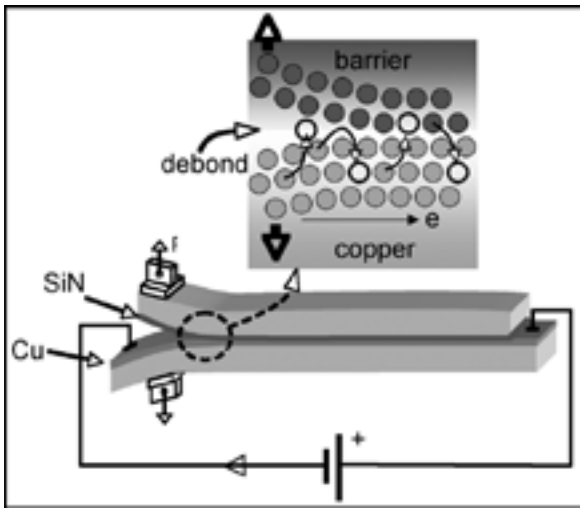

Figure 2: Schematic of samples used in standard subcritical double-cantilever beam fracture mechanics measurement, to measure crack velocity, v, versus adhesion, G, for different current densities.

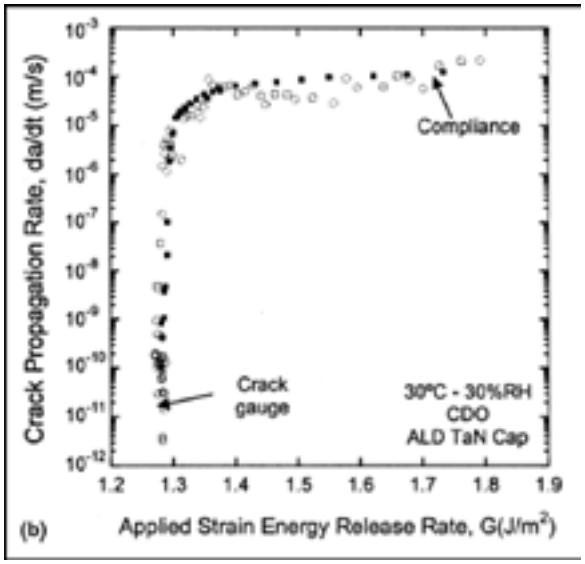

Figure 3: Previous results of our group measuring crack velocity versus adhesion without any current [3].

Results and Discussion

Figure 3 shows the results of previous work by our group [3]. This shows the relationship between crack velocity, v, versus the applied strain energy release rate, G (or driving force for cracking/debonding) for a copper/tantalum nitride interconnect without any current. In our present results, shown in Figure 4, we see v-G curves for two control specimens and two specimens with different current flow, J. Negative J represents electrons flowing opposite to the crack growth direction and positive J represents electrons flowing along the crack growth direction. We can see that these current densities are ~ 2 orders of magnitude below those used in standard electromigration tests, and there is no noticeable effect on crack growth at these low current densities.

XPS was done on the two surfaces exposed by the fracture in order to determine which interface of the structure failed. Table 1a shows XPS results of the top fracture surface (in Figure 2), indicating it is indeed a SiN layer. Table 1b shows XPS results of the bottom fracture surface (in Figure 2), indicating it is, in fact, a copper layer. From these results, we can conclude that the crack is indeed growing between the layer of Cu and the layer of SiN.

Si (2s)	34.6 %
N (1s)	24.1 %
Cu (3p)	0.5%
O (1s)	28.4 %
C (1s)	12.4 %

Cu (3p)	28.7 %
O (1s)	45.0 %
C (1s)	26.3 %

Conclusions

Using thin film fracture mechanics techniques, adhesion in copper / barrier film stacks was analyzed in the presence of electromigraton. Initial results at low current densities show no change in adhesion. X-ray photoelectron spectroscopy was performed on the fracture surfaces to show that the failure does occur at the Cu/barrier interface. Further measurements of crack propagation at higher current densities need to be done. Challenges that need to be overcome in the future are excessive Joule heating at these higher current densities, and enhanced oxidation for Cu and failure of solder joints at the higher temperatures due to the Joule heating.

Acknowledgments

I would like to thank Prof. Dauskardt for letting me work in his group, Michael Deal for being so helpful and for guiding me through the process, and Ryan Birringer for mentoring me, helping me out throughout the experiments and for answering all of my questions. Also I would like to thank the National Nanotechnology Infrastructure Network Research Experience for Undergraduates Program, CIS, and NSF for giving me this opportunity.

References

[1] Lane, M.W. et al, J. of Applied Physics, vol 93, p. 1417, 2003.

[2] Zhou, Ying, et al, AMC, 2004.

[3] Guyer, et al, J. Mater. Res., Vol. 19, No. 11, Nov 2004.

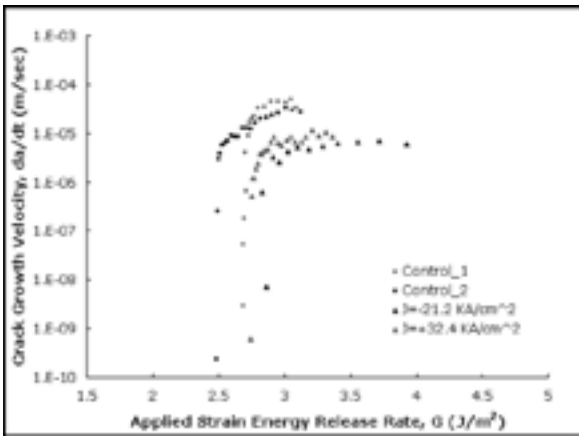

Figure 4, above: v-G curves for this work for two current densities, showing little effect on crack growth.

Table 1a, top left: XPS results of the bottom fracture surface (in Figure 2), indicating a copper layer.

Table 1b, bottom left: XPS results of the top fracture surface (in Figure 2), indicating an SiN layer.

Post-22 Nanometer Non-Classical CMOS Transistors

Austin Nelson

Electrical Engineering and Physics, University of St. Thomas

NNIN REU Site: Nanotech—The UCSB Nanofabrication Facility, University of California, Santa Barbara
NNIN REU Principal Investigator: Dr. Mark Rodwell, Electrical and Computer Engr., University of California, Santa Barbara
NNIN REU Mentor: Gregory Burek, Electrical and Computer Engineering, University of California, Santa Barbara
Contact: aanelson@stthomas.edu, rodwell@ece.ucsb.edu, burek@ece.ucsb.edu

Abstract

As silicon transistors are reaching their limits, next-generation complementary metal oxide semiconductor (CMOS) transistors may use new materials such as III-V's (i.e. indium gallium arsenide (InGaAs)). Key steps in new transistor fabrication include epitaxial regrowth, planarization, and etchback. Several planarization materials have been tested to develop a smooth and controllable protection layer during gate exposure.

Introduction

Moore's Law predicts the doubling in transistor surface area density roughly every two years. However, silicon is rapidly approaching its limit in scalability, which will require fabrication with new semiconductor materials. Currently, 65 nm gate length silicon devices are on the market, with 45 nm devices following behind. It is believed that silicon can be scaled to 22 nm devices, but beyond this limit, more exotic III-V materials such as InGaAs may be used in CMOS fabrication, which introduces a host of new engineering challenges.

The group objectives are to demonstrate a concept device showing that CMOS transistors can be reliably fabricated using III-V materials, confirm the record breaking current density of greater than 6 mA/μm that theory predicts, and then scale to sub-22 nm gate lengths.

A crucial aspect of the fabrication routine is the planarization process, whereby the source/drain contact regions are protected when the gate stack is exposed. Once the gate stack has been processed, a highly-doped InGaAs layer is conformally regrown across the wafer to provide current carriers, followed by a molybdenum (Mo) layer for ohmic contacts. These layers must be etched off the top of the gate stack, yet remain intact on the source/drain contact regions. However, the physical and chemical etch processes not only penetrate the source and drain regions, but they are also capable of damaging the InGaAs conduction channel, as shown in Figure 1.

In the planarization process, a thick layer of material is spun on a wafer to create a smooth plane at the surface. This layer is then ashed back to just below the gate height, exposing the gate but covering the source/drain regions. The InGaAs and Mo layers are then removed from the gate stack, and stripper solution removes the remaining planarization material from the source/drain regions so that contacts can be laid.

Experimental Procedure

Three different potential planarization materials were tested for the smoothest, most reliable, and most controllable characteristics: SPR510, a photoresist; PMGI SF11, a photoresist underlayer material; BCB, a plastic material.

The three planarization materials differed in their spin and curing recipes, as well as the ash process. PMGI is ashed back with MIF701 developer, SPR510 with an O_2 plasma, and BCB with CF_4/O_2 plasma. During the ash stages, samples were progressively cleaved and inspected in the scanning electron microscope (SEM) to check the planarization height relative to the gate stacks. Once they were ashed to the proper height, the Mo and InGaAs etches were performed to see if the planarization materials provided proper protection.

All materials were tested on samples that contained "pseudo" gate stacks, which were composed of chromium (Cr) and silicon dioxide (SiO_2) on a Si wafer, and differ from the final design depicted in Figure 1. The entire sample was then covered in Mo to simulate the regrowth stage.

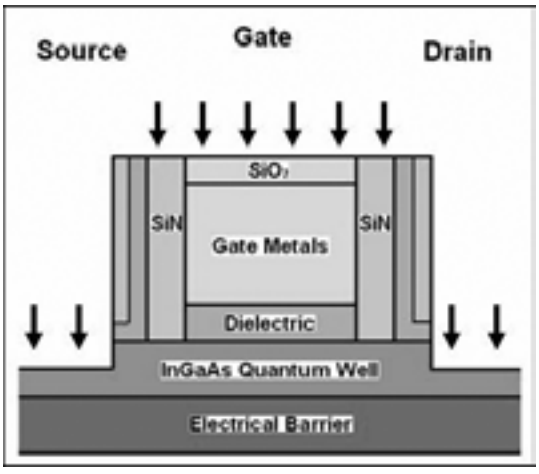

Figure 1: Mo and InGaAs etching can damage conduction channel.

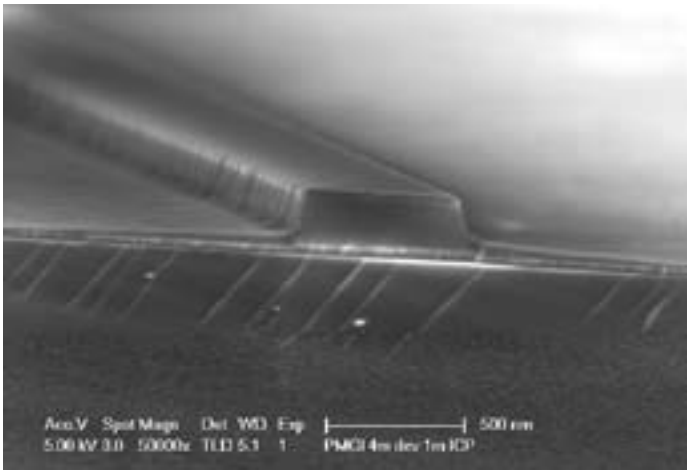

Figure 2: PMGI sample after developing and Mo etch.

Results and Conclusions

PMGI SF11 developed smoothly and evenly, creating the desired planar surface. However, it was difficult to spin on a smooth layer, and the PMGI etched off very rapidly under the Mo etch. As seen in Figure 2, almost no PMGI remains on the surface, so the source/drain regions are exposed.

The BCB samples maintained a smooth surface just below the gate height after ashing, but BCB requires a sensitive curing process, is difficult to remove, and takes much longer to process than SPR510, so it is being saved as a backup option in the final process.

SPR510 spins on smoothly and the ash rate is much slower and thus more controllable. However, when ashed with O_2 plasma, the surface was very rough and it was difficult to obtain a smooth gate stack exposure. Experiments were also executed with a post-ash reflow bake and O_3 plasma to smooth the surface, but these processes yielded little improvement—if any—on the surface roughness, as seen in Figure 3.

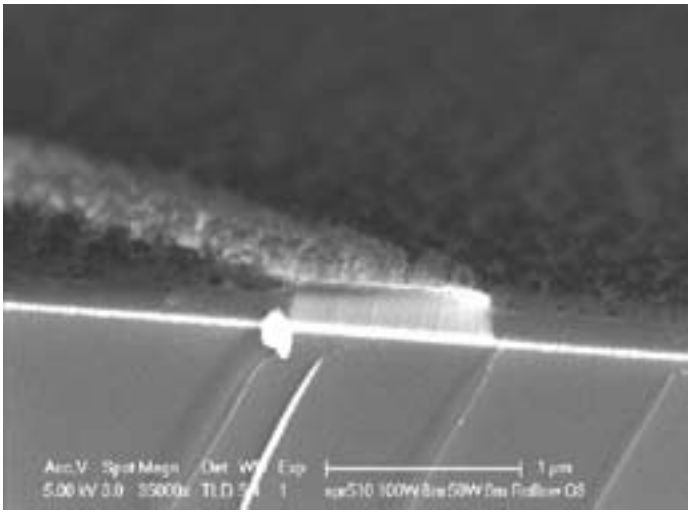

Figure 3: SPR510 after ash, reflow bake, and O_3 plasma.

It was later suggested that ashing the SPR510 in inductively-coupled plasma (ICP) rather than the capacitively-coupled plasma may yield a smoother surface. As seen in Figure 4, the sample has a much smoother surface, a cleanly exposed gate following the Mo etch, and most of the original photoresist remains at the level of the gate stack.

Each of the three materials has distinct strengths and weaknesses, but SPR510 appears to be the best candidate for the planarization process. It yields a smooth surface, controllable ash rate, and withstands the subsequent Mo and InGaAs etches. PMGI etches too rapidly, and BCB may be a strong candidate, but is much more cumbersome to work with than SPR510.

Future Work

The team must integrate the three distinct stages of the entire transistor fabrication process. The planarization process has been developed using gate stacks that mimic the samples that will be returned from the regrowth lab. The process must be fine-tuned from beginning to end with the gate stack fabrication, regrowth layers, and planarization process, as well as back-end processing.

Acknowledgements

A special thanks to the following people and organizations for their support: my principal investigator, Dr. Mark Rodwell; research mentor, Greg Burek; other team members, Uttam Singisetti and Dr. Mark Wistey; the UCSB cleanroom staff; the National Nanotechnology Infrastructure Network Research Experience for Undergraduates Program.

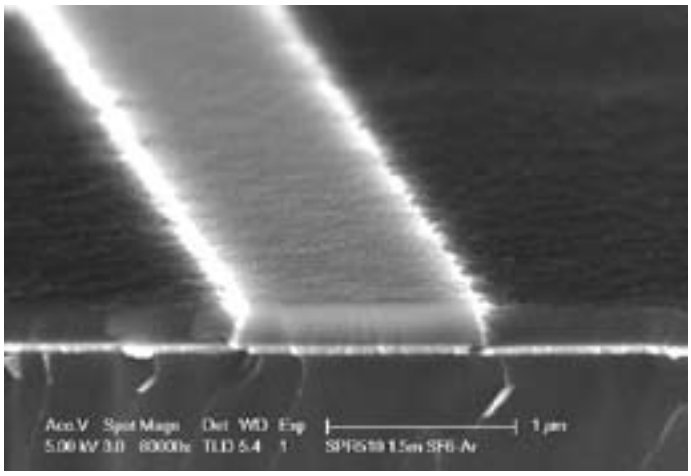

Figure 4: SPR510 after ICP and Mo etch.

Ohmic n-contacts to Gallium Nitride Light Emitting Diodes

Jonathan Aguilar

Physics, Harvard University

NNIN REU Site: Nanotech—The UCSB Nanofabrication Facility, University of California, Santa Barbara
NNIN REU Principal Investigator: Prof. Stephen P. DenBaars, Materials Department, University of California, Santa Barbara
NNIN REU Mentor: Kenneth J. Vampola, Materials Department, University of California, Santa Barbara
Contact: jaguilar@fas.harvard.edu, denbaars@engineering.ucsb.edu, kvampola@engr.ucsb.edu

Abstract:

Efficient light emitting diodes (LEDs) seek to minimize input power while maximizing optical output power. To minimize input power, the total voltage drop across the LED should be reduced. Significant loss occurs at metal-semiconductor junctions where electrical contact is made to the diode. This experiment studied different methods of minimizing the voltage drop across the LED. The p-contact on our device is made of indium tin oxide (ITO), which cannot tolerate annealing temperatures of 650°C or more [1,2]. The titanium aluminum gold (Ti/Al/Au) triple layers we use have been demonstrated to be effective n-contacts, but require annealing temperatures upwards of 750°C [3]. Therefore, our Ti/Al/Au contacts have been left unannealed, resulting in Schottky diode-like behavior of the junction.

Experimental Procedure

To improve the quality of the contact behavior, two contact schemes and methods of treating the n-type gallium nitride (GaN) surface were tested. The Ti/Al/Au scheme was compared to a copper germanide (Cu_3Ge) scheme. Cu_3Ge contacts to n-GaN can be annealed at temperatures within the tolerance of ITO [4]. Hydrogen chloride (HCl)-based wet etches are effective at removing native gallium oxides (Ga_xO_y) [5]. Lastly, etching the n-GaN surface by reactive ion etching (RIE) has been demonstrated to both improve ohmic behavior of the contact and decrease contact resistance [6]. The effect of annealing temperature on the Cu_3Ge contact scheme was also examined, but is not presented here.

Ohmic behavior and contact resistance were determined using the transmission line method (TLM). We used quarters of 2-inch Al_2O_3 wafers with epitaxial LED layers grown by metal-organic chemical vapor deposition (MOCVD). Before processing, the n-type GaN layer was exposed using an inductively coupled plasma etch to simulate etch damage that occurs during regular LED processing.

Sample	n-GaN treatment	Contact Scheme	Annealing Conditions
A	HCl	Ti/Al/Au	Unannealed
B	HCl	Cu_3Ge	550°C
C	RIE, 110W	Cu_3Ge	550°C
D	RIE, 170W	Cu_3Ge	550°C

Table 1: Contact scheme and surface treatment combinations.

Contact Deposition

Contact schemes and surface treatments were distributed across samples according to Table 1. Contact metals were deposited by electron-beam evaporation. Ti/Al/Au layer thicknesses were 200/600/3000Å. The Cu_3Ge contact scheme was deposited as Ge/Cu/Ge:400/970/400Å. This 30 at.% Ge composition has been observed to yield the low-resistivity ε_1-Cu_3Ge phase after annealing [7]. Cu_3Ge annealing was performed in a rapid thermal annealer at 550°C for 10 minutes in N_2 with a flow rate of 5 sccm. Ti/Au (200/3000Å) contact pads were then deposited on top of all n-contacts. The final step was to isolate the TLM patterns by etching around them through the n-type GaN to the Al_2O_3 substrate. The width of the resulting structure was 100 μm and the depth was 3.6 μm. Contact dimensions were 94×50 μm^2, and the TLM spacings varied from 5 μm to 40 μm.

Surface Treatment

n-GaN HCl immersion and RIE treatment were examined for their effect on ohmic behavior and contact resistance. Because these treatments affect only the n-GaN and not the contact, the resultant relative improvements in electrical performance are expected to be independent of the particular contact scheme. Therefore, these surface treatments were only tested on the Cu3Ge contact scheme. HCl treatment was performed by immersion in a HCl:DI 1:3 solution for 1 minute at room temperature. RIE dry etch was performed in $SiCl_4$ with a flow rate 10 sccm. Chamber pressure was 25 mTorr, and the etch depth was 50 nm into the n-type GaN. The samples were not temperature controlled during the RIE etch.

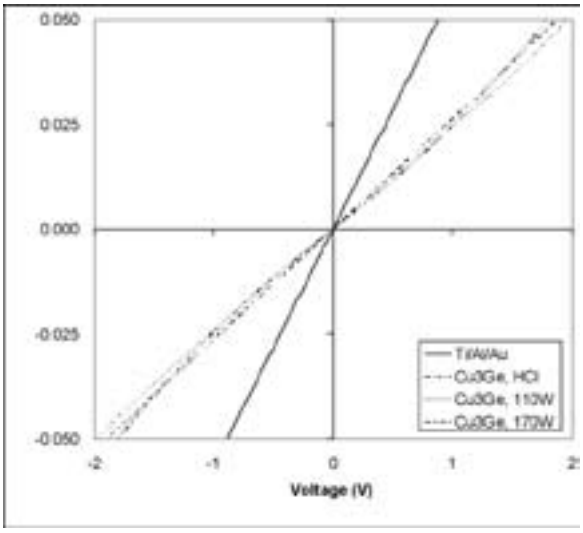

Figure 1: Current-voltage characteristics for different Cu_3Ge contacts on n-GaN.

Surface Treatment and Contact Scheme Results and Discussion

As can be seen in Figure 1, the behavior of Samples A and D were closest to ohmic. There are several possible explanations for ohmic behavior in samples. One is the removal of surface oxides and other types of surface scum that tend to accumulate during LED processing. In the case of the Sample A, the removal of gallium oxide by HCl etching is believed to be responsible for forming an ohmic contact. However, HCl immersion alone did not produce ohmic behavior in the Cu_3Ge-based samples. The emergence of ohmic behavior only after RIE treatment indicates other mechanisms besides oxide removal.

Schuette and Lu present evidence that RIE creates both Ga and N vacancies, but Ge preferentially diffuses into N vacancies and behaves as a donor, increasing the level of n-doping of the GaN [6]. $SiCl_4$ may also decrease the length of the electron depletion region [4]. Another possibility is that the RIE treatment helps remove etch damage caused by previous etching.

Figure 2 compares the contact resistances of the samples. The contact resistance of unannealed Ti/Al/Au was calculated to be $\sim 1.8 \bullet 10^{-4}$, less than half that of Cu_3Ge when both samples are treated only with HCl. However, it can be seen that RIE treatment dramatically reduced the contact resistance of the Cu_3Ge contacts.

Conclusions

Schuette and Lu show that RIE treatment reduces the length of the depletion zone in n-GaN [4]. Thus, the relative improvement of the Cu_3Ge contact with RIE surface treatment should be true regardless of contact scheme. Ti/Al/Au contacts will be used for further experimentation with RIE because of their superior performance compared to Cu_3Ge in the HCl control test. Lastly, the data indicate that there is a need to optimize RIE etching power for ohmic behavior and low contact resistance.

Acknowledgments

Thanks to Ken Vampola, Prof. Stephen DenBaars, and the rest of the SSLDC. I would also like to thank Seoul Semiconductor for supporting this work, and Angela Berenstein, the NSF, and the NNIN REU Program for the opportunity to work at UCSB.

References

[1] Determined during previous laboratory testing.
[2] Jang and Song. J. Appl. Phys. 101 (2007).
[3] Wang et. al. J. Appl. Phys. 89 (2001.)
[4] Schuette and Lu. J. Appl. Phys. 101 (2007).
[5] Ren et. al. J. Electrochem. Soc. 14 (1997).
[6] Schuette and Lu, J. Vac. Sci. Technol. B 23 (2005).
[7] Aboelfotoh et. al., J. Appl. Phys. 76 (1994).

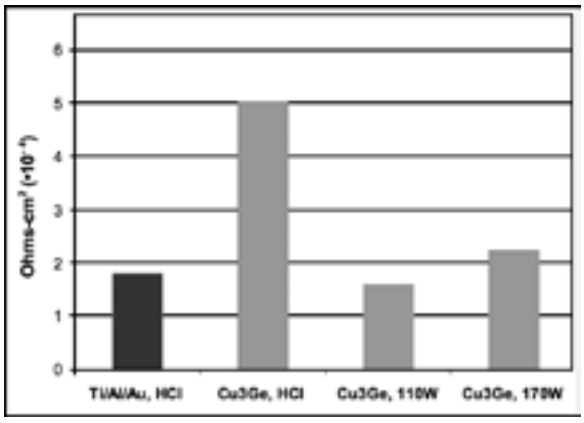

Figure 2: Specific contact resistance for different treatments.

Photoelectrochemical Etching of Silicon Carbide

Henry David Babb III

Electrical Engineering, Prairie View Agricultural & Mechanical University

NNIN REU Site: Howard Nanoscale Science & Engineering Facility (HNSEF), Howard University
NNIN REU Principal Investigator: Dr. Gary L. Harris, Director, HNSEF, Howard University
NNIN REU Mentor: Mr. James Griffin, Howard Nanoscale Science & Engineering, Howard University
Contact: babbtrey@yahoo.com, gharris@msrce.howard.edu, griffin@msrce.howard.edu

Abstract

Silicon carbide (SiC) was etched by photoelectrochemical (PEC) in a dilute solution of hydrofluoric acid (HF). PEC etch masks were formed on SiC by sputtering 10 nm of titanium and evaporating 150 nm of platinum and heating the contacts to 600ºC by rapid thermal annealing. PEC etching was performed with a UV light power density of 125 mW/cm² and a current density 0.992 mA/cm². Etching was performed for one hour at room temperature. The SiC nanopores were then oxidized at 1150ºC for four hours to form SiO_2 and subsequently placed in an HF solution to remove the oxide.

Introduction

SiC is so chemically resistive that only a few techniques are available to etch it. Hot potassium hydroxide (KOH) will etch SiC, however KOH will also remove almost all etch masks. Reactive ion etching (RIE) can be used to etch SiC also and a suitable etch mask exists for this process. RIE has very high anisotropy and good morphology, but it's an expensive process with no dopant selectivity. It does have a low etch rate but depending on the application, this can be considered an advantage or disadvantage. Photoelectrochemical etching has a more controlled etch rate from low to very high. It yields good morphology on 6H-SiC and excellent dopant selectivity. It's relatively inexpensive when compared to RIE, but only has fair morphology on 3C-SiC [1].

Photoelectrochemical etching is the process of using ultraviolet light, voltage, and chemicals to etch materials such as silicon carbide and gallium nitride. Pure silicon carbide is not a good conductor of electricity so its essential that silicon carbide be n-doped meaning more electrons are present than holes. Through photoelectrochemical etching, holes are generated with ultraviolet light by breaking some of the bonds in the SiC (Figure 1). Voltage is applied to the sample forcing holes to the surface of the sample to facilitate etching by hydrofluoric acid.

Experimental Procedure

First we characterized titanium/platinum (Ti/Pt) contacts on SiC as an etch mask by sputtering 10 nm of Ti and evaporating 150 nm of Pt and heating the contacts to 600ºC by rapid thermal annealing. The process of annealing makes sure that the Ti/Pt mask fully adheres to the surface of the SiC sample. SiC nanopores are formed on the substrate surface by PEC. PEC conditions for nanopore formation were: UV light power density of 125 mW/cm² and a electrical current density of 0.992 mA/cm² in a dilute solution of HF. Etching was performed for one hour for both 3C and 6H SiC. Nanopore formation was followed by oxidation of the SiC nanopores in a wet oxidation furnace for 4 hours at 1150ºC which changes the SiC nanopores to SiO_2. Finally a chemical etch of the newly formed SiO_2 was performed in HF.

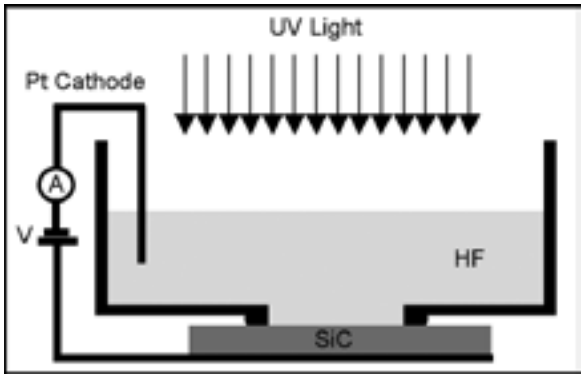

Figure 1: Photoelectrochemical setup.

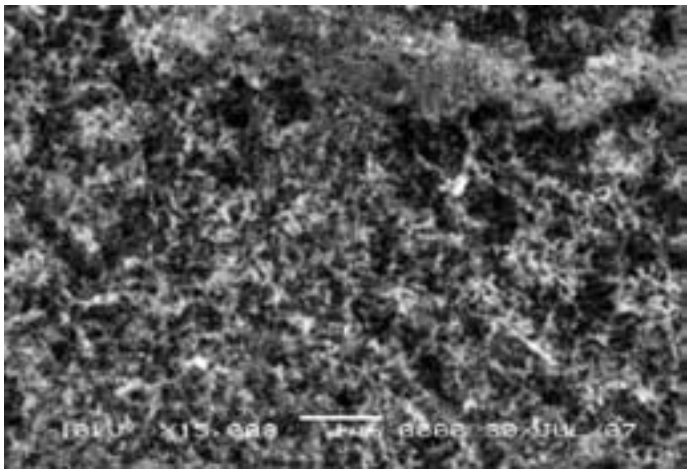

Figure 2: Porous silicon carbide.

Results

We produced nanopores on the surface of the SiC through PEC as seen in Figure 2. After oxidation, we could tell from the surface of the SiC sample that SiO_2 had formed because of the blue color that was visible on the sample where the nanopores were. SiO_2 was then removed with HF. We obtained etch depths of 13 μm for the 3C-SiC and 4.6 μm for 6H-SiC. Since 3C has a less dense lattice, we were able to obtain higher etch rates. Figure 3 is an SEM image of a 6H-SiC PEC etched sample.

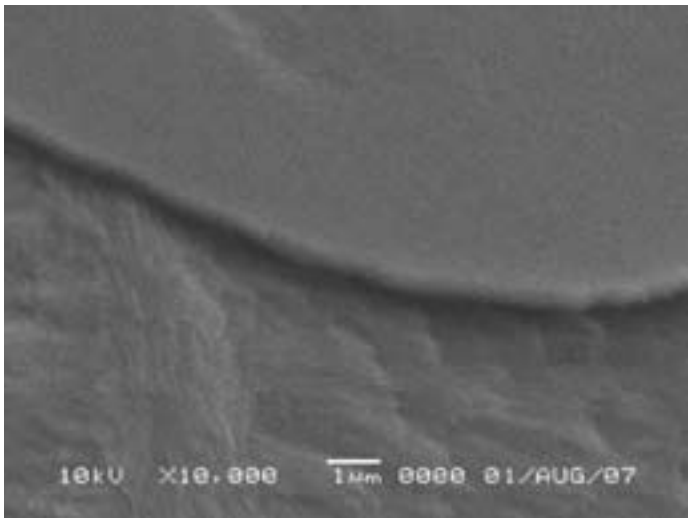

Figure 3: 6H-SiC after PEC etch.

Conclusion/Future Work

In conclusion, we were successful in forming nanopores, oxidizing the nanopores to form SiO_2, and removing the SiO_2 to get a clean etched surface on SiC. However we did have issues with getting the Ti/Pt mask to fully adhere to the SiC surface. We were able to solve this issue by heating the sample at 600ºC. Some samples were not etched because they were either undoped or low doped. In the future it would be beneficial to establish etch rates on 3C, 4H and 6H SiC based on doping concentration.

Acknowledgements

I would like to thank Dr. Gary L. Harris, Mr. James Griffin, Dr. Peizhen Zhou, the staff and students at HNF. I would also like to thank the National Nanotechnology Infrastructure Network Research Experience for Undergraduates Progam and the National Science Foundation for funding.

References

[1] "Properties of Silicon Carbide" Edited by Gary L. Harris, EMIS Datareviews Series No. 13, INSPEC, the Institution of Electrical Engineeers 1995.

[2] Hossain, T., Khan, F., Adesida, I., Bohn, P., and Rittenhouse, T. "Nanoporous Silicon Carbide for Nanoelectromechanical Systems Applications" NASA/CR 2003.

[3] Streetman, B.G. and Banerjee, S.K. "Solid State Electronic Devices" Pearson Prentice Hall 2006.

[4] Shishkin, Y., Choyke, W.J., and Devaty, R.P. "Photoelectrochemical Etching of n-type 4H SiC" 2004 J.Appl.Phys. 96, 2311.

Self-Assembly and Optical Characterization of Semiconductor and Metallic Nanocrystal Monolayers and Multilayers

Robert Bradley

Chemical and Biomolecular Engineering, North Carolina State University

NNIN REU Site: Nanoscience at the University of New Mexico

NNIN REU Principal Investigator: Prof. C. Jeffrey Brinker, Chemical and Nuclear Engineering, University of New Mexico, Sandia National Laboratories

NNIN REU Mentor: Shisheng Xiong, Center for High Technology Materials, Advanced Materials Laboratory, University of New Mexico

Contact: robradle@ncsu.edu, cjbrink@sandia.gov, ssxiong@unm.edu

Abstract

Interactions between semiconductor and metallic nanocrystals are the subject of intensive investigations. Enhanced photoluminescence (PL) yield of quantum dots in the presence of notable nanoparticles or nanohole arrays has potential applications in light-emitting diodes (LED) and sensors. Surface plasmon resonances (SPR) are believed to either increase the PL efficiency by enhancing the local exciting field or cause nonradiative damping due to energy transfer through an inverse route.

Introduction

We studied the collective interactions, in terms of linear and nonlinear optical properties, between cadmium selenide (CdSe) quantum dots, rods, cadmium telluride (CdTe) tetrapods and gold (Au) nanoparticles (NPs), comprised in monolayers and multilayers. Ultra thin films that incorporated NPs with a size of several nanometers were successfully created via an interfacial evaporation induced self-assembly (EISA) process. These films assembled on the surface of water within a polymethyl-methacrylate (PMMA) polymer matrix and were then transferred to desired substrates. Similarly, ultra thin films of pure PMMA were assembled, acting as a dielectric spacer between the two parallel layers of semiconductor and metallic NPs. Atomic layer deposition (ALD) was also utilized, allowing us to achieve precise control on the thickness of spacing layers. Finally, patterning of PMMA supported nanocrystal monolayer thin films was demonstrated. Our results indicate that the PL is affected by the distance between the semiconductor and Au nanoparticles.

Fabrication of Thin Films

Solutions of PMMA, CdSe nanocrystals or quantum dots, and Au nanocrystals, in an appropriate ratio, were dissolved in toluene. One drop of the solution was carefully released over a deionized water surface sitting in a Petri dish. The suspension of nanocrystals spread out over the surface and a thin film formed through interfacial evaporation-induced self-assembly as shown in Figure 1. The thin films consisted of the nanoparticles embedded in the PMMA polymer matrix. After the toluene evaporated, the thin film was captured on a substrate of our choice by submerging the substrate and bringing it up through the thin film. The sample was then left to dry undisturbed. The weight fraction of CdSe to Au nanocrystals within the solution was varied to explore the effect on photoluminescence. We also prepared multilayer thin films of the ratio-varied solutions to explore how stacking the layers would affect the PL.

First, we attempted to fabricate a binary nanocrystal superlattice from CdSe and Au nanocrystals dispersed with PMMA in toluene and let them co-assemble on the interfacial surface. However, the transmission electron microscopy (TEM) image in Figure 2 clearly indicates that isolated islands of nanocrystals with severe overlapping formed instead of a homogeneous monolayer thin film. Nevertheless, significant PL quenching was observed due to appropinquity of the two different types of nanocrystals when compared to the PL readings from a solution and monolayer thin film comprised solely of CdSe quantum dots.

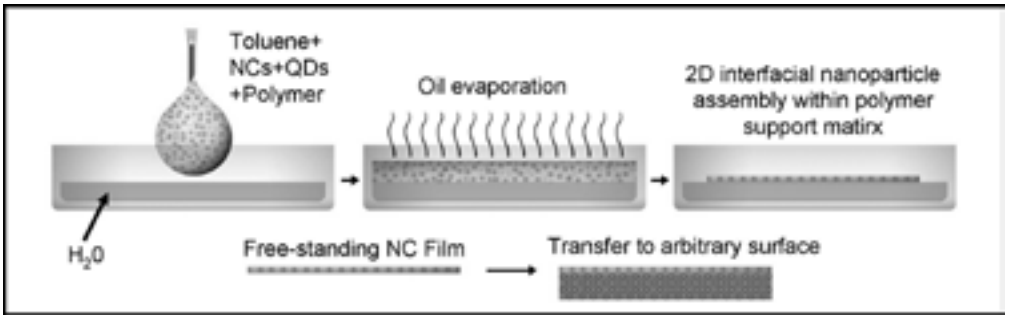

Figure 1: Schematic detailing evaporation induced self-assembly (EISA). A) Solution dropped onto surface, B) Oil evaporation, C) 2D interfacial nanoparticle assembly within polymer support matrix, D) Free-standing thin film, and E) Transfer to arbitrary surface.

Believing that the close proximity of the Au nanocrystals to the CdSe nanocrystals caused the quenching effect, we redesigned our experiment to further distance the two NPs by placing a dielectric spacing layer between a thin film composed of Au NPs and another thin film of CdSe NPs. In addition, this new strategy allowed us to tune the width of the spacing layer and this distance became the independent variable in our experiments.

Thin Films with Dielectric Spacing Layer

One thin film, composed of Au NPs, was transferred onto a glass substrate. Figure 3 shows how the solution composed solely of Au nanocrystals and PMMA creates a monolayer thin film, where the Au NPs do not coagulate, but spread out into a thin even film. Thin films composed solely of PMMA polymer were then captured on top of the Au nanocrystal layer until the desired thickness was obtained. Finally, the last thin film layer composed of CdSe NPs and PMMA was captured on top of all the other thin films. As the thin film layers were added to the sample, the surface of the sample became increasingly uneven. When the surfaces of the samples were scanned with a laser, the photoluminescence readings had no correlation to the number of PMMA spacing layers.

Seeking to better control the thickness and quality of the dielectric spacing layer, we utilized atomic layer deposition (ALD) to deposit a layer of amorphous SiO_2. We prepared 15 samples of 2 cm^2 silicon wafer chips by capturing a single Au ultra thin film layer on each wafer through EISA. The samples were then plasma-etched in order to render the surface hydrophilic and placed within the ALD instrument. All samples, heated to 50°C, were exposed to alternating cycles of vaporized $SiCl_4$ and H_2O in order to build up a dielectric spacing layer. One sample was removed from the instrument after every 30 cycles of deposition. A final thin film layer of CdSe and PMMA was captured on top of the amorphous SiO_2 to form a sandwich structure.

Electron beam lithographic patterning of Au and PMMA monolayer thin films has also been demonstrated. As a positive photoresist, PMMA can be washed away in the developer when exposed to light. Figure 4 shows an optical microscopy image of a patterned thin film. The diameter of the wheel is approximately 40 μm and the width of the lines is about 1 μm. Our patterning of these thin films suggests the ability to use interfacial assembly in device fabrication.

Results

We were able to successfully use interfacial assembly to create mono and multilayer thin films that incorporated semiconductor and noble nanocrystals. We also explored novel methods to create spacing layers between the two parallel thin films of CdSe and Au nanocrystals. Our results indicate that the photoluminescence of semiconductor nanocrystals can be affected by the appropinquity of noble metallic nanocrystals.

Acknowledgments

I would like to sincerely thank Professor Jeff Brinker and my mentor, Shisheng Xiong, for their guidance and support. Special thanks are also extended to the Brinker and Boyle Groups, the UNM coordinators, the National Science Foundation, and the National Nanotechnology Infrastructure Network Research Experience for Undergraduates Program.

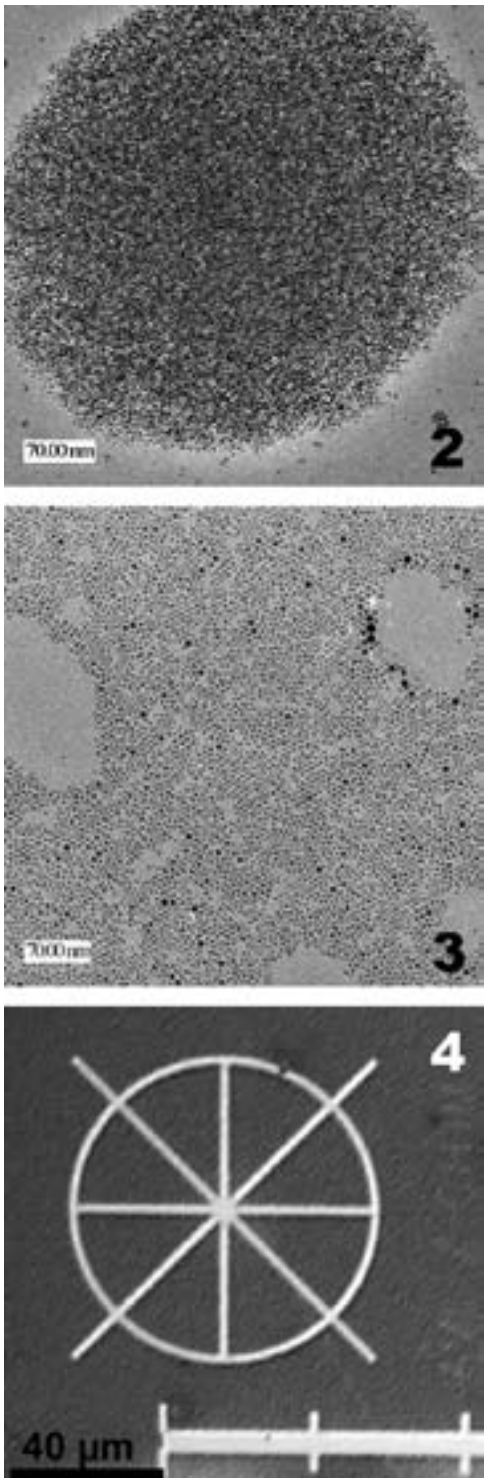

Figure 2, top: TEM image of CdSe / Au NP thin film supported by a PMMA polymer matrix.

Figure 3, middle: Ultra thin monolayer of Au NPs supported by PMMA polymer matrix.

Figure 4, bottom: Optical microscope image of patterned Au monolayer thin film.

Synthesis, Characterization, and Testing of Polyurethane Nanocomposites

Alla Epshteyn

Chemical Engineering, Tufts University

NNIN REU Site: Michigan Nanofabrication Facility, The University of Michigan Ann Arbor
NNIN REU Principal Investigator: Dr. Ellen Arruda, Mechanical Engineering, University of Michigan
NNIN REU Mentor: Amit Kaushik, Mechanical Engineering, University of Michigan
Contact: alla.epshteyn@tufts.edu, arruda@umich.edu, akaushik@umich.edu

Abstract

The dispersion of nanoscale reinforcements has been shown to raise the strength and stiffness of polymers [1]. In this project, polyurethane (PU) was reinforced with nanometer-sized clay platelets to make nanocomposites through the layer by layer (LBL) assembly process. Samples with 0, 12, 20 and 45 wt% clay were synthesized. Thermal characterization of these samples was done using a differential scanning calorimeter (DSC). Scanning electron microscopy (SEM) was used to measure the thickness, and thermo-gravimetric analysis (TGA) was used to determine the clay content in nanocomposites. Tensile tests at a constant strain rate were performed on a series of nanocomposite samples with an in-house built tensiometer. The nanocomposites were observed to exhibit enhanced mechanical stiffness, yield strength and toughness at various weight fractions of clay.

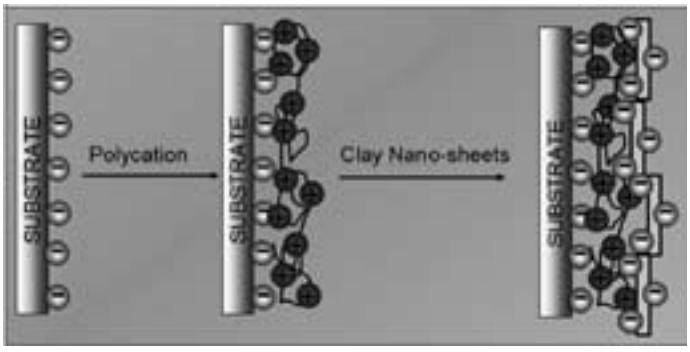

Figure 1: Adhesion of oppositely charged layers.

Synthesis (Layer by Layer Assembly)

The nanocomposites were synthesized by an emerging method of nanotechnology, the LBL assembly process. LBL is based on sequential deposition of nanometer-thick layers of oppositely charged components to build a multilayered structure. In this preparation, a glass substrate was alternately immersed into solutions of clay nanoparticles and cationic polyurethane, forming a new layer with each immersion through absorption. The oppositely charged layers adhered to each other resulting in homogeneously multilayered thin films on both sides of the glass substrate (Figure 1). These films were then separated from the substrate with a hydrogen fluoride solution. Finally, the films were treated with isopropanol alcohol.

Characterization

Clay content in each sample was determined with a Perkin-Elmer TGA. A small amount of sample (0.1-0.3 mg) was placed in a weighing pan of the instrument's ultra-sensitive balance and the sample was heated from 50ºC to 1000ºC at a heating rate of 10ºC/min while being purged with air at 20 ml/min. The weight change of each sample was recorded as a function of temperature and the results were compared to pure clay. Given that the inorganic clay has much greater decomposition temperature than the organic polymer, the content of the clay inside the samples was estimated from the comparison of curves. Thermal characterization of the films was accomplished using a Perkin-Elmer DSC machine. A small amount of the sample (3-7 mg) was encapsulated in an aluminum pan and was heat treated from 30°C to 400°C at

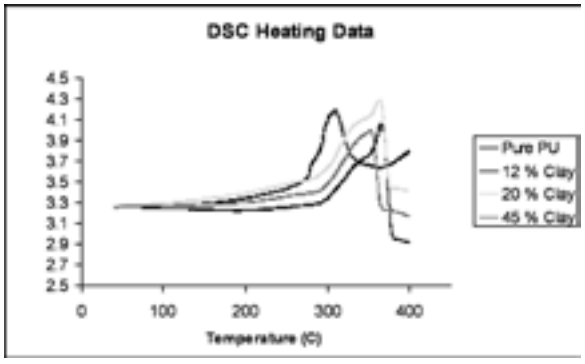

Figure 2: Thermal characterization data via DSC.

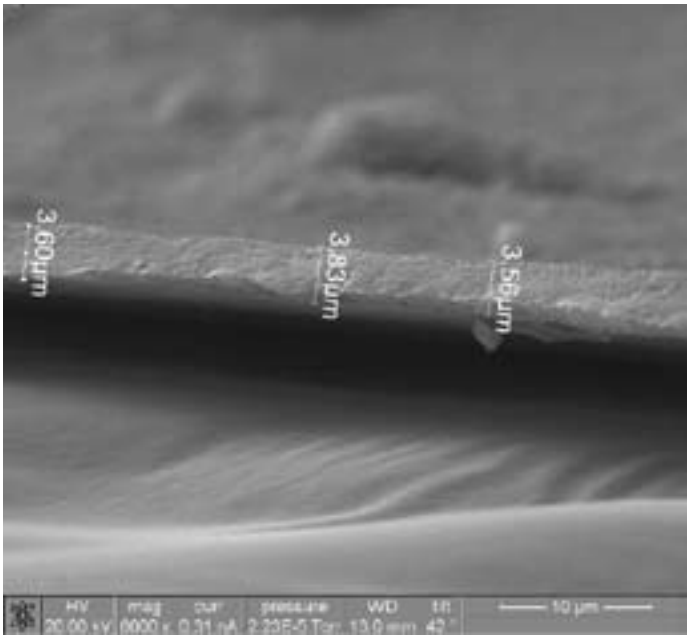

Figure 3: SEM of the 45% clay nanocomposite sample thickness.

10°C/min. The heat flow (W/g) was recorded as a function of sample temperature in order to analyze the results (Figure 3). The thickness of the nanocomposite film samples was measured via SEM to obtain the cross sectional area for stress calculations (Figure 3). The nanocomposites were gold sputtered prior to observation via SEM due to the nonconductive nature of the specimens.

Testing Methodology

Tensile testing was performed using an in-house designed tensiometer composed of a digital video camera focused on an inverted microscope (see [2] for details). Ultraspheres with a diameter of 25 μm were arranged on the specimen surface. The axial servomotors were controlled using LabVIEW software, which also synchronized data acquisition from the load element with image acquisition from the digital camera. The samples were loaded at a constant true strain rate of 0.005/s until the sample failed and LabVIEW recorded the corresponding force values and images. The load values were converted to stress and the strain was calculated using Metamorph software by tracking the distance between two ultraspheres. Nominal stress vs. nominal strain graphs were formed, the initial slope of which determined the modulus.

Results

A transition from ductile to brittle behavior was observed as the clay content increased. The addition of clay to the matrix of PU polymer increased the modulus and the yield strength significantly (Figure 4). When clay was dispersed into the PU with only 12% content, the modulus increased by 11 times and the yield strength increased by 7 times. The ultimate strain of the nanocomposite with 12% clay content was measured to be about 1/7 of the pure PU strain. The DSC data showed that the peaks of the nanocomposites were all shifted about 50ºC. The area under the curves of the DSC data decreased with the clay content increase (Figure 2B).

Conclusions and Future Work

A number of mechanical properties can be controlled with the change of clay content in the nanocomposite. As clay content increases: strength and modulus increases, while the strain (ductility) decreases. The decrease of the area under the DSC data curve also showed that the polymer becomes constrained by the clay particles. We also found that treating samples with isopropanol increased ductility of the nanocomposites. More samples should be synthesized and tested with 0% to 20% clay content to find the toughest nanocomposite of this family. Altering the polymer used in the nanocomposites could be another project. Finally, when the toughest nanocomposite is found, further characterization could be done by performing fracture tests and high strain rate tests.

Acknowledgements

The author would like to thank Ellen Arruda, Amit Kaushik, Nicholas Kotov, Paul Podsiadlo, Benjamin Pumplin, Kristen Goble, Anthony Waas, and Yaning Li for their guidance and support. Special thanks are also extended to the National Nanotechnology Infrastructure Network Research Experience for Undergraduates Program, NSF and ONR for sponsoring this internship, as well as to Sandrine Martin and Deborah Swartz for helping the program run successfully.

References

[1] Podsiadlo, P., Kaushik, A.K., Arruda, E.M., Waas, A.M., Shim, B.S., Xu, J., Nandivada, H., Pumplin, B.G., Lahann, J., Ramamoorthy, A. and Kotov, N.A., "Ultrastrong and Stiff Polymer Nanocomposites," to appear in Science.

[2] Calve, S., Mechanical and Morphological Characterization of Self-Assembling Tendons and Myotendinous Junctions *In Vitro*," PhD Thesis, University of Michigan, 2006.

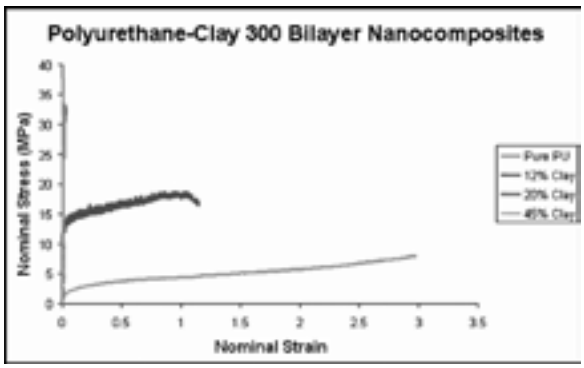

Figure 4: Nominal stress vs. nominal strain data for all nanocomposite samples tested.

Deterministic Growth of Silicon Nanowires

Jonathan Ligda

Physics, Shippensburg University

NNIN REU Site: Penn State Center for Nanotechnology Education and Utilization, The Pennsylvania State University
NNIN REU Principal Investigator: Dr. Suzanne Mohney, Materials Science and Engr., The Pennsylvania State University
NNIN REU Mentor: Chad Eichfeld, Department of Materials Science and Engineering, The Pennsylvania State University
Contact: jl3281@ship.edu, sem2@psu.edu, cme133@psu.edu

Abstract

If it were possible to grow nanowires exactly where needed, then devices could be fabricated with fewer processing steps. We are developing a method that enables silicon nanowires to be grown from the <111> sidewalls of trenches etched into silicon wafers. The nanowires are grown from a gold catalyst that is selectively plated on n-type wells patterned into the <111> sidewalls of the trenches. The goal of this summer project is to develop a process to fabricate these platforms for nanowire growth using the Penn State Nanofabrication laboratory.

Normally, nanowire growth and alignment for devices involves two separate steps, growth and then alignment. These devices' creation relies on where, and how accurately, the wires are aligned. Being able to determine where the wires are grown by creating areas for gold plating eliminates the two step process of growing and aligning.

Experimental Procedure

This process starts with <110> face silicon wafers with 380 nm of silicon dioxide (SiO_2) grown on the surface. After the oxide growth, we performed electron beam lithography on the samples. ZEP520A resist was spun on, and once applied it was ~ 400 nm thick. The electron beam patterned 200 nm lines running perpendicular to the <111> flat in the center of the wafer. After creating these lines, the samples were dry etched using reactive ion etching (RIE) to remove the SiO_2 layer exposed by the lines. Since the resist layer was very thin compared to the SiO_2 layer, an etch recipe selective to SiO_2 was created. Varying gas concentrations and bias voltages, the following recipe gave the best results; 50 sccm CF_4, 40 sccm Ar, 8 sccm H_2, 300 V DC, and an etch time of 20.5 min.

Being able to grow the wires hinges on having the n-type regions in the silicon. Therefore, applying the dopant so it fills the channels is crucial to the process. The best way to accomplish this was by incorporating spinning and vacuum techniques.

The dopant was in the form of a spin-on-glass with 10% phosphorous included. The spin-on dopant was applied at 1000-2000 rpm, allowing it to coat evenly, and placed in a vacuum chamber allowing any air to escape so the dopant could fill in the channels. The sample was then bake at 100°C for 30 sec and at 200°C for 5.5 min to remove solvents. Figure 1 shows an etch channel in SiO_2 that is filled with dopant.

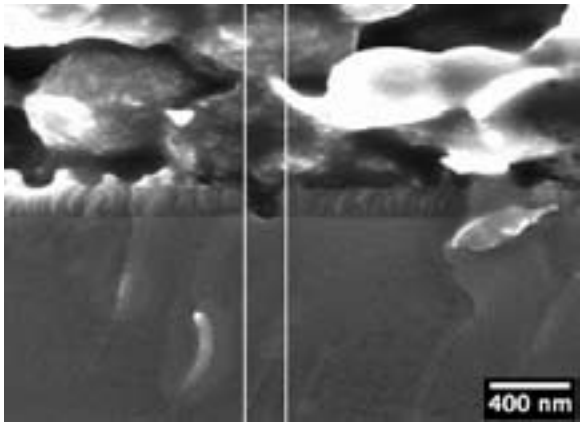

Figure 1: SiO_2 channel filled with dopant.

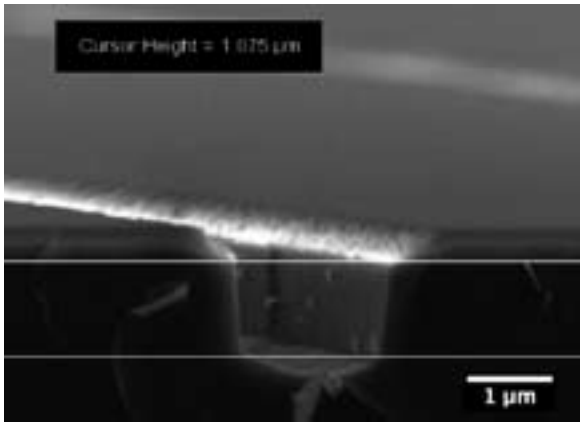

Figure 2: Two minute KOH etched trench.

Diffusing this dopant creates the n-type regions in the silicon needed during subsequent gold plating. A junction depth of 200 nm is desired. After calculations, placing the sample into at furnace for 0.5 hr at 950°C achieved this depth. Placing the sample in a 6:1 ratio of buffered oxide etch (BOE) removed the oxide layer after diffusion.

A masking layer during the future KOH etch was a necessity, and silicon nitride worked adequately. A plasma enhanced chemical vapor deposition system (PECVD) deposited 125 nm of Si_3N_4 onto the silicon surface. Samples now went through the photolithography process, using Shipley 1827 photoresist. Lines were patterned 100 nm wide, running parallel with the flat of the wafer. The photoresist was now very thick compared to the nitride, so selectivity was not a very big issue and the etch recipe used for SiO_2 worked very well. That recipe gave a nitride etch rate of about 60 nm/min, so the etch time was decreased to 3 min.

Etching silicon with KOH at 60°C is slow enough (11 nm/sec) to give a shallow enough trench in a reasonable time (1.5 min). There was now a grid in the middle of the wafer, formed from the n-type regions and the newly etched trenches in the silicon, exposing the areas where the plating of gold occurs. Figure 2 shows a trench etched for 2 min in 60°C KOH bath. The gold plating was on the n-type wells on the sidewalls.

There is a process which causes gold to selectively plate more densely onto these n-type regions [1]. These gold pads were the catalyst used for the nanowire growth step. The nanowires were grown using the vapor-liquid-solid growth mechanism with silane as the silicon precursor gas.

Conclusions

After growing the wires, scanning electron microscope (SEM) micrographs showed that wires were growing all over the surface. This was because the nitride layer which was supposed to serve as a mask during the gold plating, was no longer on the surface. We found that the gold had plated on the n-type regions—not only in the trenches, but on the top of the sample as well. Figure 3 shows an image of the n-type regions with wires growing off the surface. The nitride layer disappeared because the sample was placed in a 10:1 BOE for 2 sec. This short immersion completely removed the nitride layer and left the entire surface exposed. The nitride layer possibly had a large amount of hydrogen incorporated, making it etch aggressively in BOE. Even though the image does not show wires growing from the sidewalls, there is no reason not to believe wires were growing there as well.

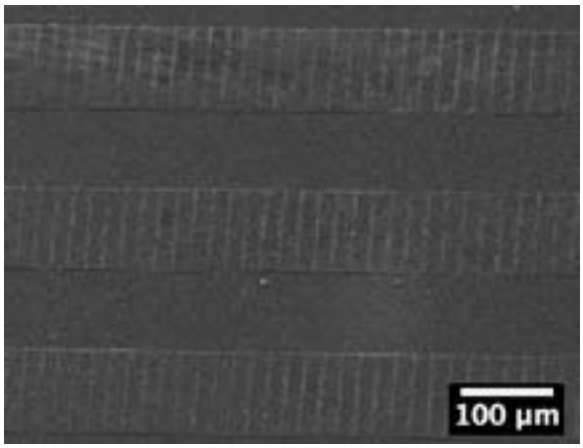

Figure 3: Sample after wire growth.

Future Work

Future work entails developing a more durable nitride layer so the BOE dip does not strip it off. Also, we need to improve the rinsing techniques after plating the gold so no gold settles onto the surface that is not n-type.

Acknowledgements

Thanks to the National Science Foundation, the National Nanotechnology Infrastructure Network Research Experience for Undergraduates Program, and The Pennsylvania State University for their funding and facilities. Also, thanks to Dr. Suzanne Mohney, Chad Eichfeld, and the staff at The Pennsylvania State University Nanofabrication Facility for their guidance and advice.

References

[1] "Selective plating for junction delineation in silicon nanowires," C. M. Eichfeld, C. Wood, B. Liu, S. M. Eichfeld, J. M. Redwing, and S. E. Mohney, Nano Lett., in press.

The Role of Surfactants in Aqueous Solution Diffusion in Hydrophobic Nanoporous Thin-Film Glasses

Katherine Mackie

Physical Chemistry, Whitworth University

NNIN REU Site: Stanford Nanofabrication Facility, Stanford University
NNIN REU Principal Investigator: Prof. Reinhold Dauskardt, Materials Science and Engineering, Stanford University
NNIN REU Mentor: Taek-Soo Kim, Mechanical Engineering, Stanford University
Contact: kmackie09@whitworth.edu, dauskardt@stanford.edu, tskim1@stanford.edu

Abstract

Nanoporous organosilicate thin-film glasses are superior candidates for use as ultra-low-κ interlayer dielectrics in advanced microelectronic devices. However, it has been recently reported that aqueous solutions containing organic species can readily diffuse in the film, despite the hydrophobic nature of the film, and increase the κ value during processing [1,2]. Of particular concern is the chemical mechanical planarization (CMP) process in which these extremely brittle materials are subjected to applied down force and shear load in the presence of chemically active aqueous solutions. This harsh process not only increases the κ value but also mechanically damages the thin-films. In this study, we demonstrate the role of surfactants, which are essential components of the CMP slurry, on the solution diffusion in nanoporous organosilicate thin-films. Surfactants were found to enhance the diffusion significantly depending on hydrophobic/hydrophilic group lengths and the structure of the surfactant molecule. Direct evidence of surfactant penetration was obtained using x-ray photoelectron spectroscopy after ion etching.

We propose a possible diffusion mechanism using the polymer reptation model to explain surfactant penetration in the nanoporous glass network. Finally, the implication of surfactant diffusion on an optimized CMP process in terms of κ value requirements is presented.

Introduction

Organosilicate ultra-low-κ dielectric glasses are incorporated into interconnect structures of advanced microelectronics to prevent parasitic transmittance. While these glasses are very effective insulators, they are also extremely vulnerable to the diffusion of solution that yields the undesirable result of an increased κ constant. Chemical mechanical planarization (CMP) is an essential process in interconnect fabrication as it results in a flat surface on which the next layer of the structure can be deposited. Now we consider the role of surfactants, which are necessary components of the CMP solution, in diffusion.

Procedure

Two types of surfactants were considered in this study: monomeric (C_mE_n) and Gemini (Surfynol®) surfactants. Various surfactant molecular weights and hydrophobic/ hydrophilic group lengths of both types were considered. Initially, solutions made with each surfactant were used, but pure surfactants in liquid phase were also considered. All surfactant solutions were 0.1 weight percent surfactant concentration in deionized water.

The ultra-low-κ dielectric thin-film considered in our study was methylsilsesquioxane (MSSQ), which is a hydrophobic, structurally modified form of silicon oxide that has the approximate atomic composition of $SiO_{1.5}CH_3$ [3]. A porous MSSQ was used that had an average pore diameter of 2.2 nm and a κ constant of 2.3.

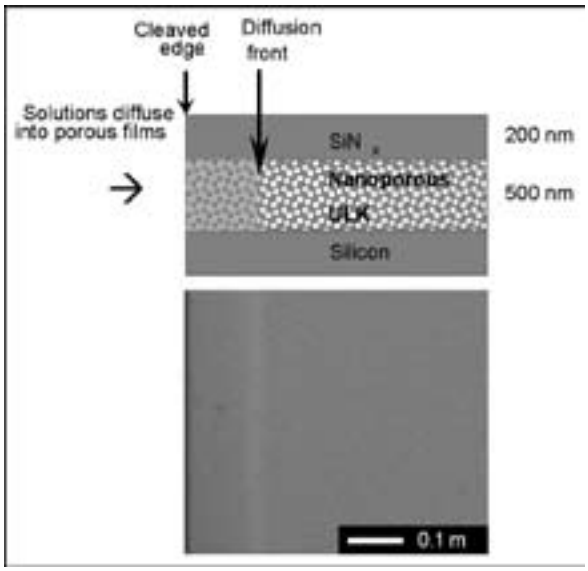

Figure 1: Solution diffusion in MSSQ.

For our study, 500 nm of MSSQ was deposited on a silicon substrate and was capped with an optically transparent silicon nitride layer (200 nm) using the plasma-enhanced chemical vapor deposition system (PECVD). The wafer was then cleaved into 1.5 × 1.5 cm specimens that were placed in Pyrex® petri dishes and submerged in either solution or liquid phase surfactant. The diffusion front was then observed and measurements were taken using an optical microscope at 50x magnification (Figure 1).

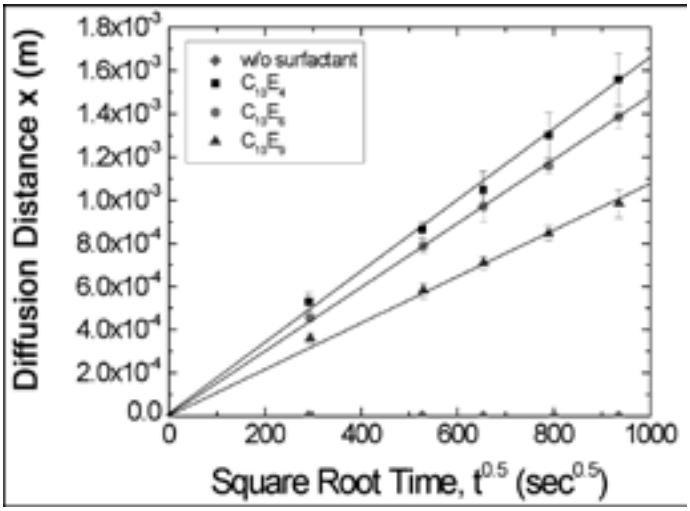

Figure 2: Fick's Law dependent diffusion of linear surfactant solutions.

These techniques were modified from previous studies used to observe the diffusion of aqueous solution [2].

Results and Conclusions

The diffusion distances of both surfactant solutions and pure surfactants showed a square-root time dependence that is characteristic of Fick's first law: $x = \sqrt{Dt}$, where x is the diffusion distance, D is the diffusion coefficient, and t is time (Figure 2). The diffusion coefficient D was observed to be a function of molecular weight, the hydrophobic/ hydrophilic group lengths, and the molecular geometry of the surfactant. For both the monomeric and Gemini pure surfactants as well as the solutions, the diffusion coefficient increased as the surfactant molecular weight decreased.

It was also observed that as the size of the hydrophilic group length of the surfactants (in both pure surfactant and solution) the diffusion coefficient decreased. The diffusion coefficients of the same surfactant at different concentrations (pure vs. 0.1 % wt) were remarkably similar. So it was determined that the surfactant is the determining factor in diffusion. However, the diffusion coefficients of the linear monomeric surfactants were significantly greater than the diffusion coefficients of the non-linear Gemini surfactants.

Despite the assumption that surfactant molecules are too large to penetrate the nanoporous network, we observed diffusion of pure surfactants. To verify this observation, we used x-ray photoelectron spectroscopy (XPS) and found that there was a significant increase in carbon content (from surfactant molecules) within the diffusion front.

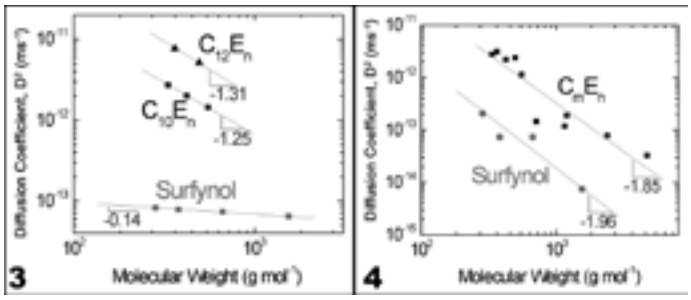

Figure 3: Pure, liquid-phase surfactant D vs. M.

Figure 4: Surfactant solution D vs. M.

Figures 3 and 4 show each calculated diffusion coefficient D of all surfactant solutions and pure liquid-phase surfactants plotted against the molecular weight (M) of the molecules. It can be noted that the slope of each regression for the surfactant solutions is approximately -2. The polymer reptation model describes the relationship between a polymer's molecular weight and the diffusion coefficient of a polymer melt so that $D:M^{-2}$. The polymer reptation model describes the self-diffusion of polymers [4]. Due to the close correlation between this model and the experimental data, we proposed that the surfactant molecules reptate through the nanoscopic pores in MSSQ.

Acknowledgements

I would like to thank the National Science Foundation for funding. I would also like to thank Professor Reinhold H. Dauskardt and Taek-Soo Kim, Michael Deal and the Stanford Nanofabrication Facility staff, and the National Nanotechnology Infrastructure Network Research Experience for Undergraduates Program.

References

[1] S. Kondo, M. Shiohara, K. Maruyama et al., "Effect of the Hydrophilic-Lipophilic Balance (HLB) of Surfactants Included in the Post-CMP Cleaning Chemicals on Porous SiOC Direct CMP," IEEE International Interconnect Technology Conference Proceedings, 172-174 (2007).

[2] E. P. Guyer, J. Gantz, and R. H. Dauskardt, "Aqueous solution diffusion in hydrophobic nanoporous thin-film glasses," J. Mater. Res. 22 (3), 710-718 (2007).

[3] M.R. Baklanov, D. Shamiryan, R. Locopi, S.H. Brongersma, K. Maex, Z.S. Yanovitskaya, "Low Dielectric Constant Materials for Microelecronics," J. of Applied Physics 93 (11), 8799 (2003).

[4] P. G. de Gennes, "Reptation of a Polymer Chain in the Presence of Fixed Obstacles," J. of Chemical Physics 55 (2), 572 (1971).

[5] G.Strobl, The Physics of Polymers, p. 283, Springer, 1997.

Charge Transport in Gold Nanocrystal Arrays

David Marsh

Chemistry, University at Buffalo

NNIN REU Site: Nanotech—The UCSB Nanofabrication Facility, University of California, Santa Barbara

NNIN REU Principal Investigator: Dr. Galen Stucky, Department of Chemistry and Biochemistry, Department of Materials, University of California, Santa Barbara

NNIN REU Mentor: Shannon Boettcher, Department of Chemistry and Biochemistry, University of California, Santa Barbara

Contact: damarsh@buffalo.edu, stucky@chem.ucsb.edu, sboettcher@chem.ucsb.edu

Abstract

This research focused on gold nanoparticles, and the single electron charging of these nanoparticles as a function of electrochemical potential. We have synthesized a variety of gold nanoparticles, processed them into thin films, and tested these films with cyclic voltammetry (CV) and dual electrode voltammetry (DEV). We have also begun to look at the effect of temperature on the conductivity. We found that conductivity is related to the electrochemical potential applied to the film as well as temperature.

Introduction

Metal nanoparticles have scientific importance because their electronic properties depend on size, shape and composition. Due to this, these properties can be controlled and manipulated [1]. It is important to understand this phenomenon in order to fabricate devices that utilize these properties. Gold nanoparticles have been studied previously, and the synthesis of purportedly monodisperse particles has been reported [2]. We optimized our synthesis such that the average diameter of our nanoparticles was 2.0±0.6 nm. The size of the nanoparticles is what governs the charging, and this size distribution was narrow enough to give reproducible electrochemical data.

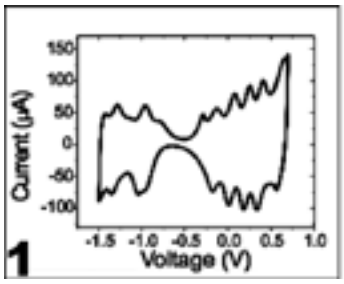

Figure 1: Cyclic voltammetry data.

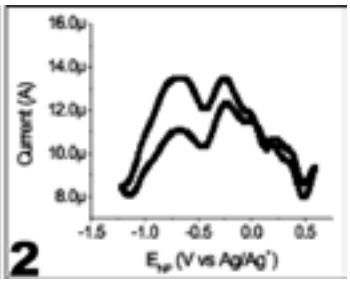

Figure 2: Dual electrode voltammetry data.

Experimental Procedure

Gold nanoparticles were synthesized using a modified Brust method [3], with hexanethiol as the stabilizing alkanethiol ligand. After the reduction reaction was complete, ethanol was added and the ethanol-soluble particles were isolated. Concentrated solutions (~ 250 mg/ml) were prepared in heptane, and thin films were spin-coated (2000 rpm) onto platinum electrodes. For DEV, gold was evaporated on top of the nanoparticle film so that conductivity could be measured through the film. All films were cross-linked in 1,9-nonanedithiol before running CV and DEV.

CV was run under argon, with tetrabutylammonium hexafluorophosphate as the electrolyte in acetonitrile. The reference electrode was Ag/Ag^+, and the counter electrode was platinum wire. DEV was conducted under the same conditions as CV. Temperature dependence studies were carried out in a cryostat to allow measurements under vacuum and down to liquid nitrogen temperature (77 K).

Results and Discussion

Gold nanoparticles exhibit discrete charging energies and this can be seen on the CV graph (Figure 1). Each peak relates to a single electron charging of half of the nanoparticles, on average. This is an average because the particles aren't all exactly the same size. At the valleys in between the peaks, all the nanoparticles are filled with electrons to the same energy level. At this potential, electron tunneling can only occur if there is thermal activation of an electron to a higher energy level. At the potentials that relate to peaks in the CV graph, electron tunneling can occur without thermal activation since half the nanoparticles already have an electron in a higher energy level. This would mean an increase in conductivity at those specific potentials.

In order to analyze the conductivity as a function of the charge on the nanoparticles, we tested our films with DEV. Figure 2 is the data from the DEV experiment, where conductivity is plotted as a function of potential. From what we know about the CV data, this potential can also be thought of as the charge potential of the nanoparticles (E_{NP}). The peaks in the DEV graph occur at similar potentials as the peaks in the CV graph. This supports the claim

$$\sigma = \sigma_0 \exp\left(\frac{-E_A}{RT}\right)$$

σ_0 = constant
E_A = activation energy
R = gas constant
T = temperature

Figure 3: Arrhenius equation describes thermal activation at low biases.

that these potentials relate to charging of half the nanoparticles, because this data shows that there is an increase in conductivity at these potentials.

Temperature Dependence

To more fully understand the mechanism of electron tunneling, it is helpful to analyze the effect of temperature. It is also a way of validating the claim that there isn't a need for thermal activation at certain potentials applied to the film. Initially we tested the effect of temperature on conductivity of the uncharged nanoparticle film, to verify that it follows the Arrhenius equation (Figure 3). The Arrhenius equation describes thermal activation of electrons and holds true at low biases. Figure 4 is the temperature dependence data and can be used to calculate the activation energy of an electron. This information would be useful if gold nanoparticles were used in electronic devices.

Conclusion

Cyclic voltammetry is a good method for analyzing the charge on the nanoparticles. In this experiment, we could detect the addition of a single electron to the nanoparticles by observing a peak. This data matched up with conductivity measurements, since there were peaks in conductivity at nearly the same potentials as the peaks in the CV graph. This is what we would expect because of the lower barrier for electron tunneling when half the nanoparticles are charged. Temperature is related to conductivity by the Arrhenius equation, and we observe this when we measure conductivity at various temperatures.

Future Work

The next step will be to combine the DEV study with the temperature dependence study. This means driving to the potentials that relate to peaks in the DEV and then running the temperature dependence experiments. This would be a way to confirm the hypothesis that there is little to no thermal barrier for electron tunneling at these potentials. Another experiment would be to vary the electrolyte used for CV and DEV, to see the effect of ion size on the charging of the particles.

Acknowledgements

I'd like to thank Shannon Boettcher for being a great mentor, as well as the entire Stucky group. Many thanks to the National Nanotechnology Infrastructure Network Research Experience for Undergraduates Program and National Science Foundation for funding.

References

[1] Boettcher, S.; Strandwitz, N.; et al. Nature Materials, 6, 592-596, (2007).

[2] Schaaff, T.; Shafigullin, M.; et al. J. Phys. Chem. B, 105, 8785-8796 (2001).

[3] Brust, M.; Walker, M.; et al. J. Chem. Soc., Chem. Commun. 801-802 (1994).

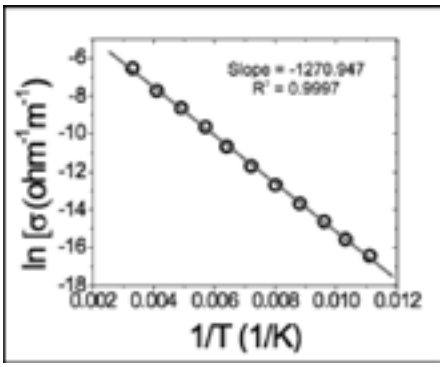

Figure 4: Temperature dependence data; from Arrhenius equation, slope = E_A/R, E_A = 0.110 eV.

Materials Ink Jet Printing of Electronic Structures

Fabiola Nelson

Chemical Engineering, New Jersey Institute of Technology

NNIN REU Site: Cornell NanoScale Science & Technology Facility (CNF), Cornell University
NNIN REU Principal Investigators: Prof. George G. Malliaras, Dr. Lynn Rathbun, CNF, Cornell University
NNIN REU Mentors: Dr. Maria Nikolou, Department of Materials Science and Engineering; Dr. Mandy Esch, Cornell NanoScale Science & Technology Facility; Cornell University
Contact: mfn6@njit.edu, ggm1@cornell.edu, rathbun@cnf.cornell.edu, mn262@cornell.edu, esch@cnf.cornell.edu

Abstract

We used poly3,4-ethylenedioxythiophene doped with poly(sterene sulfonate) (PEDOT:PSS), a commercially available conductive polymer, to fabricate electrodes for disposable sensors. We successfully printed the electrodes using an ink jet printer that utilizes piezoelectric nozzles to dispense the polymer. Printing on silicon wafer and photographic paper yielded good quality electrodes. Our goal was to fabricate electrodes that exhibit low resistance on flexible, inexpensive substrates. The first tasks were to optimize the dimension of the electrode pattern, and then optimize the drop spacing used during the printing process in order to obtain continuous films.

We found that the optimum drop spacing is different for different substrates. The optimum drop spacing for printing on paper is 5 μm. At this drop spacing, the resistance of the electrode measured with a voltmeter is around 80 kΩ. To achieve an even lower resistance for electrodes that will be used in devices, the following method was used: one layer of PEDOT: PSS was printed, and then a second layer was printed on top of the first one. The resistance of the two layered electrode was around 30 kΩ.

Introduction

Currently, commercially available sensors are unable to detect small saliva glucose concentrations. When the use of saliva is coupled with inexpensive, disposable polymer-based sensors, it is possible to create a low cost and painless glucose monitor that can lead to a much more widely used sensor [1]. Inkjet printing is a new technology that is used to print conductive polymers. A simple glucose biosensor with micromolar sensitivity utilizes a conducting polymer transistor with a channel made out of PEDOT:PSS and a platinum (Pt) gate electrode [1]. The ink jet printer allows us to print on inexpensive substrates using PEDOT: PSS as the conductive polymer.

The advantages of using the inkjet-print technology for electrodes used in chemical and biological sensors are the high speed and low cost fabrication as well as the possibility of printing onto flexible substrates [2]. Inkjet printing is one of the most promising technologies for several reasons; one of them is the capacity of depositing micro droplets of 2-12 pl on any surface such as plastics, metals, rubber, glass, silicon wafer [3].

Experimental Procedure

Initially, we designed the electrode patterns and then using the ink jet printer, we were able to optimize the parameters of the system

Figure 1: Optical microscope image, PEDOT:PSS on paper at 50 μm drop spacing.

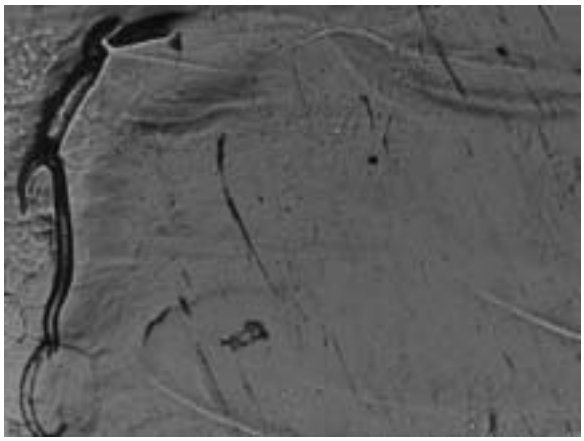

Figure 2: Optical microscope image, PEDOT:PSS on paper at 5 μm drop spacing double layers.

to print PEDOT:PSS electrodes on different substrates (glass slide, Si wafer, and photographic paper). The ideal substrate is inexpensive, flexible, and easy to print on. We predicted that the drops might behave differently on different substrates. In order to obtain continuous films, we changed the drop spacing used during the printing process. The parameter was important because the resistance was affected by drop spacing of the nozzles; large drop spacing could result in a discontinuous film.

Using the molecular vapor deposition (MVD 100) system, we treated the surfaces of the silicon wafer and the glass slide with two chemicals (APTMS and PEG). We investigated whether surface modifications would improve the characteristics of the printed electrodes or not. Photographic paper was used as a substrate to print at different drop spacing, starting with 50 μm to 5 μm single layer printed PEDOT:PSS followed by a double layer printed at 5 μm. We characterized the electrodes printed on photographic paper at 5 μm drop spacing both the single and the double layer by measuring the resistance to see whether we get good quality films. At last we measured the current in order to compare the two final results to see which one performs better.

Results and Conclusions

As a result of performing these experiments, we came to the conclusion that paper is in fact a suitable substrate to print PEDOT: PSS electrodes. Our experiments showed that printing a double layer of PEDOT:PSS on paper exhibits lower resistance and higher current than all the other substrates under investigation. This result proves that inkjet printed PEDOT:PSS electrodes on paper can be of high quality, thus they can be used in devices.

Future Work

Future work includes the use of the PEDOT:PSS electrodes in electrochemical transistors for chemical and biological applications and the study of their behavior and suitability as part of a circuit.

Acknowledgments

I would like to thank my principal investigators Prof. George G. Malliaras and Dr. Lynn Rathbun, and my mentors Dr. Maria Nikolou and Dr. Mandy Esch for their support with this project. I would also like to thank the National Science Foundation and the National Nanotechnology Infrastructure Network along with the CNF staff, Intel Foundation, and Cornell University for giving me the opportunity to perform this research.

References

[1] Macaya, D. J., Nikolou, M., Takamatsu, S., Mabeck, J. T., Owens, R. M., Malliaras. G. G. "Simple glucose sensors with micromolar sensitivity based on organic electrochemical transistors." Sensors and Actuators B 123(2007) 374-378 (2006).

[2] Mabrook, M. F., Pearson, C., & Petty, M. C. "Inkjet-Printed Polymer Films for the Detection of Organic Vapors." IEEE Sensors Journal, Vol. 6, No. 6 (2006).

[3] Ballarin, B., Fraleoni-Morgera, A., Frascaro, D., Marazzita, S., Piana, C., Setti, L. "Thermal inkjet microdeposition of PEDOT:PSS on ITO-coated glass and characterization of the obtained film." Synthetic Metals 146 (2004) 201-205 (2004).

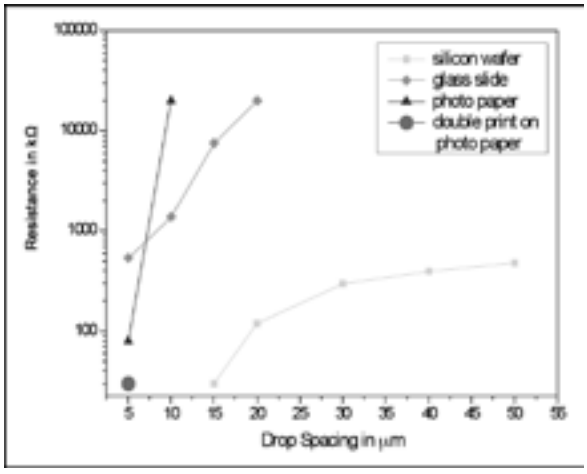

Figure 3: Resistance vs. drop spacing graph with different substrates.

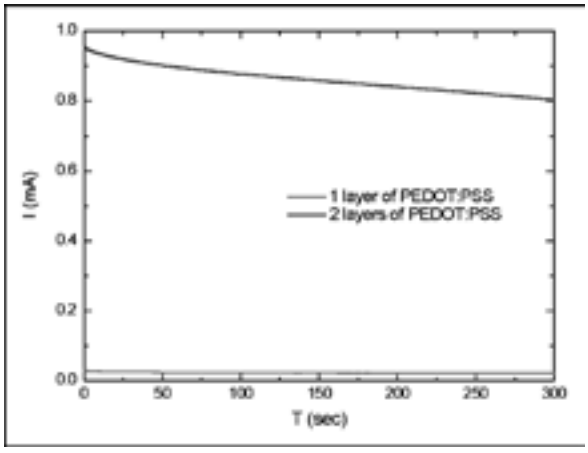

Figure 4: Current vs. time with a drop spacing of 5 μm.

Fabrication of Low Temperature Solid Oxide Fuel Cells with Ultra-Thin Film Yttria-Stabilized Zircona Electrolytes

Amrita Saigal

Mechanical Engineering, Massachusetts Institute of Technology

NNIN REU Site: Center for Nanoscale Systems, Harvard University
NNIN REU Principal Investigator: Prof. Shriram Ramanathan, School of Engineering and Applied Sciences, Harvard University
NNIN REU Mentor: Dr. Alex Johnson, School of Engineering and Applied Sciences, Harvard University
Contact: saigal@mit.edu, shriram@seas.harvard.edu, acjohns@fas.harvard.edu

Abstract

Solid oxide fuel cells (SOFCs) have the potential to become the next major breakthrough as an alternative energy conversion device. They use the simple reaction of combining hydrogen and oxygen to produce electricity and water as a by-product. A SOFC is composed of an electrolyte sandwiched between two electrodes (anode and cathode) [1]. In SOFCs, oxygen ions (O^{2-}) are transported from the cathode of the fuel cell to the anode through the electrolyte made of a material known as yttria-stabilized zircona (YSZ). Electrons are transported through an external circuit, and the flow of electrons produces electricity. The various electrochemical reaction occurring are—at the anode: $\frac{1}{2}O_2 + 2e^- = O$, at the cathode: $H_2 + \frac{1}{2}O_2 = H_2O + 2e^-$ and overall cell reaction: $\frac{1}{2}O_2 + H_2 = H_2O$. The electrochemistry of a SOFC is depicted in Figure 1.

Introduction

SOFCs operate at very high temperatures of approximately 800°C-1000°C and this leads to two major problems. First, SOFCs have to be heated up slowly or else they will break due to differential thermal expansion. Secondly, most metals oxidize or corrode at the high operating temperature of SOFCs and therefore stop conducting oxygen ions across the electrolyte. The operating temperature of the fuel cell cannot simply be reduced because the ionic conductivity of the YSZ electrolyte is reduced at lower operating temperatures [2]. Ionic resistance, $R = \rho t/A$ where resistivity $\rho \sim e^{Ea/kT}$ ($Ea \sim 0.9$ eV). Therefore, decreasing the thickness, t, of the electrolyte will allow for lower operating temperatures, T. The optimal SOFC operating temperature is ~ 300°C, since this is the temperature at which the anode and cathode can perform catalytic activity, and metal can also be used for other components of the fuel cell since they will no longer melt. In order to have a SOFC operate at 300°C, the thickness of the YSZ electrolyte should be around 50 nm.

The second goal of the research was to study the porosity of platinum, which was used for making the anode and cathode, under different sputtering conditions so as to create electrodes with smaller pores to allow for more surface area for the oxygen ions, hydrogen and electrons to travel through and react on.

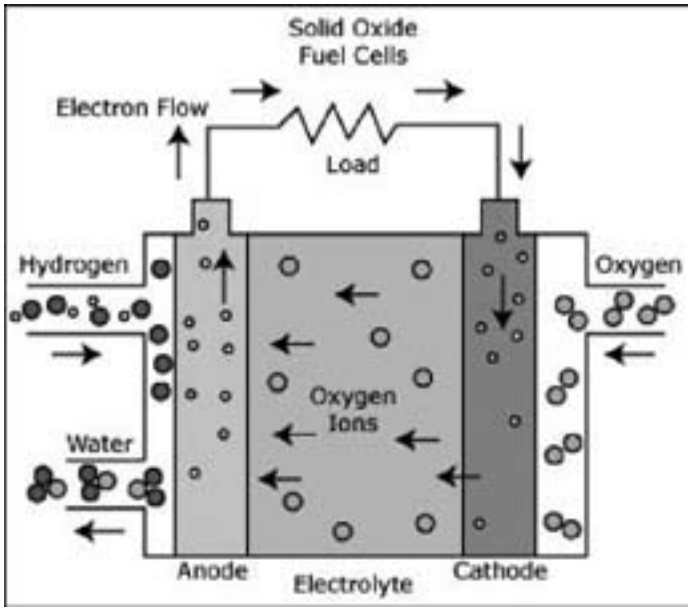

Figure 1: Electrochemistry of a solid oxide fuel cell.

Materials and Methods

Fabrication of a SOFC begins with a silicon wafer ~ 500 μm coated with silicon nitride (Si_3N_4 ~ 200 nm) on both sides using the process of low pressure chemical vapor deposition. Silicon nitride serves as an insulator to prevent any unwanted reactions from occurring between the YSZ and Si, since both are very good conducting materials. The next step is to sputter a thin layer of YSZ, the electrolyte, on top of the Si_3N_4 at a pressure of 5 mTorr, 100W power for 30 min to produce a thickness of ~ 40 nm. The next step is to pattern the back side of the chip and remove the patterned area of Si_3N_4 using reactive ion etch. The top of the chip is then patterned and a thin layer of titanium (Ti) is sputtered on the top of the chip at 4 mTorr, 250W for 2 min to produce a thickness of ~ 5 nm. Ti serves as an adhesive between the platinum electrodes and YSZ electrolyte. Platinum (Pt) is then sputtered on top of the Ti at 4 mTorr, 250W for 5 min to produce dense platinum with thickness of ~ 100 nm.

The reason for using dense platinum is that it has better electrical properties than porous platinum, so anywhere the platinum is not in direct contact with the YSZ electrolyte, as is found with the platinum on top of the titanium, there should be dense platinum.

The next step is to perform lift-off to remove the excess Ti/Pt coating. Pt is then sputtered throughout the top of the chip at 75 mTorr, 250W for 15 min to produce porous platinum which serves as the top electrode. Finally, in order to study the porosity of platinum under different conditions, we sputtered Pt by varying the following parameters; time from 5-80 min, pressure from 4-100 mTorr, and power from 100-250W, to produce platinum films with different thicknesses.

Figure 2: Fabricated solid oxide fuel cell.

Results and Discussion

Figure 2 shows the final fabricated solid oxide fuel cell. It can be seen from Figure 3 that increasing the thickness of the platinum yields larger pores with a relatively linear relationship, although neither pressure nor power have a significant effect on pore size. A possible explanation for this increase in pore size is that as more Pt atoms are added, they build outward from the existing grains, mainly upward, but also sideways so that some of the existing grains merge together to form larger pores.

Conclusions and Future Work

A SOFC with an ultra-thin YSZ electrolyte was successfully fabricated. There is a strong correlation between thickness of sputtered platinum coating and pore size where the pore size linearly increases with coating thickness. Future work includes measuring the conductivity of these fabricated SOFCs to verify that the conductivity does not decrease significantly at lower operating temperatures. Also, based on successful sputtering of platinum coatings for the anode and cathode, the next step is to create a lanthanum strontium cobalt iron oxide (LSCF) cathode and a nickel YSZ oxide anode, which are known to work well as electrodes to replace the expensive platinum.

Acknowledgments

I would like to thank Prof. Shriram Ramananthan, Drs. Alex Johnson and Kathryn Hollar for their help and support as well as Harvard's Center for Nanoscale Science, National Nanotechnology Infrastructure Network Research Experience for Undergraduates Program and National Science Foundation for funding.

References

[1] Hallie, S. Fuel cell materials and components. Acta Materialia 51: 5981-6000. 2003.

[2] Fasching, R., H. Huang, M. Nakamura, F. Prinz, Y. Satio, and P. Su. High-Performance Ultrathin Solid Oxide Fuel Cells for Low-Temperature Operation. Journal of the Electrochemical Society 154: B20-B24. 2006.

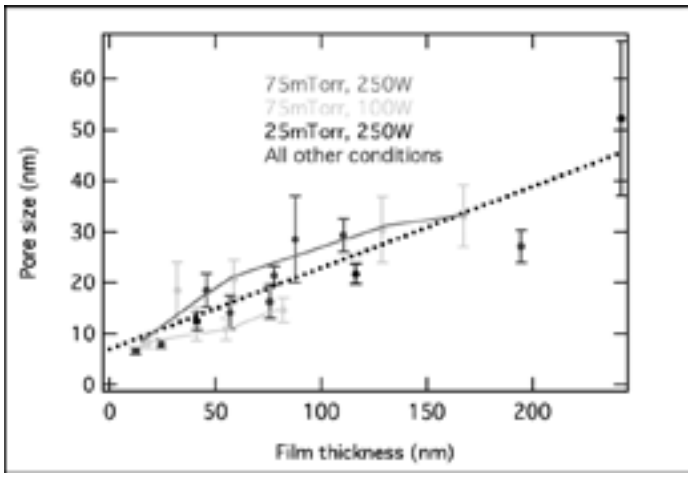

Figure 3: Effect of platinum thickness on pore size.

Probing Nanostructures of Biorenewable Polyurethane Collapsed Foams

Ryan J. Seelbach

Physics, Beloit College

NNIN REU Site: Minnesota Nanotechnology Cluster, University of Minnesota-Twin Cities
NNIN REU Principal Investigator: Dr. Christopher W. Macosko, Chemical Engineering and Materials Science, University of Minnesota-Twin Cities
NNIN REU Mentor: Ling Zhang, Chemical Engineering and Materials Science, University of Minnesota
Contact: rseelbach@gmail.com, macosko@umn.edu, zhang@cems.umn.edu

Abstract

Petroleum-based materials comprise the dominant resource going into the manufacturing of flexible foams. The rising cost of petroleum is providing the opportunity to implement vegetable-based resources into this expanding industry. 100% vegetable-based polyurethane (PU) flexible foams have been developed to exhibit viscoelastic properties comparable to their petroleum ether analogues.

Four vegetable-based collapsed foam samples were prepared and their glass transitions, mechanical moduli, and phase morphologies were studied. Glass transition temperatures and moduli were analyzed via differential scanning calorimetry (DSC) and dynamic mechanical analysis (DMA). Polyurea hard domain spacings were measured and visualized using small/wide angle x-ray scattering (SWAXS) and tapping mode atomic force microscopy (AFM). It was found that the soft domain glass transition temperature decreases as the molecular weight of the polyol structure increases.

Introduction

The chemical structure inherent to the vegetable oils varies in the degree and location of unsaturation, and determines the overall length of the fatty acid chains. By extending the polyol chain at the unsaturation points, the overall chain length increases. The goal of this experiment is to examine the effects of fatty acid chain length (i.e. polyol molecular weight) to thermal properties and phase morphology of PU foam.

During foaming, two competing reactions give rise to the phase separation of hard and soft domains. The gelling reaction is the polymerization of polyol with isocyanate to form the polyurethane soft segment (SS). The blowing reaction is the polymerization of isocyanate and water to form polyurea hard segments (HS). The hard segments eventually agglomerate during the reaction to form phase-separated hard domains throughout the continuous soft phase.

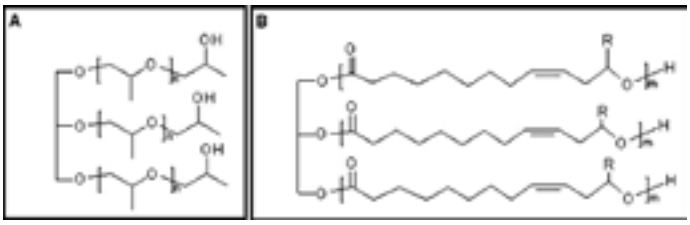

Figure 1: A] Petroleum polyether polyol. B] Vegetable-based polyol.

Experimental

Materials

The vegetable-based polyols used for this experiment were 1K, 2K, 3K, and 4K moleular weight polycondensate triols, Figure 1. These materials were polymerized using trimethylol propane (TMP) starter and ricinoleic acid via esterification synthesis. Arcol F3022 (Bayer Corporation), a petroleum polyether polyol that is comparable to the 3K polyol, Figure 1, was also used. An 80/20 mixture of 2,4 and 2,6-toluene disocyanate (TDI) was stoichiometricly balanced to completely react with the water and polyols. The blowing catalyst used to accelerate the blowing reaction was DABCO®BL-11 (Air Products).

Procedure

All samples were made into collapsed foams (CF). Polyol, water, and catalyst were added to a 50 mL plastic beaker. TDI was added last and hand mixed for 10-20 minutes in a silicon oil heat bath at 55°C until the blowing reaction was complete, and the mixture was highly viscous or crumbling. The foam was poured into a 1.5 mm thick steel mold with 25 mm diameter circular cutouts. The mold was sandwiched between a layer of Teflon® followed by a steel plate. The plates were placed in a hydraulic press (Carver, Auto Series, model 3895) at 100°C and 15000 lbs. force for 1.5 h.

Characterization

Differential Scanning Calorimetry: DSC (Q1000, TA Instruments) was used to observe the SS glass transition temperatures. About 6-10 mg of the CF was placed and sealed into an Al hermetic pan. Heat flow data was taken over a temperature range from -100°C to 200°C at a rate of 10°C/min.

Dynamic Mechanical Analysis: DMA (ARES II, TA Instruments) measured the elastic modulus, G', and loss modulus, G", over the temperature range of -100°C to 200°C. CF samples were cut to 12.65 mm width and placed in a rectangular torsion apparatus. A strain of 0.05% was applied and data was taken at a frequency of 3 rad/s.

Small/ Wide Angle X-Ray Scattering: SAXSess instrument (Anton Paar), operated at 12 kW and 50 mA, was used to determine hard domain spacings in samples. CF samples were cut and placed in a Cu sample holder and exposed to the x-ray source for 10 min. Scattering profiles were normalized to sample thickness.

Atomic Force Microscopy: An atomic force microscope (AFM) (Nanoscope III Multimode, Digital Instrument) was mounted on an optical microscope (Nikon). Tapping mode images were taken using a Si cantilever with a tip radius of about 100Å and an oscillating resonant frequency of ~ 240 kHz. All images were taken under ambient conditions. Tapping oscillations were conducted in the repulsive regime and with resolution of 512 × 512 pixels.

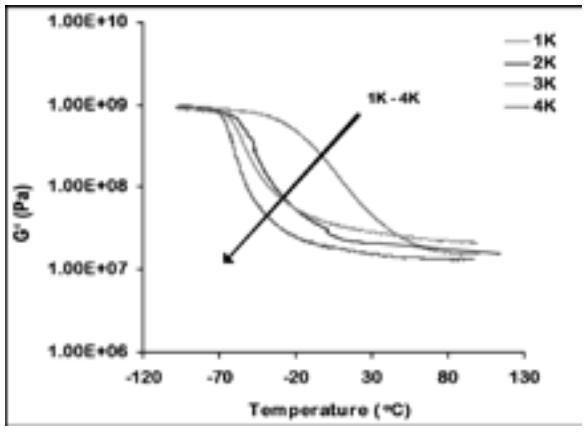

Figure 2: Dynamic mechanical analysis.

Results and Discussion

With increasing the weight of the vegetable oil structure, the PU foam's T_g. decrease as seen in Figure 2. The initial drop in G' data around -60°C corresponds to the increase in SS mobility. The temperature is the T_g of the soft domains. SAXS, Figure 3, gives an average value of hard domain spacings; a characteristic shared with the petroleum analogues. AFM provides a localized map of the phase morphology. A 500 nm phase image of 4K MW polyol is shown in Figure 4. Hard domains are brighter regions, and soft domains are darker regions. The phase scale was adjusted to show a clear contrast between the two regions. The hard domains agglomerated into tiny sphere-like orbs and distributed in the SS matrix. All images were plane-fitted to remove large scale surface curvature for better height profile displays. From experimental results, biorenewable polyols can potentially replace petroleum feedstock, making a novel substitute in industrial production of PU flexible foams. Thermal properties, such as T_g, of vegetable based PU can be tuned via the control of polyol MW.

Acknowledgements

The author would like to thank the Chemical Engineering and Materials Science Department at the University of Minnesota for allowing him to gain exposure into graduate study. The knowledge will be invaluable to his future. Also, thanks to the National Nanotechnology Infrastructure Network Research Experience for Undergraduates Program funding for this wonderful internship.

References

[1] Zhang et al. Comparison of Polyurethane Flexible Foams: Polyether vs. Soybean Oil-based Polyols. Submitted for Pub.

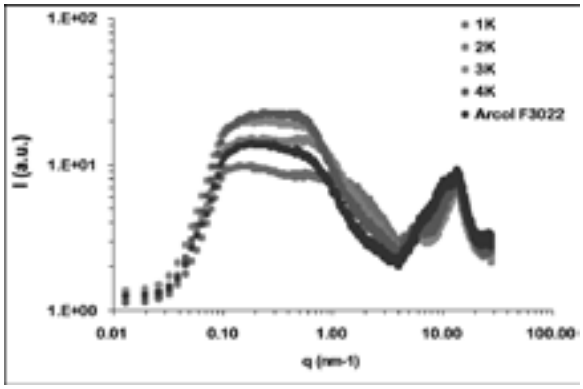

Figure 3: Small/wide angle x-ray scattering.

Figure 4: Atomic force microscopy image.

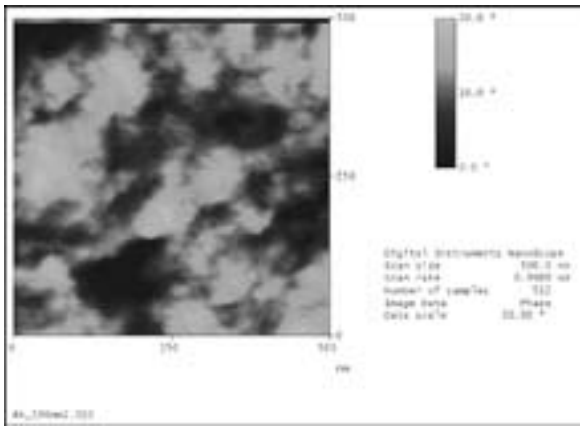

Nanostructured Photovoltaics Using Porous Alumina Templates as Structure-Directing Agents

Jessica Sherman

Department of Chemistry, University of Kentucky

NNIN REU Site: Nanotech—The UCSB Nanofabrication Facility, University of California, Santa Barbara
NNIN REU Principal Investigators: Profs. Martin Moskovits and Galen Stucky, Department of Chemistry, University of California, Santa Barbara
NNIN REU Mentor: Martin Schierhorn, Department of Chemistry, University of California, Santa Barbara
Contact: jes.carbon@gmail.com; mmoskovits@ltsc.ucsb.edu, stucky@chem.ucsb.edu; mschierhorn@chem.ucsb.edu

Abstract

Nanostructured architectures for use in type II heterojunction photovoltaic devices are explored in this report. Porous aluminum oxide (PAO) templates were employed as structure-directing agents in the electrochemical synthesis of cadmium selenium (CdSe) nanorod arrays. Arrays fabricated using a cyclic voltammetry (CV) method were subjected to photoelectrochemical measurements to determine the effect of rod dimensions on device performance. Additionally, an alternating current (AC) electrolysis method for CdSe deposition was developed and optimized.

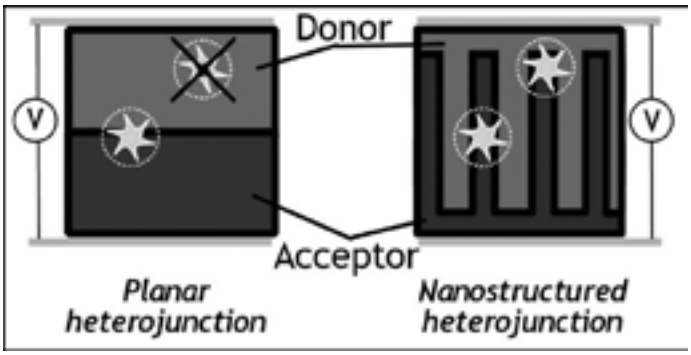

Figure 1: Solar cell schematic. Stars represent photoexcitation; X denotes exciton recombination.

Introduction

Separation of electrostatically bound charge-carrier pairs in photovoltaics is crucial to proper device function. Following photoexcitation in a solar cell, an exciton (electron-hole pair) can only diffuse a finite distance before recombination occurs. Semiconductor nanorod arrays provide a highly ordered device architecture in which an exciton can reach the donor-acceptor heterojunction prior to recombination. This strategy (Figure 1) could produce highly efficient photovoltaics.

Free-standing semiconductor nanorod arrays can be fabricated using PAO templates [1]. CdSe, due to its high electron mobility and wide (1.77 eV) bandgap, was an attractive material for this study. It has been studied in photoelectrochemical cells, which provide a means to analyze photocurrent generation in nanorod arrays with varying dimensions [2,3]. The liquid electrolyte junction eliminates problems associated with poor interface morphology found in solid bulk heterojunctions. However, since photovoltaic device operation requires a transparent electrode, usually indium tin oxide (ITO), we also sought a synthetic method that would create nanorod arrays with a surface onto which ITO could be affixed. The known CV method deposits nanorods onto a conductive substrate, but requires acidic solution which etches ITO [4]. This led us to AC electrolysis, which plates material directly onto a thin insulating layer of alumina in the pores of the template and provides a semiconductor film at the base of the rods [5].

Experimental Procedure

Photoelectrochemistry: PAO templates were prepared according to literature methods and were anodized with either sulfuric acid (45 nm pore width) or oxalic acid (60 nm pore width) [1]. Nanorod arrays were fabricated using the PAO templates and a known CV method, and characterized using x-ray photoelectron spectroscopy (XPS) [4]. The arrays were annealed for 30 minutes at 400°C under argon to increase crystal grain size. The gold backing was then attached to copper wire and the assembly was coated in epoxy, leaving the wire tip and CdSe nanorods exposed. Etching in 5 M NaOH for 3 hours removed the alumina template. The photoelectrochemical cell used a 0.2 M solution of NaOH, Na_2S and S as the electrolyte and a Pt mesh counterelectrode. All measurements were taken under argon.

AC Electrolysis: PAO templates were anodized in oxalic acid; some were also subjected to a 15 minute pore-widening soak in H_3PO_4. A solution of 0.01M $CdCl_2$ in DMSO was heated to 180°C under argon. Se was then added to saturation. The PAO template and a graphite rod were submerged in this solution and used as electrodes as an AC potential was applied. CdSe nanorod growth on the template was then characterized by scanning electron microscopy (SEM) and energy-dispersive x-ray spectroscopy (EDX).

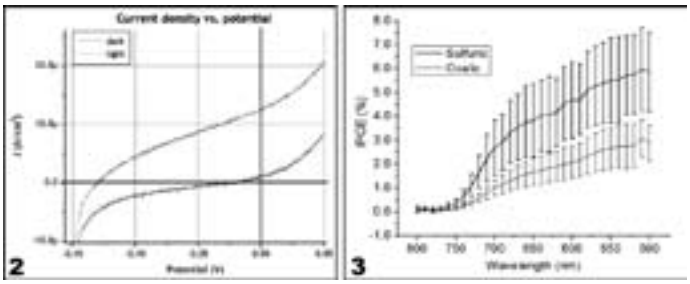

Figure 2, left: Representative J-V curve for photoelectrochemical cells.

Figure 3, right: Efficiency of nanorods produced using sulfuric vs. oxalic acid anodization.

Results

XPS measurements for the nanorods produced using the CV method revealed an average 45:55 Cd:Se stoichiometry. (Any deviation from 1:1 stoichiometry indicates point defects within the lattice, which may act as charge-carrier traps.) The nanorod arrays displayed some photoresponse in photoelectrochemical device assemblies (Figure 2), but the low short-circuit current density (12.5 $\mu A/cm^2$) indicated that optimization is necessary. The open-circuit potential (vs. Pt counterelectrode) was measured at 0.13 V. Figure 3 illustrates the efficiency (expressed as incident photons converted to electrons, or IPCE) of the sulfuric and oxalic acid-anodized templates. Sulfuric acid-anodized PAO templates produced more efficient nanorods than did oxalic acid-anodized templates. The absorption onset near 700 nm corresponds to the CdSe bandgap. The electrolyte solution absorbed strongly below 500 nm, precluding any efficiency measurements in that range.

The AC electrolysis method for nanorod array fabrication was explored using PAO templates with 200 nm average pore depth. This length of nanorods, in addition to uniform, 100 to 200 nm CdSe films, is expected to allow effective photovoltaic device fabrication. The nanorods were deposited by applying 30 V AC to a PAO template for 30 minutes. Alternatively, a pore-widened PAO template produced nanorod arrays with the appropriate CdSe film thickness with application of 45 V AC for 15 minutes. EDX analysis indicated a Cd:Se stoichiometry of 61:39. Decreasing the concentration of the $CdCl_2$ solution may bring the stoichiometry to the desired 1:1 ratio.

Future Work

The device fabrication process for CdSe arrays in photoelectrochemical cells requires optimization. Additionally, efficiency measurements of flat thin films of CdSe would allow a comparison to be drawn between thin film and nanorod performance.

The arrays produced using AC electrolysis are attached to thin films of CdSe, which may provide a useful surface onto which an ITO electrode may be sputtered. Once ITO is applied, the PAO template can be etched away, and a donor material and back electrode can be added to the photovoltaic assembly. Fabrication of proof-of-concept devices is underway.

Acknowledgments

Thanks to Martin Moskovits, Galen Stucky, Martin Schierhorn, Angela Berenstein, NSF, UCSB, Institute for Collaborative Biotechnologies, and the National Nanotechnology Infrastructure Network Research Experience for Undergraduates Program.

References

[1] O'Sullivan, J.P.; Wood, G.C. Proc. R. Soc. London, Ser. A, 1970, 317, 511.

[2] Miller, B.; Heller, A.; Robbins, M.; Menezes, S.; Chang, K. C.; Thomson, Jr., J. J. Electrochem. Soc., 1977, 124 (7), 1019.

[3] Ellis, A. B.; Kaiser, S. W.; Wrighton, M. S. J. Am. Chem. Soc., 1976, 98 (22), 6855.

[4] Norvell, E. NNIN REU Research Accomplishments, 2006, 76.

[5] Routkevitch, D.; Tager, A. A.; Haruyama, J.; Almawlawi, D.; Moskovits, M.; Xu, J. M. IEEE Trans. Electron Devices, 1996, 43 (10), 1646.

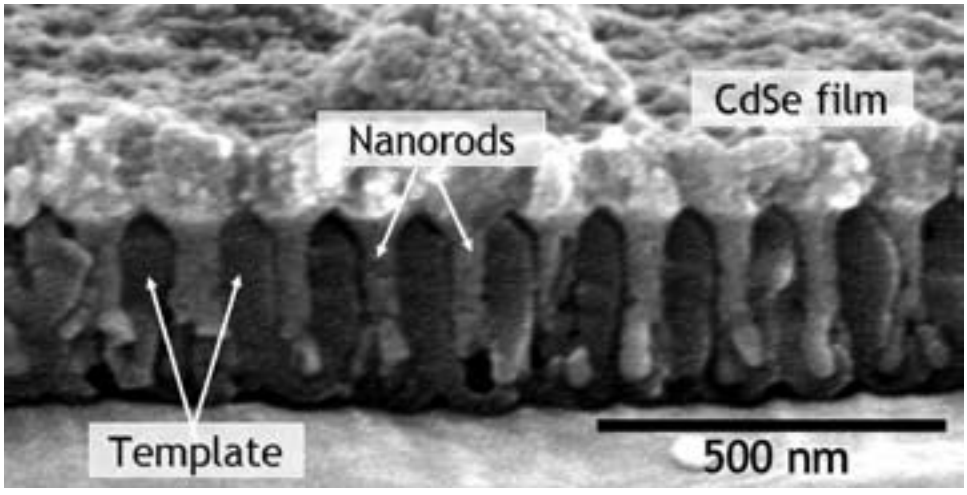

Figure 4: SEM micrograph of nanorod array produced using AC method.

Functionalization of Silicon Nanoparticles for Hyperpolarized Magnetic Resonance Imaging

Derek Smith

Chemical Engineering, University of Rochester

NNIN REU Site: Center for Nanoscale Systems, Harvard University
NNIN REU Principal Investigator: Prof. Charles Marcus, Department of Physics, Harvard University
NNIN REU Mentor: Dr. T. Fettah Kosar, Center for Nanoscale Systems, Harvard University
Contact: dsmith30@mail.rochester.edu, marcus@harvard.edu, fkosar@cns.fas.harvard.edu

Abstract

Magnetic resonance imaging (MRI) is used in the medical field for visualizing organs, tissues and structures within the body. Although MRI is widely used, it suffers from problems in certain cases due to overwhelming background signal. Silicon nanoparticles can be functionalized and introduced into the body as contrast agents, and they possess unique properties to correct many of the shortcomings of MRI. This project focuses on functionalizing silicon nanoparticles with specific molecules to target and image tumors or specific tissues and organs.

Introduction

MRI is a non-invasive medical imaging technique used to detect physiological defects within living tissues. It utilizes radio-frequency signals to measure the magnetic relaxation times of nuclei found in the body. Depending on the type of tissue, these relaxation times will differ, and through the use of magnetic gradients, a three-dimensional image of the scanned area can be created [1]. However, MRI currently suffers from image contrast issues when attempting to distinguish between healthy and cancerous tissue at small scales, and when dealing with organ systems that are in constant motion [1]. Silicon nanoparticles, which can be hyperpolarized, have the potential to correct these shortcomings.

Normal MR images are limited due to their imaging source. Since they are based on imaging the hydrogen nuclei found in water in the body, noise from other areas of the body will be a constant problem due to the abundance of water. In contrast, silicon is normally present in the body in insignificant amounts. Hence, silicon nuclei in hyperpolarized silicon nanoparticles can be imaged in place of hydrogen nuclei. This approach allows for the potential to target specific areas of the body without interference from background noise.

The aim of this project is to functionalize silicon nanoparticles to make them effective magnetic resonance imaging agents. Although silicon is already biocompatible, the surface of the nanoparticles must be modified to increase retention times in the body and to allow for specific targeting of organ systems or tumors. Functionalization of the nanoparticles is the first step to achieving both of these goals.

Experimental

The silicon nanoparticles were prepared by grinding down silicon wafers using a ball mill under varying conditions. These particles were then characterized by size using a scanning electron microscope (SEM) or by dynamic light scattering (DLS). Figure 1 shows the resulting nanoparticles. The particles shown have an average diameter of about 200 nm.

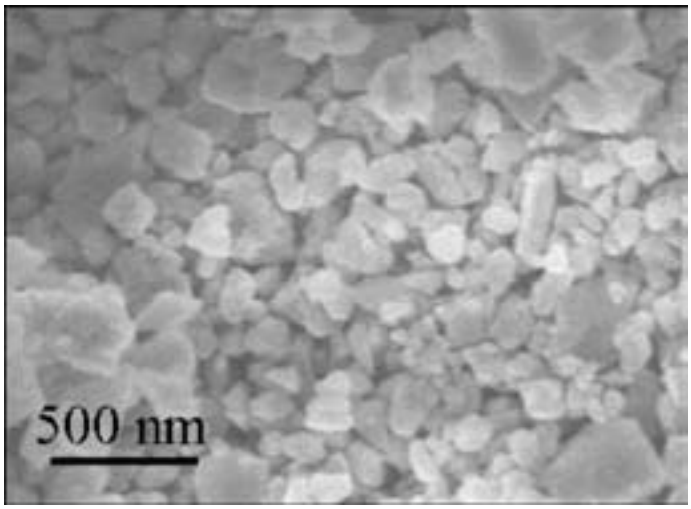

Figure 1: SEM image of silicon nanoparticles.

The functionalization of the silicon nanoparticles makes use of organosilane chemistry. The organosilane of choice for this project is 3-aminopropyltriethoxysilane (APTES). As seen in Figure 2, APTES reacts with the oxide layer on silicon through a known mechanism. The amine group present on this organosilane allows for further modification, and also provides a means to determine the success of the reaction by looking for the presence of nitrogen using elemental analysis techniques. Functionalization of a silicon surface using APTES has previously been done on silicon wafers, and attempts have been made to optimize the reaction on such surfaces [2]. Using these reports as a starting point, the organosilane reaction was first tested on small wafer squares to find the optimal reaction

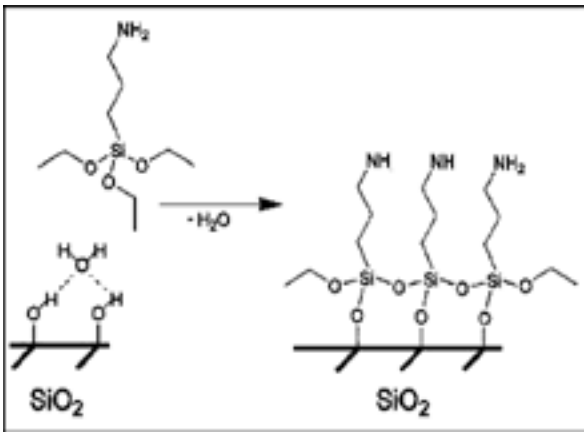

Figure 2: Reaction between APTES and native oxide on silicon [2].

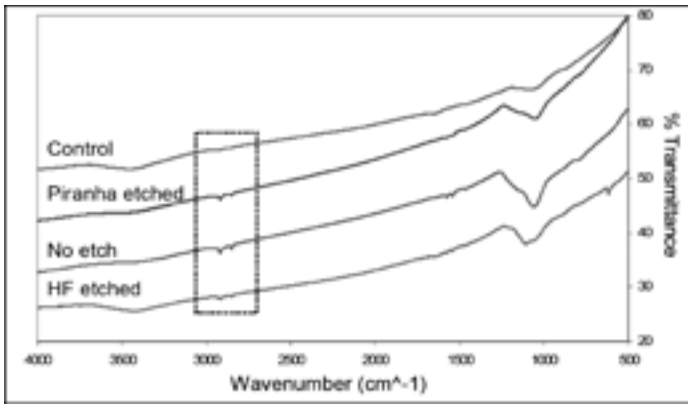

Figure 3: Full FTIR spectrum of reacted nanoparticles.

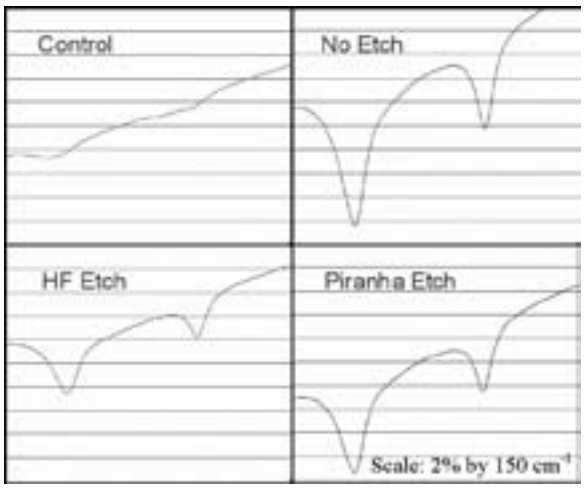

Figure 4: FTIR close-up of dashed area, showing C-H stretching region.

conditions. Untreated, Piranha etched (2:1 (v/v) sulfuric acid to hydrogen peroxide), and hydrofluoric acid (HF) etched wafers were evaluated under varying reaction parameters. The reaction was carried out under dry nitrogen atmosphere in anhydrous toluene. X-ray photoelectron spectroscopy (XPS) was used to determine if APTES was present on the surface of the wafers. We looked for a nitrogen peak that signaled the presence of APTES and compared the relative sizes of this peak.

Once the ideal conditions were determined, the silicon nanoparticles were functionalized using the same protocol. Untreated and etched nanoparticles were used to test for effects of surface treatment on the functionalization reaction, as well as for changes in the MRI properties of the nanoparticles. Both XPS and Fourier transform infrared spectroscopy (FTIR) were used to analyze the surface chemistry of the particles.

Results and Conclusions

XPS results from the wafers indicated that the optimal reaction conditions for all surface treatments were a 24 hour reaction in 1:9 APTES in toluene. Although both XPS and FTIR were used in the analysis of the nanoparticle reactions, FTIR produced the most consistent results. The primary regions compared in the FTIR graphs were the C-H stretching region from 2800 to 2950 cm^{-1} and the N-H stretching region from 1500 to 1650 cm^{-1}, both of which should only be present in those particles that had APTES on the surface. As seen in Figure 3 and 4, all three reacted particle sets exhibited relatively strong C-H peaks, particularly the "No Etch" and "Piranha Etch" particles. The N-H regions show a similar trend. These results are consistent with the presence of APTES on our nanoparticles. Further testing is needed to quantify the extent of functionalization on the silicon nanoparticle surface and confirm these results.

Future Work

Currently, work is being done to react the amine functional group present on the surface of the reacted silicon nanoparticles with monofunctional poly(ethylene glycol)-succinimidyl α-methyl-butanoate (mPEG-SMB), a functional group which will allow the nanoparticles to have a longer retention times *in vivo*. These functionalized particles will then be imaged *in vivo*.

Acknowledgements

I would like to thank Prof. Charles Marcus, Dr. T. Fettah Kosar, and Marcus group members Jonathan Marmurek, Rob Barton, and Jacob Aptekar. I'm also indebted to CNS, Harvard SEAS, the National Nanotechnology Infrastructure Network (NNIN) REU Program and the NSF for their support.

References

[1] Weishaupt, Dominik; Köchli, Victor D.; Marincek, Borut. "How does MRI work?;" Springer: New York, 2003.

[2] Howarter, J.A. and Youngblood J.P.; Langmuir, 22, 11142-11147 (2006).

Spontaneous Alignment in Self-Assembled Block Copolymers for Nanolithography

Mikael Witte

Physics and Mathematics, St. Olaf College

NNIN REU Site: Minnesota Nanotechnology Cluster, University of Minnesota-Twin Cities
NNIN REU Principal Investigator: Dr. Marc Hillmyer, Chemistry, University of Minnesota-Twin Cities
NNIN REU Mentor: Dr. Chris Leighton, Chemical Engineering and Materials Science, University of Minnesota-Twin Cities
Contact: wittem@stolaf.edu, hillmyer@chem.umn.edu, leighton@tc.umn.edu

Abstract

Block copolymers were used to create self-organizing templates for pattern transfer. The goal of the templates was to exceed 10^{12} features per square inch for use in magnetic media. The cylinder forming diblock copolymer polystyrene-polylactide (PS-PLA) has been observed to spontaneously align with cylinders of PLA oriented perpendicular to the substrate in a PS matrix after thermal annealing. The project examined spontaneous alignment of PS-PLA thin films of varying thickness on silicon (Si) and nickel-iron / gold (NiFe/Au) substrates without thermal annealing, and compares PS-PLA thin films with previously characterized polystyrene-polyisoprene-polylactide (PS-PI-PLA) triblock terpolymer thin films. In addition, the project incuded general observations of the pattern transfer process. One hypothesis was that PS-PI-PLA forms a perpendicular cylindrical pattern because of the energetic preference for PI for the film surface, thus there should be no perpendicular alignment with PS-PLA.

Introduction

The capacity of magnetic media is approaching an upper limit with current optical lithography techniques. In order to create new media with capacities in the terabit range, novel techniques must be found. Pattern transfer is one such technique, but there remain some obstacles with the block copolymer method, such as attaining long-range order (on the scale of ~ 1 cm^2), choosing the ideal block copolymer for its feature size and chemical properties, and perfecting the pattern transfer process to reproducibly create the desired pattern on a magnetic film. The ideal block copolymer has an average feature size of approximately 10 nm, with the minority component(s) self-assembling into a hexagonal pattern of cylinders aligned perpendicular to the substrate. Optimizing the pattern transfer process means, first and foremost, ensuring that the pattern is transferred. This is accomplished by trying to make the template an etch resist. Eliminating unnecessary steps in the process is also important, as this can increase reproducibility and minimize costs.

Experimental Procedure

The synthesis of PS-PLA is described elsewhere [1-3]. The sample (labeled MDR-II-85) we used had an average molecular weight of 60 kg/mol, determined from GPC, with a 2:1 mass ratio of PS to PLA and a polydispersity of 1.05. The substrates were Si/SiO_2 wafers of approximately 1 cm^2. Six were left as naked Si/SiO_2 and the other six were prepared with 5 nm NiFe (80:20 Ni:Fe) and a 5 nm Au endcap sputtered on at room temperature. Six PS-PLA solutions of varying concentration were created by adding 2 mL of chlorobenzene to varying masses of PS-PLA, from 15 mg to 35 mg. Then the solution was spin-coated onto the wafers at a constant spinning speed of 2000 rpm.

Film thickness was measured with grazing angle x-ray reflectivity (GIXR). Other characterization was performed with a Nanoscope III atomic force microscope in tapping mode. After initial characterization, the samples underwent a 45-minute 0.5 M NaOH bath followed by a 5-minute rinse in distilled water and argon drying to degrade and remove the PLA component. The samples were characterized again with the atomic force microscope (AFM).

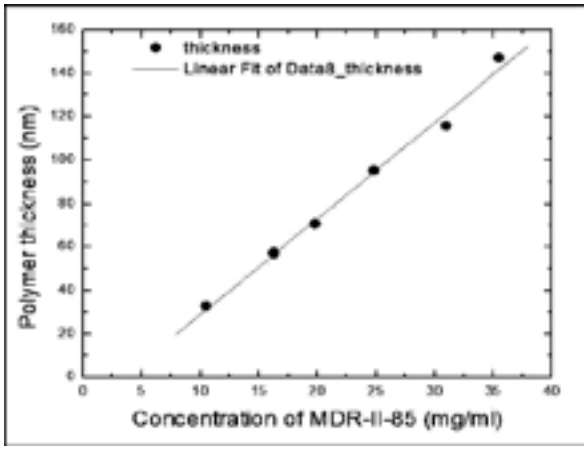

Figure 1: Thin film thickness in nm as a function of polymer solution concentration in mg/ml, as determined by GIXR.

Results And Conclusions

The thin film thickness as a function of solution concentration showed a linear relationship (Figure 1). The first round of AFM images taken of the samples as spun showed majority perpendicular cylindrical orientation for all samples but the 147.0 nm film. Perpendicular alignment looked particularly good in medium thickness samples such as the 57.1 nm and 70.5 nm samples (Figures 2 and 3). This observation undermined the hypothesis that a third component, polyisoprene, would be necessary for spontaneous perpendicular alignment.

There was no strong long-range ordering in the samples, which we determined from the lack of regular hexagonal patterning. On the other hand, initial results from the PLA-degraded samples showed more parallel cylindrical ordering in samples that appeared to have perpendicular ordering with the PLA component present. All the samples need to be further analyzed before any solid conclusions can be drawn.

Future Work

First and foremost, the remaining PLA-degraded samples need to be further characterized. Then, the images taken will be further analyzed to determine the average feature size of the perpendicular holes (i.e. from the PLA cylinders). If PS-PLA turns out to be a viable option for pattern transfer, further work will be required to determine how to create a pattern of freestanding cylinders, i.e. degrading the majority matrix. One option is to stain the PLA with a metal, which would make it an etch resist. The group is also currently pursuing techniques to hard mask the pattern. This helps to preserve the pattern while the magnetic film is etched.

Acknowledgements

The author would like to acknowledge and thank Dr. Marc Hillmyer and Dr. Chris Leighton for their direction and insight, Marc Rodwogin and Toshi Kubo for their knowledge and support, the National Nanotechnology Infrastructure Network Research Experience for Undergraduates Program and the NSF for funding, and the rest of the Hillmyer and Leighton groups.

References

[1] Zalusky, A.S.; "Mesoporous polystyrene monoliths"; J. Chem. Soc., 123, 1519-1520 (2001).

[2] Zalusky, A.S.; "Ordered nanoporous polymers from polystyrene-polylactide block copolymers"; J. Chem. Soc, 124, 12761-12773 (2002).

[3] Mao, H.; "Control of pore hydrophilicity in ordered nanoporous polystyrene using an AB/AC block copolymer blending strategy"; Faraday Discussions, 128, 149-162 (2005).

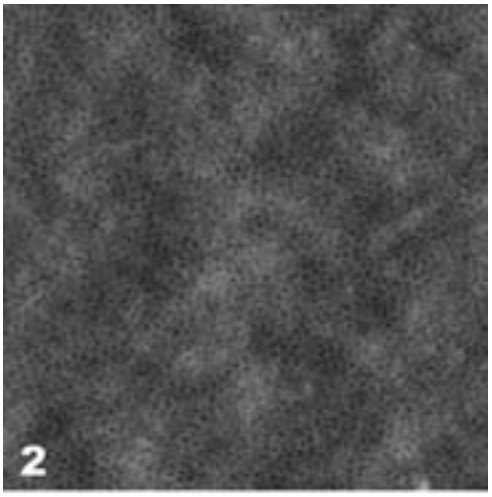

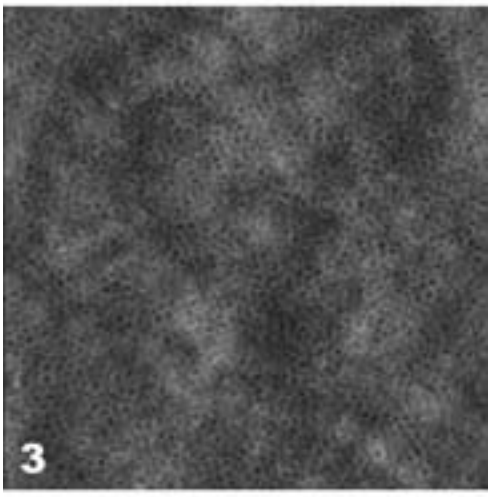

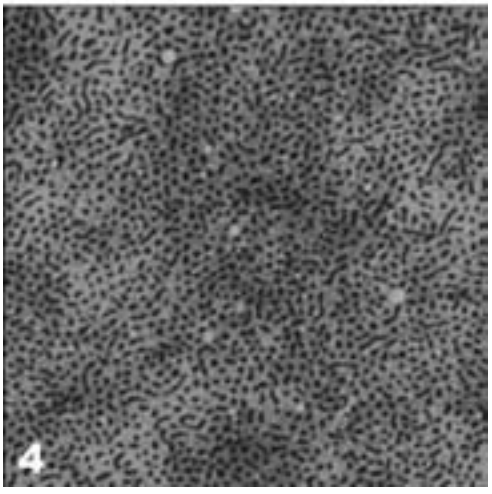

Figure 2, top: 57.1 nm thin film on Ni/FeAu substrate, as spun, 2 × 2 μm image.

Figure 3, middle: 70.8 nm thin film on Ni/FeAu substrate, as spun, 2 × 2 μm image.

Figure 4, bottom: 95.0 nm thin film on Ni/FeAu substrate, PLA degraded, 2 × 2 μm image.

Patterning of Electrical Circuits on Fluidic Assembly Microtiles

Andrew Baisch

Mechanical Engineering, Carnegie Mellon University

NNIN REU Site: Cornell NanoScale Science & Technology Facility, Cornell University
NNIN REU Principal Investigators: Drs. David Erickson and Hod Lipson, Mechanical and Aerospace Engr., Cornell University
NNIN REU Mentors: Mekala Krishnan and Michael Tolley, Mechanical and Aerospace Engineering, Cornell University
Contact: abaisch@andrew.cmu.edu, de54@cornell.edu, hl274@cornell.edu

Abstract

As an alternative to pick-and-place assembly techniques, recent research has lead to the development of microelectro-mechanical systems (MEMS) components that assemble spontaneously in fluid [1-3]. These efforts have relied heavily on surface-energy minimization and therefore work best when components are assembled by vertical stacking to obtain a product with multiple layers. Our research provides an alternative method for interfacing MEMS components assembled in fluid, which involves horizontal (in-plane) assembly. Our previous work has produced silicon microtiles with mechanical latches that can be manipulated by controlling local fluidic forces in a microchamber [4]. The goal of this research was to demonstrate electrical connection between tiles in a single plane. This was achieved by patterning tiles with gold electrodes so that their tops and sidewalls had a continuous covering of conductive material. The result of this research is a novel method for the electrical interfacing of fluidically-assembled MEMS components.

Background

Past research includes fabrication and testing a series of latching silicon microtiles of varying sizes that can be controlled and assembled in a microfluidic channel. The microtiles are manipulated by controlling the fluid flow through a polydimethylsiloxane (PDMS) microchamber with off-chip valving. The tiles are fabricated from a silicon-on-insulator (SOI) wafer using photolithography and a deep ion etch through the top silicon layer, then released from the wafer by etching the oxide using a 49% hydrofluoric acid (HF) solution.

Fabrication

We developed a fabrication method to pattern gold electrodes on 500 μm square by 30 μm high silicon microtiles. Electrode fabrication began prior to HF release, and included evaporation followed by photolithography processes, finally leading to a chemical etch of the metal to form electrodes on the tops and sides of tiles. A wet etch was chosen instead of a lift-off technique to avoid leaving unwanted metal in the trenches between the etched tiles. The consequence of residual metal between tiles would have been either damage to electrodes or no tile separation after release, both results rendering our tiles useless for in-plane fluidic assembly.

Because gold is reluctant to adhere to silicon, a 15 nm chromium adhesion layer was deposited using an electron-gun evaporator, followed by the 80 nm gold layer. After evaporation a thick (35-40 μm) layer of AZ-4903 positive-tone photoresist was spun to cover and fill the gaps between tiles. The resist was removed around electrodes using a two-step exposure and development process (Figure 1). The first exposure patterned the electrodes on the tiles.

During the first development it was necessary to under-develop the electrode pattern, with the purpose of leaving some resist to be removed during the second development. During the second exposure, the trenches between tiles were heavily exposed. A second development removed all resist between the tiles, leaving only sidewall coverage as required for the electrical connections between tiles. A wet etch of both gold and chromium removed all unwanted metal from the silicon.

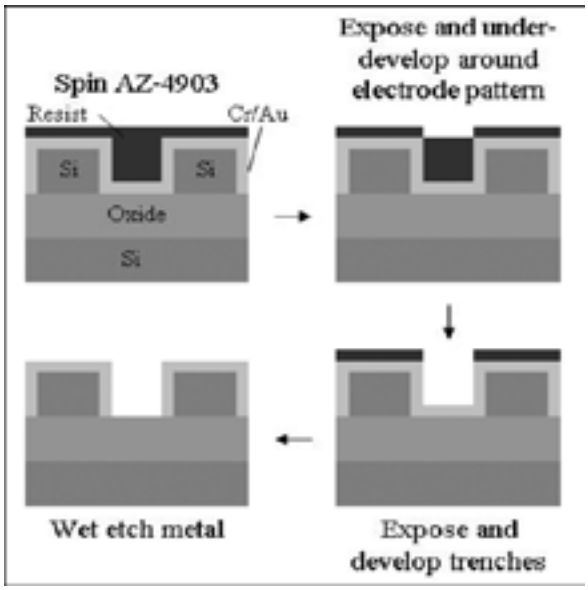

Figure 1: Diagram of two-step exposure and development process for patterning electrodes.

Without this two-step exposure and development process, we experienced either residual photoresist in the trenches between the tiles or overexposure/overdevelopment of the electrodes on the tiles. Finally, tiles were released using 49% HF solution.

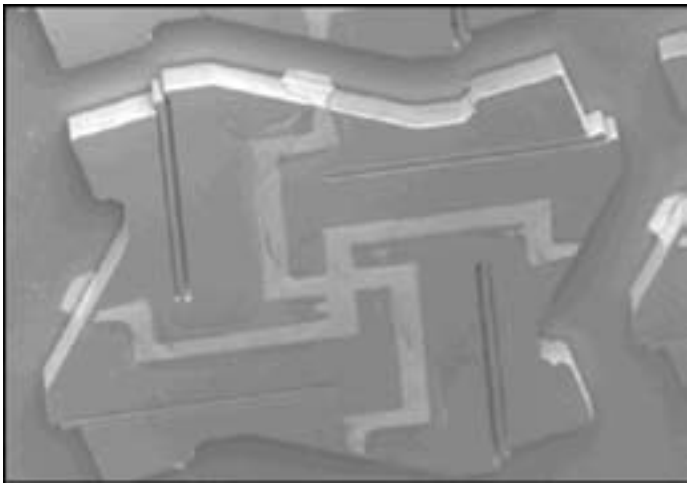

Figure 2: Scanning electron microscopy (SEM) image of silicon tile and gold electrode pattern.

Results

Our fabrication yielded many tiles suitable for electrical testing (Figure 2), though inconsistencies with the electrode pattern did arise, likely caused by variable resist thickness due to edge effects while spinning AZ-4903. Electrical testing using a multimeter probe station verified connectivity across one, two and three-tile circuits assembled in silicone oil on a glass substrate (Figure 3). The tiles were manipulated and assembled using the probe tips (Figure 4).

When compared to similar tests using a non-patterned silicon tile control, electrode-covered tiles yielded a circuit resistance four orders of magnitude smaller. To further characterize our resistance results, we used $R = \rho L/A$ to theoretically calculate circuit resistance, R (Ω). We calculated the theoretical resistance across one tile with chromium and gold wires in parallel to be 4 ohms. Since this value is much smaller than the measured resistances, we assumed that electrode resistance is negligible compared to contact resistances at the tile-tile and probe-tile interfaces. Using this assumption and a least-squares regression, the contact resistances at tile interfaces and for each probe are 880 Ω (0.00792 Ω-cm^2) and 280 Ω respectively.

Conclusion

We fabricated and tested $500 \times 500 \times 30$ μm silicon microtiles patterned with gold electrodes capable of assembling in fluid to form mechanical structures with in-plane electrical connections. By obtaining resistance data across one, two, and three tile circuits, we have verified electrical conductivity across tiles. The results indicate that electrical conduction occurred through planar assemblies of electrode-patterned tiles. Therefore, our fabrication method is capable of producing planar MEMS assembled from individual, microscale components.

Future Work

With the development of our fabrication process, it is possible to obtain simple electric connections between silicon microtiles attached in-plane. Further research will fabricate more complex circuit elements on individual microtiles, enhancing the functionality of systems built from these components.

Acknowledgements

I would like to thank the National Science Foundation as well as the National Nanotechnology Infrastructure Network REU Program for their support of this research. I would especially like to thank Mike Tolley, Mekala Krishnan, Dr. David Erickson and Dr. Hod Lipson, the Erickson Lab as well as the entire Cornell NanoScale Facility staff for their professional help and guidance on this project. Lastly, I would like to thank Dr. Garcia at Cornell for the use of his probe station.

References

[1] D. H. Gracias, J. Tien, T. L. Breen, C. Hsu, G. M. Whitesides, Science, 289 (2000), pp. 1170-1172.

[2] U. Srinivasan, D. Liepmann, & R. T. Howe, J. MEMS 10 (2001), pp. 17-24.

[3] H. J. Yeh & J. S. Smith, IEEE Photonics Technology Letters, 6 (1994), pp. 706-709.

[4] M. Tolley, V. Zykov, D. Erickson & H. Lipson, Proc. of Micro Total Analysis Systems, 2006, pp. 1552-1554.

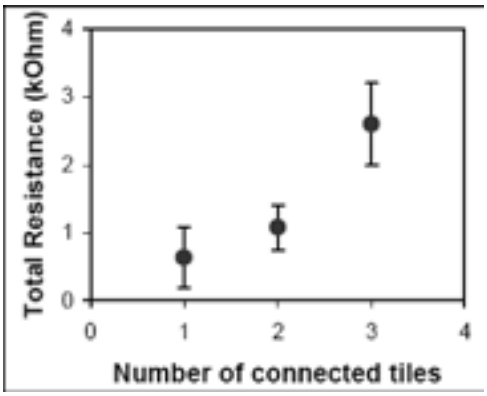

Figure 3: Resistance measurement verses number of tiles. Data points are average measured values. Error bars are minimum and maximum values.

Figure 4: Optical microscope image of resistance measurement across three assembled microtiles.

Development of a Three Degrees of Freedom Atomic Force Microscope

Courtney Bergstein
Chemistry, Carlow University

NNIN REU Site: Penn State Center for Nanotechnology Education and Utilization, The Pennsylvania State University
NNIN REU Principal Investigator: Dr. Aman Haque, Mechanical and Nuclear Engineering, The Pennsylvania State University
NNIN REU Mentor: Amit Desai, Department of Mechanical and Nuclear Engineering, The Pennsylvania State University
Contact: bergsteincl@carlow.edu, mah37@engr.psu.edu, amitdesai@psu.edu

Abstract

An atomic force microscope (AFM) easily measures forces in one direction. It can be adapted to measure force in the other directions, but it is time intensive and challenging. In this paper, a three degrees of freedom atomic force microscope (3DOF AFM) is presented. Microfabrication techniques are used to design, fabricate, and test a miniature system that can measure forces in three directions with high resolution. Typical applications for the 3DOF AFM are probing nanostructures and studying hard disk drive interactions with the reading head.

Introduction

Atomic force microscopes are used to measure surface topographies. They consist of a cantilever with a tip at the end. A laser beam deflects off the end of the cantilever and into a detector. The detector measures the deflection of the laser beam to find the displacement of the tip as it moves across different surface topographies [1, p. 1614]. AFMs typically measure forces with one degree of freedom, which is in the x direction. The y and z directions are obtainable; however it is time intensive and challenging. A three degree of freedom atomic force microscope can measure forces in all directions.

In order for this to occur, the 3DOF AFM device has to be compliant in all three directions. Compliancy is measured by a low κ value, which is calculated using a finite element simulation software called ANSYS. Figure 1 is depicting the movement of one of the devices in the x direction. This device is made of one vertical thick vertical beam (20 μm) and two thin cross beams (varying between 2 μm or 3 μm). Applications of a 3DOF AFM would be the manipulation and probing of nanostructures, studying hard disk drive interfaces, and understanding nanoscale friction and adhesion forces.

The main objective of this research was to use current microfabrication techniques to design a fabrication process by optimizing both the lithography and process steps in order to fabricate a free standing miniature system that can measure forces with three degrees of freedom.

Experimental Methods

In this research, we developed a fabrication process for free standing micro machines, specifically a three degrees of freedom atomic force microscope. The devices varied from having two cross beams to one beam, the beam thickness varied from 2 μm to 3μm, and the angle between the beams varied from 4° to 10°. Various techniques were used throughout the fabrication process.

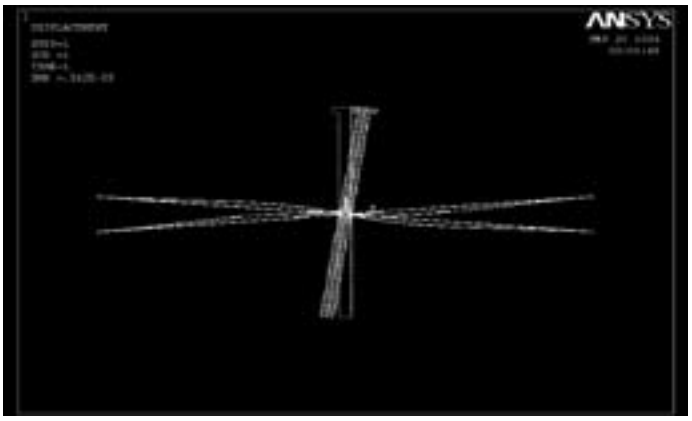

Figure 1: Depiction of the device movement in the x direction from ANSYS.

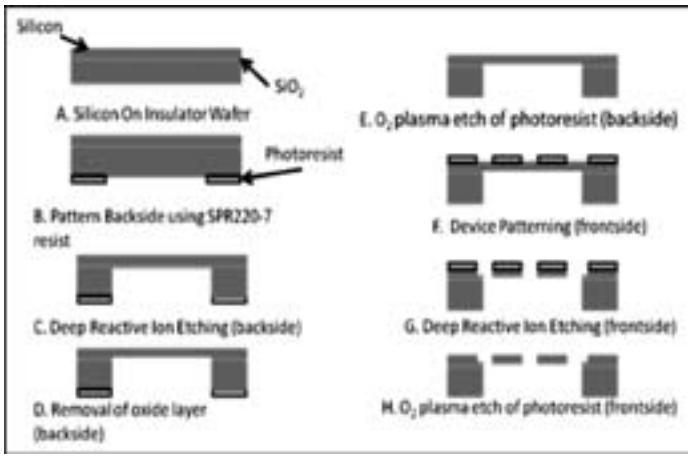

Figure 2: Schematic of the fabrication steps used to fabricate the free standing devices.

Figure 2 is a schematic showing the steps of the fabrication process. The process begins with a silicon-on-insulator (SOI) wafer. 10 m thick SPR220-7 photoresist is used to pattern the backside of the wafer. The first step of the process was to optimize lithography techniques. In order to optimize the lithography process, modifications had to be made due to the resist thickness. The first modification was to use the multiple exposure feature on the Karl Suss MA6 to prevent resist bubbling. The second modification was to skip the post exposure bake to prevent resist cracking. Deep reactive ion etching (DRIE) was used to etch the backside up until the oxide layer. The oxide layer was wet etched using a buffered oxide etch. The frontside mask was then aligned with the backside mask using the MJB3 for device patterning. DRIE is used to etch the frontside the whole way through the wafer. This resulted in free standing devices that were approximately 20 μm thick.

Future Work

We will further develop and modify the fabrication process in order to obtain a higher yield. After the devices are successfully fabricated, they will be mounted to a probe and tested in a FIB SEM. The displacement will be measured and multiplied by the spring constant, κ, (which was previously calculated in ANSYS) to find forces with three degrees of freedom of nanostructures, specifically nanowires on a silicon substrate.

Conclusions

Lithography techniques were optimized and a fabrication process was developed, but not to 100% accuracy. All of the 3DOF AFMs broke during the fabrication process; however we were able to fabricate some 2DOF AFMs. This shows that the fabrication process was successful but had a low yield. Minor modifications have to be made to the fabrication process in order to obtain a higher yield. Figure 3 is one of the 3DOF AFM devices etched 10 μm into a silicon wafer. Figure 4 shows an SEM image of one of the free standing 2DOF AFM devices that were fabricated using the proposed fabrication process.

Acknowledgements

The National Nanotechnology Infrastructure Network Research Experience for Undergraduates Program, National Science Foundation, The Pennsylvania State University Center for Nanotechnology Education and Utilization, and the Nanofabrication Staff. I also want to give a special thanks to my mentor Amit Desai, and my principal investigator Dr. Aman Haque, who are both from the Department of Mechanical and Nuclear Engineering at The Pennsylvania State University.

References

[1] Colton, Richard J. Nanoscale Measurements and Manipulation. Review Article. P. 1609-1635. 30 June 2004.

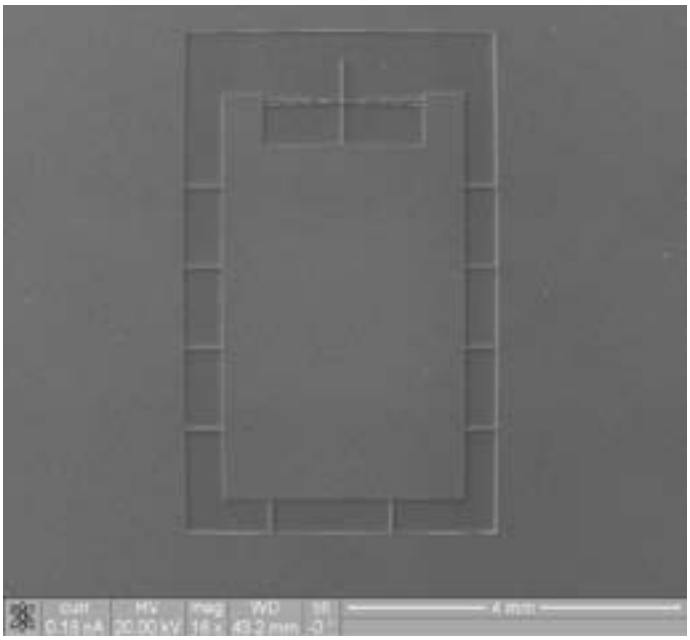

Figure 3: SEM image of a 3DOF AFM (not free standing).

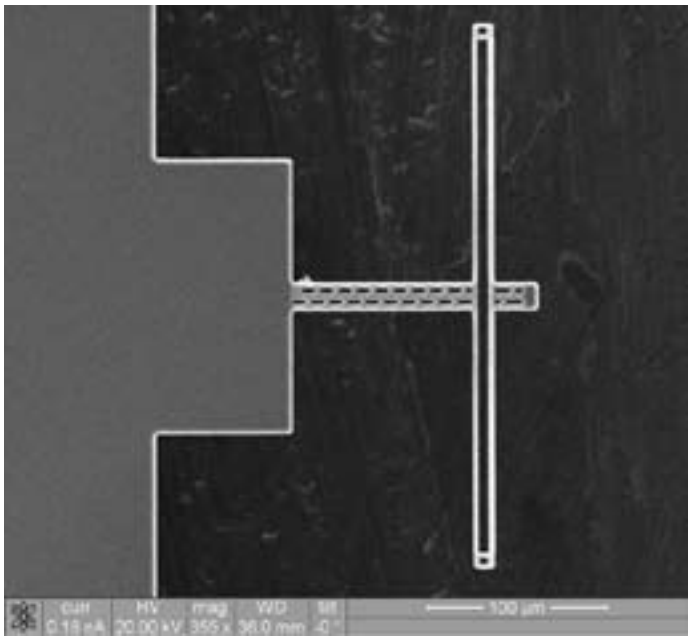

Figure 4: SEM image of a free standing 2DOF AFM fabricated using this fabrication process.

Fabrication of Active Probe Structures for Atomic Force Microscopy

Mohammad Biswas

Chemical Engineering, Auburn University

NNIN REU Site: Microelectronics Research Laboratory, Georgia Institute of Technology
NNIN REU Principal Investigator: Dr. F. Levent Degertekin, Mechanical Engineering, Georgia Institute of Technology
NNIN REU Mentor: Guclu Onaran, Mechanical Engineering, Georgia Institute of Technology
Contact: biswamo@auburn.edu, levent@gatech.edu, gte132x@mail.gatech.edu

Abstract

The atomic force microscope (AFM) launched a wide variety of applications ranging from life sciences to metrology after its invention in 1986. However, current applications are limited by several aspects of the conventional AFM technology, which uses a passive cantilever probe and typically slow and bulky piezoelectric actuators. The relatively slow piezoelectric actuators limit the attainable imaging speeds, and the complex cantilever dynamics makes the extraction of quantitative material property characterization difficult. This project addresses these issues by introducing a new probe structure for the AFM. This new probe has a sharp tip placed on an active, electrostatically actuated, micromachined membrane with an integrated displacement sensor. The membrane itself and the diffraction grating form a small phase sensitive optical interferometer for displacement detection. The project focuses on the fabrication of this probe and the experimental results obtained from the fabricated devices. Lift-off process and membrane deposition mainly involve lithography and metallization to fabricate the devices. The devices are then analyzed after being released in the critical point dryer. These results include applications such as fast tapping mode imaging, which utilizes the electrostatic actuator, and time resolving interaction force imaging, which utilizes the well-behaved dynamics of the device.

Introduction

Since its invention, the AFM has found a wide variety of applications ranging from life sciences to metrology. Moreover, AFM is one of the most widely used tools in nanotechnology. For example, applications in physics and chemistry are important for surface property characterization such as stiffness. In biology and life sciences, AFM also can be used in force spectroscopy for drug discovery and ***in vitro*** cell imaging. In engineering and nanosciences, sample information can be obtained by surface roughness analysis and process quality control.

Atomic Force Microscope

The various components of the AFM working together are what enable such diverse applications. A typical AFM has; 1) a micro-cantilever probe, 2) optical lever detection, 3) the piezoelectric tube, which is also the scanner, and 4) the controller. The probe acts as a force sensor, and the cantilever has a very sharp tip with diameter of 2-50 nm. The optical lever detection is used to determine the position of the probe by the photo detector sensing the laser reflected off the cantilever. The piezoelectric tube moves the sample or the probe in x-y-z direction. The controller keeps the cantilever deflection constant through feedback control while the probe scans the sample locally.

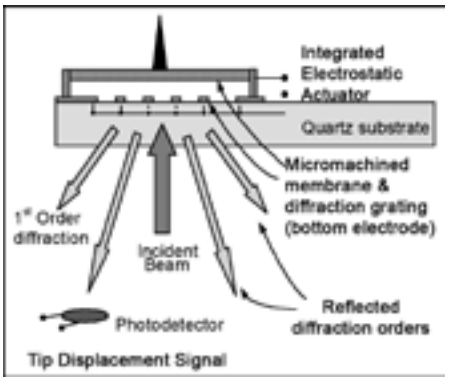

Figure 1: FIRAT probe structure and diffraction based optical interferometric detection.

Current applications are limited by some aspects of the conventional AFM technology, which uses a passive cantilever probe and typically slow and bulky piezoelectric actuators. The relatively slow piezoelectric actuators limit the attainable imaging speeds, and the complex cantilever dynamics makes the extraction of quantitative material property characterization difficult. To tackle this issue, a new probe structure called the force sensing integrated readout and active tip (FIRAT) was introduced.

This new probe has a sharp tip placed on an active, electrostatically actuated, micromachined membrane with an integrated displacement sensor as illustrated in Figure 1 [1]. The membrane itself and the diffraction grating form a small phase sensitive optical interferometer for displacement detection [1]. So the interferometric detection is more sensitive than the optical lever detection of conventional AFM, and the electrostatically actuated membrane is faster than the piezoelectric tube. In order to validate such functionalities of the FIRAT probe, it first has to be fabricated and then analyzed through various experiments.

Experimental Procedure

The fabrication of the FIRAT probe was carried out in the Microelectronics Research Center. We used a 4-inch quartz wafer on which to fabricate the probes. The process began with surface preparation of the wafer by ultra-sonication in acetone for 15 minutes and then in methanol for 15 minutes. Finally, the surface was ready after oxygen plasma cleaning using Plasmatherm reactive ion etching (RIE). Lithography, using the mask aligner,

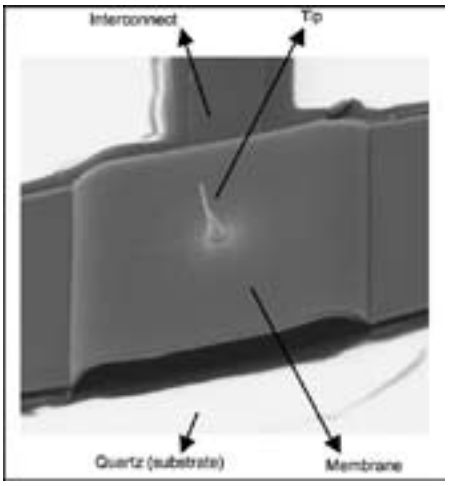

Figure 2: Image of fabricated FIRAT probe. Fingers, not shown, are under the membrane.

resulted in finger patterns. The lift-off process was then carried out to make 0.120 μm Al fingers, which were deposited using the e-beam evaporator. Next, through lithography, a sacrificial layer of about 2.5 μm thick was formed over the Al fingers in order to deposit the Al membrane.

The membrane, which had a thickness of approximately 0.8 μm, was deposited using the DC sputterer. Lithography was carried out again to perform wet etching using aluminum etchant to define the structure. After the ME dicing machine cut the wafer into several probe devices, they were released under photoresist stripper and then in the critical point dryer. A sharp tip, with a diameter of about 50-100 nm, was installed on the membrane of one of the devices using the focused ion beam tool. The final product of such a device is shown in Figure 2.

Results and Conclusions

We were able to successfully fabricate the FIRAT probes. We checked and confirmed the progress of the fabrication by taking images using a digital microscope, and gathering data using a non-optical profilometer at different intervals during the process. Similar probe devices were analyzed using the Wyko optical profilometer to confirm the fabrication of the completed structures. Using the experimental setup in Figure 3, several experiments were conducted on earlier probes, which are similar to the devices that we fabricated [1]. The time resolved integrated force (TRIF) imaging experiment demonstrated that the FIRAT probe was able to characterize stiffness and stickiness of selected samples [2].

The experimental data showed that the membrane only deflected when the probe contacted a hard material sample. However, for a soft material sample, both the membrane and the sample deflected. Thus, the softer material took more time to achieve peak contact force compared to the harder material. The amount of force required for the probe to retract from the sample determined the stickiness. In Figure 4, the fast tapping mode imaging experiment showed that the FIRAT probe was able to track the sample better than a typical cantilever at higher imaging speeds – line scan rates of up to 60 Hz [1]. These results along with other experimental data have shown great promise for the new probe, and were used to explore the extent of its functionalities.

Future Work

Although the current fabrication process does make the production of the probes simple, the probes still cannot not be commercially reproduced. The next step of this project is to design a process to enable mass installment of tips on the probes. This would make the mass production of such probes possible and facilitate the start of commercial production.

Acknowledgments

I thank my PI, Prof. F. Levent Degertekin, and my mentor, Guclu Onaran, for the project. I also thank Prof. James Meindl, director of GT Microelectronics Research Center, and Jennifer Root, site coordinator, for the research opportunity. This project was funded by National Science Foundation and National Nanotechnology Infrastructure Network REU Program.

References

[1] Onaran, A. G., M. Balantekin, W. Lee, W. L. Hughes, B. A. Buchine, R. O. Guldiken and Z. Parlak, C. F. Quate, and F. L. Degertekin., "A new atomic force microscope probe with force sensing integrated readout and active tip," Review of Scientific Instruments, 77, 023501, (2006).

[2] Onaran, A. G., M. Balantekin, W. Lee, N. A. Hall, C. F. Quate, and F. L. Degertekin., "Sensor for direct measurement of interaction forces in probe microscopy," Applied Physics Letters, 87, 213109, (2005).

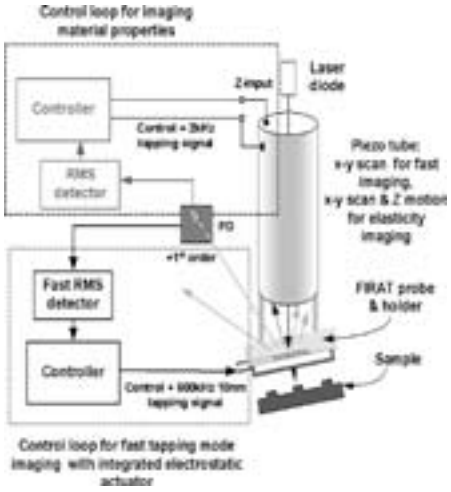

Figure 3, right: Experimental setup integrating the FIRAT probe with commercial AFM system.

Figure 4, below: Line scans of sample at different imaging speeds for each probe.

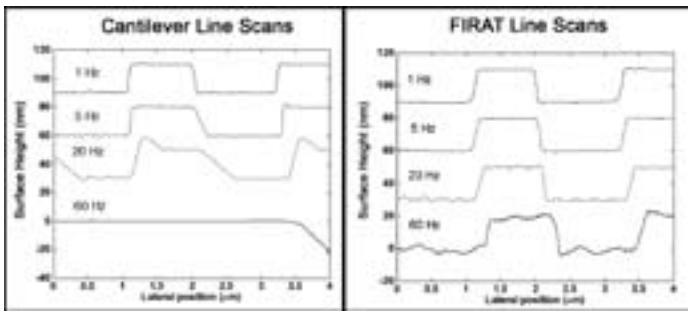

Characterization of the DRIE Process for ETWI for Piezoresistive Inertial Sensors

Maria Suggs

Physics, Southern Polytechnic State University

NNIN REU Site: Stanford Nanofabrication Facility, Stanford University
NNIN REU Principal Investigator: Prof. Beth Pruitt, Dept. of Mechanical Engineering, Stanford University
NNIN REU Mentors: Alvin Barlian and Nahid Harjee, Dept. of Mechanical Engineering, Stanford University
Contact: msuggs@spsu.edu, pruitt@stanford.edu, barlian@stanford.edu, nharjee@stanford.edu

Abstract

Electrical through-wafer interconnects (ETWI) are often integrated with inertial sensors for harsh liquid environment applications. Devices with metal interconnects are very susceptible to corrosion in aquatic environments. An alternative approach is to form highly doped, conductive polysilicon through the wafer from the back side (unexposed to harsh environments) to the front side of the device's chip. ETWI technology requires etching through the wafer. This places a high demand on the through wafer etch profile, critical dimension control, and feature size dependent etch rate (etch lag). On test structures, we measured the sidewall profile and etch rate as a function of several etch parameters (etch cycle time, platen power, current power, C_4F_8 flow, etc). In addition, we assessed practical methodologies for handling the wafer during the etch. The objective of this project is to use statistical design of experiment (DoE) to optimize the deep reactive ion etch (RIE) recipe for through wafer etching and test wafer bonding for through wafer via formation. From the development of electrical through wafer interconnects, more reliable sensor devices can be fabricated for studies in hydrodynamics in harsh environments in addition to a plethora of other applications.

Introduction

We began by optimizing a baseline recipe using STS-HRM (Surface Technology Systems). Then, we used those results to develop a reliable method for through wafer etching. STS-HRM is based on the Bosch method, which uses a process that alternates between the etch gas (SF_6) and the deposition gas (C_4F_8). Moreover, etching occurs by two mechanisms: a chemical process in which fluorine from the plasma bonds with the silicon atoms and becomes a volatile gas, and by a physical process in which the dluoride ions bombard the surface, sputtering the material away. Under proper tuning, the Bosch method achieves an anisotropic (downward direction) etching profile because of the alternating etch passivation cycles. The objective of this optimization was to achieve the following conditions: very straight walls, no grass, and small scallops. However, our major challenge for through wafer etching using STSHRM was thermal management due to backside helium (cooling gas) release, and due to photoresist burning.

As a result of etching completely through the wafer, we lose the helium that is located beneath it; hence, we lose the uniformity of the etch across the wafer, and the cooling that we need in order to prevent the photoresist from burning. Therefore, the single wafer was substituted with a polymer-bonded pair of wafers.

Experimental Procedure

The preparation of the wafers for etch optimization was as follows: spinning 3 μm SPR 220-3 positive photoresist on an SVG coater track; then, a pattern was formed by exposure using a Karl Suss MA-6 i-line mask aligner. The wafers were then developed in LDD 26W developer. The STS-HRM etcher was used for the experimental etch matrix.

Based on "Smooth Shallow Template" (Dep_{time} = 2s; $Etch_{time}$ = 3s; Throttle $Valve_{dep}$ = 15%; Throttle $Valve_{etch}$ = 12.5 %; C_4F_8 flow = 100 sccm; SF_6 flow = 400 sccm; P_{source} = 2500W, P_{platen} = 45 W, Electromagnet - $Etch_{main}$ = 1 A; Electromagnet - $Delay_{time}$ = 0 s), we selected six parameters to optimize: platen power, etch cycle time, deposition cycle time, pressure, C_4F_8 flow, SF_6 flow. We maximized and minimized the ranges and etched twelve wafers with different recipes. Following the cleaving, we proceeded to examine the samples under scanning electron microscope (SEM).

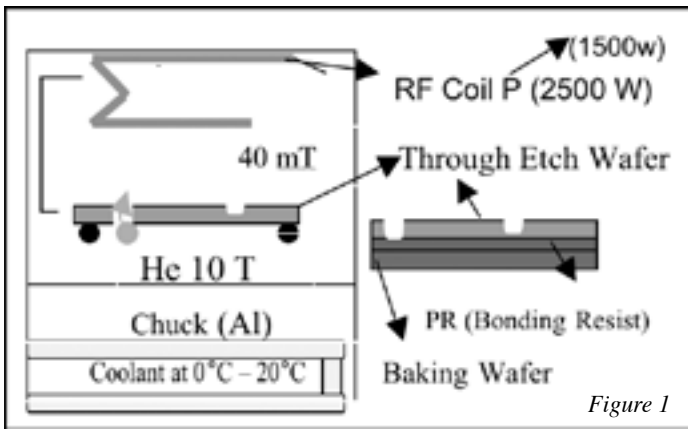

Figure 1

In order to complete a through-wafer etch, a backing wafer was polymer bonded to the through-etch wafer to prevent helium from escaping and to add structural support. First, 10 μm SPR 220-7 photoresist was spun onto the through-etch wafer and 0.5 μm oxide was placed on the backing wafer. Furthermore, 2 μm SPR 3612 photoresist was used as the bonding polymer in between the wafers (Figure 1). Then, both wafers were placed on a 90°C hot plate for 7 minutes with a weight on top. Afterwards, we tested their bond in a vacuum for 5 minutes. Then, we used STS-HRM ("Smooth Shallow Template"), but we lowered the coil power down to 1500 W, because it was discovered that the source power was the principal factor in overheating the wafer. Hence, this reduction in power to 1500 W enabled the masking resist to survive the etch. Finally, we separated the wafers by soaking in acetone for approximately one hour.

Results and Conclusions

In addition, we can conclude that based on the optimization experiment in STS-HRM, reducing the thermal load by decreasing the source power was the key to bonded wafer through etching. Moreover, a wafer-to-wafer polymer bonding technique and a release method were developed for successful through wafer etching in the high rate STS-2 machine.

Future Work

In the future, we could explore new methods for through wafer using aluminum as an etch stop. Moreover, we could set the interconnects through the device's chip and conduct tests in harsh environments.

Acknowledgements

I would like to thank the following people and institutions: Prof. Beth Pruitt, Alvin Barlian, Nahid Harjee; Michael Deal, Maureen Baran, staff at SNF; National Nanotechnology Infrastructure Network REU Program; NSF; CIS; Dr. Patrick and Dr. Pace. Special thank you to Eric Perozziello.

References

[1] Barlian, AA, Park, S-J, Mukundan, V, and Pruitt, "BL Design and characterization of microfabricated piezoresistive floating element-based shear stress sensors." Sensors and Actuators A: Physical, vol. 134, pp. 77-87, 2007.

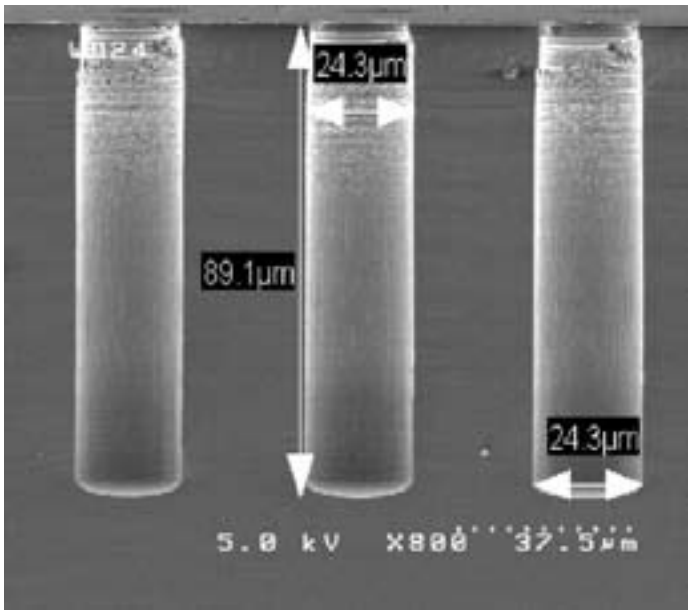

Figure 2, top: We observed very straight and vertical walls, no grass formation, and negligible scallops.

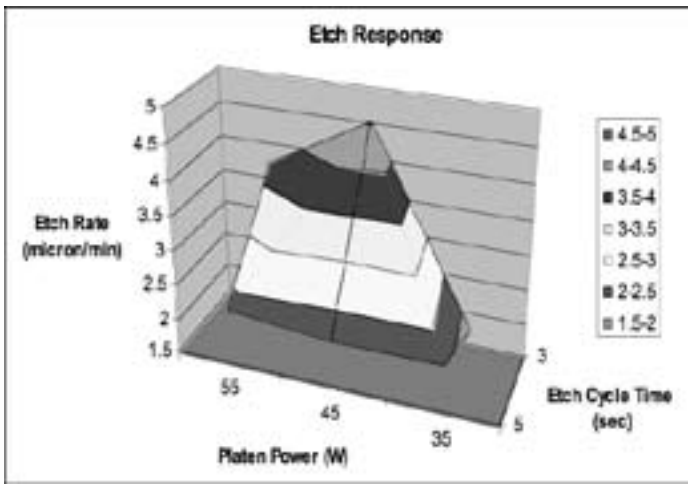

Figure 3, middle: The etch rate achieves 4.5 µm/minute.

Figure 4, bottom: The computer lights passing through the etched vias in the silicon wafer.

Fabrication of Low-Loss GaN/AlN Waveguides for Nonlinear Optics

Aydin Akyurtlu

Bradley Department of Electrical & Computer Engineering, Virginia Polytechnic Institute & State University

NNIN REU Site: Cornell NanoScale Science & Technology Facility, Cornell University
NNIN REU Principal Investigator: Dr. Farhan Rana, Department of Electrical and Computer Engineering, Cornell University
NNIN REU Mentor: Jahan Dawlaty, Department of Electrical and Computer Engineering, Cornell University
Contact: aakyur08@vt.edu, farhan.rana@cornell.edu, jd234@cornell.edu

Abstract

Nonlinear optical phenomena have well-established applications in many areas, such as optical telecommunications. Through the fabrication of low loss waveguides at micron length scales, such nonlinear phenomena can be scaled for use in integrated device applications. The purpose of this research was to fabricate gallium nitride / aluminum nitride (GaN/AlN) waveguides on sapphire substrates that demonstrate low loss and observable nonlinear effects. Because nonlinear effects require very high intensity, mode confinement becomes a very important factor. To increase mode confinement in the fabricated waveguides, a potassium hydroxide (KOH) wet etch is used to undercut the AlN base, increasing mode confinement in GaN. Waveguides were fabricated on sapphire wafers with molecular beam epitaxy (MBE)-grown GaN/AlN layers using standard photolithography and dry etching techniques yielding features ranging from 2-5 μm in width. The waveguides were tested using a femtosecond laser system.

Introduction and Background

Optoelectronic and photonic devices are a class of semiconductor devices that utilize and process light signals. One of the primary components of many of these devices is waveguides that are used to guide the light signals within the device. For device efficiency and information integrity, it is important that waveguides exhibit very low scattering losses. While the guiding properties of waveguide structures are very important to the functioning of such devices, waveguides can also be used to process optical signals through the use of nonlinear optical effects. At very high intensities, such as those provided by a laser, the polarization of the guiding medium interacts nonlinearly with the incident field in ways that are modeled using a power series representation of the electrical susceptibility with terms exceeding linear order. These nonlinearities give rise to many interesting phenomena, such as second and third harmonic generation, sum frequency generation, and Raman shifting. Nonlinear effects are already utilized in macroscale waveguiding structures such as optical fibers. Because nonlinear effects only become pronounced at high intensities, loss and mode confinement become critical properties that must be optimized.

Waveguide Fabrication

The wafers used for manufacturing were 3″ sapphire wafers with various epitaxially grown III-V layers. The two layer types used were; (1) a 500 nm AlN layer with alternating layers of GaN/AlN quantum wells and (2) a 1.4 mm bulk GaN layer on top of 100 nm bulk AlN. A thick layer of silicon dioxide (SiO_2), ~ 1 μm, was deposited on the wafer using pressure-enhanced chemical vapor deposition (PECVD) to act as a more robust mask for the III-V dry etch process. After standard photolithography using a 10x i-line stepper for exposing, the SiO_2 layer was etched using a CHF_3/O_2 dry etch chemistry in a reactive ion etcher (RIE). The III-V layers were etched using an $Ar/BCl_3/Cl_2$ RIE dry etch in an ICP etcher. The samples were finally treated with resist stripper and HF to remove the photoresist and SiO_2 masking layers. With minimal optimization, the process was found to achieve good sidewall smoothness for features ≥ 3.5 μm, but there was noticeable damage during the nitride etch process to 2 μm and 2.5 μm features. Increased sidewall smoothness and reduction in damage to small features could most likely be improved by utilizing a thicker oxide mask layer and further optimization of the III-V etch process.

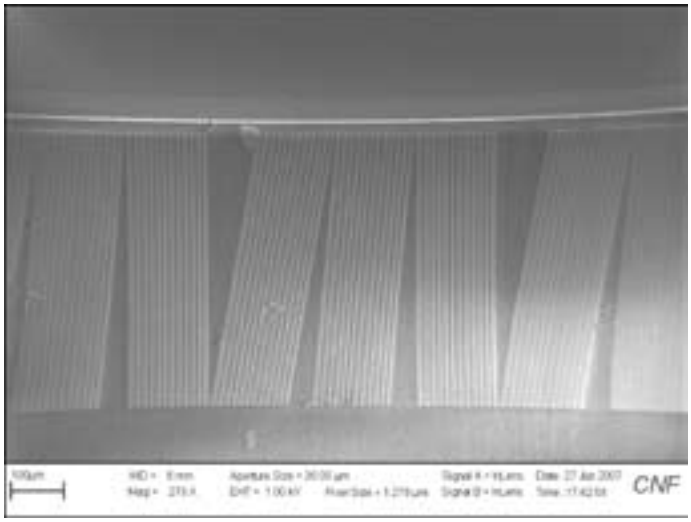

Figure 1: Row of fabricated waveguides.

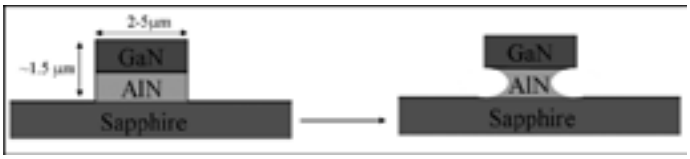

Figure 2: Diagram of KOH undercut.

KOH Undercut

In order to increase the nonlinear effects in the waveguides, an undercut in the lower AlN layer of the bulk GaN/AlN waveguides was created. The undercut would reduce the cross-sectional area of the AlN layer, which would cause the mode to be confined more strongly in the GaN layer, reducing mode volume. Previous research [1,2] had indicated that KOH solutions were capable of selectively etching AlN over other III-V compounds. Waveguides fabricated in the bulk GaN/AlN sample were treated in heated AZ400K developer for 30 minutes at 90ºC ± 5ºC. The solution selectively etched the AlN over the GaN such that a noticeable undercut was formed. A rough scanning electron microscopy (SEM) measurement showed the etch rate to be very approximately 20 nm/min.

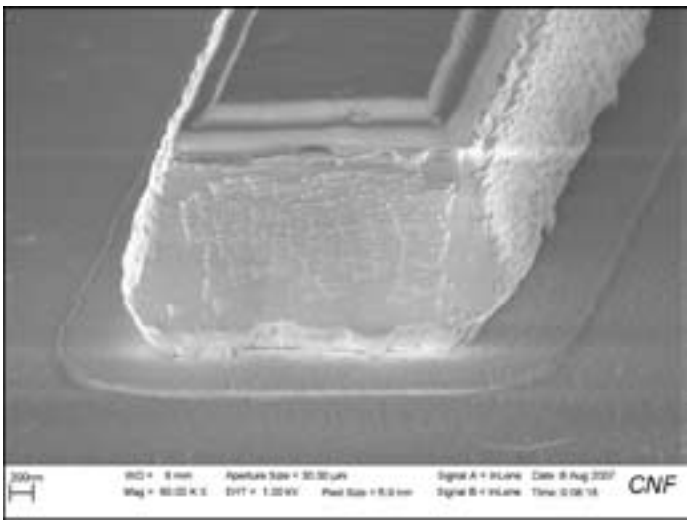

Figure 3: Profile of bulk GaN/AlN waveguide with KOH undercut.

Testing Results and Conclusions

Testing the fabricated waveguides was accomplished using a bright white light source generated by nonlinear interaction of a pulsed fiber laser with a photonic crystal fiber. The laser was coupled to the waveguide by focusing the beam through a lens and the output was observed using a CCD. Only qualitative data could be taken due to equipment and time limitations. The CCD was used to capture various mode profiles for qualitative comparison of waveguides with different material composition and fabrication processes. Comparison of mode profiles in the three tested samples is shown in Figure 4. All fabricated waveguides were shown to support guided modes, but exhibited visible scattering loss. Due to the conservative undercut and significant surface scattering at the facet, there was no concrete difference in mode confinement between the bulk GaN waveguides with and without undercutting, but the initial results show enough potential to warrant further study.

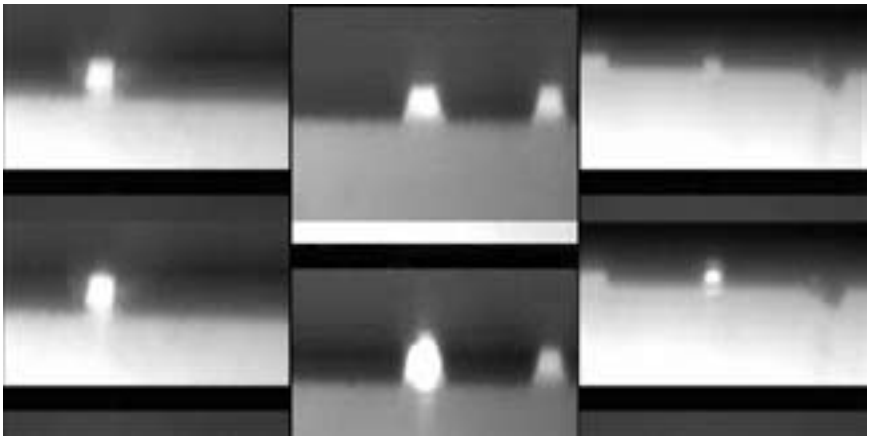

Figure 4: Guide and mode profiles. From left to right: Bulk GaN/AlN with undercut, Bulk GaN/AlN without undercut, Bulk AlN with GaN/AlN quantum wells.

Acknowledgements

I would like to thank Dr. Farhan Rana and Jahan Dawlaty, as well as everyone in the Rana Group, for their help in this project. I would like to thank the entire CNF staff for their assistance in making the technical side of my project possible. I would also like to thank Melanie-Claire Mallison, Lynn Rathbun, the NSF, and the National Nanotechnology Infrastructure Network Research Experience for Undergraduates Program for coordinating this program and giving me this opportunity.

References

[1] Mileham, J.R.; Pearton, S.J.; Abernathy, C.R.; Mackenzie, J.D.; Shul, R.J.; Kilcoyne, S.P.; "Patterning of AlN, InN, and GaN in KOH-based solutions."; Journal of Vacuum Science & Technology A: Vacuum, Surfaces, and Films; Volume 14; Issue 3, May 1996; pp. 836-839.

[2] Simeonov, D.; Feltin, E.; Buhlmann, H.-J.; Zhu, T.; Castiglia, A.; Mosca, M.; Carlin, J.-F.; Butte, R.; Grandjean, N.; "Blue lasing at room temperature in high quality factor GaN/AlN microdisks with InGaN quantum wells."; Applied Physics Letters; Issue 90 (2007).

Quantum Dot Light Emitters

Rehan Kapadia

Electrical Engineering, University of Texas at Austin

NNIN REU Site: Minnesota Nanotechnology Cluster, University of Minnesota-Twin Cities
NNIN REU Principal Investigator: Dr. Steven Campbell, Electrical Engineering, University of Minnesota-Twin Cities
NNIN REU Mentor: Gagan Aggarwal, Electrical Engineering, University of Minnesota-Twin Cities
Contact: Kapadia.rehan@gmail.com, campb001@umn.edu, aggar014@umn.edu

Abstract

Quantum confinement effects allow radiative recombination of holes and electrons in silicon nanoparticles (NP), also referred to as quantum dots (QD). This is an area of considerable interest as QDs have the potential for high efficiency, and have the ability to tune the emission wavelength with the QD size. Currently, devices use organic polymers to inject holes and electrons onto the QDs, where 1-2% radiatively recombine. Inorganic materials are generally deposited at elevated temperature. The low thermal stability of QDs result in a belief that they are incompatible with inorganics. The objective of the current approach is to demonstrate how a layer of QDs behaves when trapped between two inorganic materials. To test the photoluminescence (PL), we deposited QDs on silicon nitride and used atomic layer deposition (ALD) to grow a thin layer of hafnium oxide (HfO_2) at very low temperature. The PL was measured after deposition of QDs and HfO_2. Results show no degradation in PL intensity. For electroluminescence (EL) measurements, we used a structure of ITO-ZnO-QDs-AlN-Pt. The silicon NPs used were generated by decomposition of silane in plasma and were directly deposited onto the substrates. The devices were created by ALD deposition of zinc oxide (ZnO) on an indium tin oxide (ITO) covered glass slide and sputtering of the aluminium nitride (AlN) onto the QD-ZnO-ITO layers.

Introduction

We can exploit the quantum confinement effects in quantum dots (QDs) to cause photoluminescence (PL) and electroluminescence (EL). Current direct-gap inorganic light emitting diode (LED) technology is efficient but expensive. The organic LEDs used today have reliability problems as well as poor color depth. By using QDs as the electroluminescent element, we can tune the emission wavelength and potentially create high efficiency reliable EL devices. Presently, to conduct electrons and holes to the QDs, organic polymers are used as the electron and hole conducting layers. The use of these materials presents many of the same stability problems seen in organic light emitters. We will attempt to use inorganic materials instead.

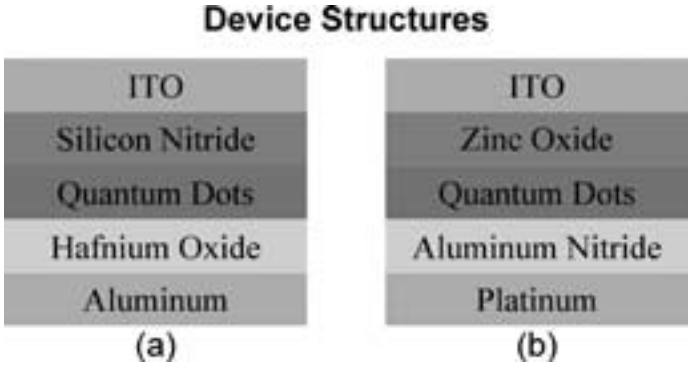

Figure 1

Experimental Procedure

The focus of this project was two-fold. First, we must determine if the intensity of the PL of QDs is reduced when sandwiched between inorganic materials. This will allow us to determine whether the quantum confinement effects or the crystalline structure of the QDs are damaged. Second, we must find if electroluminescent devices can be created using only inorganic materials.

The device to test the PL was fabricated on a glass slide that was covered with ITO. The structure, as shown in Figure 1a, was plasma enhanced chemical vapor deposition (PECVD) Si_3N_4, a layer of QDs, and ALD HfO_2. The Si_3N_4 layers were between 60Å and 90Å, grown at a rate of 75Å/min. The QDs were deposited by placing the samples in the exhaust stream of the plasma where the QDs were formed. The samples were placed in the exhaust stream for 30s, 45s, 1 min,2 min, 3 min, 4 min and 6 min. Following QD deposition, 60Å of HfO_2 were grown on the samples by ALD at 130°C using trimethyl aluminum and water. The PL was tested after both the QD deposition and the ALD.

To test the EL, the device shown in Figure 1b was fabricated. 70Å of ZnO was deposited at 250°C on the ITO covered glass slide using ALD. The QDs were deposited in a similar fashion as the first set of devices. The layer of AlN was sputtered for 1 min using an Al target and N_2 in the environment. Platinum electrodes were then sputtered on top of the AlN.

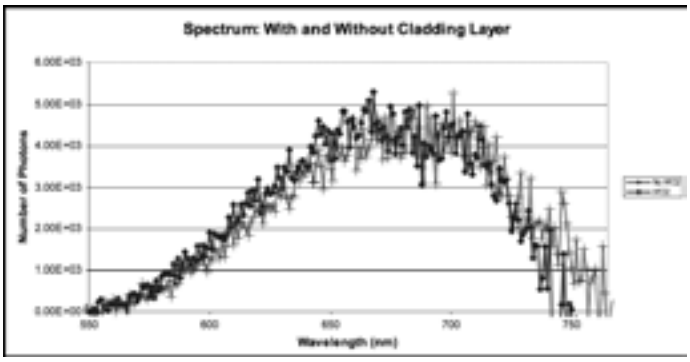

Figure 2

Results and Conclusions

The spectrums of the Si_3N_4/HfO_2 devices, shown in Figure 2, indicate that there was no noticeable change in intensity of the PL after HfO_2 deposition. The tests were run under the same conditions, so that the magnitudes of the spectrums were comparable. This indicates that the crystalline structure and the quantum confinement effects of the QDs were intact. Thus, ALD growth methods can now be used to create novel device structures.

The ZnO/AlN devices should have behaved as a diode due to the band alignment. However, the I-V curves in Figure 3 show that the behavior was ohmic. We believe there were pinholes in the thin sputtered films, causing all the current to flow through only one material and to be localized near the pinholes. This also would explain why no EL was observed. None of the current went through the QDs. When a constant voltage was applied to the devices and the devices were excited by UV light, PL was clearly visible, but the current flowing through the device did not appreciably change.

These results do not rule out the possibility that inorganic layers may be used as electron and hole transport layers. However, the films that were grown over the QD layer were only characterized using ellipsometry and profilometry on test wafers. This does not tell us what types of films were actually being grown on the QDs. Therefore, the results indicated that the structure of the devices were not as expected. Due to the extreme uniformity of ALD layers, we suspect that the pinholes were in the sputtered films, although this has yet to be proven.

Future Work

Since the quality of the films appeared to be a problem, careful study of the nucleation and growth of films on quantum dots needs to be pursued. The layer of QDs should also be characterized, as it would allow us to determine what type of surface we are depositing the materials onto. There should also be tests on control substrates so we can determine what thickness of materials are necessary to reliably gives us diode characteristics.

Acknowledgments

I would like to thank my PI, Dr. Campbell, as well as graduate students in his group: Gagan Aggarwal, Rick Liptak, and Sang Ho Song, and postdoctoral fellow, Dr. Xiaodong Pi,. I would also like to thank University of Minnesota, National Nanotechnology Infrastructure Network Research Experience for Undergraduates Program, and NSF.

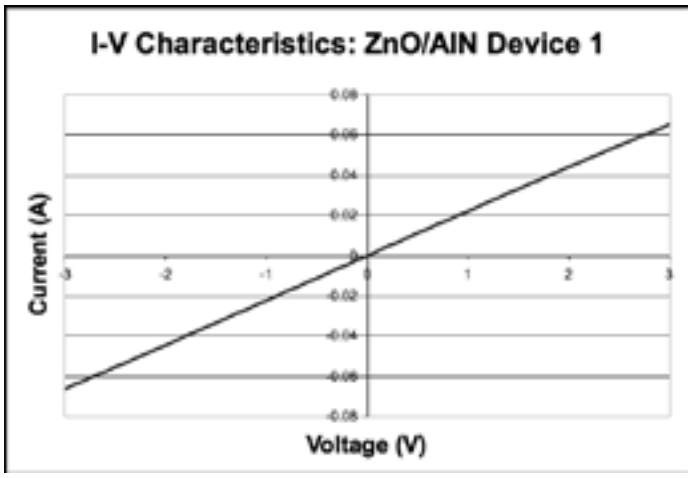

Figure 3

Characterization and Optimization Study of Silicon Evanescent Racetrack Lasers

Brian McSkimming

Electrical & Computer Engineering, University at Buffalo, State University of New York

NNIN REU Site: Nanotech—The UCSB Nanofabrication Facility, University of California, Santa Barbara
NNIN REU Principal Investigator: Dr. John Bowers, Electrical and Computer Engr., University of California, Santa Barbara
NNIN REU Mentor: Alexander Fang, Electrical and Computer Engineering, University of California, Santa Barbara
Contact: bmm6@buffalo.edu, bowers@ece.ucsb.edu, awfang@ece.ucsb.edu

Introduction

The *electrically pumped hybrid silicon evanescent laser* has been presented as a novel device which satisfies the desire to manufacture low cost, high volume silicon lasers with the goal of using photonic circuitry to replace traditional metal interconnects for board to board and chip to chip applications. The hybrid silicon evanescent device platform has already been demonstrated in the form of a photodetector, an optical amplifier and a racetrack laser [1]. The silicon evanescent laser is achieved through bonding a III-V multiple quantum well (MQW) active layer structure to a silicon waveguide. For efficient current flow to the active region, protons are implanted into the cladding layer of the III-V structure in order to prevent lateral carrier diffusion and thereby increasing the current and optical mode overlap in the quantum wells.

We report here the optimization of this proton implant profile for two laser characteristics, threshold lasing current and device capacitance, and show an improvement of both these characteristics. This technique was implemented and used in the design of the silicon evanescent laser in an attempt to maximize the injection efficiency into the MQW active layer. Injection efficiency is the fraction of injected carriers which contribute to light generation, is one factor used to characterize lasers. Another factor which can affect performance of the silicon evanescent laser is the capacitance between the n contact layer and the p contact layer.

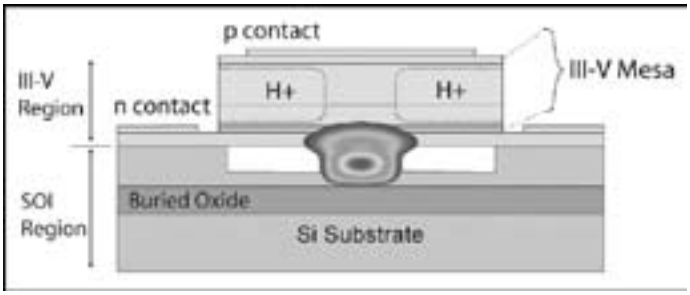

Figure 1: Cross-sectional illustration of device platform.

Device Structure/Fabrication

The silicon evanescent laser device platform consists of two separately regions bonded together. Figure 1 is an illustration of the cross-sectional view of the device. The top portion is a III-V heterostructure consisting of a n-region, multiple quantum well (MQW) active region and p-cladding region which are epitaxially grown on an indium phosphide (InP) substrate. The bottom portion is a silicon waveguide structure processed from a silicon-on-insulator (SOI) substrate. The two pieces are bonded using a low temperature O_2 plasma assisted wafer bonding technique [2]. The InP is then etched using both reactive ion etching (RIE) through the p region, and wet etching through the MQW to create a mesa ~ 10 μm wide in order to access the n layers. n and p contact pads are subsequently deposited and annealed in forming gas. The sides of the mesa are implanted with protons of varying energies in order to allow for efficient current flow as well as preventing lateral current diffusion. Detailed descriptions of the fabrication process of the hybrid silicon evanescent laser can be found in [3].

An illustration of the silicon evanescent racetrack laser device topography is shown in Figure 2. It consists of a racetrack resonator, two integrated photodetectors, and a directional coupler, which couples light from the resonator and directs it towards the photodetectors.

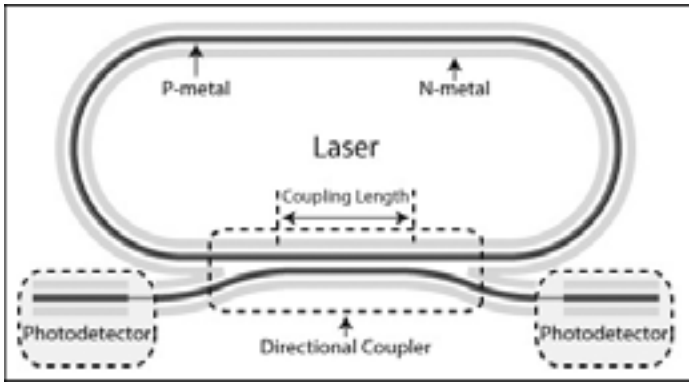

Figure 2: Illustration of silicon evanescent racetrack laser.

Experimental Procedure

This experiment used two different proton implantation profiles, the first being the standard baseline implantation profile as shown. The second implantation profile increased the depth of the protons to correspond to the top of the MQW active region while increasing the height of the protons implanted to correspond to the top of the mesa. By increasing the depth of the implantation to the top of the MQW active region, we intended to improve the injection efficiency into the active region directly above the silicon waveguide. Bringing the implantation profile to the top of the mesa is intended to reduce the capacitance between the p and n layers by decreasing the available area which is behaving as a parallel plate capacitor, in particular the highly doped P-InGaAs contact layer.

During testing, the laser was driven from 0-500 mA in 25 mA increments through the top p-contact. The photodetectors were reverse biased at -5V, and the current across them is measured as the driving current is increased. In order to determine the effect which the deeper proton implant profile has on the injection efficiency, we compared devices implanted with the two different profiles based upon their lasing threshold current. The capacitances of the devices were measured directly.

Results and Conclusions

Eight devices from each profile were tested and analyzed. Using the L-I (Power vs. Current) curve taken from the silicon evanescent racetrack lasers, the lasing threshold current can be determined experimentally. As a result of increasing the proton implant depth the lasing threshold current decreased. Devices 2-4, with a directional coupler length of 100 μm, demonstrated a 17.31% improvement in the average threshold current for proton implant profile 2 over profile 1. As can be seen in Figure 3, the average threshold current for devices 2-4 improved from ~ 192 mA, for proton implant profile 1 to ~ 158 mA for proton implant profile 2. Devices 6-10, with a directional coupler length of 300 μm, demonstrated a 4.71% improvement in the average threshold current for proton implant profile 2 over profile 1. The average threshold current for devices 6-10 improved from ~ 175 mA, for proton implant profile 1, to ~ 167 mA for proton implant profile 2. This decrease in the threshold current for these devices demonstrates that the injection efficiency was in fact improved by increasing the depth of the proton implant profile.

As can be seen in Figure 4, the capacitance decreased from an average of ~ 4.6 pF to ~ 3.6 pF with the increase in proton implant height. Overall there was a 21.4% decrease in the capacitances measured for the devices.

Acknowledgements

Thanks to Alex, Dr John Bowers and his group, Intel, and all the supporters of the Bowers Lab. Special thanks to the National Nanotechnology Infrastructure Network Research Experience for Undergraduates Program for this opportunity and to the NSF for funding.

References

[1] A. W. Fang, et al., "Hybrid Si evanescent devices" Materials Today 10, 7-8, (2007).

[2] D. Pasquariello, et al. "Plasma-Assisted InP-to-Si Low Temperature Wafer Bonding," IEEE J. Sel. Top. Quantum Electron. 8, 118, (2002).

[3] A. W. Fang. et al., "Electrically pumped hybrid AlGaInAs-silicon evanescent laser," Opt. Express 14, 9203-9210 (2006).

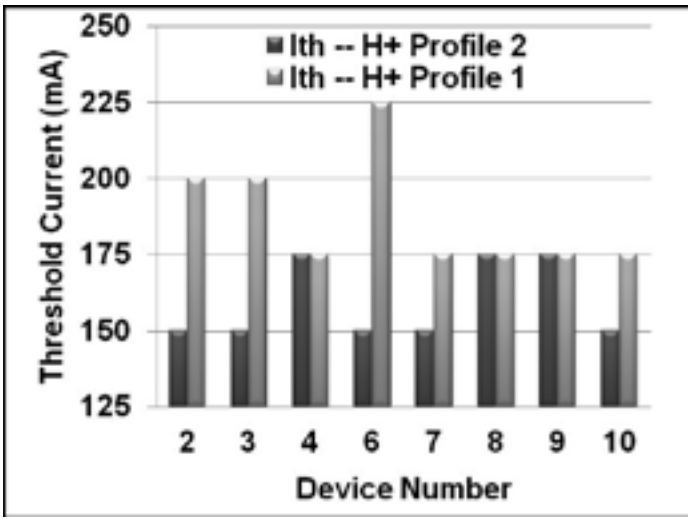

Figure 3: Threshold current comparison between proton implant profiles.

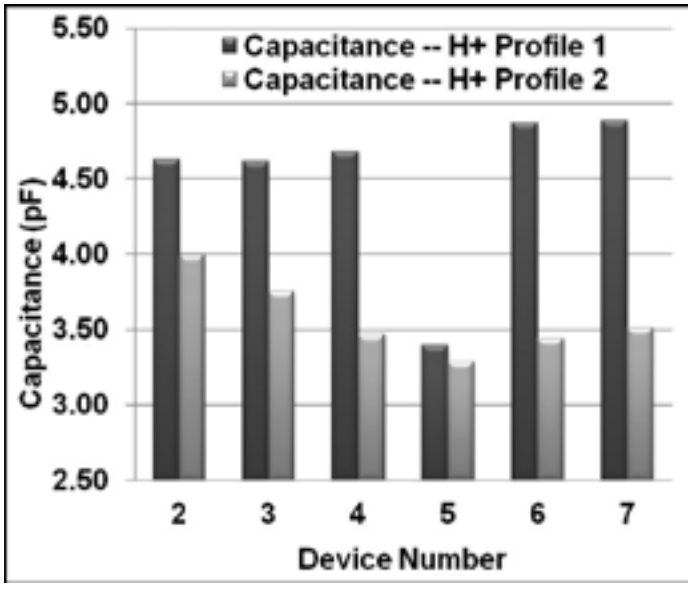

Figure 4: Capacitance comparison between proton implant profiles.

Observation of Harmonics in a Uni-Directional Mode-Locked Fiber Laser Incorporating a Carbon Nanotube Saturable Absorber

Zachary Nishino

Physical Science, St. John's University

NNIN REU Site: Nanoscience at the University of New Mexico
NNIN REU Principal Investigator: Ravi Jain, Electrical & Computer Engineering/Physics, University of New Mexico
NNIN REU Mentor: Li Wang, Electrical & Computer Engineering; Alex Braga, Physics & Astronomy; University of New Mexico
Contact: zachary.nishino06@stjohns.edu, ravijain@unm.edu, liwang@unm.edu

Abstract

The relationship between peak power, pump power, pulse width, spectral width, and repetition frequency with respect to the various harmonics was studied in a uni-directional mode-locked fiber laser incorporating a carbon nanotube saturable absorber. The saturable absorber, which was designed to work at 1550 nm, was composed of 0.8-nm-diameter carbon nanotubes. This laser produced a fundamental frequency of 11.23 MHz, of which the harmonics were multiples. By varying the pump power, an increasing linear relationship developed between repetition frequency and harmonic. We also observed a decreasing linear relationship between spectral width and peak power with the harmonic.

Introduction

Carbon nanotubes exhibit many interesting physical, electrical, thermal, and optical properties. Recently, an interest in their optical properties has made them the point of interest for mode-locked lasers. Due to their fast recovery times, nonlinear absorption of light intensity, and relatively easy fabrication, these nanosized carbon tubes make for a suitable saturable absorber in fiber lasers [1-3]. Coupled with harmonic mode locking, the equal spacing of pulses within the laser cavity, these lasers can be used in optical communication systems for ultra fast data transfer [4-6]. In this experiment, we studied the characteristics of harmonics in a passively mode-locked fiber laser with a carbon nanotube saturable absorber (CNSA).

Experimental Procedure

A uni-directional ring laser cavity was designed with components and measurements as labeled in Figure 1. A fiber pigtailed 980 nm diode (capable of > 100 mW output) was used to pump the 4 meter long erbium doped fiber (EDF). An isolator (> 30 dB isolation) was put in the cavity to ensure uni-directional lasing. A 15 meter long standard single mode fiber was used to compensate the dispersion. The laser was coupled out the cavity through an 88/12 coupler. The carbon nanotube saturable absorber was provided from SouthWest Nanotechnologies and consisted of 0.8-nm-diameter carbon nanotubes. Through the laser output, we utilized a spectrum analyzer to measure the spectrum and spectral width. A digital oscilloscope was used to measure the repetition frequency and to estimate the peak power.

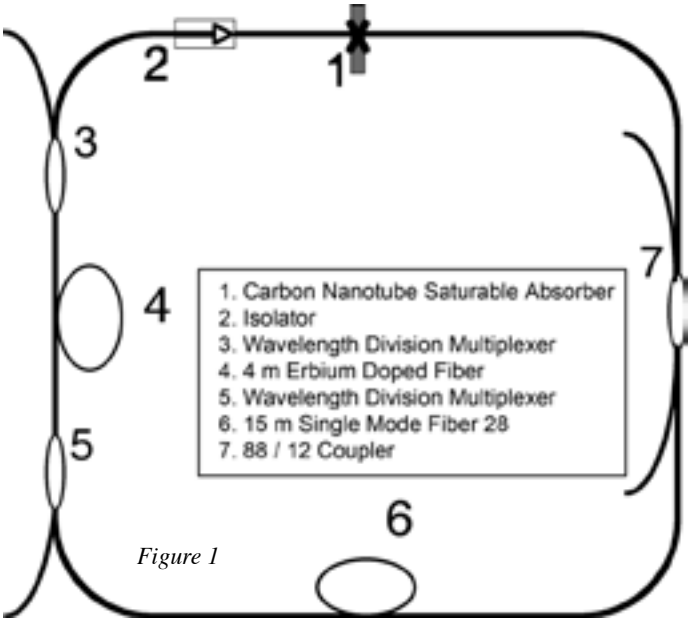

Figure 1

Results

This mode-locked laser operated at a fundamental frequency of 11.23 MHz, of which the harmonics were multiples. Depending on the pump power, the laser operated at different harmonics (up to 14th), see Figure 2. It is almost a linear relationship between the pump power and order of harmonics.

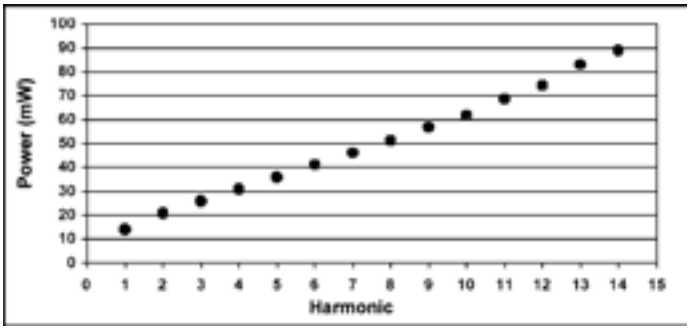

Figure 2

This is the first time that such stable and controllable harmonics have been observed in experiments in such fiber lasers.

To verify that pulses from our laser were from the mode-locked operation instead of another mechanism, like oscillation relaxation or Q-switching, pulse width measurement of the laser was attempted. Although we were not able to determine the actual pulse width from an auto-correlation measurement, we did use the spectrum analyzer to have a preliminary study of the pulse width. The 3-dB widths of the spectra were about 15-16 nm (see Figure 3), depending on the order of harmonics at which the laser was operating.

Directly from $\Delta \nu \times \Delta t \approx 1$ and $\Delta\nu/\nu = \Delta\lambda/\lambda$, it was easy to estimate the pulse width was on the order of 500 fs, which was much smaller than expected for oscillation relaxation or Q-switching. From Figure 3, it was also observed that the overall spectral width decreased (implying the pulse width increased) with increasing harmonics, which has also been observed by other researchers.

Finally, peak powers at different harmonics were measured (see Figure 4). The majority of the data followed a trend of declining as the harmonic increased, which has also been observed by other researchers. However a small section of data developed a trend of slightly increasing as the harmonic increased. This was more than likely due to a change in the digital oscilloscope's settings while the data was being taken.

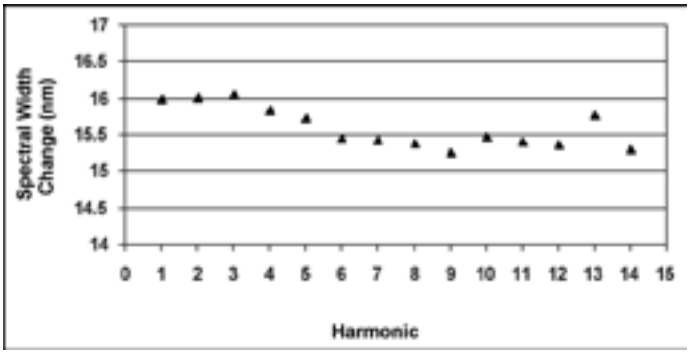

Figure 3

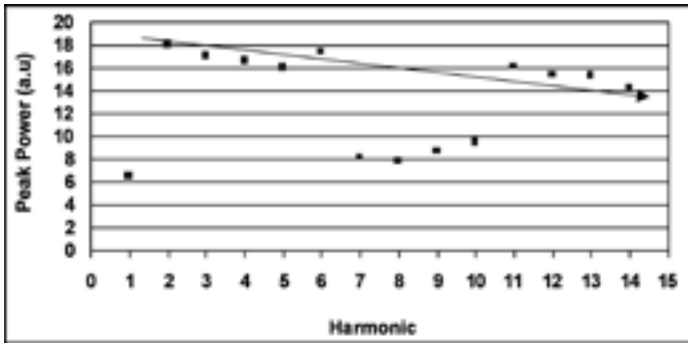

Figure 4

Conclusion

We have demonstrated harmonic mode-locking in a fiber laser incorporating carbon nanotubes. For the first time, it has been demonstrated that reliable harmonics can be tuned by changing the pump power of the laser. Spectral width has been measured to estimate the actual pulse width of the laser.

Acknowledgements

I would like to thank the National Nanotechnology Infrastructure Network Research Experience for Undergraduates and the National Science Foundation for this opportunity. I would like to thank my professor R. K. Jain, my mentors Li Wang and Alex Braga. I would like to make special mention of Jeff Nicholson for his help.

References

[1] L. Vivien, D. Riehl, and P. Lancon et al. Optics Lett. 26, 223 (2001).

[2] Sze Y. Set, Hiroshi Yaguchi, Yuichi Tanaka, and Mark Jablonski, J. Lightwave Technology 22, 51 (2004).

[3] J. W. Nicholson, "Optically assisted deposition of carbon nanotube saturable absorbers." OFS Laboratories (2006).

[4] A. N. Pilipetskii, E. A. Golovchenko, and C. R. Menyuk, Optics Lett. 20, 907 (1995).

[5] A. B. Grudinin and S. Gray, J. Opt. Soc. Am. B 14, 144 (1997).

[6] Bülend Ortaç, Ammar Hideur, and Marc Brunel, Optics Lett. 29 (2004).

On-Chip Microfluidic Integration of Ultra-High Quality Silicon Optical Microdisk Resonators for Lab-On-Chip Applications

William J. Roman

Biomedical and Electrical Engineering, University of Rhode Island

NNIN REU Site: Microelectronics Research Laboratory, Georgia Institute of Technology
NNIN REU Principal Investigator: Dr. Ali Adibi, Electrical and Computer Engineering, Georgia Institute of Technology
NNIN REU Mentor: Dr. Siva Yegnanarayanan, School of Electrical and Computer Engineering, Georgia Institute of Technology
Contact: roman.will@gmail.com, ali.adibi@ece.gatech.edu, sivay@ece.gatech.edu

Abstract

Silicon on insulator (SOI) technology platform enables the dense monolithic integration of planar nanophotonic optical components and electronic devices. Applying SOI technology to optical sensing, lab-on-chip applications can be envisioned that test for virtually any biomolecule. This project focuses on the design, fabrication, and testing of polydimethylsiloxane (PDMS) channels filled with varying refractive index oils that induce a shift in the resonance wavelength of ultra-high quality (Q) planar microresonators fabricated on SOI substrate, in order to create an effective biosensor. Detection of specific chemical and biological molecules through suitable selective surface coatings on such resonators allows for the rapid, inexpensive production of label-free sensor architectures for lab-on-chip systems [1].

Introduction

SOI substrates offer ultra-compact, ultra-high Q nanophotonic components that are completely compatible with silicon (Si) VLSI technology. Monolithic optical resonators in such SOI substrates, offer the further advantage of micron-scale size, and through suitable designs of the waveguide-cavity coupling, a complete 100% transmission of energy from the waveguide to the cavity is possible. Any molecule present over the resonator is sensed through the resonance wavelength shift induced by the refractive index of the molecule. Successful detection of indices leads to the development of an ultra-compact label-free biosensor.

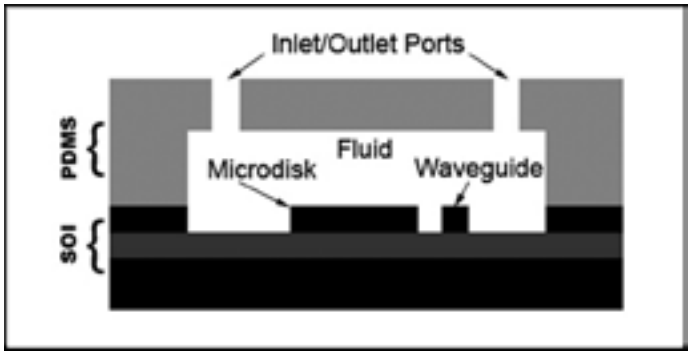

Figure 1: Resonator integrated with microfluidic channel. (Resonator radius: 20 µm, height: 230 nm.)

Experimental Procedure

SOI resonator chips were developed with several add-drop and single disk and ring resonators on each chip for comparison and finding optimal wavelength shifts. PDMS (Sylgard 184) fluidic channels with punched inlet and outlet ports were activated with O_2 plasma and aligned under a microscope to cover the resonators, ensuring index changes (Figure 1). Refractive index oils (Cargille Laboratories) ranging from index 1.32 through 1.395 were individually injected into the channel through a 23-gage polyethylene tubing (Intramedic Clay Adams) using syringes (Norm-Ject 5mL). Each micro-resonator covered with oil from the channel was evaluated for performance using a swept-wavelength test setup that recorded the resonances over a given group of wavelengths. The setup consisted of a tunable laser (Agilent Technologies Model 81680A, line width 100 kHz) for the wavelength sweep, a standard objective lens (Newport M-40x, 0.65NA) for input/output coupling to the device, followed by a photoreceiver (Thorlabs PDB 150C) that was interfaced to a personal computer through a data acquisition (DAQ) card (National Instrument PCI-6251, 16-Bit, 1 MS/s). All light coupled to the resonators used TE-polarized light (Figure 2).

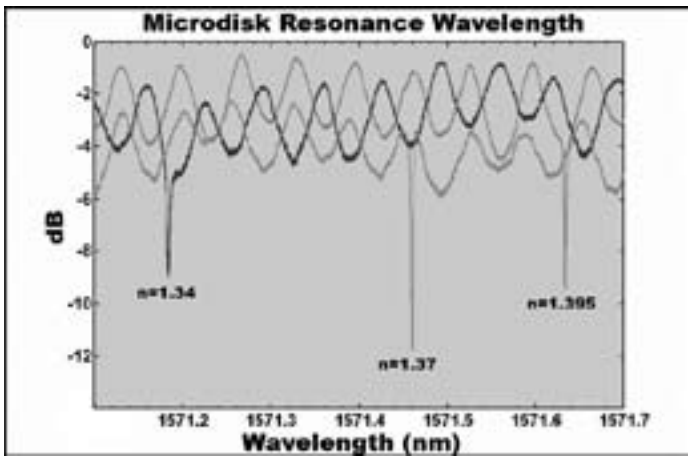

Figure 2: Microdisk spectral response.

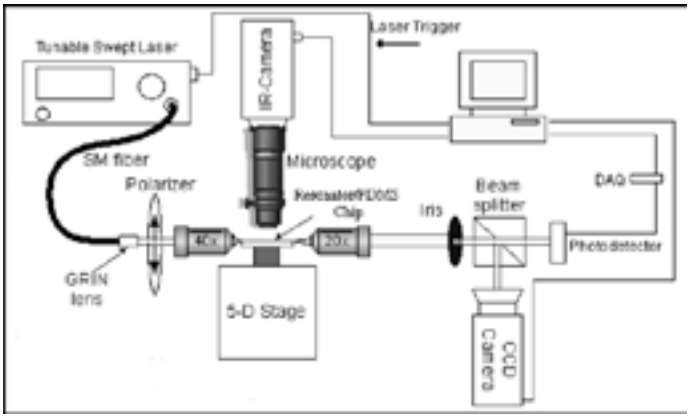

Figure 3: Test setup.

Initial tests of microdisk resonators yielded promising results with high quality factors ($Q > 10^6$; $Q = \lambda/\Delta\lambda$) and noticeable shifts between indices (Figure 3). Microrings, however, yielded greater shifts and were pursued in further tests due to the ease of detecting the index changes (Figure 4).

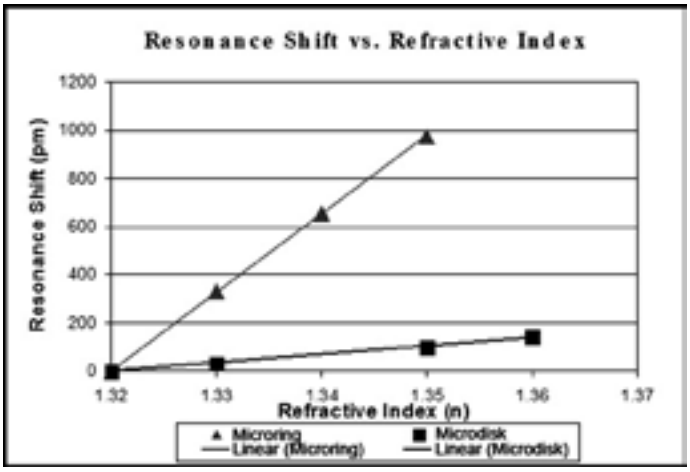

Figure 4: Resonator performance.

Some leaking was observed to come from the bottom of the channel, indicating a poor seal that resulted in a progressive difficulty in coupling the waveguides to the laser to begin the experiment. The imperfect seal resulted in a new channel designs with larger contact areas between the PDMS and Si. After new channel fabrication, real-time data acquisition methods were explored to simulate real-time detection. It was found that by applying a weight to an inverted syringe in a test tube rack (Lake Charles Manufacturing), gravity provided a linear flow rate in the range of 1 μL/s, suitable for further experimentation and easy index switching.

To rapidly identify indices in real-time, the DAQ program was revised to sweep 10 nm, thereby covering the free-spectral range of the resonator and hence capturing two resonances. Real-time detection resulted in 350 pm shifts between 0.01 index changes. Repeated measurements revealed that resonance wavelengths were consistent to within 1 pm, for the same index oil under flow conditions. However, it was observed during the real-time tests that the introduction of fluid flow, through applied pressure on the syringe, caused the resonance wavelengths to shift higher by up to 10 pm, when compared to the no-flow condition.

In order to understand this effect, we developed a complete model for the flow-channel under the external applied pressure. Initial results from this model indicate that the fluid pressure induced change in the oil index accounted for the shift. More detailed modeling of this effect is under further investigation.

Results and Conclusions

Early channels demonstrated the detection of a linear relationship between refractive index changes and resonance wavelengths over a given wavelength interval regardless of their type. Experimentation with ring resonators was pursued because their display of large shifts would provide for small index change identification. The second generation of channels allowed the development of a method of obtaining real time data. Given the high quality factors (10^6) observed from the resonators and that subsequent readings varied by less than 1 pm, index sensitivity was 2.85×10^{-5} for this device. With optimized device, wavelength shift of nanometers and detection on a picometer scale will be achievable for true lab-on-chip applications.

Future Work

At the time of this paper, microring resonators attached to micospectrometers are being fabricated for real-time lab-on-chip analysis function. Surface functionalization with biotin for testing with the highly specific protein Streptavidin in real-time is also being pursued for a biological approach. Future plans include multiple protein detection on the same chip as well as chemical sensing.

Acknowledgements

I would like to express my appreciation to the NSF, National Nanotechnology Infrastructure Network Research Experience for Undergraduates Program, and the Georgia Institute of Technology for their funding and facilities. A special thanks to site coordinator Jennifer Tatham Root for a productive research environment. I would also like to express my gratitude to Dr. Ali Adibi and Dr. Siva Yegnanarayanan for inclusion in their research and to the MSMA Group and Photonics Research Group for their guidance.

References

[1] De Vos, Katrien et alia, "Silicon-on-Insulator microring resonator for sensitive and label-free biosensing," Opt. Express 15. 7610-7615 (2007).

Development of Optical Fiber Packaging for Planar Lightwave Circuits by Microfabrication

Kylan Szeto

Physics, Rensselaer Polytechnic Institute

NNIN REU Site: Cornell NanoScale Science & Technology Facility, Cornell University
NNIN REU Principal Investigator: Prof. Michal Lipson, Electrical and Computer Engineering, Cornell University
NNIN REU Mentor: Dr. Carl Poitras, Electrical and Computer Engineering, Cornell University
Contact: szetok@rpi.edu, ml292@cornell.edu, cbp8@cornell.edu

Abstract/Introduction

Testing integrated sub-micrometer light guiding structures typically involves precisely nanopositioning tapered lens fibers to couple light into nanotapered waveguides [1]. This is done through optimization using piezoelectric stages and optical microscopes. While this method works well in a research environment, this time consuming and expensive process remains slow and impractical for packaging and makes it difficult to test waveguiding chips with multiple devices. More importantly, it makes it impractical for industry. This project proposes a solution by defining and etching trenches into the substrate in front of waveguides, in which inexpensive cleaved optical fibers are easily aligned and fixed in place with UV curable index matching epoxy. Cleaved fibers have a mode field diameter of about 8 μm, greatly reducing misalignment errors with sub-micrometer waveguides. This method involves etching trenches into silicon dioxide (SiO_2) and Si so that cleaved fibers can be easily aligned with the waveguides. The final phase of testing will measure the optical efficiency of light coupling into the chip's devices. This process is easily reproducible and offers a solution for mass production of integrated optical circuits.

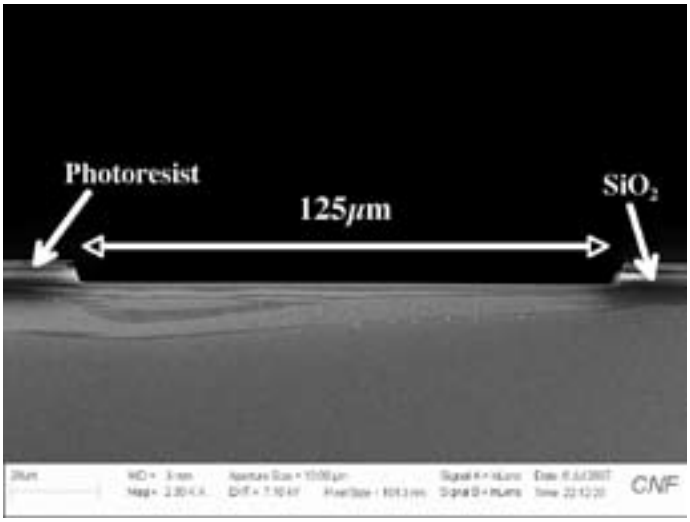

Figure. 1: Oxide etch down to silicon substrate.

Experimental Procedure

The first phase of this project involved designing 125 μm wide trench patterns to match the diameter of single mode SMF-28 optical fibers. A mask was created using the GCA/Mann 3600F optical pattern generator and used to characterize and define fabrication protocols on test Si wafers with a 3 μm thick layer of thermally grown SiO_2. By analyzing etch rates and selectivities of the Oxford 100 and Unaxis 770 etchers to SPR 220 photoresist, we decided to spin SPR 220-3.0 to a thickness of 3.3 μm. Characterization of the exposure dose for this thickness on the EV 620 contact aligner was best for 3 seconds using a 90 second MIF 300 development.

After photolithography, our wafer was subjected to a 20 second descum in the Glenn 1000 oxygen asher, and underwent 3 μm of oxide etching in the Oxford 100 using the CHF_3/O_2 recipe for 35 minutes. This etch had to be characterized in order to determine how the trench profiles matched the desired dimension, as shown in Figure 1. Throughout fabrication, the depth of our trenches and etch rates were monitored using the F50 Filmetrics optical film measurement tool and the Tencor P10 profilometer.

Next we characterized the silicon etch with the Unaxis 770. This required 120 loops to remove the 59.5 μm of Si, as shown in Figure 2.

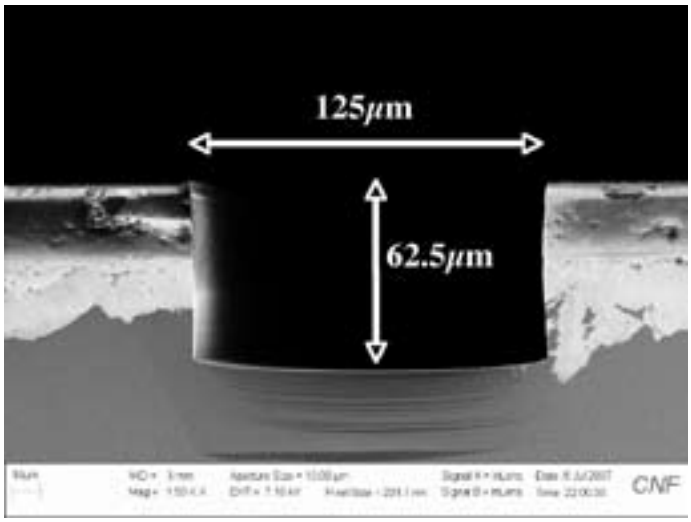

Figure 2: Deep etch into silicon substrate.

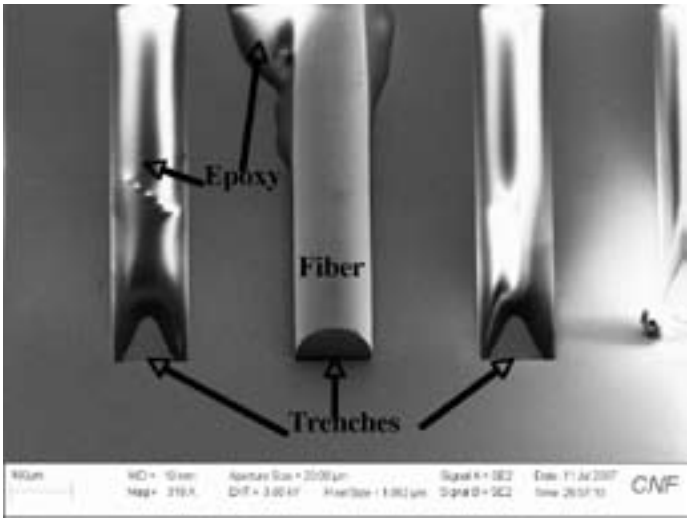

Figure 3: Dropped fiber held in place by epoxy.

The last steps were a hot resist strip and a 10 minute descum in the Glenn 1000. The wafer was then cleaved into individual chips, and a chip was mounted on a 3 axis rotation stage. Cleaved optical fibers were positioned using a 3 axis linear stage. Using this simple set up with an optical microscope we aligned and dropped fibers into the trenches. Finally, we glued them into place using UV curable index matching epoxy.

After mounting several fibers, we took scanning electron microscopy (SEM) images to characterize the position of the fibers (see Figure 3), and corrected our computer-aided design (CAD) to account for improper trench dimensions. We determined that 127 μm wide trenches with sacrificial trenches (epoxy drains) in between active sites were appropriate.

Our final step was to test these protocols on an SOI chip with waveguides, ring and disk resonators. After patterning the waveguides by e-beam lithography on an SOI sample, the devices were etched using the PT 770 and cladded with 2.8 μm of SiO_2 (GSI PECVD tool). We then spun 3.8 μm of resist onto our chip to account for the removal of the additional SiO_2 cladding, exposed our trench pattern using the ABM mask aligner for 9 seconds (used to expose small samples), and carried out the rest of the etch protocols as described above. We determined that the etch rates on both the Oxford 100 and the Unaxis 770 were much slower for small samples, but that the selectivities remained unchanged.

Results and Conclusions

The positioning of fibers into our functionalized chip was good, and the epoxy drains worked well; but this step was still sensitive to the epoxy drop size and placement. Also, trench and waveguide alignment was not accurate due to deterioration of alignment marks during e-beam lithography, forcing us to align the mask by eye (this problem can be easily resolved by adjusting the exposure doses of the alignment marks). After fixing fibers onto both ends of the chip, we used a broadband amplified spontaneous emission light source and an Optical Spectrum Analyzer to test the devices. The best output graph is shown in Figure 4. This plot illustrates the resonant frequencies from the associated 8 μm ring resonator. This plot is also evidence that dropping optical fibers into pre-aligned trenches can be used to achieve good transmission, showing that this method is applicable for testing devices.

Future Work

Continued work should be put into perfecting the epoxy step to prevent defunctionalizing adjacent waveguides, or the need to space them far apart. Alternatively, further research into the use of multi-fiber systems such as ribbon fiber could prove beneficial. The ability to pre-space waveguides, drop, and epoxy many fibers simultaneously would greatly add to the efficiency of the drop-fiber method.

Acknowledgments

I would like to thank Professor Michal Lipson for the research opportunity in her lab, and Dr. Carl Poitras for providing me with the knowledge, and encouragement to complete my project. I'd also like to thank the Cornell Nanophotonics Reseach Group for all of their help. Special thanks to Ms. Melanie-Claire Mallison and Dr. Lynn Rathbun for making my experience the best it could be. Finally I'd like to thank the National Nanotechnology Infrastructure Network Research Experience for Undergraduates Program and the National Science Foundation for their funding.

References

[1] Almeida, V; Panepucci, R; Lipson, M; "Nanotaper for Compact Mode Conversion"; Optics Letters, Vol. 28 No. 15, pages 1301-1304, August 1, 2003.

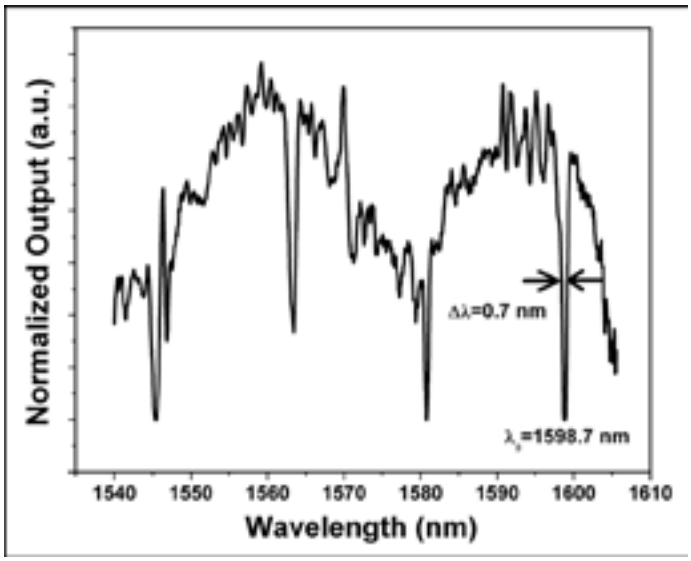

Figure 4: Power output graph from coupling tests.

Modeling the Resolution for Photoacoustic Bio-Microscopy in the Giga-Hertz Frequency Range

Chukwunomso Agunwamba

Mathematics and Physics, Worcester Polytechnic Institute

NNIN REU Site: Center for Nanoscale Systems, Harvard University

NNIN REU Principal Investigator: Shriram Ramanathan, School of Engineering and Applied Sciences, Harvard University

Contact: nomnso@wpi.edu, shriram@seas.harvard.edu

Abstract

Photoacoustic (PA) methods promise higher image resolution with an increase in the acoustic wave's frequency. However, they are effectively limited by the wave's penetration depth as the frequency enters the gigahertz range [1,2]. In this project, we explored the relationship between depth, initial center frequency, and amplitude for the acoustic pulse. First, arrangements of transducers and metallic particles were specified for the PA microscope. For the setup, a discrete time model was used to show how to obtain an image, to develop relations both for the resolution. This model was simulated in MATLAB®.

Introduction

Previously, in a paper [3] by Daniel Wulin and Shriram Ramanathan, curves relating the center acoustic frequency for metallic and silica particles to their radii were generated and discussed. For a fluid, they also showed how the initial center frequency of a Gaussian acoustic pulse is downshifted as a function of depth traveled. This project proposes several transducer and metallic particle arrangements for a PA bio-microscope. It can be useful for non-invasive examination of the structure of biological media and molecules (such as fat) and individual cells or tissues. It uses acoustic waves generated from the elastic response of nano-sized metallic particles to a laser pulse train. The lateral and axial resolutions from the resulting image are modeled in terms of the maximum center frequency allowed by selected biological media and the acoustic pulse's bandwidth.

Theory

The acoustic pulse, *h(m)*, would pass through a sequence of interfaces while experiencing reflections represented as r_k, transmission represented as $(1\text{-}r_k)$, and attenuation between interfaces represented as $\alpha(\omega l)$. The absorption coefficient is a function of the center frequency. Its expression depends on the medium. In the MHz range, this curve has been determined for several biological media. For example, attenuation coefficient for water is known to have an f^2 relationship with frequency in the MHz range [4]. It is assumed that the signal containing reflected-acoustic pulses and the signal containing emitted-acoustic pulses are spatially and temporally sampled once they are received.

The signal coming from the imaged sample is a superposition of scaled and delayed pulses that have the same profile as the original emitted pulse. It is assumed that there is weak temporal dispersion of the composite acoustic pulse formed by the superposition of several center frequencies, ω_l. The de-convolved spectrum is, therefore, a linear combination of scaled and delayed sinusoidal functions in the frequency domain. $S(\omega)$ is the impulse response of the transducer, while $H(\omega,\omega_l)$ is the spectrum of Gaussian acoustic pulse with a center frequency of ω_l. The spectrum, $X(\omega,\omega_l)$, contains the information about attenuation, reflection, and the time delay for each echo pulse in the signal.

The axial resolution [5,6] is treated as being quite independent of the center frequency. The stress and thermal confinements of the laser pulse temporal width is given by t_s and t_{th} [7]. This, in turn, limits the temporal width of the acoustic pulse it modulates. V_o is the velocity of the acoustic pulse in the medium housing the metallic particles and the transducers. V_j is in the space after the *jth* interface. To calculate depth, the velocity of the acoustic pulse is assumed constant within the imaged medium, only depending on the center frequency. It is also assumed that the medium housing the metallic particles and the transducers has an impedance matching the imaged sample.

The lateral resolution is obtained using the diameter of the transducer, d_t, its focal length, the maximum center frequency, $\omega_{l_{att}}$. The frequency, $\omega_{l_{att}}$, is the highest frequency with the minimum detectable intensity in the signal.

$$Y(\omega) = S(\omega)\sum_{j} X(\omega,\omega_j)H(\omega,\omega_j),\ X(\omega) = \sum_{k=0}^{J} C_k^2(\omega_j)\,e^{-\alpha(k,\omega_j)\omega}$$

$$H(\omega,\omega_j) = \left(\frac{1}{\sigma_j\sqrt{2\pi}}\right)\left[e^{-\left|\omega-\omega_j\right|^2/\left(2\sigma_j^2\right)}\right]$$

$$C_k^2(\omega_j) = C_{k-1}^2(\omega_j)\left[e^{-\left(\alpha(\omega_j)-\alpha(\omega_j)\right)\Delta z_k(\omega_j)}\right]\left[(1-r_{k-1}^2)^2\right](r_k)^2(r_{k-1})^2$$

Here, $\omega = 2\pi\frac{k}{F_s}$, k = frequency in Hz, and F_s is the sampling frequency in Hz satisfying the Nyquist rate.

$$\text{Single Transducer Axial resolution} = R_A = \frac{V_o}{2*FWHM\left(\left|S(\omega)\sum_j H(\omega,\omega_j)X(\omega,\omega_j)\right|\right)} + t_{sh} = \min\left(t_s, t_{th}\right)$$

Here, the initial acoustic pulse temporal width $= t_{sh} = \min\left(t_s, t_{th}\right)$

Highest center frequency detected at the transducer after being attenuated by the medium $= \omega_{l_{att}}$

$$\text{Lateral resolution} = R_L = \frac{\lambda_0 * \text{focal length}}{d_t} = \frac{2\pi V_o * \text{focal length}}{\omega_{l_{att}} * d_t}$$

The depth profile is resolved with time, under the assumption of a linear relationship between reflection depth and 'time-of-flight'. Here, the time-of-flight is the time for the wave to travel from the metallic particle(s) to an interface in the sample and to a receiving transducer. The assumption of a linear relationship implies that the wave maintains a constant velocity within each sub-medium of fixed characteristic impedance. The velocity only changes to a new value when the wave enters a region having a different characteristic impedance.

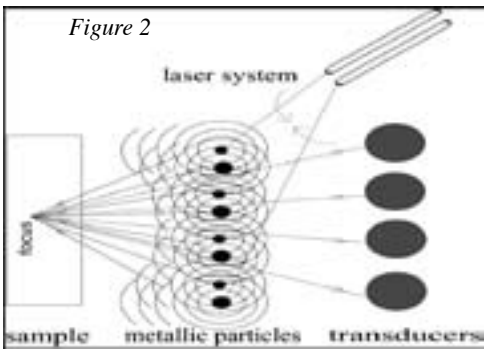

Figure 2

Design

In Figure 2, a single laser beam excited a metallic particle or a cluster of metallic particles. (The black and the blue arrows trace the path of the rays to the transducer.) To direct and focus the beam, the light, from two lasers, swept in the directions indicated by the green arrows. The sweeping can also be done by one laser and a beam splitter. The sweeping action caused a relative time delay and a sequential excitation of the metallic particles. A curved wave front was created, according to Huygens's principle. This idea was adapted from a description in a paper by P. N. T. Wells [8]. There, he describes how the sequential excitation of elements in a transducer array focuses and directs the acoustic wave beam. The difference is that a laser system and metallic particles are used in generating the acoustic wave in this paper.

The pulse-echo method relied on waves that are reflected at interfaces with mismatched acoustic impedances (See Figures 3 and 4). At any such interface, a fraction of the wave was transmitted into the new medium while the other portion was reflected. Each transducer element recorded the amplitude of the acoustic wave that passed by its position.

Conclusion

A discrete pulse-echo model was developed and simulated in MATLAB to explore how the combination of high acoustic frequency, with the transducer setup, density of metallic particles, and choice of center frequencies, can make possible very fine resolutions in the range between micrometer and nanometer scales. Some follow up studies include: modeling how the nanoparticles control and shape the wave fronts in time and space, studying different materials and fluids for housing the nano-particles and the transducer, and making measurements of the attenuation coefficient of biological media in the giga-hertz range.

Acknowledgments

The author acknowledges funding from the NNIN Research Experience for Undergraduates Program through Harvard University for this part of the research.

References

[1] "Photoacoustic imaging in biomedicine" by M. Xu, and L.V. Wang, Rev. Sci. Instrum. 77, 041101 (2006).

[2] "Acoustic Microscopy: Biomedical Applications" by Ross A. Lemons, and Calvin F. Quate, Science, New Series, Vol. 188, No. 4191. (May 30, 1975), pp. 905-911.

[3] "Non-invasive high-resolution acoustic microscopy technique using embedded nanostructures" by Daniel Wulin, and Shriram Ramanathan, Mater. Res. Soc. Symp. Proc. (2007).

[4] "Ultrasonic imaging of the human body" by P N T Wells, Rep. Prog. Phys. 62 (1999) 671-722.

[5] "Advances In Ultrasound Biomicroscopy" by F. Stuart Foster, Charles J. Pavlin, Kasia A. Harasiewicz, Donald A. Christopher, and Daniel H. Turnbull, Ultrasound in Med. & Biol., Vol. 26, No. 1, pp. 1-27, 2000.

[6] "Analytic explanation of spatial resolution related to bandwidth and detector aperture size in thermoacoustic or photoacoustic reconstruction" by Minghua Xu and Lihong V. Wang, Phys. Rev. E 67, 056605 (2003).

[7] "Photoacoustic imaging in biomedicine" by M. Xu, and L.V. Wang, Rev. Sci. Instrum. 77, 041101 (2006).

[8] "Ultrasonic imaging of the human body" by P N T Wells, Rep. Prog. Phys. 62 (1999) 671-722.

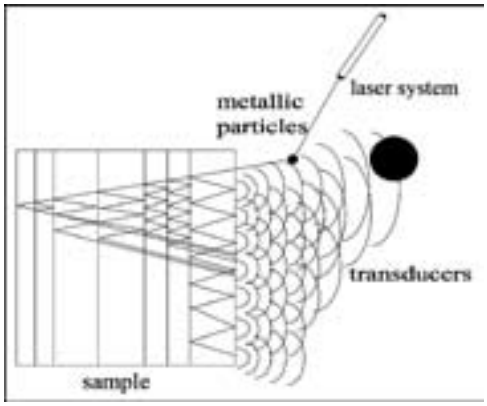

Figure 3: Reflections, transmissions, and absorptions occur each time a ray path meets an interface.

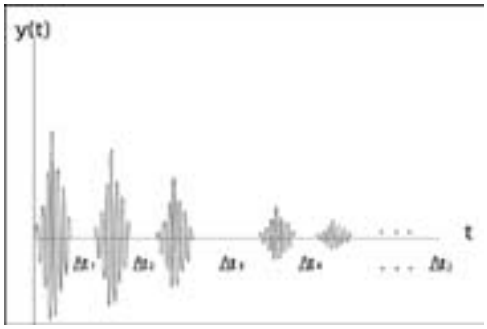

Figure 4: The echo signal as a combination of delayed pulses. The delay depends on the acoustic wave velocity in the sample and the distance between interfaces. These dependencies could cause the echoes to overlap.

Electrical Charge on a Nanofiltration Membrane

Kasiem Anderson

Biomedical Engineering, Georgia Institute of Technology

NNIN REU Site: Howard Nanoscale Science and Engineering Facility, Howard University
NNIN REU Principal Investigator: Dr. Kimberly Jones, Civil Engineering, Howard University
NNIN REU Mentor: Dr. Jermey Matthews, Civil Engineering, Howard University
Contact: gth707m@mail.gatech.edu, kljones@howard.edu, jermeym@gmail.com

Abstract

Nanotechnology applications have become useful in the optimization of filtration membranes. The extended Nernst-Planck (ENP) equation is a complex mathematical model that can be manipulated to calculate and predict flux, rejection, or electric charge across a membrane. Using the MATLAB® software, a program can be created to calculate these theoretical values that will guide the fabrication of membranes with optimized performance as well as shed light on the understanding of experimental data. With this knowledge, progression with nanofiltration membranes will be quickened, and we can sooner be able to use them for more practical applications of filtering water such as the purification and reuse of drinking water.

Introduction

The ENP equation is a complex equation using the ionic diffusion, electric field gradient, and convection of a membrane to solve flux, or the ability of a particular species to pass through the membrane, such that flux is equal to the convection minus the diffusion and electric field gradient. As such, the equation does not have any relation to the mechanistic structure of the membrane, but rather the performance of the membrane.

As a complex differential equation needing the Runge-Kutta method to be solved, manipulation of the ENP equation can be quite time consuming and difficult. Therefore, it is quite appropriate to create a program that will solve for the various variables needed to progress in nanofiltration membrane optimization.

The Runge-Kutta is a method of integration that involves a recursive method of averaging the derivative at several points, then adding this new number to a sum variable until the last point of integration is reached. There are multiple versions of the Runge Kutta with varying levels of accuracy. This alone may require many iterations, so using a computer will not only save time, but allow for a more accurate version of the Runge Kutta, and likewise attain a most accurate result.

Using the Model to Write Program

Using the MATLAB software, it is essential to write the ENP equation and its associated equations into the .m file. The ENP equation solutions must fall under the restrictions stated by the electro-neutrality condition and the under zero current condition. Using the Runge-Kutta method of solving the system of differential equation for the potential and concentration gradients, we are able to move between the flux, the electric potential across the membrane, as well as solve for the rejection of ions within a few more steps.

Future Progress

We were not able to complete the program using the ENP equation but have made some progress with it. As such, the first step is to continue the work we have done, and find a way to complete an efficient and accurate method of programming the ENP equation into MATLAB, or some other programming software application.

A logical next step to take is to continue working with the extended Nernst Planck equation to allow one to solve for any of the many variables of the model. Practically speaking, what is necessary is to find out how to reach the desired settings of the nanofiltration membrane, especially the charge across the membrane. Eventually, with work, nanofiltration will be used more and more for drinking water filtration, to medical uses throughout the world. Naturally this will be expedited by the use of computers wherever possible, such as the math calculations assigned.

Acknowledgements

National Nanotechnology Infrastructure Network Research Experience for Undergraduates Program; Howard Nanoscale Science and Engineering Facility; Dr. Kimberly Jones; Dr. Jermey Matthews; Dr. Gary Harris; Mr. James Griffin; Mr. Aaron Jackson.

Electron Transport in Silver Silicon Composite Film

Ian Broderick

Physics, Carleton College

NNIN REU Site: Howard Nanoscale Science and Engineering Facility, Howard University
NNIN REU Principal Investigator: Dr. Clayton Bates, Electrical Engineering, Howard University
NNIN REU Mentor: Dr. Chichang Zhang, Electrical Engineering, Howard University
Contact: broderii@carleton.edu, bates@msrce.howard.edu

Abstract

Composite films of silver (Ag) nanoparticles embedded in an n-doped silicon (Si) matrix exhibit strong photo responses when exposed to infrared spectrum, especially in the 1-15 μm wavelength range. The focus of this project is to quantify the Hall effect on a 3 μm thick composite film composed of 18% Ag grown on a highly resistive Si substrate. The measured Hall current is related to the electron mobility and reflects the responsivity of the future infrared detector. Samples were created via magnetron co-sputtering at 550°C using Argon plasma at 3.5 mTorr. Four ohmic contacts of chromium (Cr) and gold (Au) were evaporated on the sample, using e-beam and thermal deposition followed by rapid thermal annealment, to employ the Van Der Pauw method of Hall measurement. Hall measurements were taken at the National Institute of Standards and Technology between 77 K and 300 K.

Introduction

Silver nanoparticles display strong photo responses to infrared spectrum. To create a device that takes advantage of this characteristic, Ag will be co-sputtered with highly n-doped Si to form a matrix with embedded Ag nanoparticles. In order to fabricate this device, we must characterize its responsivity, electron mobility and potential lifetime. Fortunately all this can be extracted from measurements of the Hall currents, which is a direct measurement of the mobility and rapidity of the electrons in the material. Essential to the film are isolated small non-chemically bonded Ag nanoparticles; isolated to avoid shorts, small to increase the surface area and response strength, and non-chemically bonded to avoid unwanted silicides. To avoid the silicides, we made depositions at 550°C which is low enough to prevent silicides and high enough that we get our silicon in crystal form. Taking into account the other specifications, this project aimed to accurately sputter a 3 μm thick composite film of 18% Ag, 82% n-doped Si onto a Si substrate.

Figure 1: Sample 25B.

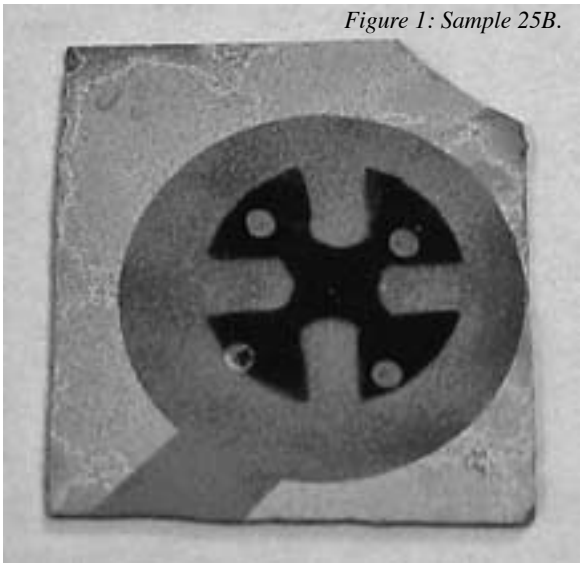

Experimental Procedure

Our Ag and n-doped Si (resistivity: 1-5 Ωcm) targets were placed in the Kurt J. Lesker CMS-18 Magnetron Plasma co-sputtering system. This system uses argon plasma and using different voltages can co-sputter two targets at varying rates. For both of our trials, 25A and 25B, the deposition temperature was 550°C and the Ar pressure was 3.5 mTorr. Both depositions ran for precisely 2.5 hours. Our first sample 25B had the following deposition specifics: base pressure of $2.7*10^{-7}$ Torr, Ag power supply of 12W (~ 260V across target), Si power supply of 330 W (~ 470V). Our second sample, due to a realization that 25B had too much Ag, had a much lower Ag voltage: base pressure of $5.0*10^{-8}$ Torr, Ag power supply of 7W (152V), same Si power supply. After deposition, four ohmic contacts had to be placed on the film for the future Hall measurements. To achieve this, we evaporated a 200Å layer of chromium followed by a 1500Å layer of gold, using e-beam and thermal evaporation respectively. The sample then underwent thermal annealing at 600°C for 30 seconds. The final product is shown in Figure 1.

At this point, we went to make the Hall measurements using the Van Der Pauw method. Detailed info on the exact specifics of this technique can be found at http://www.eeel.nist.gov/812/hall.html. The key variable defined by this experiment is ΣV_i which is the sum of all the positive magnetic field voltages minus the sum of all the negative field voltages (we used a magnetic field of 8000 Gauss). This value plugs into $n_s = ((8*10^{-8})IB)/(q* \Sigma V_i)$ to get the number of mobile carriers. Finally this value, along with

the average resistivity, R_s, gives us the electron mobility of $\mu = (R_s * qn_s)^{-1}$. We took these mobility measurements at different temperatures from 77K to 290K to define the optimal operating temperature.

Results and Discussion:

Figures 2 and 3 display the resistivity and electron mobility vs. temperature for both samples. As can be seen from Figure 3, the resistivity of sample 25B is far too low, implying too much silver. Later Rutherford back-scattering tests showed that indeed sample 25B was 22.5% Ag and that our corrective measures resulted in 11% Ag in 25A. Thus sample 25B was relatively useless for this project.

25A was more hopeful, in that it displayed the expected mobility vs. temperature relationship; initially a positive relationship due to decreased impurity scattering, later to taken over by a negative relationship caused by lattice vibrations. The final issue we took with sample 25A was how low the Hall mobility was, which should have been in the 10^3, 10^4 range. This could probably be solved by using a more highly doped Si target (of resistivity around 0.001-0.006 Ωcm) which was our original intent (but the target cracked). Also more accurately attaining 18% Ag would help in this matter.

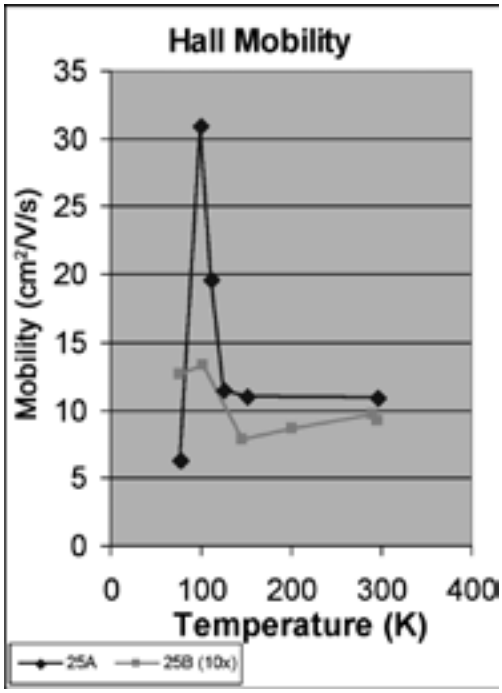

Figure 2: 25A, 25B Hall mobility.

Future Work

For the future creation of an infrared detector, more characterization is required. Specifically, the measurement of the responsivity of the device to different incident wavelengths at varying operating voltages. After that, this project only needs optimization of the fabrication process and creating the final product.

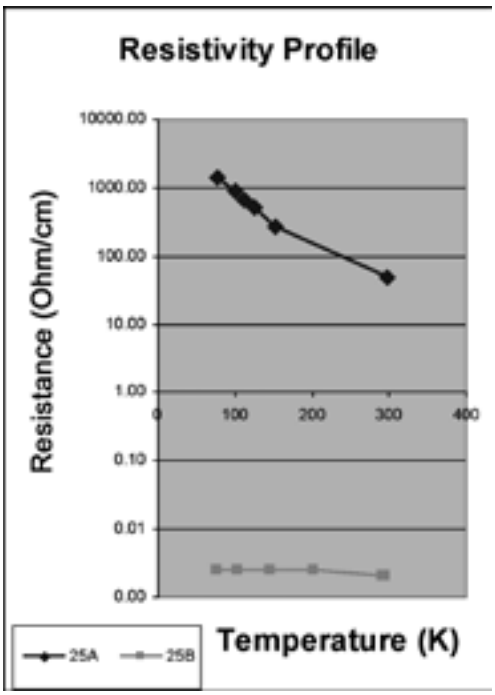

Figure 3: 25A, 25B Resistivity profiles.

Acknowledgements

I would like to thank Dr. Clayton Bates and my mentor Dr. Chichang Zhang for guidance and assistance during my research. I would also like to thank the National Nanotechnology Infrastructure Network Research Experience for Undergraduates Program and the National Science Foundation for funding. Finally I want to acknowledge Robert Thurber from the National Institute of Standards and Technology for providing the Hall measurement equipment.

References

[1] Shur, Michael. Physics of Semiconductor Devices. Prentice Hall. NJ, 1990.

[2] Sze, Simon. Physics of Semiconductor Devices. Wiley-Interscience. 1981.

[3] Zeghbroeck, Bart Van. "Principles of Semiconductor Devices" http://ece-www.colorado.edu/~bart/book/ 2004.

Simulation of Room-Temperature Terahertz Quantum Cascade Lasers with Varying Degrees of Transverse Confinement

Nikhil Chandra

Applied and Engineering Physics, Cornell University

NNIN REU Site: Microelectronics Research Center, The University of Texas at Austin
NNIN REU Principal Investigator: Dr. Matthew Gilbert, Microelectronics Research Center, The University of Texas at Austin
NNIN REU Mentor: Dr. Leonard F. Register, Electrical and Computer Engineering, The University of Texas at Austin
Contact: nsc22@cornell.edu, mgilbert@mail.utexas.edu, register@mer.utexas.edu

Abstract

The transport and scattering of electrons through quantum wire aluminium gallium arsenide (AlGaAs)/GaAs heterostructures were simulated for various diameters. The effects of transverse confinement on non-radiative electron transitions were studied in an attempt to improve lasing efficiency at room-temperature.

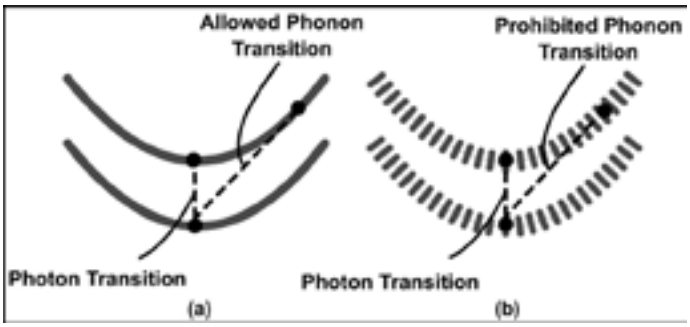

Figure 1: Energy bands; (a) without transverse confinement, and (b) with transverse confinement.

Introduction

Quantum cascade lasers (QCLs) emit radiation when electrons passing through a layered heterostructure undergo transitions between energy eigenstates and then emit photons. Currently, terahertz QCLs only operate at very low temperatures, as electrons absorb thermal energy and rise in energy bands associated with dimensions transverse to the direction of transport, undergoing transitions to lower eigenstates by emitting LO-phonons instead of photons (Figure 1a). LO-phonons are bosons that correspond to high-frequency longitudinal lattice vibrations. Applications of terahertz QCLs would be significantly economized by successfully achieving room-temperature operation. Theoretically, transverse confinement of the superlattice in quantum wires would discretize energy bands associated with dimensions transverse to the transport direction. This would obstruct the absorption of thermal energy by electrons, and subsequent transitions between eigenstates would result in the radiative emission of photons instead of the non-radiative emission of phonons (Figure 1b).

The focus of this project lay in qualitatively determining the efficacy of transverse confinement in improving the radiative efficiency of a terahertz QCL operating at room-temperature. We designed a heterostructure that possessed desirable spacings and resonances between energy eigenstates. This was followed by the simulation of the transport and scattering of electrons through quantum wires of various diameters with this heterostructure, using a quasi-three-dimensional non-equilibrium Green's function (NEGF) simulator entitled "Schrödinger Equation Monte Carlo 3D" (SEMC3D). Only scattering by phonon emission was considered. Reductions in non-radiative phonon transition rates were associated with increased radiative photon transition rates, and vice versa. Transitions triggered by phonon absorption were ignored.

Method

We found the energy eigenstates of a potential profile using a shooting-point eigenvalue solver. The profile consisted of wells and barriers that corresponded to the GaAs/AlGaAs heterostructure of a single QCL module, over which a potential drop of 46 meV was applied. The widths of the wells and barriers were adjusted and the effective mass of each region was tuned until desirable spacings and resonances between energy eigenstates were obtained.

Figure 2 displays the final heterostructure designed, along with the energy eigenstates superposed with their probability densities. E_5's wavefunction was concentrated in the first two wells to ensure that electrons injected into this level would fall to E_4 or E_3 within these wells, preferably by emitting a photon. Population inversion was promoted by evenly spreading out the probability densities of E_4 and E_3 between all three wells to provide rapid tunneling, and by setting the energy gap between

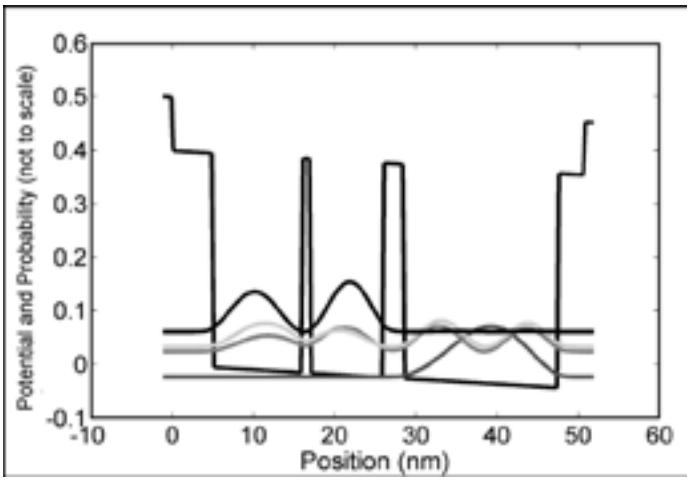

Figure 2: Potential profile with energy eigenstates and probability densities.

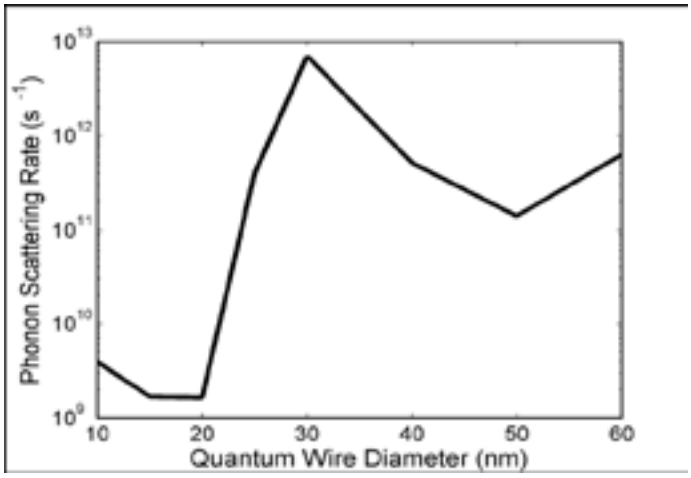

Figure 3: Variation of non-radiative phonon scattering rate with diameter.

E_3 and E_2 to roughly equal the LO-phonon energy of GaAs, as this would encourage rapid transitions between these levels by phonon scattering.

We built three-dimensional potential fields corresponding to quantum wires of different diameters using this heterostructure, to be loaded into SEMC3D. However, since the heterostructure would no longer be isolated from the "outside world," a slight offset in the spacings between the energy eigenstates as calculated by SEMC3D was expected. To discover the true spacings between the eigenstates, we configured SEMC3D to inject electrons into the profile over a range of energies, and calculated the transmission probability (i.e., the likelihood that an injected electron would traverse the entire length of the module). Energies for which there was a spike in the transmission probability corresponded to the now quasi-bound eigenstates.

To ensure the qualitative accuracy of the simulation, we varied the LO-phonon energy until the electron scattering rate by the emission of phonons in the third well was maximized. This was vital to ensure rapid depopulation of E_4 and E_3, promoting population inversion. The LO-phonon energy settled upon was 36.263 meV. For each quantum wire diameter, we used SEMC3D to calculate the energies and wavefunctions of the two-dimensional transverse energy subbands. We followed this by injecting electrons into E_5 for each of these subbands. In each case, the average phonon scattering rate in the first two wells was calculated using the average self energy. A Fermi-weighted average of the subbands' scattering rates was used at 300 K to understand the effects of transverse confinement on scattering by phonon emission at room-temperature. We performed this procedure for quantum wires with diameters of 10 nm, 15 nm, 20 nm, 25 nm, 30 nm, 40 nm, 50 nm and 60 nm.

Results

The phonon scattering rate decreased precipitously for wires with diameters below 30 nm (Figure 3). The peak in scattering rate observed for 30 nm was attributed to resonances between the transverse subbands. The lowest scattering rate was achieved at a diameter of 20 nm. Further reduction in diameter led to an increase in the scattering rate. This was attributed to an increase in the overlap between the initial and final carrier states between the ground states of E_5, and E_3 and E_4.

Conclusion

We have qualitatively demonstrated that the discretization of energy bands by transverse confinement decreases the likelihood of non-radiative scattering by phonon emission. New methods for the construction of quantum wire heterojunctions may provide a means to implement transverse confinement in terahertz QCLs, enabling room-temperature operation.

Acknowledgements

I would like to thank Dr. M.J. Gilbert, Dr. L.F. Register, Dr. S. Banerjee, Ms. Jean Toll, the National Nanotechnology Infrastructure Network Research Experience for Undergraduates Program and the NSF.

References

[1] B.S. Williams, S. Kumar, and Q. Hu, Opt. Soc. of Amer. (2005).

[2] R. Köhler, A. Tredicucci, F. Beltram, H.E. Beere, E.H. Linfield, A.G. Davies, D.A. Ritchie, R.C. Iotti, and F. Rossi, Nature 417, 156 (2002).

[3] B.S. Williams, H. Callebaut, S. Kumar, Q. Hu, and J.L. Reno, Appl. Phys. Lett. 82, 1015 (2003).

Enhanced Laser Cooling Using Ion-Doped Nanopowders: Engineering and Harvesting Atomic Vibrations

Philip Hebda

Mathematics and Physics, Purdue University

NNIN REU Site: Michigan Nanofabrication Facility, The University of Michigan Ann Arbor
NNIN REU Principal Investigator: Dr. Massoud Kaviany, Department of Mechanical Engineering, University of Michigan
NNIN REU Mentor: Jedo Kim, Department of Mechanical Engineering, University of Michigan
Contact: phebda@purdue.edu, kaviany@umich.edu, jedokim@umich.edu

Abstract

This research focused on maximizing the overall cooling rate to cool solids from room temperature to the cryogenic temperature range by advancing the existing theoretical treatments. At the atomic level, laser cooling is described through the energy transfer mechanisms among photons, electrons, and phonons. The cooling rate is dependent on the interactions and properties of the host atoms, the optically-active dopant, and the coupling between these three carriers [1]. Investigated parameters included the electron-phonon coupling coefficient and the phonon density of states (DOS) using the Debye-Gaussian model, both of which affect the phonon-assisted photon absorption rate, the target phonon energy, and the nonradiative decay rate. To enhance the cooling rate, doped nanopowders are used over bulk since the DOS of nanopowders has broader peaks [2].

Background

The ultimate goal in laser cooling research is to create a refrigeration unit capable of reaching the cryogenic temperature range. Since it lacks moving parts, such a device would have a longer lifetime than other coolers. The largest reported temperature drop has been 70 K from room temperature, and the process has been observed as low as 77 K [3].

Laser Cooling Process

The solid to be cooled is composed of an ionic host doped with an optically-active rare-earth ion. Incident photons have a frequency tuned slightly lower than the resonance transition of the dopant. In order for an electron of the dopant to absorb an incident photon, a phonon from the host must also be absorbed so that the sum of the photon and phonon energies equals the resonance transition. The electron then decays back to the ground state either radiatively, with the emission of a photon, or nonradiatively, with the emission of phonon(s) and a photon. Cooling occurs if the average emitted photon has a greater energy than the incident photon.

Cooling Rate Equation

In Figure 1, the cooling rate equation is given in the unit of watt [1]. The variables which vary with the selection of host include the effective mass of the constituent atoms m_{eff}, the electron-phonon coupling coefficient $\varphi'_{e\text{-}p,O}$, the phonon DOS D_p, the target phonon energy E_p, the Bose-Einstein distribution f_p^o, and the internal quantum efficiency $\eta_{e\text{-}ph}$. Other factors from the equation, which vary with the properties of the optically-active dopant, laser irradiation, and the structure of the sample, include the photon-electron coupling coefficient $\boldsymbol{s}_\alpha \bullet \boldsymbol{\mu}_e$, the frequency $\omega_{ph,i}$ and wavelength $\lambda_{ph,i}$ of the laser photons, the number density of the dopant n_d, the length of the solid L, the speed of light u_{ph}, the incident laser power $Q_{ph,i}$, and the average wavelength of the emitted photons $\lambda_{ph,e}$.

$$\dot{S}_{ph\leftarrow e\text{-}p} = \frac{\pi\hbar}{2\varepsilon_o m_{eff}^2}(\boldsymbol{s}_\alpha \cdot \boldsymbol{i}_e)^2 \varphi'^2_{e\text{-}p,O} \frac{D_p(E_p) f_p^{o2}(E_p)}{E_p^3} \frac{\hbar\,\omega_{ph,i} n_d L}{u_{ph}} Q_{ph,i}\left(1 - \frac{\lambda_{ph,i}}{\lambda_{ph,e}}\eta_{e\text{-}ph}\right)$$

Figure 1: Cooling rate equation.

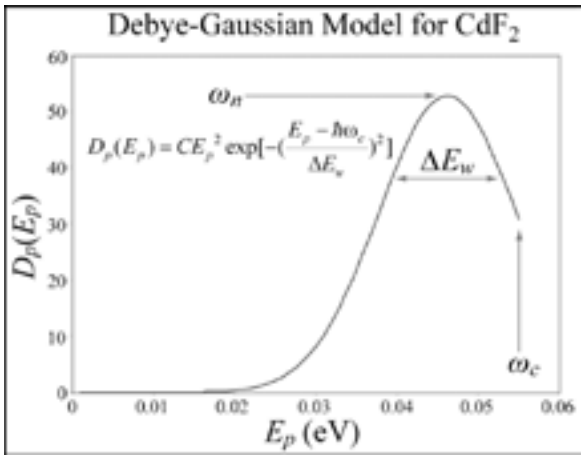

Figure 2: DOS for CdF_2 using the Debye-Gaussian model, shown with the DOS equation, where the constant C is dependent on the cut-off frequency ω_c ($C = 26587.7\ eV^3$ for CdF_2).

Phonon DOS

The density of states (DOS), which gives the number of phonon modes for a given energy, was estimated using the Debye-Gaussian model (Figure 2). The peak value was calculated from the natural frequency ω_n, the cut-off frequency ω_c, and the width of the peak ΔE_w. The area under the curve was normalized to one, so a lower cut-off frequency increased the peak value.

By using the harmonic oscillator model, cut-off frequencies were calculated for various fluorides, chlorides, and oxides from the spring force constant and effective mass between the anion-cation pair. In addition to increasing the peak DOS value, lower cutoffs augment the cooling rate by increasing the internal quantum efficiency and decreasing the target phonon energy. From the calculations, chloride paired with a heavy cation would maximize the cooling rate through these factors.

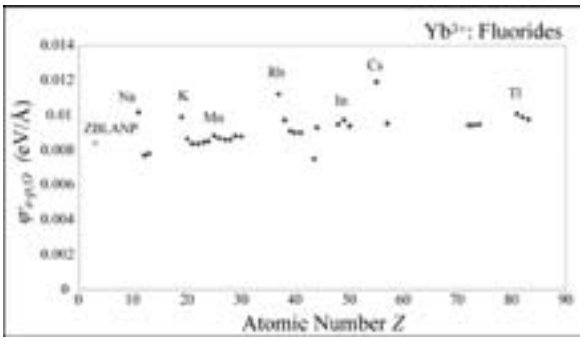

Figure 3: Electron-phonon coupling coefficient for various cations in fluoride glass.

Electron-Phonon Coupling

In the harmonic oscillator model, the dopant absorbs phonons from the vibrations of a neighboring anion. When an anion-cation pair oscillates with respect to the dopant, the anion-dopant bond length changes, changing the potential of the dopant's valence electrons. As the coupling factor is increased through host selection, the same anion-dopant contraction or dilation increases the potential change of the electrons. The electron-phonon coupling coefficient was calculated for Yb^{3+}-doped fluorides (Figure 3). Electron-phonon coupling increases slowly with atomic number and peaks at the alkali metals. Rubidium and cesium fluorides are the optimal cations for maximizing electron-phonon coupling.

Nanopowders

The properties of nanopowders have been found to enhance the cooling rate over bulk materials by increasing the number of energy carriers in laser cooling, specifically phonons and photons [2]. Calculations show that the DOS of nanopowders is on average larger at the relevant phonon energies. Photon scattering in random nanopowders leads to photon localization, where photons do not propagate through the solid but are spatially restricted to a region. This leads to a much higher photon density per input power.

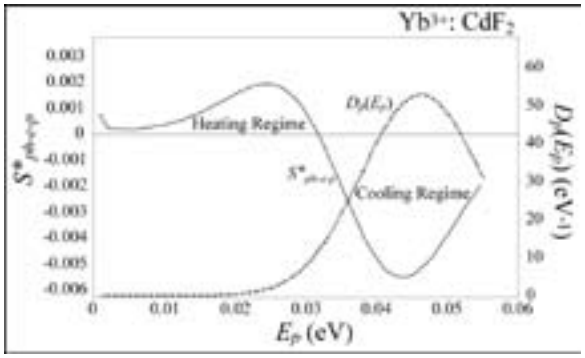

Figure 4: Calculated cooling rate (normalized per unit of input power $Q_{ph,i}$) and normalized DOS vs. target phonon energy.

Conclusions

The selection of an ionic host material has been discussed through the DOS and the electron-phonon coupling coefficient. From the results, ideal cations are rubidium and cesium. Currently, fluoride is used as the anion because it is known to be optically transparent to the laser photons; more research is needed for other anions.

In Figure 4, the normalized cooling rate varies with the target phonon energy. In the heating regime, the target phonon energy is too low, so each instance of radiative decay does not remove a sufficient amount of phonon energy to overcome the heating of nonradiative decay. The target phonon energy which provides the maximum cooling rate (most negative) is shifted slightly to the left of the DOS peak value due to the Bose-Einstein distribution and the E_p^3 term in the denominator of the cooling rate equation.

Acknowledgements

I would like to thank Dr. Massoud Kaviany for allowing me to work in the Heat Transfer Physics Laboratory and Jedo Kim for mentoring me on my project. This project was supported by the National Nanotechnology Infrastructure Network Research Experience for Undergraduates Program and the National Science Foundation.

References

[1] Kim, J. and M. Kaviany, "Material Selection Optimization for Ion-Doped Laser Cooled Diatomic Crystals," (unpublished).

[2] Ruan, X. L., and M. Kaviany, Phys. Rev. B 73, 155422 (2006).

[3] Ruan, X. L., and M. Kaviany, J. Heat Transfer 129, 3 (2007).

What Makes Peacock Feathers Colorful?

Suntrana (Tran) Smyth

Physics, University of Alaska, Fairbanks

NNIN REU Site: Cornell NanoScale Science & Technology Facility, Cornell University
NNIN REU Principal Investigator: Professor Sandip Tiwari, Electrical and Computer Engineering, Cornell University
NNIN REU Mentor: Brian Bryce, Electrical and Computer Engineering, Cornell University
Contact: suntranafs@hotmail.com, st222@cornell.edu, babryce@gmail.com

Introduction

The iridescence of peacock feathers is fascinating because of their range of colors and their brightness in a filament. Color can arise from wavelength selective absorption and wavelength selective reflection. Bright colors of many butterflies are now known to arise from reflection. Yoshioka and Kinoshita [1] found that the pigmentation in peacock feathers, instead of reflecting light, serves "...to absorb the randomly scattered light and [thus] make vivid the interference color." Zi et al. concluded that periodic structures caused the reflection properties that lead to the colors [2]. We undertook this effort to clarify the nature of the color phenomena in peacocks in view of earlier seemingly contradictory reports.

Previous Work

Zi et al. [2] of Fudan University reported that two mechanisms are the cause of the iridescent colors in peacock feather barbules: varying size of the lattice constant and varying numbers of melanin rod layers normal to the cortex surfaces. Zi found that the green and blue barbule lattice constants were ~ 150 nm and ~ 140 nm respectively. The authors concluded that that Fabry-Perot interference was central to the coloration phenomena; the number of melanin rod layers parallel to the cortex surface was reported as "~ 9-12 for the blue and green barbules, and ~ 4 for the brown barbules." Zi et al. also reported that the brown barbules possess a (non-square) rectangular lattice structure. They observed ~ 185 nm along the direction perpendicular to the cortex surface by ~ 150 nm along the parallel, and that brown barbule structures possess no air hole array between the melanin layers nearest to the surface [3].

Methods and Observations

A peacock feather consists of a shaft from which barbs extend spirally. Tiny barbules protrude from each barb shaft. Visible under a scanning electron microscope (SEM), the perimeter of the cross-section of every barbule contains an ordered structure (Figure 1). This structure consists of melanin rods interspaced with air holes, possibly integrated with keratin. We probed the structures by taking SEM images of feather cross-sections, measuring the geometries, and modeling the interaction of light striking those geometries with the M.I.T. electromagnetic equation program (MEEP).

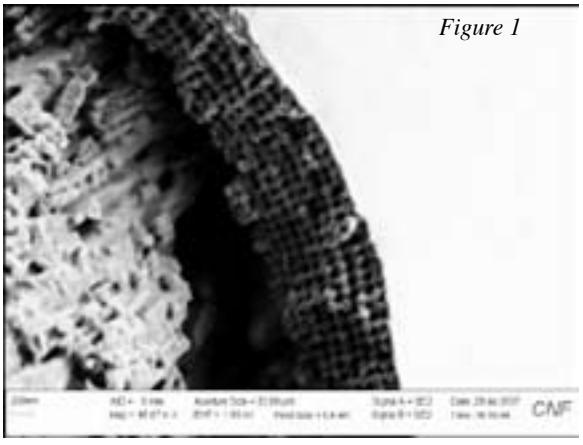

Figure 1

A spatially periodic dielectric material (in the case of peacock feather, melanin rods interspaced with air holes and keratin) that inhibits the propagation of light waves at certain frequencies and energies is called a "photonic crystal." It creates blocking and passing bands for photons similar to those of electrons in a semi conducting crystal. The feather structures give rise to what's known as a "partial" band gap, in which light is blocked (and therefore reflected) only at certain polarizations and angles of incident.

A variety of sampling techniques were attempted intending to produce high quality SEM images: barbule slices were imbedded in polymer which was cut to expose cross sections; glass and diamond microtomes were used to slice microscopic samples; an ineffectual attempt was made to break barbules cleanly using a hardened structure by cooling it with liquid nitrogen.

The most effective sampling strategy consisted of simply laying a barb down on copper tape, slicing the barbules from it with a razor blade, removing the stem, and gold sputtering to reduce charging by incident electrons. This yielded good quality SEM images of the barbule cross sections and of their longitudinal structure. However, there remained difficulties in structural measurement. First, even with sputtering, prolonged charging due to the electron beam was still apt to destroy parts of the sample. Second, the sputtering itself caused error, as it obscured the actual structures. Third, it was difficult to make a precise judgment as to the angles of the lense versus the cross-sectional face. Random errors were greatly reduced by averaging sizes of several lattices measured simultaneously.

With geometric data from these images, MEEP was used to simulate a Gaussian pulse of light with various frequencies and polarizations striking a square photonic crystal lattice of cylindrical void tubes of the observed diameters encased in melanin.

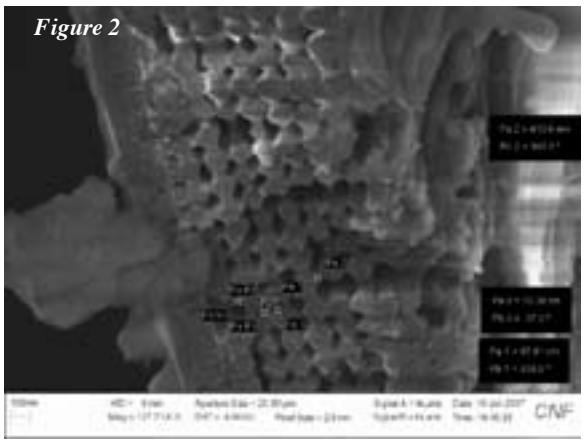

Results

Our SEM images indicate that the blue and green barbule structures possess 7.5 ± 1 melanin rod layers interspaced with air-holes parallel to the cortex surface. The brown barbule structures apparently possess 7 ± 1 melanin rod layers interspaced with air-holes plus two outside layers of melanin without air-holes (Figure 2).

However, when the melanin rods were examined from a longitudinal view, large, previously unreported spherical distortions (Figure 3) were observed, indicating that the lattice structures are in fact three dimensional. In cross section, the green and blue barbule lattice structures appeared to be 2D and square, with lattice constants of 154 ± 10 nm and 156 ± 10 nm for the green and blue barbules respectively. We detected no difference in the perpendicular and parallel dimensions of the lattice structure of the brown barbules, and observed a lattice constant of 172 ± 10 nm.

Utilizing this data in our MEEP model produced a graph of light wavelength versus reflected power (Figure 4). There is correlation between the cylinder diameter to lattice constant ratio and wavelength of reflected light. Further work is needed in order to generalize these results for a complete model.

Conclusions

We find, as did Li et al that the brown barbules, in contrast to blue and green, possess two melanin layers at the cortex lacking air spacing. Our data does not show a significant difference in number of total melanin layers parallel the cortex surface in differently colored barbules, differing with Zi et al.

Insofar as the structures are 2D, we find in contrast to Li et al, that the lattice structures of not only blue and green but also brown barbules are square. Our model does not show the cylindrical air hole radius to lattice spacing ratio affecting the range of the reflectance spectra as directly as theorized.

Over all, we find that a 2D model is insufficient to cause the broad range of light frequencies reflected from the different barbules and that 3D lattice, with spherical distortions along the melanin rods, are important to determining the color reflection properties of the peacock feather.

Acknowledgements

The Intel Foundation; National Nanotechnology Infrastructure Network REU Program; National Science Foundation; Cornell NanoScale Facility; The Tiwari Group esp. Dr. Tiwari, and Brian Bryce; Cornell NanoScale Facility Staff; Cornell NanoScale Facility REU group.

References

[1] Yoshioka, S. and Kinoshita, S. 2002. Effect of Macroscopic Structure in Iridescent Color of Peacock Feathers. Forma, 17, 169-181.

[2] Zi, J., Xindi, Y., Li, Y. et al. 2003. Coloration strategies in peacock feathers. PNAS. 100:12576-12578.

[2] Li, Y. et al. 2005. Structural origin of the brown color of barbules in male peacock tail feathers. Physical Review E 72: 01902-1-01902-4.

Figure 3: These bumps are of 60nm+/-20nm in radius.

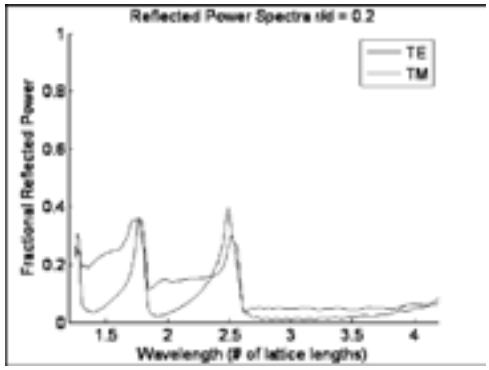

Figure 4: The right-most peak in the graph represents blue light.

Thermal Transport in Silicon Nanowires

Prem Vuppuluri

Mechanical Engineering, University of Portland

NNIN REU Site: Cornell NanoScale Science & Technology Facility, Cornell University
NNIN REU Principal Investigator and Mentor: Dr. Derek Stewart, Cornell NanoScale Facility, Cornell University
Contact: vuppulur08@up.edu, stewart@cnf.cornell.edu

Abstract

The thermal conductance of small diameter silicon (Si) nanowires was determined using a Density Functional approach. Nanowires were isolated from a bulk clathrate system with a unit cell of 30 Si atoms. The equilibrium coordinates of the atoms in the unit cell were determined through structural relaxation based on Hellmann-Feynman forces. Additionally, coordinate relaxations of a clathrate nanowire with terminating hydrogen atoms were also done. The force constant matrix was evaluated for a SiH nanowire with three unit cells. Phonon bands were obtained from the force constant matrix, and the transmission function was used to calculate thermal conductances for 20 temperature values. The high temperature conductance limit was 4.75×10^{-10} W/K.

Introduction

Heat dissipation is a critical variable in the design and analysis of electronic systems. As device sizes approach the nanoscale order, constructing effective, thermally conductive fins becomes increasingly difficult. Transport of phonons and heat is ballistic in thermal conduits with length scales on the order of a nanometer. As a result, the analysis of the thermal conductance of nanowires requires a different approach from macroscopic systems. In this research, the thermal conductance was calculated by predicting how phonons would transmit through the system.

Phonons are the primary carriers of thermal energy in semiconductors. Phonons are waves created by the vibration of atoms in crystalline structures. The propagation of phonons through a lattice is responsible for thermal transport. In order to quantify the propagation of the phonons through the system, the force constant matrix of the nanowire system has to be determined. The phonon band diagram can be produced from the force constant matrix, and using this information, the transmission function of the system can be calculated as a function of frequency.

The transmission function T(ω) can then be used to calculate the thermal conductance, σ, with the following equation [1]:

$$\sigma = \frac{1}{k_B T^2} \int_0^\infty (\hbar\omega)^2 \frac{e^{\hbar\omega / k_B T}}{(1+e^{\hbar\omega / k_B T})^2} \mathrm{T}(\omega) d\omega / 2\pi$$

where T is the temperature, ω is the phonon frequency, k_B is the Boltzmann constant, and ħ is the reduced Planck constant.

Coordinate Relaxation

The first step in calculating the thermal conductance was to determine the atomic coordinates of the silicon nanowire taken directly from the bulk system. Figure 1 shows a top view of an isolated clathrate nanowire [2] with a unit cell composed of 30 Si atoms (dark grey) and 20 hydrogen (H) atoms (light grey).

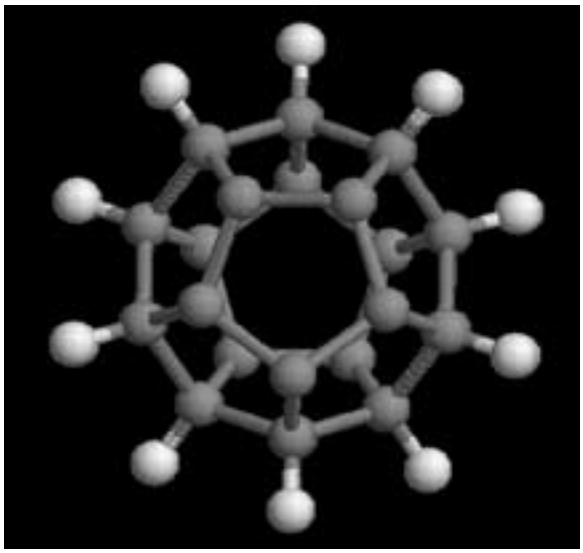

Figure 1: Isolated clathrate silicon nanowire with terminating hydrogens. Diameter (d) = 9.66 Å.

Figure 1 was created using Si-Si bond lengths of 2.38 Å and Si-H bond lengths of 1.50 Å [3]. The structure contains only regular pentagons. Structural relaxations were done using SIESTA, a self consistent density functional code with a atomic orbital basis set [4]. For the relaxation analysis, a cutoff energy of 200 Ry and a double-ζ basis set were used. A force tolerance of 0.0025 eV/ Å was taken for the calculation. Pseudopotentials were generated using Troullier and Martins' method [5]. 16 k-points in the z direction were used for the calculation.

The calculation of the relaxed coordinates produced a structure that looked very similar to the isolated structure shown in Figure 1. The relaxed nanowire had a diameter of 9.60 Å, as compared to the isolated nanowire which had a diameter of 9.66 Å. The lattice constant of the relaxed system was 10.31 Å, as opposed to a lattice constant of 10.59 Å.

Force Constant Matrix Generation

A force constant matrix for the relaxed Si nanowire was generated by linking three unit cells together and disturbing atoms in the middle unit cell. The forces induced on neighboring atoms by the disturbance were used to generate the force constant matrix. The force constant matrix was used to create a phonon band diagram, and the transmission of phonons was calculated as a function of frequency. The phonon band diagram is shown in Figure 2, and the transmission function is shown in Figure 3.

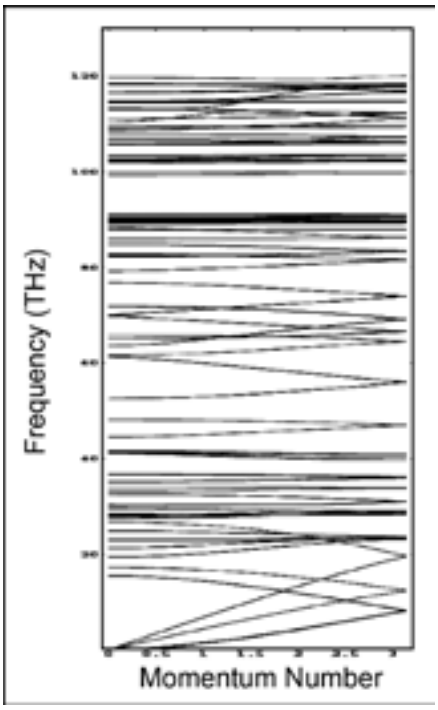

Figure 2, left: Phonon band diagram for terminated clathrate system.

Figure 3, below: Transmission function for terminated clathrate system.

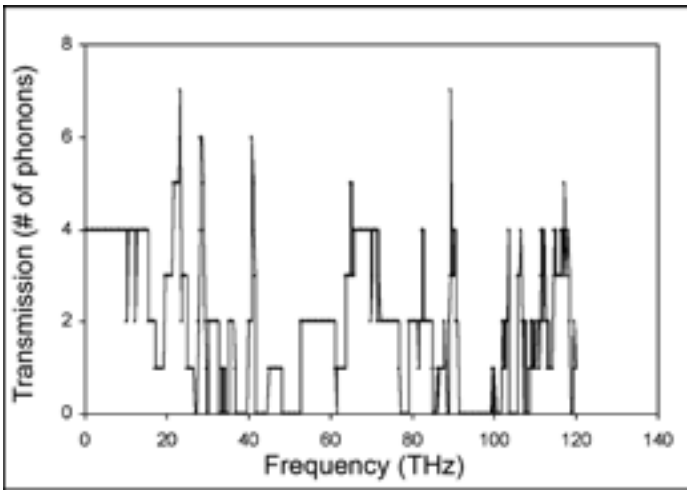

The transmission function was generated from the phonon band diagram by observing the density of phonon bands at each frequency. The transmission function has sharp peaks at frequencies where the bands are flat and dense, and is zero for frequency ranges with no bands.

Thermal Conductance Calculation

Using the transmission function shown in Figure 3, the thermal conductance of the silicon clathrate nanowire with terminating hydrogens was calculated as a function of temperature, by numerically solving the conductance equation for temperatures ranging from 0 to 500 K, in increments of 20 K. The resulting graph is shown below in Figure 4, and the high temperature conductance limit of this system was determined to be approximately 0.475 nW/K. In comparison, a (7,0) carbon nanotube was determined to have a greater high temperature conductance limit of 4.50 nW/K [1].

Acknowledgments

I would like to thank Dr. Mingo for his help in creating the phonon band diagram and collecting the transmission function data. I also appreciated the guidance of my mentor, Dr. Derek Stewart, and the financial contributions of the National Science Foundation, the National Nanotechnology Infrastructure Network Research Experience for Undergraduates Program, and the Cornell NanoScale Facility.

References

[1] N. Mingo, D.A. Stewart, D. A. Broido, and D.A. Shrivastava, "Phonon Transmission through Defects in Carbon Nanotubes from First-Principles", submitted to Phys. Rev. B.

[2] B. Marsen and K. Sattler, Phys. Rev. B 60, 11593 (1999).

[3] M. Durandurdu, Physica Status Solidi B, 243, R7-R9 (2006).

[4] J. M. Soler et al,, J. Phys. Condens. Matt., 14, 2745 (2002).

[5] N Troullier and J.M. Martins, Phys. Rev. B 43, 1993.

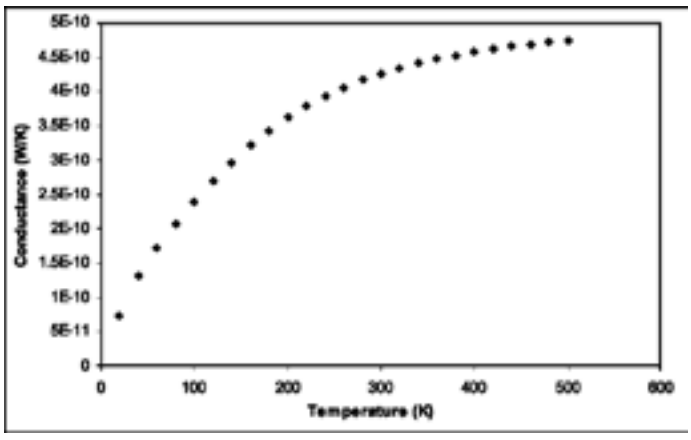

Figure 4: Thermal Conductance as a function of Temperature.

Effect of a Magnetic Field on the Synthesis of Single-Walled Carbon Nanotubes

Myriam Alexandre

Geophysical Science, University of Chicago

NNIN REU Site: Michigan Nanofabrication Facility, The University of Michigan Ann Arbor
NNIN REU Principal Investigator: Dr. Michael Keidar, Aerospace Engineering, University of Michigan Ann Arbor
NNIN REU Mentor: Tamir Arbel, Engineering, University of Michigan Ann Arbor
Contact: myriam@uchicago.edu, keidar@umich.edu, arbelt@umich.edu

Abstract

The full potential of carbon nanotubes for applications in engineering cannot be achieved until synthesis techniques are refined and methods to control nanotube characteristics are discovered. In this research project, the arc discharge method for producing single-walled carbon nanotubes (SWNTs) was used to test whether the addition of a magnetic field to the arc chamber will create longer SWNTs. Through analysis using scanning electron microscopy (SEM), samples taken from the arc chamber showed that, statistically, the average length of SWNTs produced with the magnetic field were longer than those produced without the addition of the magnetic field.

This suggests that with the addition of a magnetic field, the arc discharge method is an efficient and inexpensive method for producing longer SWNTs. From these results, it is predicted that increasing the magnitude will further increase the length of the SWNTs and produce more consistent results.

Introduction

SWNTs have extremely high tensile strength, elasticity, flexibility and high thermal conductivity. They can also be electrically conducting like metals or semiconducting depending on their structure; making them suitable for a wide range of applications from reinforcement material to microscale machinery. Several techniques have been developed for carbon nanotube synthesis. The most common methods are chemical vapor deposition (CVD) and arc discharge. These techniques are potentially viable as large-scale processes of producing SWNTs; however, they struggle with producing high quality, uniform and homogenous SWNTs that will hopefully make it easier to take advantage of the nanotubes' many potential applications.

CVD, at relatively low temperatures, uses a metal catalyst coated substrate in a heated chamber. Then two gases are introduced to the chamber; a process gas and a hydrocarbon gas. Its perk is that it does not require high temperatures, but the nanotubes it produces usually have defects in their structure. The arc discharge method involves the evaporation of a graphite anode filled with metal catalyst mixture by discharging an electric current between the electrodes. It offers poor flexibility and produces excessive amounts of unnecessary carbonaceous material.

In this research project, the arc discharge method for producing SWNTs is used to test whether the addition of a magnetic field to the arc chamber will affect the length of SWNTs. The theory behind adding the magnet predicts that if we can increase the density of the plasma between the electrodes, then we can increase the growth rate and consequently produce longer SWNTs. Adding the magnet has been shown to collimate the plasma in the chamber, specifically confining the plasma to the space between the electrodes and spreading it across the electrodes evenly as shown in Figure 1.

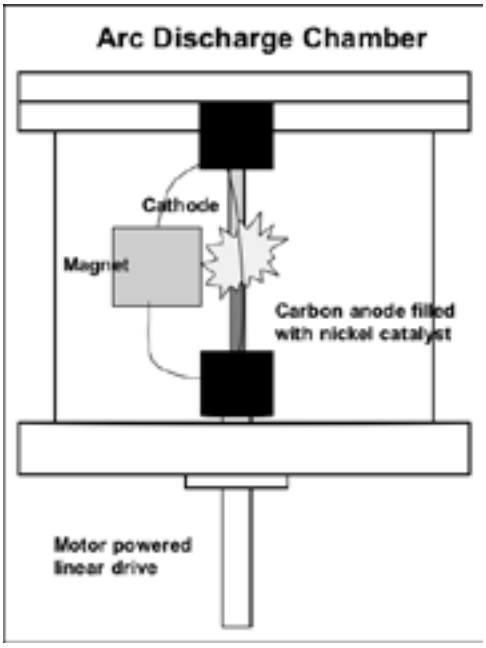

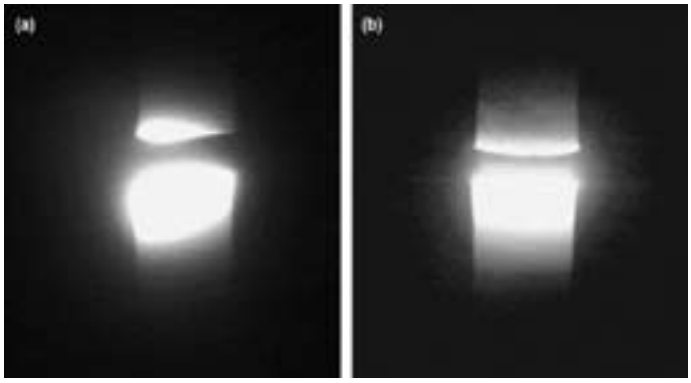

Figure 1: Photo of arc discharge; (a) without magnetic field, (b) with magnetic field.

Experimental Procedure

We tested whether a magnetic field would make longer SWNTs by executing the arc discharge method of production with and without the magnet. The graphite anode was prepared by filling the 3″ graphite rods with metal catalyst (Ni: Yt: C = 4:1: 95 %) and placing it in the chamber. Attached to the lid of the chamber was the stainless steel cathode. After the anode had been prepared, the lid was placed on the chamber. The chamber was vacuumed down and then pumped with helium at 650 Torr. The current that was sent between the electrodes was usually between 70 and 80 amps. While the current ran through the chamber, particles from the anode evaporated and condensed on the cathode and other regions of the chamber. As the anode shrank, the gap between the anode and the cathode was maintained by the chamber's motor-powered linear drive, thus maintaining the target current. The magnet was propped so that the magnetic field ran axially through both electrodes.

Samples from different regions of the chamber were collected. Samples from the deposit were found on a rod-like hard carbonaceous material that formed between the electrodes, and those taken from the collaret were found on material that formed above the cathode and around the deposit. Collected samples were analyzed under the SEM, which allowed us to take measurements of the SWNTs that were found.

Results and Discussion

Our SEM data indicated that the presence of a magnetic field made a significant difference in the average length of the SWNTs produced by the arc discharge method. Of the entire measurements taken without the magnetic field, 50% were under 600 nm and 90% were under 1300 nm; while 50% of the measurements taken from samples with the magnet were under 1100 nm and 90% were under 2600 nm.

Thus, the presence of the magnetic field seemingly doubled the length of the SWNTs produced. Additionally, samples from the deposit with magnetic field produced some of our longest SWNTs of over 6 μm in length. Hystograms are shown in Figure 2.

Conclusion

Our results indicate that, with the assistance of a magnetic field, the arc discharge method can consistently produce SWNTs of up to or over 6 μm in length. However, our main sources of error arise from limitations with the SEM. It only allows us to analyze a small area at a time and it severely lacks vertical resolution. Thus, there needs to be a more efficient and precise method of taking length measurements. Improving our understanding of SWNT formation and developing efficient techniques to disperse and purify the nanotubes will hopefully make our results more conclusive.

Acknowledgements

I would like to thank the National Nanotechnology Infrastructure Network Research Experience for Undergraduates Program, Intel Foundation, NSF, Sandrine Martin, and everyone else who has made this opportunity feasible. Your effort and contribution has been fruitful and has educated me about the endless research opportunities in nanotechnology. Thanks!

References

[1] Keidar, M., "Modeling of the Anodic Arc Discharge and Conditions for Single-Wall Carbon Nanotube Growth." Journal of Nanoscience and Nanotechnology 2006.

[2] Doherty S.P., "Semi-continuous production of multiwalled carbon nanotubes using magnetic field assisted arc furnace." Carbon 2005.

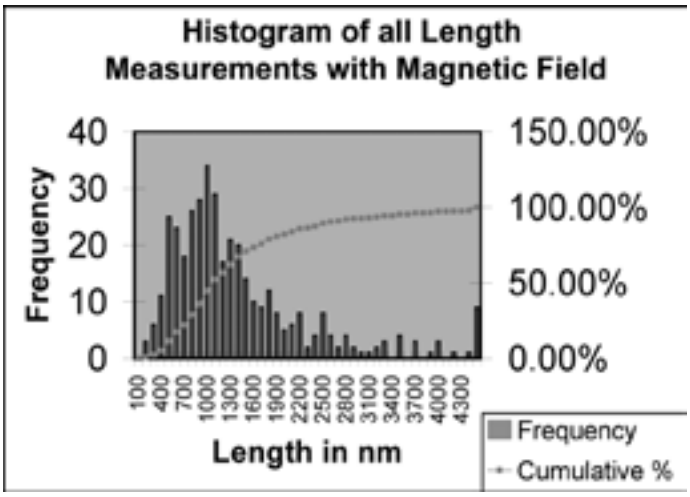

Figure 2

Nanowire Sensors

Andrea Boock

Engineering Science and Mechanics, The Pennsylvania State University at Altoona

NNIN REU Site: Penn State Center for Nanotechnology Education and Utilization, The Pennsylvania State University
NNIN REU Principal Investigator: Dr. Stephen J. Fonash, Center for Nanotechnology Education and Utilization, Pennsylvania State University
NNIN REU Mentor: Pilyeon Park, Materials Science and Engineering, Pennsylvania State University
Contact: aeb247@psu.edu, pxp908@psu.edu, fonash@engr.psu.edu

Abstract

The approach for growing nanowires (NWs) used here was the step-and-grow method, which combines the NW synthesizing and positioning step in an economic and safe way [1]. Template molds containing growth-controlling nanochannels were created with polydimethylsiloxane (PDMS) by using a master mold and placed over electrodes pre-positioned on a substrate. Polyaniline (PANI) NWs were then synthesized electrochemically in growth channels positioned between a biased anode and grounded cathode electrodes. The template molds could be stepped and the process repeated. After the synthesis of PANI NWs, they were tested for their sensitivity to humidity as a function of their surface to volume ratio. PANI NWs (110 nm) showed a linear response to humidity and could potentially function as a humidity sensor.

Introduction

Nanowires possess a high surface to volume ratio. This makes them excellent candidates for sensing applications, since a high surface to volume ratio improves detection sensitivity and response time due to more reaction area per volume and reduced diffusion time [2,3]. Most current approaches to growing nanowires require a synthesizing step, as well as a positioning step [4-6]. The overall approach for growth of the nanowires used here for sensing is the step-and-grow method, a novel approach that combines the two steps and eliminates the production of excess nanostructures [1].

Experimental Procedure

The first step was to create PDMS template molds using a previously created master mold. The master mold was made from a silicon wafer coated with 1 μm silicon dioxide, and was a positive image in relationship to the nanochannels, which would be created in the template mold. The template molds were created by spinning h-PDMS onto the master mold, curing at 65°C for 30 minutes, and adding s-PDMS mixture. They were then placed under vacuum, followed by a cure at 65°C for 3 hours. The template molds were then separated from the master molds and cut into rectangular slices with nanochannels located in the center of each piece.

The creation of the substrate began with patterning the electrodes onto a 2000Å silicon oxide coated Si wafer. The top surface of silicon oxide contained trenches patterned by dry etching and filled with platinum, with a titanium adhesion layer, deposited level with between the surface of the wafer.

In the synthesis of nanowires, the PDMS template molds were laid across the surface of the electrodes. An aniline monomer solution was then introduced to the opening of the nanochannels. 1V was applied to the anode by HP 4284a. PANI started to grow from the anode and filled the nanochannels until it reached to the grounded cathode. After carefully removing the PDMS template from the electrodes, PANI NWs are characterized by field emission scanning electron microscope (FESEM) and atomic force microscope (AFM). Figure 1 shows FESEM image of 111.6 nm PANI NW, and Figure 2 shows AFM image of the surface of PANI NW. Finally, PANI NW was tested for sensitivity to humidity, the results of which can be seen in Figure 3.

Results and Conclusions

Nanowire synthesis using the step-and-grow method is effective for synthesizing and positioning nanowires in a potentially economic manner. The PANI NWs were responsive to humidity and could potentially function as a humidity sensor.

Future Work

The step-and-grow approach can be used for synthesizing nanowires of many different materials. This opens up the opportunity for different types of nanowire sensors, as well as nanowire array structures.

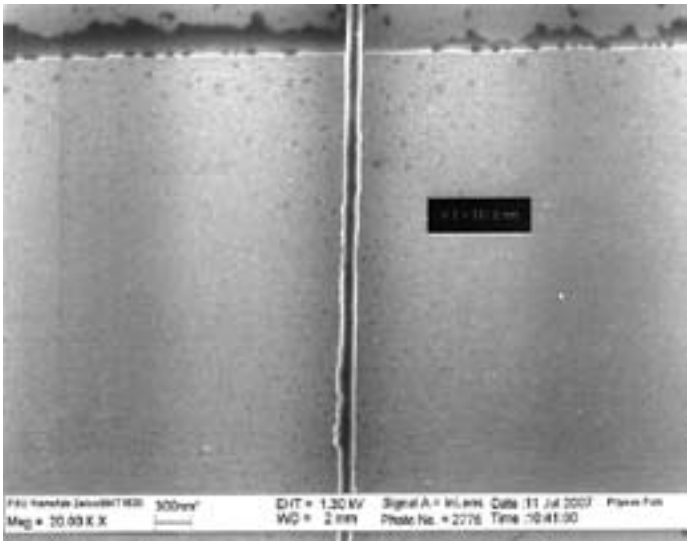

Figure 1: FESEM image of 111.6 nm polyaniline nanowire at 20.00 K X.

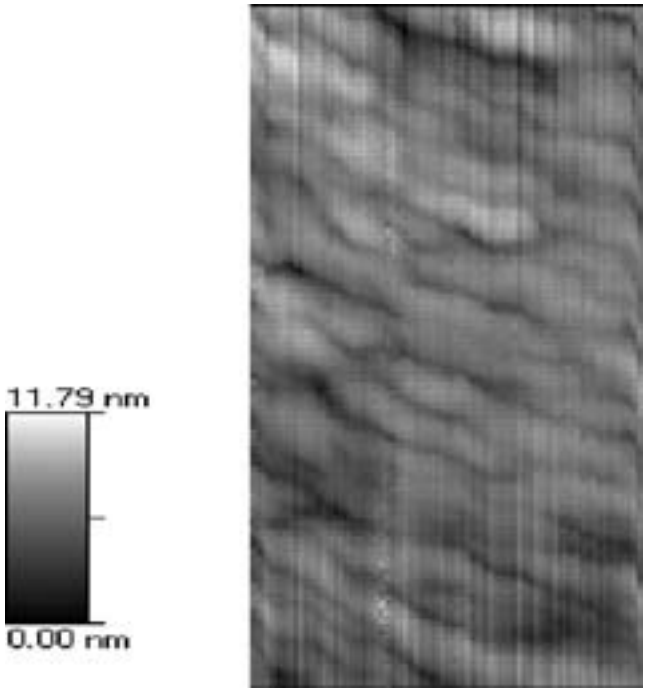

Figure 2: AFM image of polyaniline nanowire topology.

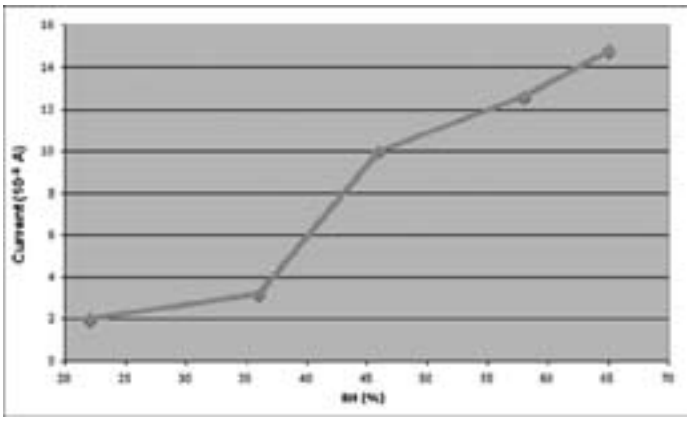

Figure 3: Relative humidity versus current when I V of electrical bias was applied to the device.

Acknowledgements

I would like to thank Pilyeon Park and Dr. Stephen J. Fonash for their support and guidance. Also, I am very grateful to the Penn State Nanofabrication Facility staff, as well as the staff of the Center for Nanotechnology Education and Utilization for a great experience. I would also like to thank the National Science Foundation and the National Nanotechnology Infrastructure Network REU Program for funding.

References

[1] Nam, W. J, Carrion, H., Park, P., Garg, P., Joshi, S., Fonash, S. J., Proceedings of the 2007 International Manufacturing Science And Engineering Conference, 2007, Atlanta, Georgia, USA.

[2] J. Huang, S. Virji, B. H. Weiller, and R. B. Kaner, Chem. Eur. J. 10, 1314 (2004).

[3] D. Xie, Y. Jiang, W. Pan, D. Li, Z. Wu, and Y. Li, Sens. Actuators B, 81, 158 (2002).

[4] L. Roschier, J. Pentilla, M. Martin, P. Hakonen, M. Paalanen, U. Tapper, E. I. Kauppinen, C. Journet, and P. Bernier, Appl. Phys. Lett. 75, 728 (1999).

[5] Y. Huang, X. Duan, Q. Wei, and C. M. Lieber, Science, 291, 630 (2001).

[6] P.A. Smith, C.D. Nordquist, T. N. Jackson, T. S. Mayer, B. R. Martin, J. Mbindyo, and T. E. Mallouk, Appl. Phys. Lett. 77, 1399 (2000).

Synthesis and Characterization of ZnO and PbI_2 Colloidal Nanoparticles

Shin Bowers

Biomedical Engineering, Brown University

NNIN REU Site: Nanoscience at the University of New Mexico
NNIN Principal Investigator: Dr. Marek Osinski, Professor of Electrical and Computer Engineering, Center for High Technology Materials, University of New Mexico
NNIN REU Mentor: Dr. Gennady Smolyakov, Research Asst Professor, Electrical & Computer Engineering, Center for High Technology Materials, University of New Mexico
Contact: shin_bowers@brown.edu, osinski@chtm.unm.edu, gen@chtm.unm.edu

Abstract

Many applications have been found for various nanocrystals. Specifically, zinc oxide (ZnO) can be used for various biomedical applications such as tissue imaging and deoxyribonucleic acid (DNA) detection while lead iodide (PbI_2) can be used as an x-ray detecting nanoscintillator. This project focused on the synthesis of quantum dots which emit in narrow spectral band for subsequent biomedical applications. ZnO was first synthesized by a low temperature colloidal process utilizing a Schlenk line set up. In an attempt to increase the intensity of the photoluminescence (PL) that the ZnO nanoparticles emit, the quantum dots were annealed at various temperatures and time intervals. PbI_2 was also synthesized through a low temperature colloidal process.

In order to characterize the nanoparticles, a spectrofluorometer was used to measure the excitation spectra. Low-temperature photoluminescence was measured using a closed-circuit helium cryostat and a helium-cadmium laser. Tunneling electron microscopy (TEM) and scanning electron microscopy (SEM) were performed to measure the size of the nanoparticles.

Experimental Procedure

ZnO was synthesized through a one-pot low temperature method utilizing a Schlenk line apparatus. First, 25 mL of *m*-xylene (≥ 99.0%, Fluka) and 50 mL of 1-pentanol (≥ 99.0%, Fluka) were added to a three-neck flask. Subsequently, 0.68g of *p*-toluene sulfonic acid (*p*-TSA) (≥ 98.5%, Sigma-Aldrich) was added under the assumption of a decrease of spectral band width and increase of PL intensity [1]. The solution was stirred, and 2.5 g of zinc acetate dihydrate (≥ 99.0%, Fluka) was added to the solution.

Under argon and reflux, the solution was heated for 1 hour and 20 minutes at 130°C and 1 mL aliquots were taken every 20 minutes. The solution was then centrifuged at 4000 rpm in 5 minute cycles with the addition of a 50% ethanol and deionized water stock solution until a white precipitate formed. The precipitate was diluted with ethanol and the solution was placed under vacuum until ZnO powder was obtained.

Annealing measurements for ZnO were conducted with a tube furnace. The ZnO powder was annealed at 200, 300, 400, and 500°C. At each temperature the powder was annealed in three 10 minute cycles. Cryostat measurements were conducted using a cold finger at decreasing temperatures up to 10 K.

PbI_2 was similarly synthesized through a low-temperature one-pot synthesis with a Schlenk line [2]. 100 mg of lead iodide powder (≥ 99.999%, Aldrich) was dissolved in 15 mL of tetrahydrofuran (THF) (≥ 99%, Sigma). The solution was sonicated until the powder was completely dispersed in the THF. The solution was then centrifuged at 4000 rpms in 10 minute cycles until a deep yellow colored solution formed above a precipitate. The deep yellow colored solution was decanted into a three-neck flask.

10 mL of anhydrous methanol was injected into the solution under nitrogen and the solution was stirred at room temperature for 24 hours. 1 mL aliquots were taken at 10 minute, 1, 2, 4, and 8 hour intervals. 1 mg of dodecylamine (≥ 98.0%, Fluka) was added to each aliquot immediately after it was taken. After 24 hours, the amount of solution inside the three-neck flask was measured and dodecylamine was added according to a 1 mg/mL ratio.

Results and Conclusions

ZnO synthesis was highly successful, producing nanoparticles that ranged from 4 to 10 nm. Figure 1 shows a 4 nm sized nanoparticle with parallel lines indicating the presence of a crystalline structure. The PL of the ZnO in Figure 2 shows the band-to-band emission of ZnO located at 380 nm, but also reveals a shoulder mound at longer wavelengths peaking at ~500 nm. In the cryogenic measurements under vacuum, as the temperature decreases, it is possible to see that this shoulder mound decreases in intensity, suggesting the possibility that this mound is caused by solvent-related defects on the surface of the ZnO. The annealing measurements (Figure 2) also showed this shoulder, and the ratio of shoulder to ZnO band-to-band emission decreased until 300°C.

Subsequent increases in temperature resulted in an increasing ratio, until the ZnO band-to-band emission was barely visible at 500°C. The ZnO sample at high annealing temperatures turned a dark charcoal color, indicating the possibility of carbon decomposition, the carbon possibly present from the solvents in the synthesis.

PbI_2 synthesis also proved to be highly successful. Figure 3 indicates that there is a distinct, narrow spectral range emitted from the lead iodide suggesting the presence of nanoparticles. Furthermore, the TEM in Figure 4 shows nano-structures on the range of 4 nm. The three differing parallel line structure present on the PbI_2 particle suggests that the crystal might be pyramidal in structure.

Future Work

Although distinct spectra existed for both ZnO and PbI_2, in order to increase PL intensity and minimize surface defect related PL, the particles will need to be coated. For subsequent biomedical applications, ZnO will need to be made water-soluble and bioconjugated. Water solubility will be achieved through the process of cap exchange, while bioconjugation will be made possible through the attachment of a protein layer. Finally, various tests and characterization methods must be conducted in order to prove the validity of these successive results.

Acknowledgements

I would like to thank Professor Marek Osinski and Dr. Gennady Smolyakov for their continual support and insight; Brian Akins, Tosifa Memon, and Krishnaprasad Sankar for their help with various syntheses; and Nathan Withers for the annealing experiments. Thanks to the National Nanotechnology Infrastructure Network Research Experience for Undergraduates Program, the National Science Foundation and the University of New Mexico for making this research experience possible.

References

[1] Demir, M. M. et al.; "Precipitation of monodisperse ZnO nanocrystals via acid-catalyzed esterification of zinc acetate"; J. Mater. Chem. 28, 2940 (2006).

[2] Finlayson, C. E. et al.; "Highly efficient blue photoluminescence from colloidal lead-iodide nanoparticles"; J. Phys. D-Appl. Phys. 39, 1477 (2006).

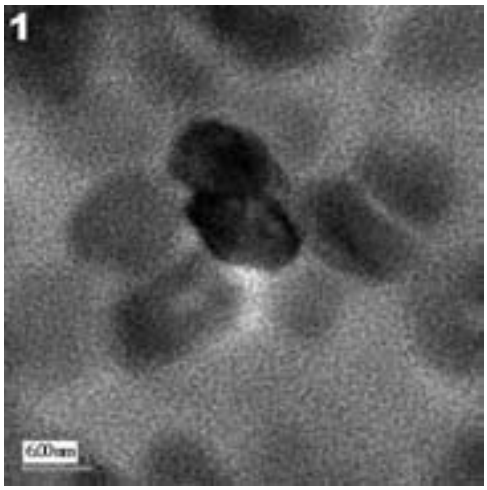

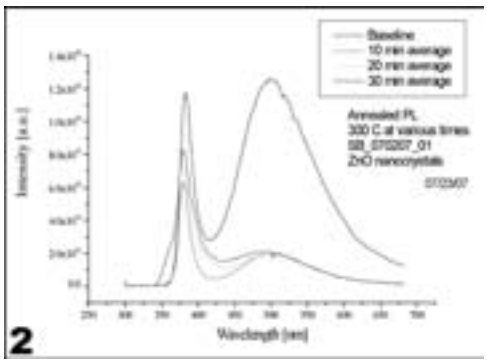

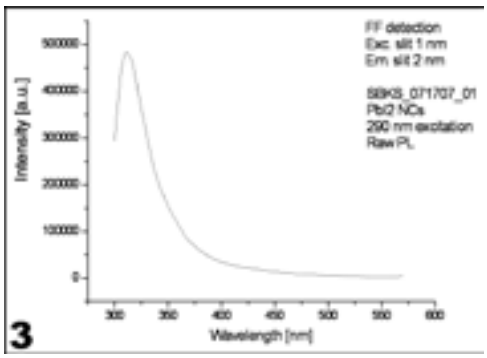

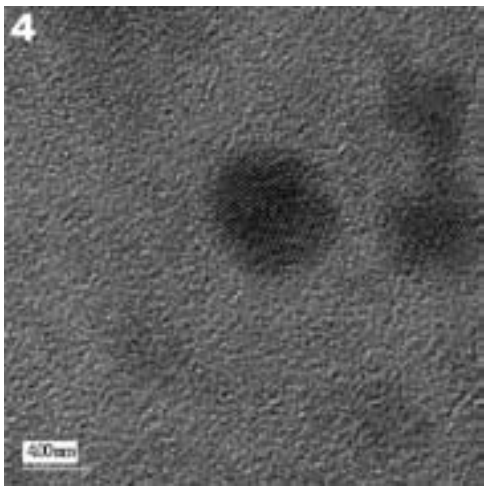

Figure 1, top: TEM image of ZnO nanoparticles.

Figure 2, upper middle: PL of ZnO annealed at 300°C for varying time intervals.

Figure 3, lower middle: PL of PbI_2 nanoparticles at 290 nm excitation.

Figure 4, bottom: TEM of PbI_2 nanoparticles.

Maskless Nanolithography Using an Atomic Force Microscope

Ian Frank

Physics, Pomona College

NNIN REU Site: Center for Nanoscale Systems, Harvard University
NNIN REU Principal Investigator: Prof. Marko Loncar, School of Engineering and Applied Sciences, Harvard University
NNIN REU Mentor: Dr. Jiangdong Deng, Center for Nanoscale Systems, Harvard University
Contact: ian.frank@pomona.edu loncar@seas.harvard.edu jdeng@cns.fas.harvard.edu

Abstract

We demonstrated possible applications for nanolithography using an atomic force microscope (AFM). We were able to anodically produce lines of aluminum oxide (AlO) on a thermally evaporated aluminum thin film by scanning the microscope tip across the substrate while applying a bias. Line widths < 70 nm were routinely obtained. A wet etch with phosphoric acid was shown to selectively etch the aluminum; leaving behind the aluminum oxide pattern creating what we hope will be an effective mask for reactive ion etching. We also demonstrated that this lithography method can be used to work with nanowires by drawing patterns near to and on top of zinc-oxide nanowires that had been coated with aluminum.

Introduction

Atomic force microscopy (AFM) nanolithography has been around for some time in various forms. The simplest method is merely scratching the surface of a substrate with the AFM tip. A more reproducible method, used in this work, is to create a bias between the tip and the surface while the AFM is in alternating current (AC) mode [1].

In AC mode, the AFM tip on the end of a cantilever is driven up and down at high-frequency and is not in contact with the surface, although it is within 5-10 nm of the surface. The result is an extremely high electric field between the sample and the tip which, combined with the water vapor in the air, anodically oxidizes certain surfaces. By optimizing the tip speed relative to the sample, the tip bias, and the tip-surface distance line widths as low as 10 nm on Al substrates have been reported [2].

AFM nanolithography is desirable for a number of reasons. Perhaps most importantly, the technology is far less expensive and more available than electron-beam lithography (EBL) and focused ion beam (FIB) milling technology which are the more traditional methods of achieving features of similar dimension. Beyond cost issues, AFM lithography is also advantageous over EBL and FIB because of its speed and relative simplicity.

Procedure

Our work was based mostly on the oxidation of aluminum thin films, though we made a few attempts to perform oxidation of silver layers as well. An important first step in achieving controlled oxidation on an aluminum substrate is to have as smooth a surface as possible. We optimized the operation conditions of thermal evaporation (TE) and yielded smooth Al surface with roughness less than 2 nm. Beyond having a smooth surface, we established that the substrate must be treated by exposure to oxygen plasma immediately prior to the lithography. This treatment lasts for only a few hours and was essential for the success of the lithography. During the actual lithography, the best indicator of success was the tip being pulled into the surface. This could be easily monitored by watching the phase output of the AFM. If the phase dropped down into the attractive regime then oxidation of the substrate was almost certainly occurring.

Our Asylum Research AFM's internal power supply is limited to ± 10V while literature suggests that the best results were obtained in the -12 to -30 V region [2]. Subsequently we built a circuit that would allow the AFM to turn an external power supply on and off at the appropriate times during the lithography. Once this circuit was in place, we noticed significant improvement in the contrast and quality of the oxidation lines we were able to produce on the aluminum.

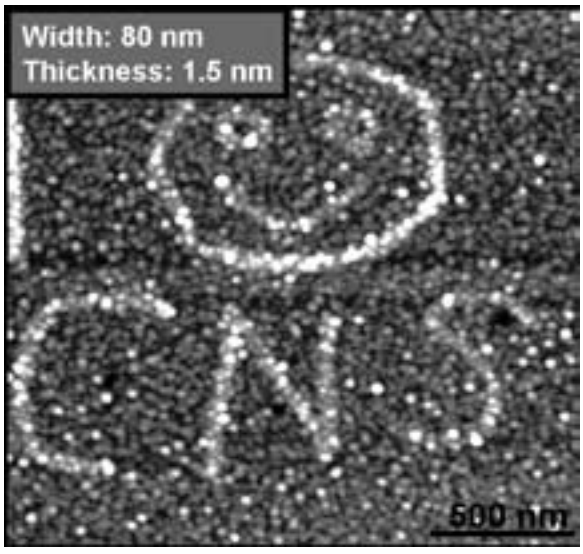

Figure 1

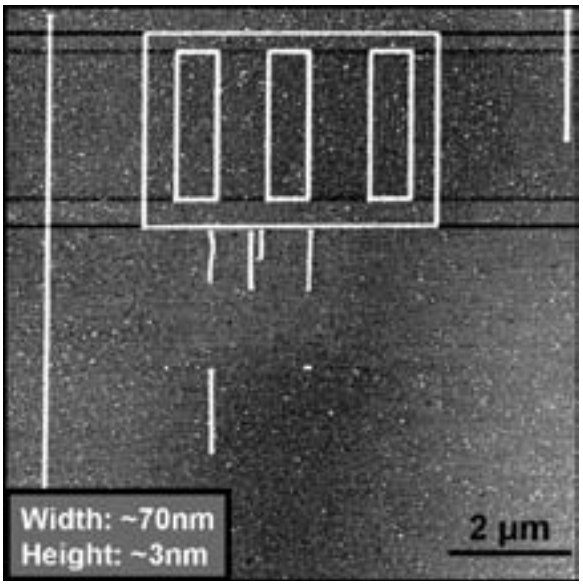

Figure 2

Figure 1 is an example of an oxide pattern drawn at -10 V. As you can see, the lines, while visible, are not solid and the pattern of the aluminum grains below are clearly visible. Figure 2 is an example of patterns drawn at -14 V with the help of the external power. These lines are more robust and solid.

Applications

Once oxidized, patterns were written on the aluminum substrate; a method for selectively removing either the aluminum or the oxide was required. This step was equivalent to the mask developing step in EBL for example. This would then allow the pattern to be transferred to the sample below the mask.

It was reported that phosphoric acid, diluted in deionized (DI) water, would very selectively etch the aluminum, leaving behind the aluminum oxide [1]. Figure 3 shows SEM images of three oxide lines on an aluminum thin film before and after the substrate was etched in phosphoric acid. As it can be seen, the contrast improves considerably in the right hand image as the lines go from being 3 nm thick to over 10 nm thick.

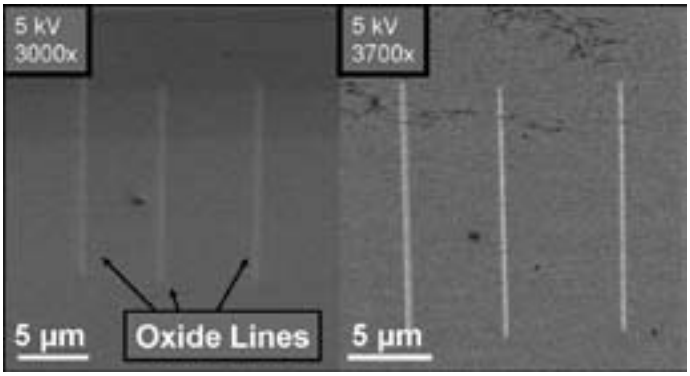

Figure 3

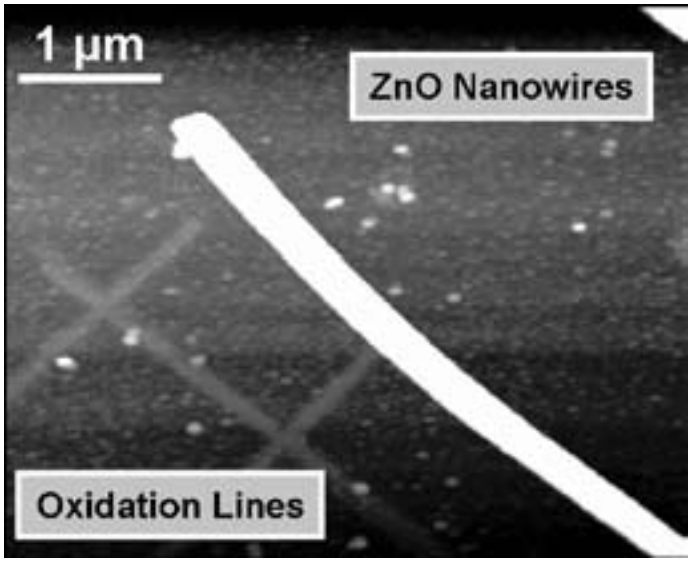

Figure 4

Figure 4 is an AFM image showing an example of oxide lines drawn around a zinc-oxide nanowire; demonstrating that this lithography technique can be used to create structures on and around nanowires. The dominating feature in the figure is the nanowire which is approximately 200 nm wide and 100 nm high. We believe that there is oxidation on top of the nanowire which is coated with aluminum; however, it is impossible to know with certainty due to the surface roughness and the color scale of the image.

Conclusions and Future Work

We demonstrated that AFM nanolithography can be a useful tool for cheaply and quickly creating RIE masks, as well as creating structures that will allow easier interaction with nanowires. We routinely achieved line widths < 70 nm, a number which promises to decrease as the process is optimized. Our future plans include using these demonstrated techniques to build working devices in the field of nano-optics. We are also attempting this technique on surfaces other than aluminum to allow for more diversity in the available applications.

Acknowledgements

I would like to thank Marko Loncar and J.D. Deng for their mentoring, Jim MacArthur for his help with electronic circuitry, and the NSF, National Nanotechnology Infrastructure Network Research Experience for Undergraduates Program and Center for Nanoscale Systems for their support.

References

[1] Cochran, P., NNIN REU Research Accomplishments, 34 (2004).

[2] Davis, Z.J. et Al. , Ultramicroscopy 97, 467 (2003).

Photo-CVD Coating of Nanoparticles with Silicon Dioxide

Brayden Glad

Mechanical Engineering and Materials Science, Duke University

NNIN REU Site: Minnesota Nanotechnology Cluster, University of Minnesota-Twin Cities
NNIN REU Principal Investigator: Dr. Steven Girshick, Mechanical Engineering, University of Minnesota-Twin Cities
NNIN REU Mentor: Adam Boies, Mechanical Engineering, University of Minnesota-Twin Cities
Contact: beg3@duke.edu, slg@umn.edu, aboies@me.umn.edu

Abstract

Extending previous research [1-6], the ability to coat nanoparticles with silicon dioxide (SiO_2) using a xenon (Xe_2) excimer lamp at standard atmospheric temperature and pressure was demonstrated using a photo-chemical vapor deposition (CVD) process. Sodium chloride (NaCl) was used as at the core particle, and tetraethyl orthosilicate (TEOS) in concentrations up to 0.70 sccm was provided as the SiO_2 precursor. NaCl particles of approximately 40-50 nm diameter received coatings of repeatable thickness after an exposure time of approximately 1 second in 172 nm light. The ability to control coating thickness by modifying TEOS flow rate was considered, and coating thickness was shown to increase with TEOS flow rate up to a maximum thickness of up to 2.0 nm in these conditions. Characterization showed the process provided a practically uniform covering of amorphous silica on approximately spherical particles.

Procedure

To verify the coating of particles, a straightforward tandem differential mobility analyzer setup (TDMA) was used. Sodium chloride, atomized with a nitrogen carrier gas, was dried and size selected using a differential mobility analyzer (DMA). Extra flow was vented to assure 1.0 slm through the DMA. The flow was mixed with varying quantities of tetraethyl orthosilicate (TEOS) with the appropriate amount of carrier nitrogen to maintain vapor pressure at the ambient 21°C.

The mixture then received 50 mW/cm^2 of 172 nm radiation from a Ushio UER20H-172C excimer lamp. Intensity was periodically verified using a Coherent Fieldmate laser power meter. A particle residence time in the illumination chamber of between 1.7-2.3 s was derived from an Ansys 10.0 flow simulation.

After receiving radiation, the aerosol passed through a charger, then a second DMA before entering a TSI 3025A condensation particle counter. Stepping through a range of voltages, the second DMA passed different mobility diameters to the counter, and provided a complete distribution of particles in the flow. Controls were created using the same setup with the lamp off, with TEOS varying between none and 0.70 sccm. To capture particles for characterization, electrostatic precipitation was used, with a voltage of 2.5 kV. For each collection, a standard Cu TEM grid was attached to the positive terminal of the precipitator. Additionally, for each collection used for the FTIR analysis, an uncharged stainless steel screen was placed directly across the flow path of the particles.

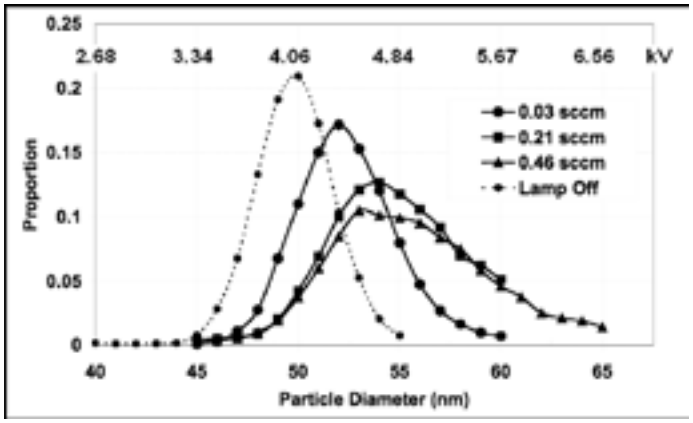

Figure 1: Mobility diameter by precursor quantity.

Results

The TDMA data demonstrate a size increase of the original particles as a result of the particle processing. Further TEM analysis indicates that the increased particle diameter is due to a coating process occurring as a result of photo-CVD. Both 40 and 50 nm particles experienced coating, however, most analysis was conducted on 50 nm particles because the atomizer produced a larger sample at that size.

In Figure 1, 50 nm particle results generated from the averages of five trials are presented. With increasing TEOS concentration, the particle coating thickness (half the difference between final and initial sizes) increased until a probable saturation thickness of about 2.0 nm. Thickness variation was approximately normally distributed, with more variance for larger TEOS flow rates. Tests without NaCl yielded minimal particles, implying that no self-nucleation of TEOS occurred.

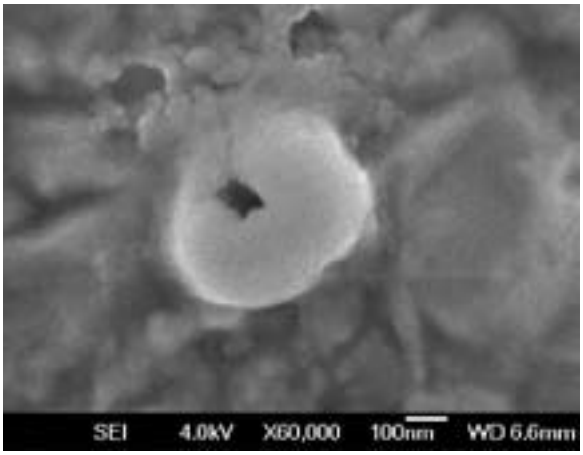

Figure 2: SEM image of an accumulation of coated nanoparticles.

Figure 2 displays a cluster of approximately spherical coated nanoparticles. There was evidence of some agglomeration, but individual particles of the appropriate size and consistent shape were clearly identifiable. This image was captured using a JEOL 6500 field transmission scanning electron microscope, operating with an excitation voltage of 4.0 kV, and a working distance of 6.6 mm. Figure 3, captured with a JEOL 1210 transmission electron microscope, clearly illustrates coatings of approximately uniform thickness despite a variety of vaguely spherical base particle shapes.

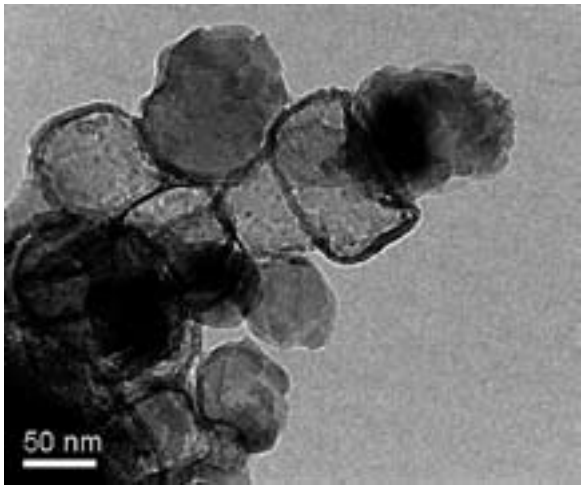

Figure 3: TEM image of nanoparticles and coatings.

X-ray diffraction characterization was conducted using a Bruker-AXS D5005, with a step size of 0.08 degrees 2-0 and 6.0 s step duration. Samples tested were polydisperse coated and uncoated particles, because no DMA was used. The results were analyzed using Jade 7.0, and no evidence of SiO_2 crystallization was found. Fourier-transform infrared radiation results were obtained with a Magma-IR 550 spectrometer.

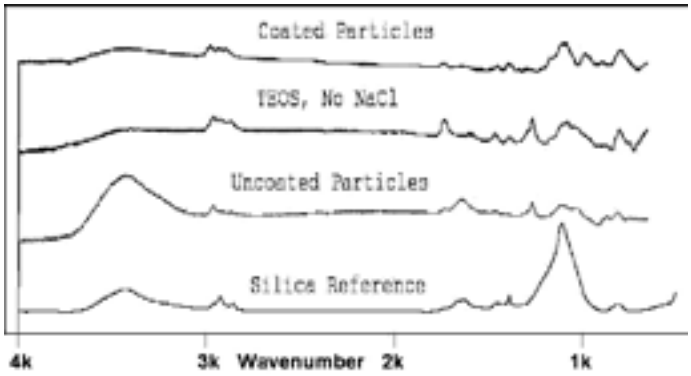

Figure 4: FTIR results.

Step size was 1 wave number with 30 samples per step, and the data was analyzed with Essential FTIR 1.20. Figure 4 shows that the difference between the coated particles and the uncoated control is only a few peaks, but each of those match a peak for silica, again providing strong evidence of coating. Particularly noticeable is the Si-O-Si asymmetric stretching peak at ~ 1120 wave number [5]. These silica peaks are more clearly pronounced in the coated particle data than the TEOS alone, demonstrating that the NaCl base contributes to silica formation.

Acknowledgements

We thank the Nitto Denko Corporation, the National Nanotechnology Infrastructure Network Research Experience for Undergraduates, and the National Science Foundation for material support. For their assistance on the project, Yuanqing He and Jami Hafiz also deserve thanks. Most importantly, I personally thank Dr. Steven Girshick, principal investigator, and Adam Boies, my mentor, for providing this opportunity.

References

[1] Konuma, M; Film Deposition by Plasma Techniques; Springer-Verlag, Berlin (1992).

[2] Kurosawa, K, et al.; "Silica Film Preparation by Chemical Vapor Deposition using Vacuum Ultraviolet Excimer Lamps"; Applied Surface Science, Vol. 168, pp. 37-40 (2000).

[3] Lan, W, et al,; "Reaction Mechanism of Mercury-Sensitized Photochemical Vapor Deposited Silicon Oxide"; Japanese Journal of Applied Physics, Vol. 32 pp. 150-154 (1993).

[4] Takezoe, N, et al.; "SiO_2 Thin Film Preparation using Dielectric Barrier Discharge-Driven Excimer Lamps"; Applied Surface Science, Vols. 138–139, pp. 340–343 (1999).

[5] Yokotani, A, et al.; "Analysis of the Photochemical Reaction on the Surface for Room Temperature Deposition of SiO_2 Thin Films by Photo-CVD using Vacuum Ultraviolet Light"; Japanese Journal of Applied Physics, Vol. 44, pp. 1019–1021 (2005).

[6] Zhang, B; "Growth of coatings on nanoparticles by photoinduced chemical vapor deposition"; Journal of Nanoparticle Research, online first, DOI: 10.1007/s11051-007-9238-2.

Controlling Fluid Flow to Conducting Polymer Biosensors Using Surface Modification

Thomas Gobert

Electrical and Electronic Engineering, McNeese State University

NNIN REU Site: Cornell NanoScale Science & Technology Facility, Cornell University
NNIN REU Principal Investigator: Prof. George Malliaras, Materials Science and Engineering, Cornell University
NNIN REU Mentor: John Defranco, Applied and Engineering Physics, Cornell University
Contact: t_gobert@yahoo.com, ggm1@cornell.edu, jad93@cornell.edu

Abstract

Fluoroctatrichlorosilane or FOTS, which is a hydrophobic monolayer (contact angle = 110°) that is used to modify substrate surfaces, is described for use in biosensor arrays. By lithographically patterning FOTS into arrays of hydrophilic channels with a hydrophobic background, confined passageways for fluid flow are created which allows a liquid sample to reach the sensing section of the substrate with low flow resistance. The sensor incorporates organic electrochemical transistors that are designed using poly(3,4-ethylenedioxythiophene) poly(styrenesulfonate) or PEDOT:PSS as the active layers for the gate and source-drain connections. This active layer represents the conducting polymer which interacts with the enzymatic ionic process and lowers the drain current depending on the concentration. The placement of deferent enzymes on each sensor in the array is used to measure the concentration of each unique parameter in the solution.

Introduction

Biosensors are used to detect and sense various materials, gases, and chemical compounds in an environment. The organic electrochemical biosensor that is used in this experiment senses for analytes in a chemical solution. Examples of such analytes are lactose, glucose, etc. A distribution array in order for different biosensors to sense unique analytes on the same platform has been designed using surface treatment techniques. This will enable users to detect multiple concentration levels at once and have micro-molar precision.

In previous designs, polydimethylsiloxane (PDMS) was used to control the fluid flow because of its barrier characteristics and simple fabrication methods. A technique that has been developed was to use a nanoscale monolayer as a surface treatment. This monolayer created a hydrophobic surface that could be placed anywhere on the surface.

Fabrication

The fabrication process consisted of developing two separate masks. The first mask had the fluidic pattern and the second mask had the source, drain, and gate placements for the multiple sensing sections. In order to fabricate the PEDOT:PSS connections, parylene has been coated on the silicon oxide wafer. The photolithographic process consisted of spinning SPR220-3.0 photoresist on the substrate and exposing it under the HTG System III-HR contact aligner for approximately 6 seconds. Before developing the substrate, it was placed in a 115°C heating plate for approx. 90 seconds. The substrate was developed using 30 MIF and then placed in the PlasmaTherm 72.

This process caused the exposed areas of the wafer to be etched away so that placement of the conducting polymer (PEDOT:PSS) could be placed. Acetone and IPA were used to rinse off the remaining photoresist so that the parylene could be the only layer left on the wafer. Spin-coating the PEDOT:PSS on the wafer allowed the polymer to fill in the patterns on the wafer. The parylene was then lifted off of the substrate by a peeling technique which only left the conducting layer. The substrate was then placed in a 120°C oven for 90 minutes. This process fabricated the source, drain, and gate onto the wafer.

The next process consisted of fabricating the distribution array of fluidic channels on the previously fabricated wafer. Again using the photo-lithographic techniques, the second mask was used to expose the fluidic channel regions onto the wafer. The wafer was developed using 300MIF and then was placed in the molecular vapor deposition tool, where it deposited a 5 nm hydrophobic layer of FOTS. Acetone and IPA was then used to remove the excess photoresist leaving only the outlined pattern and the connections hydrophilic.

Experimental Procedure

The substrates were tested by injected fluid via a syringe that held 40 ml. The fluidic channels were 3 mm in width and 5 mm in length. The fluid that was used to test the flow was de-ionized water. The water reached the testing sections effectively and enough fluid remained in the sensing area to test from. The PEDOT:PSS strips were tested for conductivity by using a voltmeter for ohmic resistance. By depositing an analyte as

the dielectric between the gate and source-drain electrodes, the biosensor was tested. Varying the gate voltage proved that the biosensor was functional because of the output drain current.

Results and Conclusions

The design enabled the surface-controlled fluid to flow with low resistance. Crosstalk between the channels was eliminated because of the hydrophobic gaps between the channels and the sensing sections. The multiple organic electro-chemical transistors were operable from the numerous fabrication processes and displayed functional voltage biasing.

Acknowledgements

I would like to thank George Malliaras, J. A. Defranco, Melanie-Claire Mallison, and Lynn Rathbun. Special thanks to the Intel Foundation, National Nanotechnology Infrastructure Network Research Experience for Undergraduates Program, and National Science Foundation for funding.

References

[1] J.T. Mabeck, J. A. Defranco, D. A. Bernards, and G. G. Malliaras, Applied Physics Letters 87, 013503 (2005).

[2] J. A. Defranco, B. S. Schmidt, M. Lipson, G. G. Malliaras, Organic Electronics 7 (2006) 22-28.

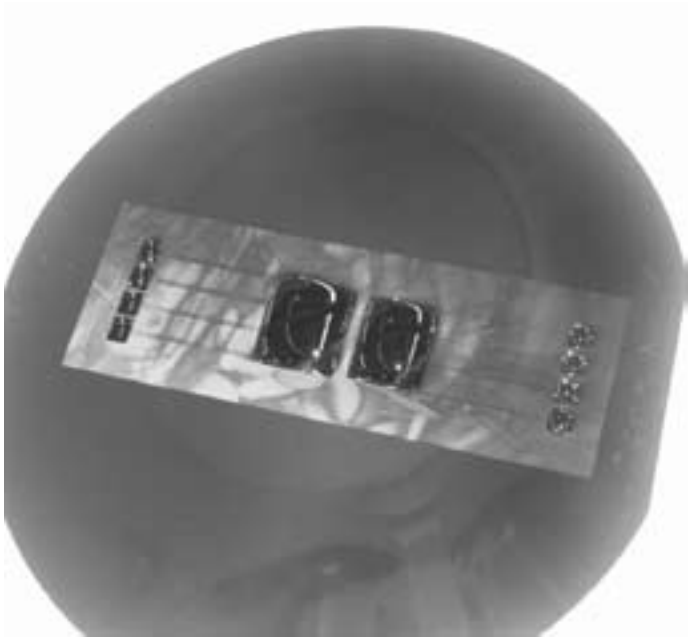

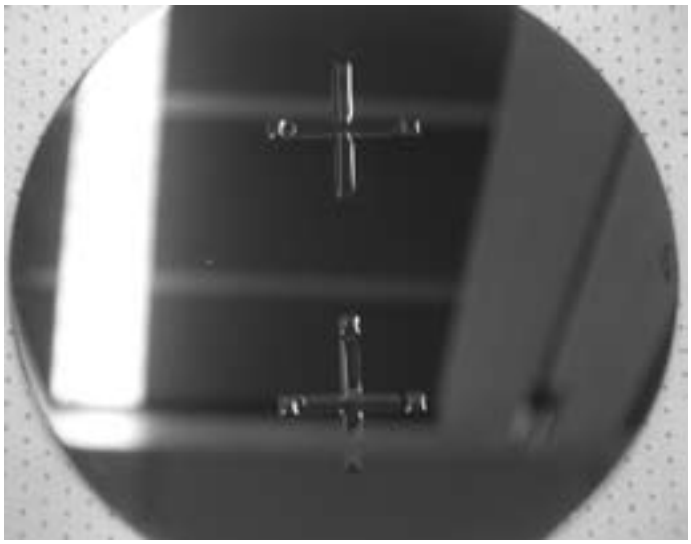

Figure 1, top: Shows early design of fabricated substrate with 100 µm channels. The wafer has FOTS monolayer present which prohibits water-based solutions from adapting to the surface. The lightest area is covered with FOTS and the remaining is hydrophilic.

Figure 2, bottom: The design that worked best with the FOTS monolayer incorporated hydrophobic gaps that eliminated crosstalk between devices and the channel width allows fluid to flow with low resistance.

Synthesis of Palladium Nanoparticles for Methanol Steam Reforming Catalyst

Michael P. Johnson
Chemistry, Dana College

NNIN REU Site: Nanoscience at the University of New Mexico
NNIN REU Principal Investigator: Dr. Abhaya Datye, Center for Microengineered Materials, University of New Mexico
NNIN REU Mentor: Patrick D. Burton, Center for Microengineered Materials, University of New Mexico
Contact: mpjohnso@dana.edu, pburton@unm.edu, datye@unm.edu

Introduction

There is a need for energy in remote corners of the world. An energy storage technology is needed that can last longer than current batteries and is easily transportable. One possibility is to use hydrogen to power a fuel cell. However, the trouble with hydrogen is that it is hard to store and is also highly volatile. Our approach to hydrogen production and storage is through methanol steam reforming (MSR). Steam and methanol produce three moles of hydrogen and one mole of carbon dioxide. Methanol offers a high conversion rate and produces less by-products than other hydrocarbon fuels. The challenge is to make stable catalysts that work at low temperatures.

Current MSR catalysts are made of a copper/zinc oxide alloy and are active at 230ºC. The problem is that these catalysts deactivate quickly. A palladium/zinc oxide (Pd/ZnO) catalyst offers the possibility of high methanol conversion over a longer time but is active at a higher temperatures and a greater mass of catalyst. Since catalysis is a surface phenomenon, the Pd/ZnO alloy can be made more active by increasing the surface area. The optimal particle diameter is 6 nm.

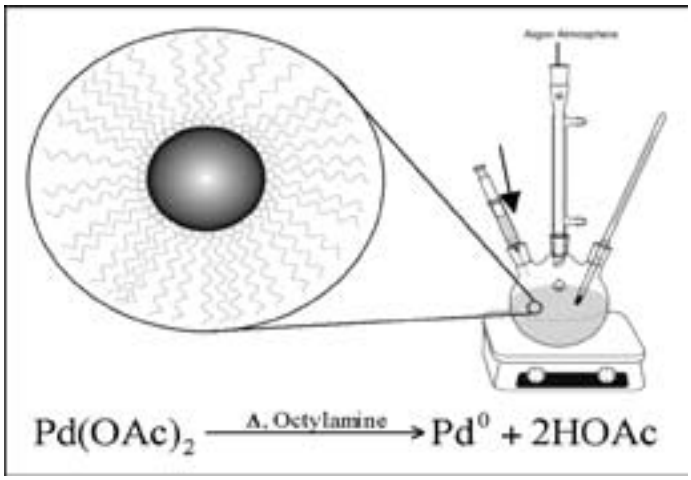

Figure 1: Solution precipitation.

Experimental Procedure

Palladium acetate was reduced with octylamine in hexadecanediol at 270ºC for 30 minutes. As the organometallc decomposed, Pd metal precipitated out of solution. During this process, the amines coated the surface of the Pd to protect against interparticle agglomeration. The Pd nanoparticles were washed in chloroform and methanol to remove excess amine ligands. The final product was a suspension of black nanoparticles in chloroform. The solution precipitation route was effective in synthesizing nanoparticles of Pd of ~ 4.5 nm in all samples as transmission electron microscopy (TEM) and scanning electron microscopy (SEM) reveal.

Once the Pd particles are synthesized, they were impregnated on a ZnO support to make a catalyst.

In order to preserve the morphology of the ZnO powder, it was necessary to use an organic medium rather than an acidic environment, as other methods use. The method for attaching the Pd to ZnO was to perform a ligand replacement on the Pd. 12-mercaptododecanoic acid was mixed into the suspension of nanoparticles for 10 minutes. A theoretical amount of 10% of the thiol/acid ligand was added based on the mass of the nanoparticles. Infrared spectroscopy (IR) showed that a ligand substitution did take place. The theory of ligand substitution is that the thiol produces a stronger bond with Pd than an amine and the acid tail will bond with the surface of the ZnO. Pd will not agglomerate after amines are removed to reveal the Pd surface, because the particles will be anchored to the ZnO.

Problems in the synthesis came when depositing the Pd onto the ZnO surface. Several dispersion techniques were tested including incipient wetness, calcination at 80ºC, mixing ZnO into the suspension, and a control of reducing palladium acetate on ZnO. (This is how the current Pd/ZnO alloys are formed.) The nanoparticles were prone to clump and form clusters rather than spread evenly onto the surface of ZnO.

Characterization

Pd decorated ZnO was partially formed. Spectroscopy measurements showed that ligand exchange took place. IR showed correct octylamine stretches before ligand replacement and clearly showed carboxylic acid stretches of the 12-mercaptododecanoic

acid after. X-ray diffraction showed that we had two crystalline phases of Pd and ZnO. Energy dispersive x-ray spectroscopy confirmed the composition.

Methanol is also capable of decomposing into hydrogen and carbon monoxide. Carbon monoxide (CO) binds to the Pd and deactivates the catalyst. However, this is not a problem as CO oxidation runs showed that the catalyst had a high selectivity to carbon dioxide (CO_2) over CO at reaction temperatures.

MSR was then performed on the catalysts. About 200 mg of catalyst was used in MSR and the average conversion was taken over four fifteen minute runs at 250ºC. The control Pd/ZnO performed better because of the lack of ligands prohibiting the methanol interacting with the surface of the palladium. The best novel catalyst (Figure 2) had a methanol conversion of 41% and 35% selectivity towards CO_2. The best control catalyst was the 10% Pd:ZnO with 100% conversion and 87% selectivity.

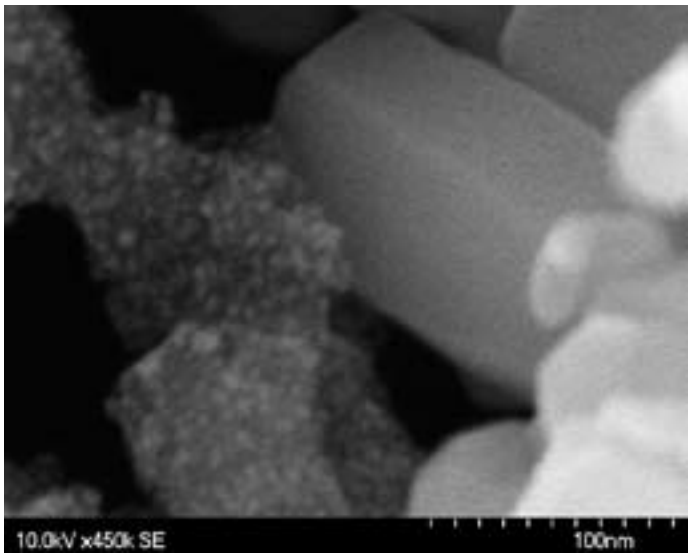

Figure 2: Pd/ZnO-incipient wetness.

Results

In this work, we have shown that it is possible to synthesize a catalyst from components of ligand-capped metal nanoparticles and metal oxide powders. The catalytic activity demonstrated by our catalysts using CO oxidation and MSR was low. The activity was hindered by residual ligands on the particles, resulting in a poor nanoparticle dispersion and overall powder coverage, as illustrated by TEM and SEM images.

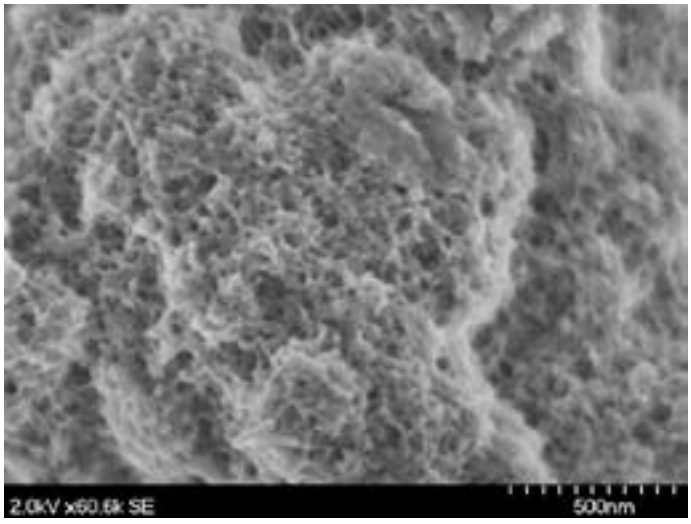

Figure 3: Pd/ZnO-ZnO doping.

Future Work

To improve our catalyst, it is necessary to enhance the particle dispersion over the oxide surface and remove excess ligands. Possible ways to coat the ZnO surface might be to funtionalize the surface before adding nanoparticles or testing different ligands. Alternative deposition techniques also might need to be discovered. Even after coating with Pd, the amines need to be removed before any accurate MSR testing can occur. Possible techniques include an oxygen plasma etching process to gently remove excess amines. Although not yet perfect, this synthesis method offers a very promising way to collect hydrogen for fuel in the future.

Sample (dispersion technique)	Methanol Conversion	Selectivity
2% Pd/ZnO (reduced on surface)	79%	90%
5% Pd/ZnO (reduced on surface)	5%	39%
8% Pd/ZnO (reduced on surface)	81%	95%
10% Pd/ZnO (reduced on surface)	100%	87%
15% Pd/ZnO (reduced on surface)	83%	96%
20% Pd/ZnO (reduced on surface)	75%	98%
Amine Coated Pd NPs (incipient wetness)	33%	53%
Thiol replaced Pd NPs (incipient wetness)	41%	35%
Thiol replaced Pd NPs (ZnO soaked in NP solution)	2%	37%

Figure 4: MSR conversion and selectivity.

Acknowledgments

I would like to send a personal thank-you to Patrick Burton and Timothy Boyle of the Advanced Materials Laboratory. I would also like to thank the National Science Foundation and the National Nanotechnology Infrastructure Network Research Experience for Undergraduates Program for granting me this amazing experience.

Nanoimprinted Plasmonic Nanoparticles for Biosensor Applications

Emma Kamnang

Electrical Engineering, Corning Community College

NNIN REU Site: Michigan Nanofabrication Facility, University of Michigan Ann Arbor
NNIN REU Principal Investigator: Professor L. Jay Guo, Applied Physics; Engr. & Computer Science, University of Michigan
NNIN REU Mentor: Brandon D. Lucas, Applied Physics, University of Michigan
Contact: ekamnang@corning-cc.edu, emmacarole87@yahoo.com, guo@eecs.umich.edu, bdlucas@umich.edu

Abstract

Localized surface plasmon resonance (LSPR), free-electron density oscillations found in gold (Au) and silver (Ag) nanoparticle (NP) systems, has been studied extensively over the last decade in part because of the NP's ability to behave as nanoscopic transduction elements. In this study, metallic nanoparticle arrays (NPAs) were fabricated using the mold-based nanoimprint lithography (NIL) technique. The NIL approach, compared to other methods, allowed the complete control of the fabrication of nanopatterns possessing different sizes, shapes and interparticle spacing on a variety of substrates. The ability of these NPAs to transduce changes in their dielectric environment was exhibited through a controlled study using electron-beam deposited silicon dioxide (SiO_2). Additionally, the ability of these plasmonic NPAs to detect biological interactions was demonstrated using a high-affinity biotinstreptavidin model system.

Introduction

Surface plasmon resonance (SPR) biosensors have been utilized extensively to study biological interactions by monitoring changes in the resonance condition (i.e. critical angle and reflectance) of a suitably modified metal film. Similarly, its nanoparticle (NP) system analog known as localized surface plasmon resonance (LSPR) can be monitored using UV-Vis spectroscopy to transduce changes near the NP surface. These changes result in shifts of the resonance wavelength that is characterized by enhanced absorption and scattering of the NP system. Therefore, a suitably modified NP system offers the ability to also detect bimolecular interactions with commercially available spectroscopic systems.

Nanoparticle Array Fabrication

Glass substrates were first cleaned in a piranha solution, thoroughly rinsed with deionized water and dried using nitrogen (N_2). Nanoimprint resist was spin cast onto the substrates to achieve the appropriate film thickness and baked on a hot plate to remove residual solvent. Imprinting was performed by heating the mold and substrate assembly above the resist glass transition temperature while in the imprint chamber, followed by an increase in the chamber pressure for approximately 5 minutes. The mold-substrate assembly was then cooled and separated to yield an imprinted pattern as shown in Figure 1. The final NP (Figure 1) was achieved by residual layer removal using oxygen (O_2) plasma reactive-ion etching (RIE), and Au electron-beam evaporation to the desired thickness and lift-off.

Experimental Methods

Extinction measurements of our fabricated NP system were accomplished through UV-Vis spectroscopy using a system comprised of an inverted microscope (Nikon TE300) and miniature spectrometer (Ocean Optics HR4000). In order to ascertain the distance-dependent dielectric response of Au NPAs possessing different height characteristics (40 nm; 60 nm; 80 nm),

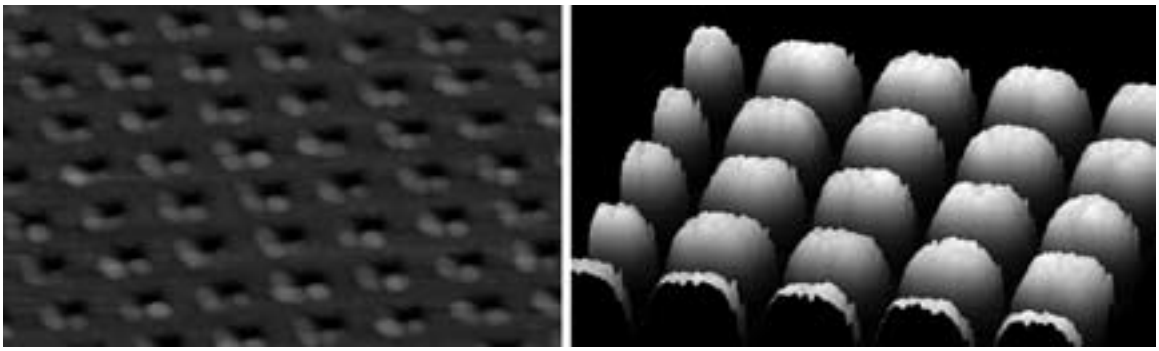

Figure 1: AFM images of imprinted sample and Au NPA.

evaporation of SiO_2 was performed to modify the dielectric environment of the NPA in a controlled manner. After ascertaining the initial resonance wavelength of the NPAs in ambient, extinction measurements were performed for multiple SiO_2 layer depositions on each NPA, iteratively.

Next, a Au NPA possessing a height of 40 nm was used to detect the specific binding interaction of a biotin-streptavidin system. This was accomplished by biotinylating the NPA through overnight incubation in a commercially available biotin-thiol self-assembled monolayer. The sample was incorporated into the experimental setup with a custom made flow cell that allowed increasing concentrations of streptavidin to flow across the biotinylated NPA surface using a peristaltic pump. Changes in LPR were acquired in real-time using data acquisition software. A standard commercially available SPR system was used as a control for the biological experiment.

Experimental Results

Figure 2 shows the resulting resonance shift due to changes in the SiO_2 layer thickness. It was found that the resonance peak amplitude, width and wavelength all increase with increasing SiO_2 layer thickness. Additionally, the 40 nm NPA was found to be the most sensitive to the SiO_2 layer thickness. All NPA systems also show a reduction in sensitivity as the oxide layer increases, and approach a saturated response. This demonstrates the ability of these NPAs to detect changes that occur only in the surrounding nano-environment. Figure 3 shows the ability of the NPAs to detect and monitor in real-time the specific binding of the biotinstreptavidin system. Each exposure of the biotinylated NPA to increasing streptavidin concentrations, followed by a wash in phosphate buffered solution to remove unbound streptavidin, were clearly observed for both the LSPR and SPR systems. The saturation of biotin binding sites with streptavidin was clearly observed through the saturated LSPR response which occurred much faster and at lower concentrations than found in the SPR system.

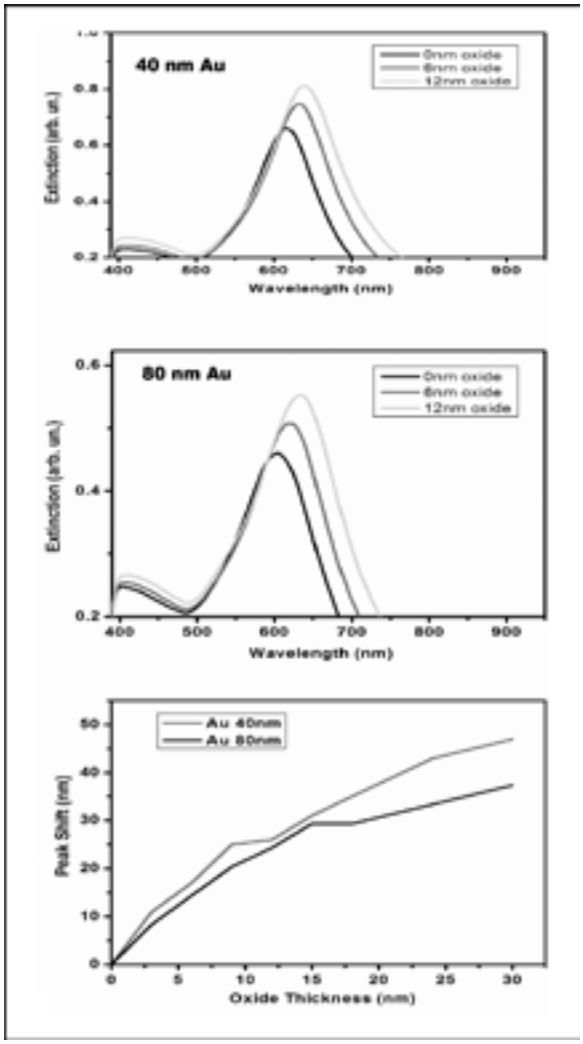

Figure 2: SiO_2 dielectric layer testing.

Conclusions

The ability of Au NPAs to detect changes in the local dielectric was exhibited using electron-beam evaporation of SiO_2. An increase in oxide film thickness caused an increase in the amplitude, width and wavelength of the LSPR. Shorter Au NPA constructs were found to be more sensitive to increases in oxide layer thickness. Additionally, all NPAs exhibited a reduction in their dielectric sensitivity with increasing oxide layer thickness and approached saturation. The relevance of these NPAs to biosensor applications was demonstrated through the detection of specific binding in a biotin-streptavidin system.

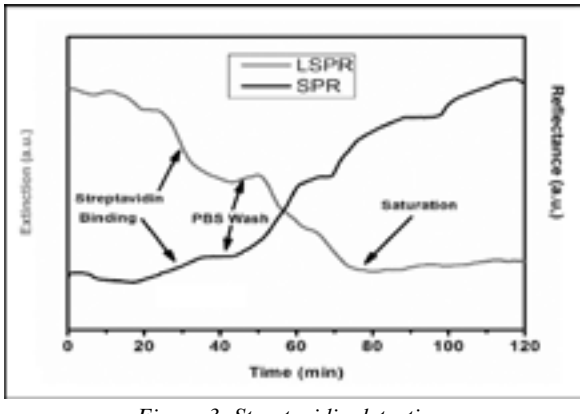

Figure 3: Streptavidin detection.

Acknowledgements

I would like to thank the National Science Foundation (NSF), Intel Foundation, Professor L. Jay Guo, Brandon Lucas, Dr. Vladimir Chegel, Dr. Sandrine Martin, Prof. Guo's research group, Michigan Nanofabrication Facility staff members, the National Nanotechnology Infrastructure Network Research Experiences for Undergraduates, and fellow NNIN REU 2007 interns at the MNF site for their help and support. Also, I would like to thank Professor Lawrence Josbeno for introducing me to the program.

Use of Engineered Proteins for Organization of Nanostructures

Sarah Lee

Chemistry, Brigham Young University-Idaho

NNIN REU Site: Center for Nanotechnology, University of Washington
NNIN REU Principal Investigator: Beth A. Traxler, Microbiology, University of Washington
NNIN REU Mentors: Eliora Gachelet and Ruth Hall, Microbiology, University of Washington
Contact: lee04003@byui.edu, btraxler@u.washington.edu, gachelet@u.washington.edu

Abstract

The *Escherichia coli lac* repressor (LacI) is a deoxyribonucleic acid (DNA)-binding protein that regulates the production of proteins involved in lactose metabolism. Permissive sites within LacI have been previously identified, where short peptide sequences can be inserted without affecting the normal function of the protein. The sequence for the inorganic silica binding motif, QBP3, was inserted into a permissive site at residue 338 of the *E. coli lac* repressor, endowing LacI with the ability to bind both DNA and inorganic silica. After PCR screening for the QBP3 insert, six candidates were sequenced. Two were chosen for continued characterization. Western blot analysis of these constructs showed good protein expression, and β-galactosidase assays indicated LacI clones maintained normal function. The constructs showed some binding to fine silica and minimal binding to coarse silica. These analyses suggest the insertion at residue 338 binds less favorably to silica than the previously isolated QBP3 insertion at residue 317. Engineered proteins like these, that bind both DNA and inorganic compounds, can be utilized to arrange nanostructures in complex predictable patterns, using DNA as a scaffold.

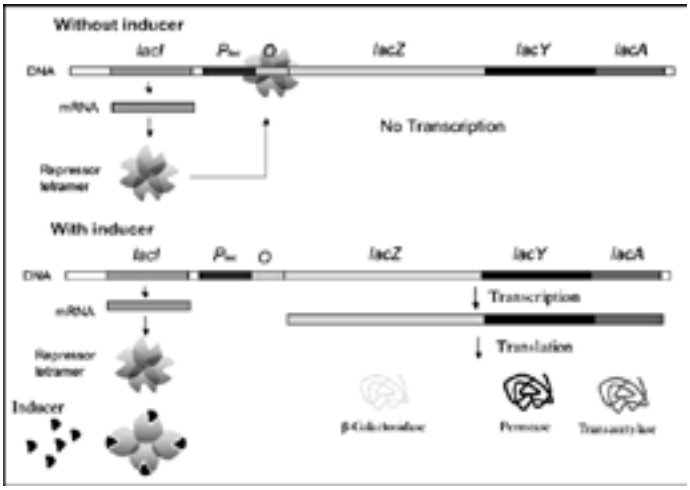

Figure 1: Diagram describing the function of the lac repressor (LacI).

Introduction

The expression of proteins involved in lactose metabolism in *Escherichia coli* are regulated by the DNA-binding protein *lac* repressor (LacI). LacI normally functions as a tetramer which binds to the *lac* operator (Figure 1). RNA polymerase binding is inhibited, repressing lac transcription and protein production. In the presence of lactose, allolactose binds to the tetramer inducing a conformational change. This new shape cannot bind to the *lac* operator, so transcription of the lactose metabolism genes occurs. Permissive sites have been previously identified within LacI [1]. These sites are permissive because short sequences can be inserted there without affecting the normal function of the protein. QBP3, a known amino acid sequence with the ability to bind silica [2], was inserted into the permissive site at residue 338 of LacI, endowing LacI with the ability to bind both DNA and silica. Expression, function and silica binding capability of the Lac-I derivatives were characterized.

Proteins with this dual binding ability can use DNA as a scaffold to organize nanostructures in complex predictable patterns. As more proteins are engineered to bind DNA and inorganic compounds, organization of complex nanostructures will become a more efficient process.

Experimental Procedure: Construction of LacI-338::QBP3

A plasmid with the lacI-338::i31 gene, *plac*I-338::i31 [1], was used as a cloning vector and digested with the restriction enzyme BamHI. The coding sequence for the silica binding motif, QBP3 (Leu-Pro-Asp-Trp-Trp-Pro-Pro-Pro-Gln-Leu-Tyr-His), was PCR amplified using engineered primers (5'TTCGCAATTCCTTTAGATCTACCTTTCTATTCTCACT CT3' and 5'ACTTTCAACAGTTTCGGCCAGATCT CCA CC3') which were designed to amplify the QBP3 coding sequence and introduce BglII restriction sites. The PCR product was purified via ethanol precipitation and digested with BglII. BglII and BamHI restriction sites leave identical overhangs which facilitated the ligation of QBP3 and *plac*-338::i31. To minimize ligation of the vector without the QBP3 insert, a background BamHI digest followed the ligation. Reactions were transformed into DH5α competent *E. coli* and plated onto LB plates, supplemented with 100 μg/ml ampicillin, and incubated overnight at 37ºC.

90 reactions were screened by PCR with the engineered primers QBPINT and 3'LacIR, which bind within and downstream of the QBP3 insert. Six candidates were further screened by sequencing. QBP3 contains a BseRI restriction site not present

in the vector. Two candidates were cut with BseRI to confirm the insertion, and chosen for further characterization (denoted 29 and 38 in the figures).

Characterization of LacI-338::QBP3

Protein expression of the clones was determined by western blotting, using the monoclonal anti-LacI primary antibody. β-galactosidase assays were carried out as described by Kleina and Miller [3] to determine DNA binding activity, in high and low plasmid copy number *E. coli* strains, CSH140 and BN29, respectively.

Silica binding assays were done with cell extracts containing various LacI derivatives supplemented with fine or coarse silica powders. Assays were incubated for 10 minutes with rotation at room temperature, then harvested. The ability of protein to bind to silica (indicated by fractionation to the pellets) was measured. Protein was detected using the LacI antibody on a Western blot.

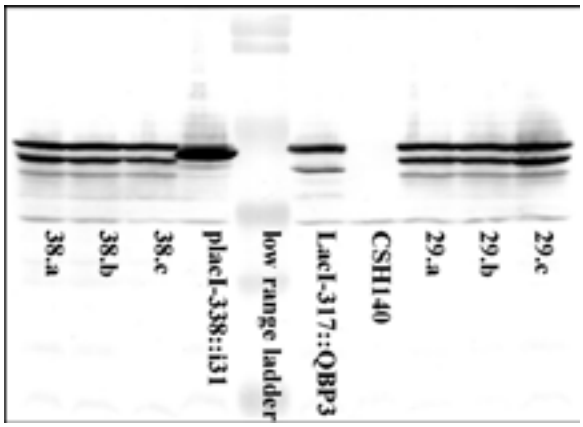

Figure 2: Western blot analysis of protein expression.

Results and Conclusions

Two LacI-338::QBP3 clones were isolated and characterized. The LacI-338::QBP3 derivatives displayed good protein expression [Figure 2]. Smaller LacI-related bands were present in the Western blot, suggesting these proteins were somewhat more susceptible to degradation than the positive controls. β-galactosidase assays showed good repression activity was maintained in both strains, indicating DNA binding by LacI-338::QBP3 (Table 1). The clones displayed some fine silica binding and even less affinity for coarse silica (Figure 3). The silica binding assays also suggested the insertion at residue 338 binds less favorably to silica than the insertion at residue 317.

Future Work

It will be of interest to determine whether the affinity for binding various inorganic compounds varies by motif insertion at different locations, as seen here. Also, this project can be continued with the characterization of QBP3 and other inorganic binding sequence inserts into various DNA-binding proteins. As more constructs are built and characterized, organization of nanostructures using these engineered proteins will become a more efficient process.

Acknowledgments

The National Nanotechnology Infrastructure Network Research Experience for Undergraduates Program and the National Science Foundation. Special thanks to Beth Traxler, Eliora Gachelet, Ruth Hall and Rembrandt Haft.

References

[1] Nelson, B.; C. Manoil; B. Traxler; J. Bacteriol., 179, 3721-28 (1997).

[2] Oren, E.E.; C. Tamerler; D. Sahin; M. Hnilova; U.O.S. Seker; M. Sarikaya; R. Samudrala; Bioinformatics, (2007), in press.

[3] Kleina, L. G.; Miller, J. H.; J. Mol. Biol., 212, 295-318 (1990).

mutant	β-gal activity
(assayed in CSH140)	
pTrc99A (wt LacI)	0.0010
LacI-317::QBP3	0.0003
placI-338::i31	0.0005
29.a	0.0007
29.b	0.0008
29.c	0.0009
38.a	0.0006
38.b	0.0008
38.c	0.0006
(assayed in BN29)	
BN29	152.863
pTrc99A (wt LacI)	0.598
placI-338::i31	7.200
29.a	17.300
38.c	10.39

Table 1: β-galactosidase activity in Miller units.

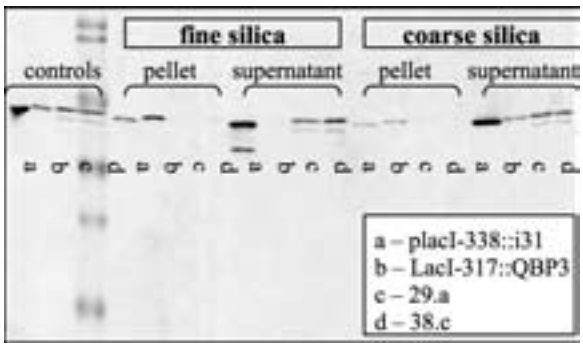

Figure 3: Western blot analysis of silica binding assays.

Atomic Force Microscopy Grain Structure Characterization of Perpendicular Magnetic Recording Media

Alexander Luce

Engineering Physics, University of Arizona

NNIN REU Site: Stanford Nanofabrication Facility, Stanford University
NNIN REU Principal Investigator: Professor Robert Sinclair, Materials Science and Engineering, Stanford University
NNIN REU Mentor: Faraz Hossein-Babaei, Department of Materials Science and Engineering, Stanford University
Contact: aluce@email.arizona.edu, bobsinc@stanford.edu, farazhb@stanford.edu

Abstract

Magnetic recording technology plays a key role in the development of computer, audio, and video storage devices. The nanoscale grain size of current hard-disk media determines important recording properties and thus requires accurate characterization methods. In this work, we developed a new method to characterize the nanostructure of thin film magnetic recording media using a phase-imaging tapping-mode atomic force microscope (AFM). In this study, clear images obtained with the AFM were compared to those obtained with a transmission electron microscope (TEM). A statistical distribution of grain size was analyzed. This novel method is an important development because phase imaging tapping mode AFM could provide a cheaper and faster characterization alternative to TEM.

Introduction

In order to continue increases in information storage density for personal computers, advanced nanofabrication techniques are being used to produce magnetic media with grain structures in the nanometer size range. The grain size of the media determines important recording properties including aerial density, signal to noise ratio, and thermal stability [1]. In order to successfully fabricate media with nanometer grain size, advanced characterization techniques are required to accurately assess grain sizes.

Because of the nanoscale size of current PMR grains, the TEM has been the tool of choice for grain structure analysis. The TEM provides excellent resolution [2]; however, sample preparation is difficult and time consuming. The AFM can be easily used to image surface topography with little sample preparation. However, to our knowledge, there exist few other efforts using the AFM to analyze nanoscale grain sizes of magnetic thin films [3].

In tapping-mode AFM, an oscillating cantilever scans the sample surface, and tip to sample height is kept constant through the use of an electronic feedback loop. Phase-imaging is an extension of tapping-mode, which measures the contrast in the phase angle between the driving and response frequencies. This data is gathered simultaneously with topographic data. The difference in phase angle is sensitive to several material properties including composition, viscoelasticity and surface adhesion [4]. This data may be used to enhance grain boundary resolution [3]. In this study, we present grain size distributions of PMR media obtained using phase-imaging tapping-mode AFM for the first time.

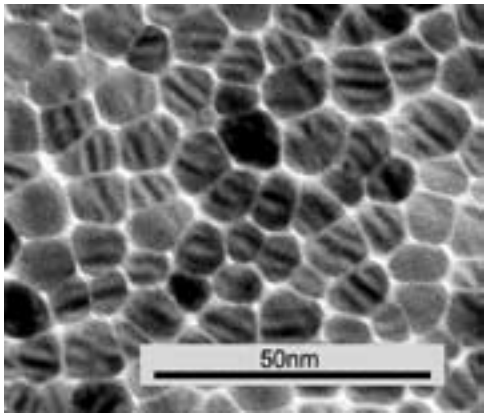

Figure 1: Bright field TEM image of PMR media with 9 nm grain size.

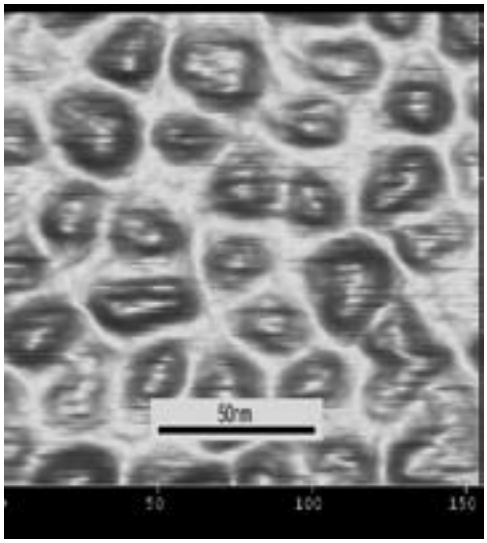

Figure 2: Phase-image tapping mode AFM scan of PMR media with 20 nm grain size.

Experimental Procedure

Two discs of CoPtCr-O PMR with different grain size were analyzed. Samples were etched for 2 minutes in an oxygen plasma to remove a 5 nm protective diamond-like carbon (DLC) layer on the surface of the media and to improve imaging response. A Digital Instruments multimode scanning probe microscope operating in tapping mode was used to characterize the samples both before and after the plasma etch process. Silicon nitride cantilevers with a resonant frequency

between 285-315 kHz, and a tip radius of curvature (ROC) of 10 nm were used. TEM images of the samples were obtained before etching. Grain size was determined by taking the average of the large diameter and small diameter of a single grain, with a sample size of 30 grains used for statistical analysis.

Results and Conclusions

In Figure 1, we present a TEM image of a PMR media sample with 9 nm grain size. We compare this with Figure 2, which is an AFM phase image of a different sample of PMR media, having a measured grain size of approximately 20 nm. Note in both images, the individual grains and grains boundaries are clearly visible.

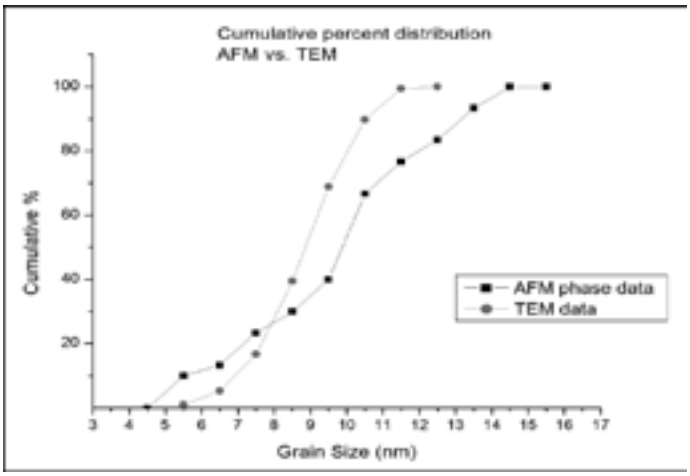

Figure 3: Cumulative percentage plot of grain sizes obtained by TEM and AFM methods.

In Figure 3, we present the measured grain size data for the sample with 9 nm average grain size in a cumulative percentage frequency plot, which has been shown to give reasonable grain size distributions even with small grain size populations [5]. The AFM method yielded slightly larger grain sizes than the TEM method. This may have been because the radius of curvature (ROC) of the AFM tip, at approximately 10 nm, approached the measured grain size and became a limiting factor in the resolution of the scans. In fact, the AFM phase image data agreed quite well with the TEM data as the calibration error of the AFM is approximately 10%.

In Figure 4, we compare the grain size distributions for the 20 nm grain size sample obtained with the AFM topography method and the phase image method. The phase image data was gathered before the sample was etched. This shows the phase difference is sensitive enough to be detected through the 5 nm amorphous DLC layer.

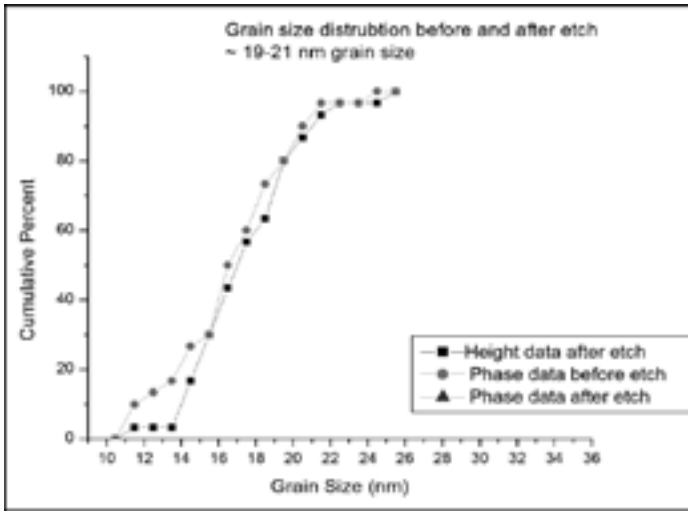

Figure 4: Cumulative percentage plot of grain sizes obtained from AFM height data, and AFM phase-image data.

In this study, we have presented the first images of PMR nanoscale grain structure captured using phase imaging tapping-mode AFM. These are found to compare to TEM nanographs. This work demonstrates that tapping mode AFM can be used for reasonably accurate grain size analysis of magnetic recording media.

Acknowledgements

Sinclair Group, Dave Gage, Dr. Jim Kruger, Mike Deal, Maureen Baran, REU Staff, NNIN REU Program, support from NSF and Center for Integrated Systems.

References

[1] Piramanayagam, S. N.; "Perpendicular recording media for hard disk drives"; Journal of Applied Physics, 102, 11301-11323 (2002).

[2] Risner, J.; "Transmission electron microscopy analysis of computer hard disc, magnetic thin films"; Materials Chemistry and Physics, 81, 241-143 (2003).

[3] Pang, C.H.; "Application of phase-imaging tapping-mode atomic-force microscopy to investigate the grain growth and surface morphology of TiSi2"; Journal of Vacuum Science and Technology B, 20, 1866-1869 (2002).

[4] Bhushan, B.; "Phase contrast imaging of nanocomposites and molecularly thick lubricant films in magnetic media"; Nanotechnology, 14, 886-895 (2003).

[5] Park, D.W. and Sinclair, R; "Grain size analysis of longitudinal thin film media"; Journal of Applied Physics, 87, 5687-5689 (2000).

Optical Characterization of Nanostructured Wide Bandgap Semiconductors for Energy Applications

Jessica Smith

Physics and Mathematics, Austin College

NNIN REU Site: Michigan Nanofabrication Facility, The University of Michigan Ann Arbor
NNIN REU Principal Investigator: Professor Pei-Cheng Ku, Electrical Engineering & Computer Science, University of Michigan
NNIN REU Mentors: Min Kim and Luke Lee, Electrical Engineering and Computer Science, University of Michigan
Contact: jmsmith@austincollege.edu, peicheng@umich.edu, minwkim@umich.edu, leelk@umich.edu

Abstract

Illumination applications for light emitting diodes (LED's) have been increasing. Therefore, LED's are the dominant focus in the field of solid state lighting. The issue concerning lighting today is the trade-off occurring between high efficiency and high color rendering capabilities. For high efficiency, a white light can be constructed using blue and yellow components. However, to render the color faithfully, the white light must contain at least the primary components blue, green, and red. We explored improving color rendering in a highly efficient dichromatic system.

Introduction

To increase the color rendering index of the dichromatic white light, we broadened the spectral line widths of light emitted at blue and yellow to cover also the green and red components. To prove this concept, we used the selective area epitaxy (SAE) technique for growing indium gallium nitride quantum wells (InGaN QWs). Our methods included changing the pattern of the dielectric mask including pitch and area, and changing the indium incorporation and growth rate of InGaN QWs in different areas to achieve a broader linewidth. To characterize variations of emission wavelengths on the pattern, we used micro-photoluminescence (PL) to locally concentrate high energy. We plan to stack blue and yellow QWs on one LED, and characterize the color rendering index and efficiency of the proposed LED.

When having two layers of GaN separated by a layer of InGaN, a QW forms. Because electrons can occupy a lower energy state in InGaN than GaN, excited electrons tend to go to lower energy states in the InGaN layer. The QW increases the probability of electrons recombining with holes. When electrons and holes recombine, photons are emitted.

Previous results revealed linewidth broadening at blue emission using SAE. To further prove our concept in attaining high color rendering index dichromatic white light, we increased the wavelength to green/yellow. This was achieved by increasing the indium composition of the material to create a different lattice for emitting light and increasing the QW thickness to lower the energy of the photon released. To broaden the emission linewidth, we varied the growth rate of the QW across the wafer by SAE, in turn creating varying QW thicknesses. We adjusted the conditions affecting the concentration gradient that the molecules form, and altered the pattern at which our QWs grew. The pattern had multiple sites that included different shapes and densities to have different QW thicknesses that emit slightly different wavelengths of light at each site, thus the one LED will have a broader spectrum of emission.

Experimental Process

To define the pattern for SAE, we deposited a layer of silicon dioxide (SiO_2) then a layer of S1805 resist on a GaN template. We used photolithography to expose selected areas of resist to UV light. Then we developed those certain areas by removing the exposed resist with MF AZ 300. Finally, we etched those certain areas into the SiO_2 with a solution of BHF and water.

For QW growth, we used metal-organic chemical vapor deposition. The product that forms when the gas phases of indium and gallium, both attached to an organic molecule when added to ammonia, is InGaN. When incorporating the indium, we used ~ $In_{0.2}Ga_{0.8}N$. The concentration gradient of the molecules was increased/decreased and the pattern was altered, each partially determining how fast the molecules reached the exposed GaN template. Since the materials always wants to grow at the most stable planes in SAE, the GaN oriented in a hexagonal pyramidal shape.

For micro-PL, we arranged a beam splitter, UV objective lens, as well as other lenses and mirrors to concentrate the UV light onto one micro-pyramid and measure variations of the wavelength emitted from site to site on the pattern. We used the spectrometer to read the spectrum emission.

Results and Conclusions

With the planar QW results, we obtained an InGaN peak at about 510 nm, with the GaN peak at a less intensity. The micro-pyramid QWs were obtained using the same recipe as the planar QWs; however, the micro-pyramid InGaN signal was low as shown in Figure 1. Unfortunately we were not able to obtain micro-PL signal from individual micro-pyramids, possibly due to the weak signal. (Micro-pyramid growth at the ~ 10 μm site is shown in Figure 2. The SEM was under maintenance at the time of measurement.) We also cannot know how the QW thickness and indium incorporation separately affected the wavelength emitted, since both together must be qualities of the QW.

With further testing of possible causes for unattainable micro-PL measurements, we can detect if there is a problem with laser alignment on a micro-pyramid or sample defects. One possible cause could be due to the micro-PL setup. We used a UV objective lens that is coated for light in the non-visible wavelength range, thus the lens was not ideal for light in the green wavelength range when the signal is weak.

Nonetheless, we have proven it is possible to get green emission from micro-pyramid QWs in our PL measurements. Once we have increased the wavelength of light emission and characterized the light produced by measuring each site of our pattern, then we will stack blue and yellow QWs accordingly to improve efficiency. Finally, we will have one LED, and with anticipation the LED will have improved color rendering properties and efficiency.

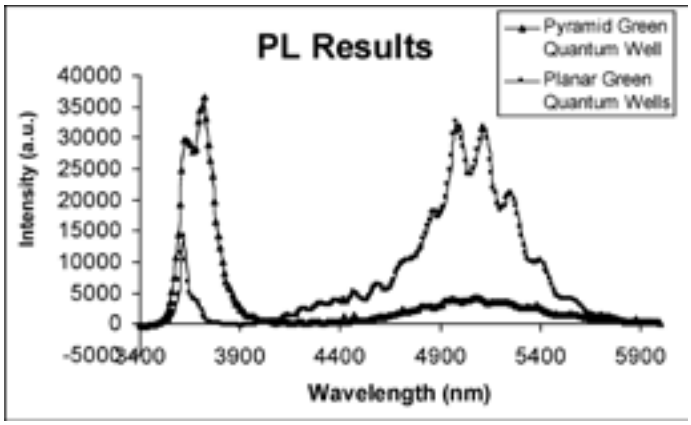

Figure 1: Compared photoluminescence results of planar and micro-pyramid quantum wells.

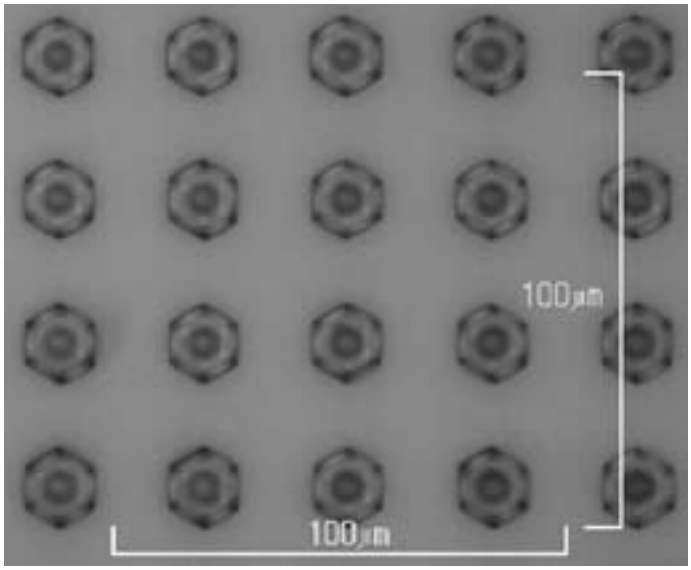

Figure 2: ~ 10 μm diameter array of micro-pyramids.

Acknowledgements

This work was performed in part at the Michigan Nanofabrication Facility, a member of the National Nanotechnology Infrastructure Network Research Experience for Undergraduates Program, which is supported by the National Science Foundation. Thank you to Dr. Sandrine Martin and Prof. Pei-Cheng Ku, along with his research group.

References

[1] Schubert, E. Fred (2006). "Light Emitting Diodes (2nd ed.)." New York: Cambridge University Press.

[2] H. Yu, T. Jung, L. Lee, and P. C. Ku, "Multiple Wavelength Emission from Semipolar InGaN/GaN Quantum Wells Selectively Grown by MOCVD," Conference of Laser and Electro-Optics, Baltimore, MD (2007).

Investigation of TMAH Release of Stretchable Silicon Networks

Allison Solanki

Physics, Whitman College

NNIN REU Site: Stanford Nanofabrication Facility, Stanford University
NNIN REU Principal Investigator: Prof. Peter Peumans, Electrical Engineering, Stanford University
NNIN REU Mentor: Kevin Huang, Electrical Engineering, Stanford University
Contact: solankak@whitman.edu, ppeumans@stanford.edu, kevhuang@stanford.edu

Abstract

The development of stretchable silicon networks is an important step to realizing cost-effective large area electronics. Devices were fabricated using conventional complementary metal oxide semiconductor (CMOS) processing on wafers which were etched into networks of nodes connected by spiral springs and then stretched to desired size and shape. This investigation focused on developing an approach to release these networks following deep reactive ion etching using a tetramethylammonium hydroxide (TMAH) etch on <111> wafers. To achieve effective release of these networks, etching parameters such as etch time and temperature of etchant bath were varied until optimal process parameters such as etch rate and oxide selectivity were determined. The ability to successfully create a device on a standard 4″ silicon wafer and stretch it to a size ten times or larger is important in the implementation of many large area electronics applications, such as structural health monitoring sensors and solar cells.

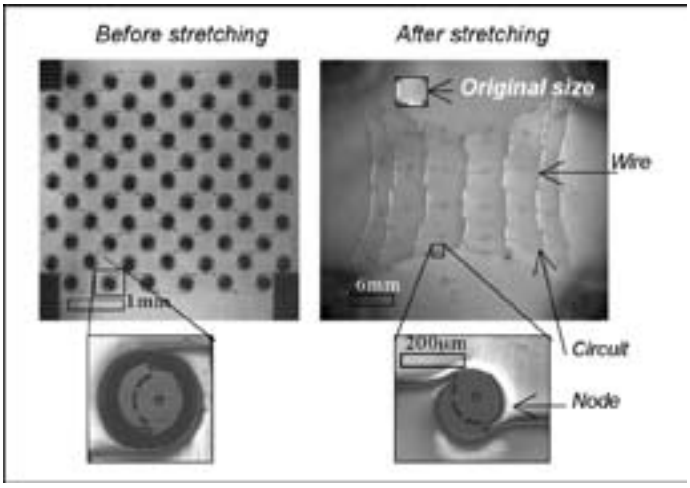

Figure 1: Stretchable silicon network before and after stretching.

Introduction

This research investigated a cost-reducing, consumption friendly fabrication process to release two-dimensional stretchable silicon structures. Eventually, devices or sensors will be placed on individual nodes, in which the spiral springs serve as built-in circuit interconnects for creation of an integrated, robust system as shown in Figure 1.

Previously, stretchable silicon network fabrication required using silicon on insulator (SOI) wafers and employed the xenon difluoride (XeF_2) isotropic dry etch process to release the devices from the substrates. This process was expensive due to the cost of the SOI wafers and inability to reuse the wafers following a single process run. In addition, it was prone to structural problems stemming from pinhole defects particularly in the sidewalls. In response to these consequences, a new wet etch process was employed.

TMAH is a well known non-toxic, anisotropic wet etch solution that was chosen for its ability to etch specific crystal planes at specific rates, its high selectivity to oxide, and for its compatibility with the CMOS process as it does not contain harmful alkali ions [1]. Because TMAH etches the <111> plane at the slowest rate, it can act as an etch stop much like the buried oxide does in the SOI wafer when bulk Si <111> wafers are used.

Device Fabrication

The substrates for this investigation consisted of 4″ diameter, <111> oriented Si wafers which were selected for their compatibility with the TMAH target etch planes. The device fabrication process started with the blanket deposition of a 1.6 μm thick layer of silicon oxide via low pressure chemical vapor deposition (LPCVD). Next, standard photolithography steps were performed. A dry fluorine etch was subsequently used to etch the exposed network pattern in the oxide. Si was then etched using the Bosch deep reactive ion etch (DRIE) process which consisted of an alternating sulfur hexafluoride (SF_6) etch process and a deposition of octafluorocyclobutane (C_4F_8), which served as a protective passivation layer over the etched structures to create a smooth sidewall.

Next, a 2 μm layer of oxide was blanket deposited using LPCVD. A second oxide etch removed the bottom layer of oxide, preparing the wafer for another DRIE. This prepared the Si wafer for the wet etch release. Figure 2 shows the resulting device structure following the second DRIE step. Finally the wafers were subjected to a TMAH bath heated over a hotplate to ensure thorough undercutting of the nodes, spirals, and pads. The bath was closely monitored to ensure a constant temperature and the solution was agitated to help decrease the quantity of hydrogen bubbles, which can disrupt the etching process.

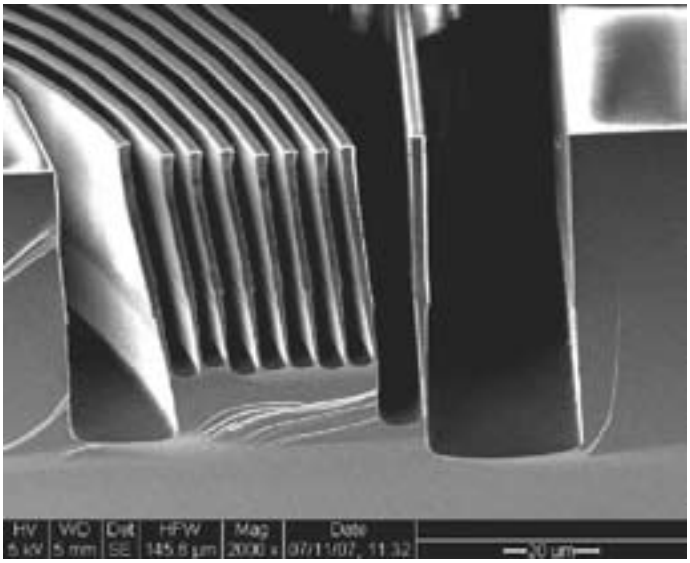

Figure 2: Cross-section of device prior to TMAH wet etch.

Results and Conclusions

Complete structure fabrication was achieved in a clean room environment, and optimal production specifications were determined to successfully release the Si structures from the wafer.

It is well known that planar etch rates are inversely related to the TMAH concentration, thus for optimum results, a 5% TMAH: 95% water bath ratio was used at a temperature of 90ºC [2]. With an optimum etch rate of 1.4 μm/min in the <110> plane, the TMAH etch process time was determined to be 80 minutes to effectively undercut the silicon nodes, interconnects, and pads. However, transferring the networks between liquid and gaseous states proved difficult.

Traditionally, critical point dryers (CPD) are used to reduce the negative consequences of surface tension. However, the stretchable Si structures are delicate, hence they became easily entangled due to the gas flow in the dryer, as shown in Figure 3. This prompted a new investigation directed at successful removal of the structures following the TMAH bath. One solution was found by increasing the distance between the released structure and the substrate during the final DRIE step, followed by air drying the samples after release. Although the substrates still had to be removed from the TMAH solution and thus were subject to some tangling, the networks were nevertheless released without being introduced to the CPD.

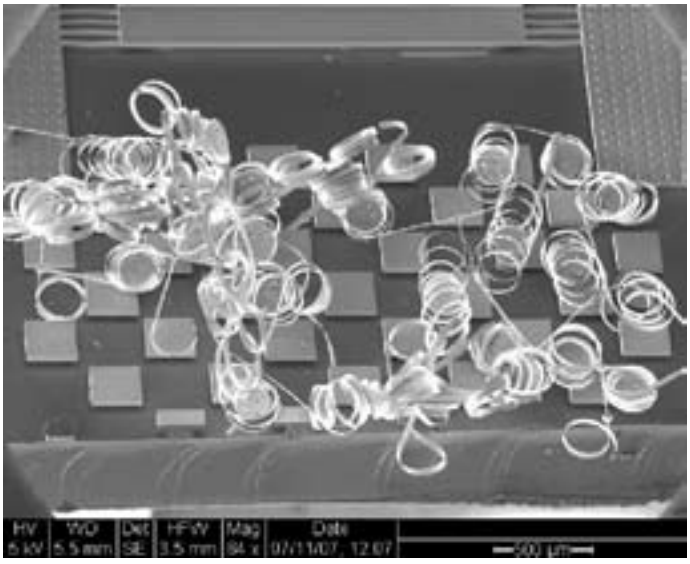

Figure 3: Tangled node network following TMAH etch.

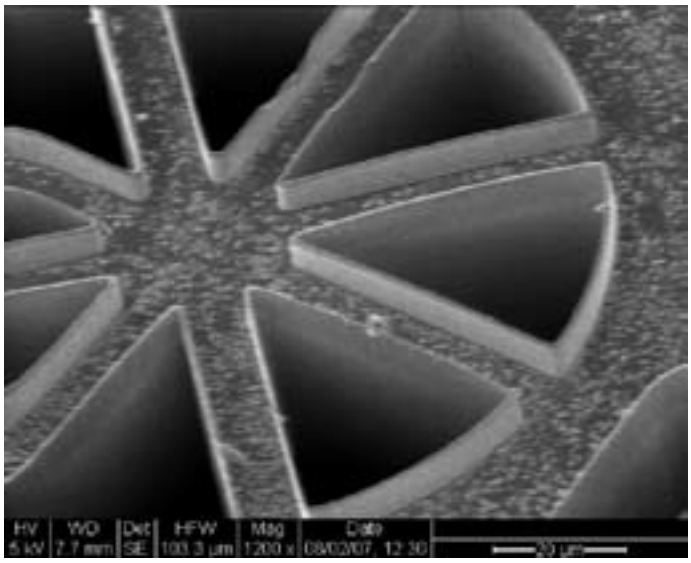

Figure 4: Underside of node showing clean release.

Figure 4 shows a cleanly released node structure. Future work will involve improving this release mechanism. However, we have shown that a cost-effective method to fabricate stretchable silicon networks is viable and important in the implementation of various sensor devices.

Acknowledgements

The author would like to thank Kevin Huang and Dr. Peter Peumans for their guidance and support throughout this research, the Stanford Nanofabrication Laboratory staff, and Dr. Michael Deal and the Stanford Research Experience for Undergraduates program. This work was supported by the Stanford Center for Integrated Systems, the National Nanotechnology Infrastructure Network Research Experience for Undergraduates and the National Science Foundation.

References

[1] Tsaur, J., et. al. "Development of TMAH Anisotropic Etching Manufacturing Process for MEMS". Micromachining and Microfabrication Process Technology VI, Proceedings of SPIE, Vol. 4174, 142-153 (2000).

[2] Laconte, J., et. al. "Micromachined Thin-Film Sensors for SOI-CMOS Co-Integration". New York: Springer, 2006. p. 17-46.

Index
(NNIN REU Interns are in Bold)

NNIN Sites

Cornell University.....vii, 10, 20, 22, 38, 70, 82, 90, 100, 112, 114, 126
Georgia Institute of Technology..... vii, 6, 30, 50, 86, 98
Harvard University..... viii, 72, 78, 102, 122
Howard University..... viii, 4, 16, 58, 104, 106
The Pennsylvania State University .....ix, 8, 18, 64, 84, 118
Stanford University..... ix, 44, 46, 52, 66, 88, 134, 138
University of California Santa Barbara.....x, 48, 54, 56, 68, 76, 94
University of Michigan Ann Arbor .....x, 42, 62, 110, 116, 130, 136
University of Minnesota-Twin Cities..... xi, 36, 74, 80, 92, 124
University of New Mexico..... xi, 2, 60, 96, 120, 128
University of Texas at Austin..... xii, 14, 24, 32, 40, 108
University of Washington ..... xii, 12, 26, 28, 34, 132

A

Adibi, Ali 98
Afshari, Kamran..... vii, 38
Aggarwal, Gagan..... 92
Aguilar, Jonathan ..... x, 56
Agunwamba, Chukwunomso .....viii, 102
Ahsan, Syed Saad ..... xii, 40
Aillaud, Melissa..... xi, 2
Akinwade, Deji..... 46
Akyurtlu, Aydin ..... vii, 90
Alexandre, Myriam ..... x, 116
Anderson, Kasiem..... viii, 104
Anderson, Winston 4
Arbel, Tamir..... 116
Archer, Paul 34
Arruda, Ellen 62
Ayres, Ebony ..... viii, 4

B

Babb III, Henry David ..... viii, 58
Baisch, Andrew ..... vii, 82
Bakir, Muhannad 50
Baler, Kevin..... x, 42
Barlian, Alvin 88
Bates, Clayton..... 106
Batt, Carl..... 22
Bergstein, Courtney..... ix, 84
Birringer, Ryan 52
Biswas, Mohammad ..... vii, 86
Boduroglu, Serhan..... 18
Boettcher, Shannon..... 68
Boies, Adam 124
Bolz, Brian..... vii, 6
Boock, Andrea..... ix, 118
Bowers, John 94
Bowers, Shin..... xi, 120
Bradley, Robert..... xi, 60
Braga, Alex 96
Brinker, C. Jeffrey 60
Broderick, Ian ..... viii, 106
Brower-Thomas, Tina..... 16
Bryce, Brian..... 112
Burek, Gregory 54
Burton, Patrick D..... 128

C

Campbell, Steven..... 92
Chandra, Nikhil ..... xii, 108
Chen, Hang 50
Chiu, Daniel..... 26
Colletti, Ashley ..... ix, 8
Copeland, Naresh W. ..... ix, 44
Crockett, Latisha ..... ix, 46

D

Dai, Hongjie 44
Dattoli, Eric 42
Datye, Abhaya 128
Dauskardt, Reinhold..... 52, 66
Dawlaty, Jahan..... 90
Defranco, John..... 126
Degertekin, F. Levent 86
Demirel, Melik C..... 18
DenBaars, Stephen P..... 56
Deng, Jiangdong..... 122
Desai, Amit..... 84
Deufel, Chris..... 10

E

Eichfeld, Chad 64
Epshteyn, Alla ..... x, 62
Erickson, David 82
Esch, Mandy 70

F

Fang, Alexander..... 94
Farrell, Robert M. 48
Fonash, Stephen J. 118
Forth, Scott 10
Frank, Ian..... viii, 122
Friez, Nathan..... viii, 10

G

Gachelet, Eliora 132
Gamelin, Daniel..... 34
Gilbert, Matthew..... 108
Girshick, Steven 124
Glad, Brayden ..... xi, 124
Gobert, Thomas ..... vii, 126
Gopal, Ashwini 40
Griffin, James 58
Guo, L. Jay 130

H

Haeger, Daniel..... x, 48
Hainley, Christopher J. ..... xii, 24
Hall, Ruth 132
Haque, Aman 84
Harjee, Nahid..... 88
Harris, Gary L..... 4, 58
Harrison, Ryan M..... xii, 12
Hawkins, Benjamin 20
Hebda, Philip..... x, 110
Hillmyer, Marc 80
Ho, Man Kin Derek ..... xii, 14
Hoshino, Kazunori..... 40
Hossein-Babaei, Faraz..... 134
Hou, Tuo-Hung..... 38
Huang, Kevin..... 138
Huang, Tony Jun..... 8

J

Jain, Ravi 2, 96
Jeffries, Gavin..... 26
Johnson, Alex 72
Johnson, Michael P. ..... xi, 128
Jones, Kimberly..... 104

K

Kamnang, Emma ..... x, 130
Kan, Edwin 38
Kapadia, Rehan ..... xi, 92
Kaushik, Amit 62
Kaviany, Massoud 110
Keidar, Michael 116
Kelley, Kevin ..... xii, 26
Kennedy, Matthew 22
Kim, Jedo 110
Kim, Min 136
Kim, Taek-Soo 66
Kirby, Brian 20
Korgel, Brian A. 32
Korte, Kylee ..... xii, 28
Kosar, T. Fettah 78
Kranz, Christine 6
Krishnan, Mekala 82
Kuilan León, Ruth Enid ..... xiii, 16
Kumar, Karthik 14
Ku, Pei-Cheng 136

L

Lambson, Brian ..... vii, 30
Lee, Luke 136
Lee, Sarah ..... xii, 132
Leighton, Chris 80
Ligda, Jonathan ..... ix, 64
Linford, Daniel ..... vii, 50
Lipson, Hod 82
Lipson, Michal 100
Loncar, Marko 122
Lopez, Gerald 30
Lucas, Brandon D. 130
Luce, Alexander ..... ix, 134
Lui, Clarissa 22
Lu, Wei 42

M

Mackie, Katherine ..... ix, 66
Macosko, Christopher W. 74
MacQueen, Alice ..... xii, 32
Makowski, Jan 36
Malliaras, George G. 70, 126
Mangan, Ashlee ..... ix, 18
Mao, Xiaole 8
Marcus, Charles 78
Marsh, David ..... x, 68
Matthews, Jermey 104
McSkimming, Brian ..... x, 94
Mitchell, James W. 16
Mizaikoff, Boris 6
Mohney, Suzanne 64
Moskovits, Martin 76
Murali, Raghunath 30

N

Naderseresht, Nasim ..... ix, 52
Nakamura, Shuji 48
Nelson, Austin ..... x, 54
Nelson, Fabiola ..... vii, 70
Nguyen, Van ..... xii, 34
Nikolou, Maria 70
Nishino, Zachary ..... xi, 96
Noia, Brandon ..... vii, 20

O

Onaran, Guclu 86
Osinski, Marek 120

P

Park, Pilyeon 118
Patrick-Boardley, Nefertiti 4
Perkins, Sasha ..... vii, 22
Peumans, Peter 138
Poitras, Carl 100
Pruitt, Beth 88

R

Ramanathan, Shriram 72, 102
Rana, Farhan 90
Rathbun, Lynn 70
Register, Leonard F. 108
Rodwell, Mark 54
Roman, William J. ..... vii, 98

S

Saigal, Amrita ..... viii, 72
Schierhorn, Martin 76
Seelbach, Ryan J. ..... xi, 74
Sharma, Shivani 12
Sherman, Jessica ..... x, 76
Shi, Jinjie 8
Shin, Heungjoo 6
Sinclair, Robert 134
Skrabalak, Sara 28
Smith, Danielle K. 32
Smith, Derek ..... viii, 78
Smith, Jessica ..... x, 136
Smolyakov, Gennady 120
Smyth, Suntrana ..... vii, 112
Solanki, Allison ..... ix, 138
Stewart, Derek 114
Stucky, Galen 68, 76
Suggs, Maria ..... ix, 88
Szeto, Kylan ..... vii, 100

T

Talghader, Joey 36
Thomas, Wendy 12
Tiwari, Sandip 112
Tolley, Michael 82
Traxler, Beth A. 132
Tu, AnYue 12
Tutuc, Emanuel 24

V

Vampola, Kenneth J. 56
Varahramyan, Kamran 24
Vuppuluri, Prem ..... vii, 114

W

Wang, Li 2, 96
Wang, Michelle 10
Wang, Xinran 44
Witte, Mikael ..... xi, 80
Wong, Philip 46

X

Xia, Younan 28
Xiong, Shisheng 60

Y

Yakovenko, Olga 12
Yegnanarayanan, Siva 98
Yeung, Christina ..... xi, 36

Z

Zhang, Chichang 106
Zhang, John X.J. ..... 14 , 40
Zhang, Ling 74

The 2007 NNIN REU Research Accomplishments are on the web in PDF at: http://www.nnin.org/nnin_2007reu.html.
This book was formatted by Ms. Melanie-Claire Mallison. She welcomes your comments at mallison@cnf.cornell.edu